FINAL REPORT

AN EXPERIMENTAL STUDY OF THE PRESSURE LOSSES IN CONVERGING FLOW FITTINGS USED IN EXHAUST SYSTEMS

by

Charles F. Sepsy

Donald B. Pies

The Ohio State Research Foundation

December, 1972

The project upon which this report is based was performed pursuant to Contract No. HSM 099-71-28 with the National Institute for Occupational Safety and Health, Department of Health, Education, and Welfare.

50272-101

REPORT DOCUMENTATION PAGE	1. REPORT NO.	2.	3. Recipient's Accession No. PB89 188239/AS
4. Title and Subtitle An Experimental Study of the Pressure Losses in Converging Flow Fittings Used in Exhaust Systems			5. Report Date 72/12/00 6.
7. Author(s) Sepsy, C. F., and D. B. Pies			8. Performing Organization Rept. No.
9. Performing Organization Name and Address College of Engineering, Ohio State University, Columbus, Ohio			10. Project/Task/Work Unit No. 11. Contract (C) or Grant(G) No. (C) HSM-099-71-28 (G)
12. Sponsoring Organization Name and Address			13. Type of Report & Period Covered 14.

15. Supplementary Notes

16. Abstract (Limit: 200 words) A study was conducted to correlate pressure losses for all fittings normally used in industrial ventilation exhaust systems. The project was divided into two parts. In the first part an experimental investigation was made of pressure losses in 16 converging flow fittings with 8 inch common seam diameters which covered a wide range of branch tap and main fitting body styles. The second part of the study correlated pressure losses on a generalized basis which would be valid for all converging flow fittings normally used in industry. Fittings with take/off diameters from 3 to 16 inches were studied. Flow conditions most commonly used in industrial ventilation systems were used; branch to main upstream velocity ratios varied from 0.75 to 6. Branch entry angles of 30, 45, and 90 degrees were studied. Branch and main loss coefficients were found to correlate with good agreement when plotted against the ratio of branch to upstream volume flow rate. Branch and main loss coefficients were found to be significantly affected by the three types of branch tap entrance (sharp, rolled, and round edge). A simple energy/mass balance model was found to be unreliable, due to heat transfer from the fitting to the ambient due to viscous dissipation of turbulent eddies as the branch flow enters the mainstream flow. A negative loss coefficient was seen when the upstream flow rate was high enough compared to the branch flow rate; the upstream flow added sufficient energy to the flow between the branch and downstream to cause an increase in total pressure.

17. Document Analysis a. Descriptors

b. Identifiers/Open-Ended Terms NIOSH-Publication, NIOSH-Contract, Contract-HSM-099-71-28, Ventilation-systems, Ventilation-equipment, Exhaust-ventilation, Exhaust-systems, Air-flow, Industrial-ventilation

c. COSATI Field/Group

18. Availability Statement	19. Security Class (This Report)	21. No. of Pages 345
	22. Security Class (This Page)	22. Price PMF $25.95 $6.95

TABLE OF CONTENTS

TABLE OF CONTENTS (Cont'd)

TABLE OF CONTENTS (Cont'd)

TABLE OF CONTENTS (Cont'd)

LIST OF FIGURES

LIST OF FIGURES (Cont'd)

LIST OF FIGURES (Cont'd)

NOMENCLATURE

Symbol	Description	Dimensions
A_b or AB	cross-sectional area of branch	in. sq.
A_d or AD	cross-sectional area of downstream	in. sq.
A_u or AU	cross-sectional area of upstream	in. sq.
CB	branch loss coefficient	
CB'	experimental branch loss coefficient including wall friction	
CB_t	theoretical branch loss coefficient	
CLC_s	centerline coefficient at a section	
CM	main loss coefficient	
CM_t	theoretical main loss coefficient	
C_p	specific heat for constant pressure	$BTU/lb_m-°R$
C_v	specific heat for constant volume	$BTU/lb_m-°R$
D_b or DB	diameter of branch	in.
D_d or DD	diameter of downstream	in.
D_u or DU	diameter of upstream	in.
ΔCB	empirical branch loss coefficient correction term	
ΔCM	empirical main loss coefficient correction term	
ΔP_{fb}	friction pressure drop in branch	in. of H_2O
ΔP_{fd}	friction pressure drop in downstream	in. of H_2O

ΔP_{fu}	friction pressure drop in upstream	in. of H_2O
ΔP_{tbd}	total pressure drop between branch and downstream	in. of H_2O
ΔP_{tud}	total pressure drop between upstream and downstream	in. of H_2O
γ	specific heat ratio	
h_b	enthalpy of the branch flow	BTU/lb_m
h_d	enthalpy of the downstream flow	BTU/lb_m
h_u	enthalpy of the upstream flow	BTU/lb_m
H_{vb}	velocity head in branch	in. of H_2O
H_{vCLs}	centerline velocity head in a section	in. of H_2O
H_{vd}	velocity head in downstream	in. of H_2O
H_{vs}	velocity head in a section	in. of H_2O
H_{vu}	velocity head in upstream	in. of H_2O
m_b	mass flow rate in branch	lb_m/min
m_d	mass flow rate in downstream	lb_m/min
m_u	mass flow rate in upstream	lb_m/min
P_b	static pressure in branch	in. of H_2O
P_{bar}	ambient barometric pressure	psia
P_d	static pressure in downstream	in. of H_2O
P_{da}	absolute pressure of the dry air	psia
P_s	static pressure in a section	in. of H_2O
P_{svwb}	saturation pressure of water vapor at the wet-bulb temperature	psia
P_u	static pressure in upstream	in. of H_2O

P_{wv}	partial pressure of water vapor	psia
Q_b or QB	volume flow rate in branch	cfm
Q_d or QD	volume flow rate in downstream	cfm
Q_u or QU	volume flow rate in upstream	cfm
R	gas constant for air equal to 53.34 ft-lb_f/lb_m-°R	
ρ	density of the air	lb_m/ft^3
ρ_s	density of the air at a section	lb_m/ft^3
T_b	temperature in branch	°R
T_d	temperature in downstream	°R
T_{db}	dry-bulb temperature	°F
θ	branch angle	degrees
T_{wb}	wet-bulb temperature	°F
T_u	temperature in upstream	°R
u_b	internal energy of the branch flow	BTU/lb_m
u_d	internal energy of the downstream flow	BTU/lb_m
u_u	internal energy of the upstream flow	BTU/lb_m
V_b or VB	mean velocity in branch	fpm
V_d or VD	mean velocity in downstream	fpm
V_s	mean velocity in a section	fpm
V_u or VU	mean velocity in upstream	fpm

CHAPTER I

INTRODUCTION

1.1 Background

Considerable emphasis has recently been directed toward assuring that health and safety standards in industry be kept at a safe level for the workers. Many industrial processes release toxic fumes and vapors, or harmful particulates to the surroundings which humans would breathe if no measure were taken to capture these pollutants at their source. One of the most efficient means to eliminate contaminates is by an exhaust ventilation system.

Since contaminates may be produced by a number of individual processes within one building, an exhaust ventilation system might require a network of ventilation lines which connect to a common main discharge header. In order to properly design a ventilation system, the pressure drops across each component of the system must be known. The primary reference used to determine pressure drops in ventilation systems is the book entitled Industrial Ventilation, A Manual of Recommended Practice, published by the American Conference of Governmental Industrial Hygienists.

This manual recommends that converging flow fittings have a tapered main stream body with a length at least twice

the diameter of the main upstream connection. The pressure drop in the flow from branch to common stream is given as a fraction of the branch velocity head depending on the particular branch inlet angle. The manual also assumes there is no pressure drop in the flow from main upstream to common stream for all branch inlet angles.

A study of other literature available which deals with the pressure losses in converging flow fittings for exhaust ventilation systems and joining water flow pipe lines shows that losses are a function of the ratio of branch to upstream volume flow and not solely branch flow rate. Also, this literature shows pressure losses do occur in the flow from upstream to common stream. Unfortunately, this pressure loss information was limited to fittings with constant mainstream diameters as opposed to the fittings commonly used in industrial ventilation which have tapered body mainstreams. The reliability of these results was felt questionable because the only experimental work performed in this area used water flow in pipes with diameters much smaller than normally required in ventilation ductwork. Experimental work had been conducted by Healy, Patterson, and Brown (Ref. 12) on converging flow fittings, but this investigation was limited to rectangular ducts normally used in heating and cooling return air systems.

1.2 Statement of Purpose

Since pressure loss information for converging flow fittings was found vague and incomplete, an investigation was felt necessary to correlate pressure losses for all fittings normally used in industrial ventilation exhaust systems. The National Institute for Occupational Safety and Health, Department of Health, Education and Welfare, has felt that such a study is vital to the needs of people and therefore, sponsored a one and a half year project to make available pressure loss design data. This project was divided into two programs. The first program was a solely experimental investigation of pressure losses in sixteen converging flow fittings with eight inch common stream diameters which covered a wide range of branch tap and main fitting body styles. Results from this first study were given in Reference 18.

The second program was an investigation to correlate pressure losses on a generalized basis which would be valid for all converging flow fittings normally used in industry. Since the fittings covered in Reference 18 were restricted to eight inch common stream diameters, it was felt additional fittings should be studied which had take-off diameters over the range from three to sixteen inches in order to assure the generality of results. The results of this

generalized pressure loss program are presented in the following context. All experimental portions of this investigation were made over the range of flow conditions most commonly used in industrial ventilation systems. Branch velocities varied from 1000 feet per minute to 6000 feet per minute, velocities in the main upstream ranged from 1000 feet per minute to 5000 feet per minute, and the ratio of branch velocity to main upstream velocity was allowed to vary from seventy-five hundredths to six. The branch entry angle covered thirty, forty-five, and ninety degrees. All fittings studied in the experimental investigation conformed to those fittings manufactured for industrial exhaust systems.

CHAPTER II

APPROACH

2.1 Introduction

An important guideline in developing pressure loss information for duct design work requires that design data be available in a concise, easy-to-use form. The most commonly accepted presentation of design data for divided flow fittings uses a dimensionless pressure loss term as a function of some dimensionless flow condition and dimensionless fitting geometry parameter. Conventional data is usually given in graphical form where the dimensionless geometry parameter is fixed for a particular curve and the dimensionless pressure loss and dimensionless flow condition parameters are allowed to vary. This chapter defines the dimensionless parameters used in this investigation and describes the approach to determine values for these parameters.

2.2 Fitting Parameter Definitions

Figure 2.1 depicts a typical fitting used in this study where flow parameters and geometry parameters are designated at their proper locations. The different parameters are

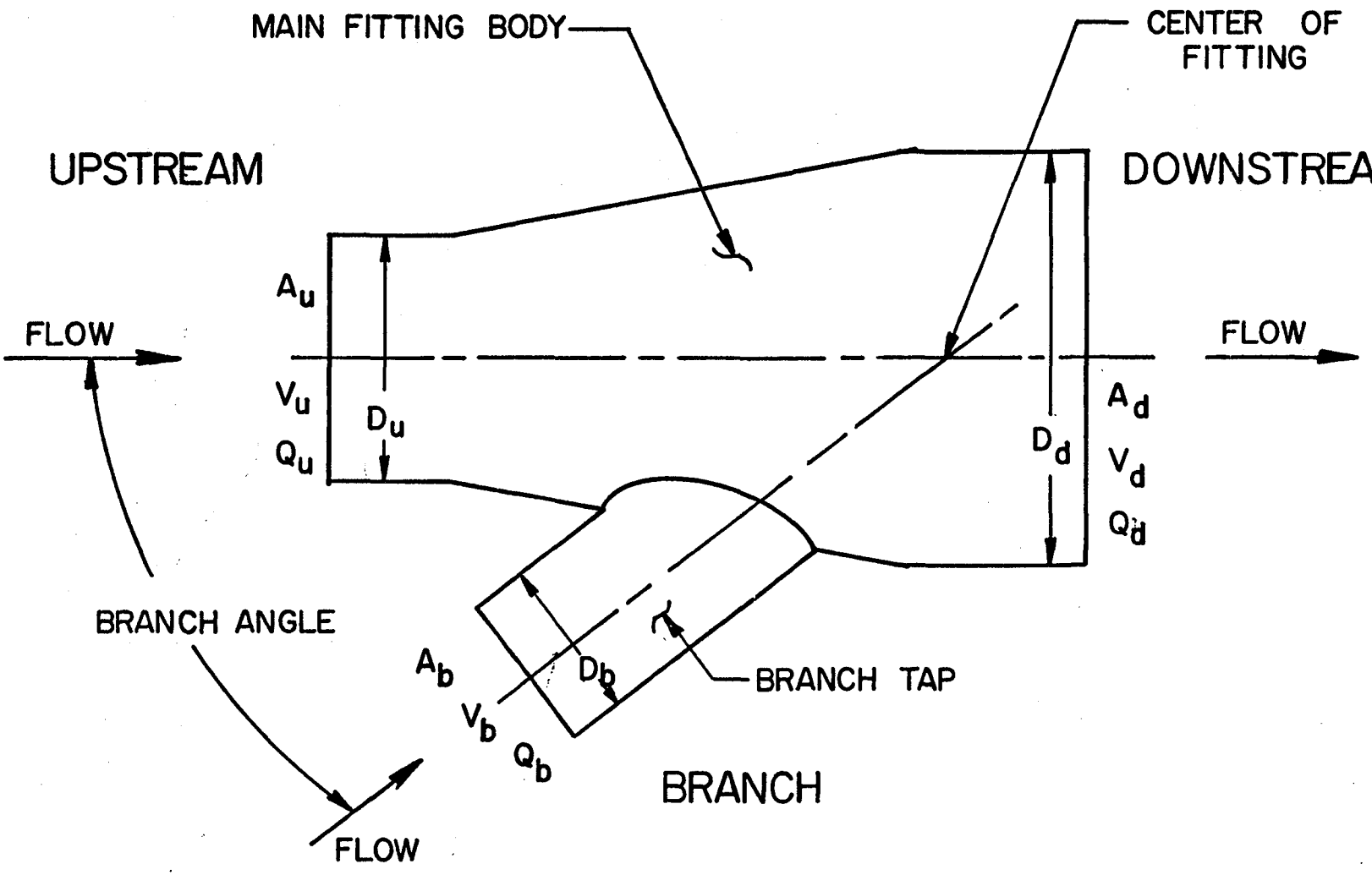

FIGURE 2.1 DEFINITION OF PARAMETERS FOR A TYPICAL FITTING

defined as:

$D_b \triangleq$ diameter of branch take-off, inches

$D_u \triangleq$ diameter of upstream take-off, inches

$D_d \triangleq$ diameter of downstream take-off, inches

$A_b \triangleq$ cross-sectional area of branch, inches sq.

$A_u \triangleq$ cross-sectional area of upstream, inches sq.

$A_d \triangleq$ cross-sectional area of downstream, inches sq.

$V_b \triangleq$ mean velocity of branch flow, fpm

$V_u \triangleq$ mean velocity of upstream flow, fpm

$V_d \triangleq$ mean velocity of downstream flow, fpm

$Q_b \triangleq$ mean branch volume flow, cfm

$Q_u \triangleq$ mean upstream volume flow, cfm

$Q_d \triangleq$ mean downstream volume flow, cfm.

2.3 Loss Coefficient

With the exception of Reference 13, past literature shows that pressure losses exist between branch to downstream sections and upstream to downstream sections. Therefore, two dimensionless pressure loss parameters were required to describe the pressure drops encountered in converging flow fittings. These two pressure drop parameters were defined as the drop in total pressure between either the branch to downstream or upstream to downstream sections divided by the kinetic energy of the downstream

flow. The expressions for these parameters were:

$$CB = \Delta P_{tbd}/(V_d/4005)^2 \qquad 2.1$$

$$CM = \Delta P_{tud}/(V_d/4005)^2 \qquad 2.2$$

where CB $\triangleq$ branch loss coefficient, dimensionless

CM $\triangleq$ main loss coefficient, dimensionless

ΔP_{tbd} $\triangleq$ total pressure drop at standard conditions from branch to downstream sections, inches of water

ΔP_{tud} $\triangleq$ total pressure drop at standard conditions from upstream to downstream sections, inches of water

V_d $\triangleq$ mean velocity at the downstream section, fpm

The branch and main loss coefficients were defined by equations 2.1 and 2.2 because these relations gave convenient forms for design work and equations 2.1 and 2.2 also were consistent with similar works by other authors.

Previous work with converging flow fittings showed that CB and CM would correlate against Q_b/Q_u. Other parameters which were felt to influence the branch and main loss coefficients included A_b/A_d, A_u/A_d, and branch angle.

2.4 Numerical Values for CB and CM

An accurate theoretical approach to determine the branch and main loss coefficients would require complex

mathematical expressions to describe turbulence, separation, vortex formation, and a number of other effects within the fitting which cause drops in total pressure. Expressing CB and CM solely in terms of the dimensionless forms Q_b/Q_u, A_b/A_d, A_u/A_d, and branch angle by a pure theoretical approach might prove nearly impossible. A pure theoretical "black box" or system boundary approach was not sufficient because certian nonusable static pressure terms appeared when conservation of mass and momentum were applied around the system boundary. Even if a pure theoretical approach would have given a workable solution, the information would only be valid for ideal fittings and not those fabricated in production processing for the commercial market.

It was felt that reliable data could only be determined by an experimental investigation. It was hoped that general expressions could then be found by empirical means using the experimental results, and this would allow the branch and main loss coefficients to be determined for any fitting geometry.

The experimental program set forth was to cover thirty-three fittings over a wide range of diameters and three commonly used branch angles. The branch and upstream diameters varied from three to fourteen inches, the downstream diameter varied from four to sixteen inches, and the branch

angle was thirty, forty-five, or ninety degrees. The combinations of branch, upstream, and downstream diameters were representative of fitting diameters used in practice.

The analytical program consisted of first theoretically describing the branch and main loss coefficients by the system boundary approach using conservation of mass, momentum, and energy. The equations were then rearranged to express as many terms as possible in the form of Q_b/Q_u, A_b/A_d, A_u/A_d, and branch angle. All terms that could not be equated by Q_b/Q_u, A_b/A_d, A_u/A_d, or branch angle were dropped. The remaining equation was felt to give a first approximation of the branch and main loss coefficients. Experimental results could then be used to empirically fit the approximate theoretical equations to meet the experimental values. These semi-empirical equations could then be compared with the experimental work in this investigation and with other authors of similar studies to determine the degree of reliability in the final analytical expressions.

CHAPTER III

EXPERIMENTAL PROGRAM

3.1 Introduction

The experimental investigation set forth was divided into five basic subdivisions. These five areas included: equations needed to reduce raw data; choice of equipment; choice of instrumentation; raw data collection; and reliability limits of reduced data. Each of the above considerations is discussed in this chapter.

3.2 Experimental Determination of the Loss Coefficients

Proper evaluation of the branch and main loss coefficients, equations 2.1 and 2.2 respectively, required that the basic loss coefficient definitions be broken down into a combination of parameters that could be measured in the laboratory. Certain correction factors were also necessary to standardize results with duct design information used in the design field.

The velocity head downstream at standard conditions was related to the velocity downstream by

$$H_{vd} = (V_d/4005)^2 \quad \text{(Ref. 3)} \qquad 3.1$$

and the change in total pressure from branch to downstream was given by

$$\Delta P_{tbd} = (H_{vb} - H_{vd}) + (P_b - P_d) \qquad 3.2$$

Equation 2.1 was then rearranged into the form

$$CB' = \frac{(H_{vb} - H_{vd}) + (P_b - P_d)}{H_{vd}} \qquad 3.3$$

where, H_{vb} $\triangleq$ mean velocity head of the branch, inches of water

H_{vd} $\triangleq$ mean velocity head of the downstream, inches of water

P_b $\triangleq$ static pressure of the branch, inches of water

P_d $\triangleq$ static pressure of the downstream, inches of water

CB' $\triangleq$ branch loss coefficient less friction loss terms, dimensionless.

The velocity heads of the branch and downstream were not the centerline velocity pressures directly given from raw data, but were velocity pressures determined from the mean velocities in the duct. Mean velocities were related to measured centerline velocity pressures by

$$V_s = 1096.5\ CLC_s \left(\frac{H_{vCL_s}}{\rho_s}\right)^{1/2} \quad \text{(Ref. 3)} \qquad 3.4$$

where, $V_s \triangleq$ mean velocity in a section, fpm

$CLC_s \triangleq$ centerline coefficient of a section, dimensionless

$H_{vCL_s} \triangleq$ velocity head measured at the centerline of a section, inches of water

$\rho_s \triangleq$ density of air at a section, lb_m per cubic feet.

Velocity heads in equation 3.3 were then determined by

$$H_{vs} = (V_s/4005)^2 \qquad 3.5$$

where, $H_{vs} \triangleq$ velocity head in a section at standard conditions, inches of water

$V_s \triangleq$ mean velocity in a section, fpm

Equation 3.3 was also corrected for friction in the straight duct by the equations presented in Appendix C. The new equation for branch loss coefficient was

$$CB = \frac{(H_{vb} - H_{vd}) + (P_b - P_d) - (\Delta P_{fb} + \Delta P_{fd})}{H_{vd}} \qquad 3.6$$

where, $\Delta P_{fb} \triangleq$ friction pressure drop in branch, inches of water

$\Delta P_{fd} \triangleq$ friction pressure drop in downstream, inches of water.

In using equation 3.6, all pressures must be converted to standard conditions or remain at experimental conditions. Any experimental pressure can be multiplied by $(0.075/\rho)$

to obtain pressure at standard conditions provided temperatures are near standard room temperature, where ρ is the density of air during the experiment in lb_m per cubic foot. Since ΔP_{fb} and ΔP_{fd} in Appendix C were given at standard conditions, all experimentally determined pressures were converted to standard conditions in order to preserve the homogeneity of data.

All terms have been accounted for except the calculation of density. Since the experiments were run at near standard conditions, the perfect gas law was assumed to hold. Density was related by

$$\rho = \frac{P_{da}\ (144)}{R(T_{db} + 460)} \qquad \text{(Ref. 15)} \qquad 3.7$$

where, $\rho \triangleq$ density of the dry air, lb_m per cubic feet

$P_{da} \triangleq$ absolute pressure of the dry air, psia

$R \triangleq$ gas constant for air equal to 53.34 ft-lb_f/lb_m-°R

$T_{db} \triangleq$ dry-bulb temperature, °F.

P_{da} was determined by

$$P_{da} = P_{bar} - P_s - P_{wv}$$

where, $P_{bar} \triangleq$ ambient barometric pressure, psia

$P_s \triangleq$ static gauge pressure at a section, psig

$P_{wv} \triangleq$ partial pressure of the water vapor, psia.

The static gauge pressure was subtracted from the ambient barometric pressure because gauge pressures are negative in exhaust systems. Partial pressure of the water vapor, P_{wv}, was calculated by the Carrier equation as follows:

$$P_{wv} = P_{svwb} - \frac{(P_{bar} - P_s - P_{svwb})(T_{db} - T_{wb})}{2800 - 1.3\,T_{wb}} \qquad \text{(Ref. 5)}$$

where, P_{svwb} ≙ saturation pressure of water vapor at the wet-bulb temperature, psia

T_{wb} ≙ wet-bulb temperature, °F

Curve fitting pressures of saturated water vapor near standard temperature gave

$$P_{svwb} = 0.0292\, e^{0.036 T_{wb}} \text{ psia}$$

where, T_{wb} is in °F.

The procedure to determine the equation for the main loss coefficient with correction terms followed the same routine as just presented for the branch loss coefficient. Equation 2.2 then became

$$CM = \frac{(H_{vu} - H_{vd}) + (P_u - P_d) - (\Delta P_{fu} + \Delta P_{fd})}{H_{vd}} \qquad 3.8$$

where, H_{vu} ≙ mean velocity head upstream, determined by equations 3.4 and 3.5, inches of water

P_u ≙ static pressure upstream, inches of water

ΔP_{fu} ≙ friction pressure drop in upstream, inches of water.

An alternative method to calculate H_{vd} was by a mass balance. Since Mach Numbers never exceeded one-tenth, the flow could be considered incompressible (See Ref. 20). The mass balance related downstream velocity by

$$V_d = \frac{A_b}{A_d} V_b + \frac{A_u}{A_d} V_u \qquad 3.9$$

where, $V_b \triangleq$ mean velocity in the branch, fpm

$V_u \triangleq$ mean velocity in the upstream, fpm

$A_b \triangleq$ cross sectional area of the branch, in. sq.

$A_u \triangleq$ cross sectional area of the upstream, in. sq.

$A_d \triangleq$ cross sectional area of the downstream, in. sq.

Substituting V_d from equation 3.9 into equation 3.1 gave the velocity head downstream in terms of conservation of mass.

Both the measured and mass balance methods to determine H_{vd} were completely correct, although variation could occur due to inaccuracy of a manometer reading. To determine which method yielded a more precise loss coefficient, an uncertainty analysis was devised for both cases. This uncertainty analysis followed the precedures outlined in Reference 6 and the case for H_{vd} calculated via mass balance is given in Appendix E. Observing uncertainties in the two loss coefficients showed that determining H_{vd} simply through measurement placed an uncertainty interval of over twice the uncertainty interval by using the mass balance

basis. Therefore, it was decided that equations 3.6 and 3.8 could be more precisely calculated by using equations 3.9 and 3.1.

3.3 Equipment

Air flow for this investigation was made available by connecting the duct work to the suction inlet of a centrifugal fan. The apparatus first used in this study produced adequate flow rates for fittings with downstream diameters of eight inches or less, but a higher-capacity centrifugal fan was required for fittings with downstream diameters greater than eight inches. The lower volume flow system was similar to the higher volume flow system and both apparatus are depicted by the schematics in Figures 3-1 and 3-2 respectively.

The low volume flow set-up used an American Blower Company centrifugal fan with a capacity of 3,000 cubic feet per minute at a static pressure rise of five and one-half inches of water. A five horsepower direct current motor drove the fan. Variable motor speed was accomplished by a rheostat which allowed the motor to run from 1,000 to 1,250 revolutions per minute.

Higher volume flow rates were achieved by a Sirocco centrifugal fan also made by American Blower Company. The capacity of this fan was 7,000 cubic feet per minute at a

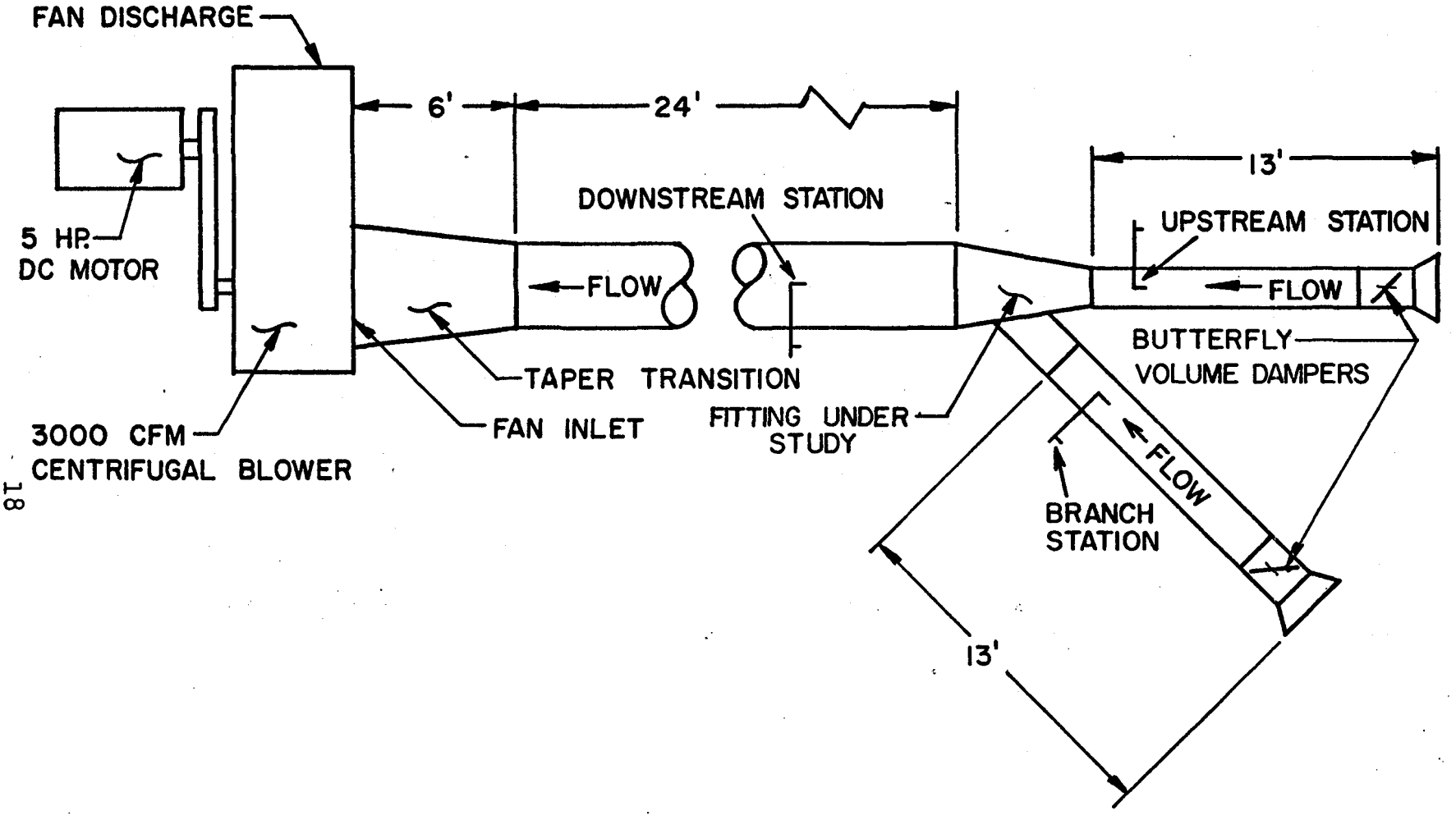

FIGURE 3-1 SCHEMATIC DIAGRAM OF TEST APPARATUS FOR THE DOWNSTREAM DIAMETER EQUAL TO 4", 6", OR 8".

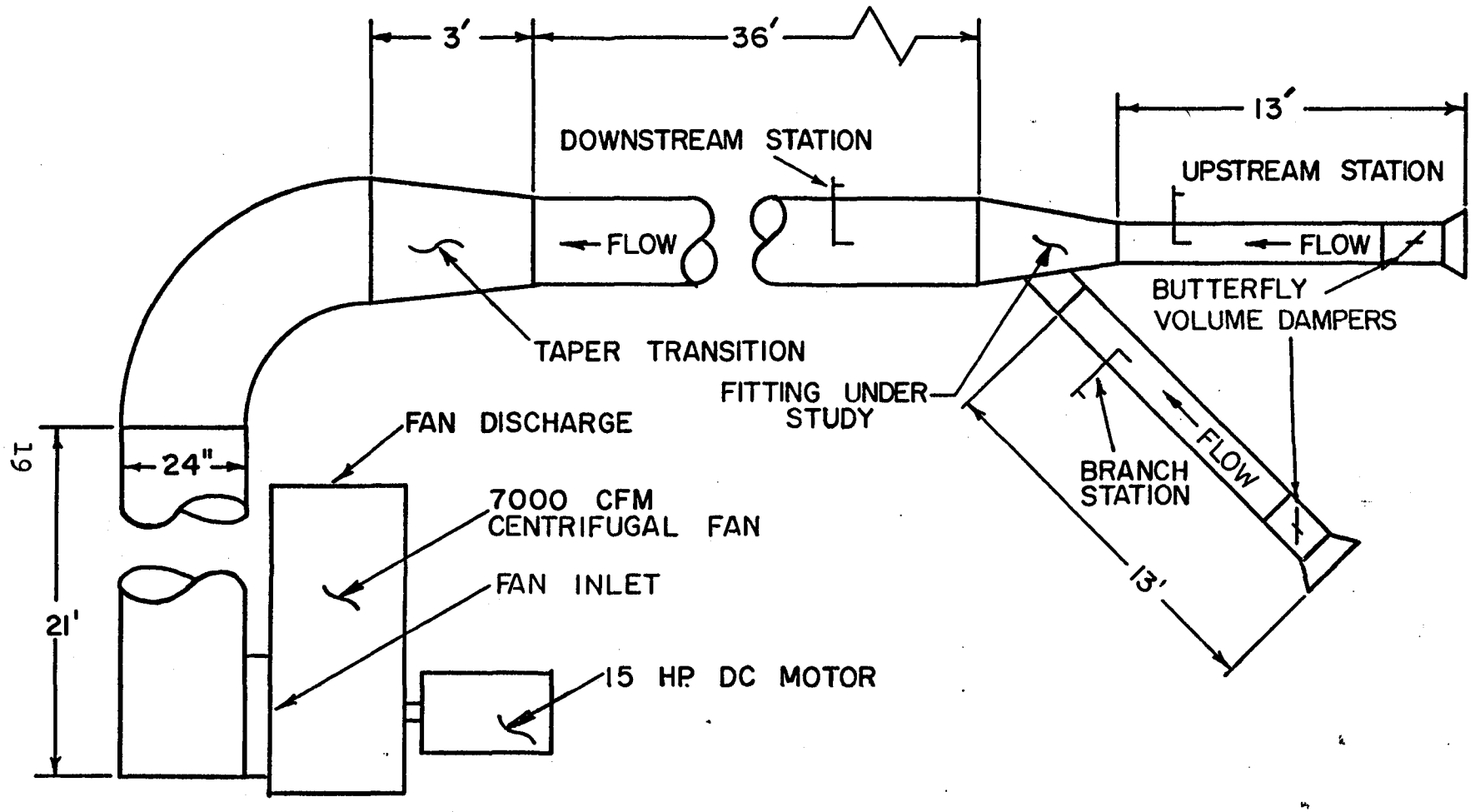

FIGURE 3-2 SCHEMATIC DIAGRAM OF TEST APPARATUS FOR THE DOWNSTREAM DIAMETER EQUAL TO 10", 12", OR 16"

static pressure rise of four inches of water. A direct current fifteen horsepower General Electric motor was used to power this fan at speeds between 400 to 700 revolutions per minute. Motor speed was controlled by varying the voltage to the motor.

Simple round concentric taper transitions were used on the smaller fan for reduction from the fan inlet diameter to test section diameter. Because of space limitations, two elbows plus additional straight duct were needed to connect the fan to the test section on the higher flow apparatus. Supply outlets on both fans were left open to the surrounding room.

The duct work was obtained from United Sheet Metal, a division of United McGill Corporation in Westerville, Ohio, and was of the circular spiral type manufactured by this company. Butterfly type volume dampers at the branch and main duct inlets provided additional control of air flow. Bellmouth fittings at the inlets helped reduce inlet losses and provided more uniform flow. The fittings tested were of the type manufactured by United Sheet Metal for the commercial market. Standard "off the line" production fittings were used with no attempt made to selectively pick good or bad ones. Fittings that are machine-made do not have variations as great as exist for handmade fittings. A complete

list and description of the fittings investigated is presented in Appendix B.

Straight duct was connected to the fittings by slipping the duct over fitting take-offs and securing by sheet metal screws. To prevent air leakage, the joints were sealed with standard duct tape. The system was self-sealing, since the negative gauge pressure tended to draw the tape into any cracks or holes. The ductwork was supported from the floor by means of stands made from wood. Other than the bellmouth fittings at the two inlets, no special precautions were felt necessary to straighten flow patterns or smooth turbulence since the experiment was conducted on the suction side of the fan where flow disturbances from fan blades do not exist.

3.4 Instrumentation

Since many fittings of various sizes were studied, a versatile means to measure air flow was required. The pitot-static tube was chosen because such a device is portable, easily used, and not restricted to one size duct as in the case of the flow nozzle. Standard size pitot-static tubes normally have outside diameters of either one-eighth inch or five-sixteenths inch. The larger of the two pitot-static tubes is generally a better measuring probe because it has a much faster response to pressure changes. On

the other hand, this tube had a diameter large enough compared to duct diameters of eight inches or less to increase the velocity head by one to two percent due to the Bernoulli effect. Therefore, both size tubes were used depending on the duct diameter. One-eighth inch outside diameter tubes measured flow in ducts up to eight inches in diameter, and five-sixteenths inch tubes were used in ducts with diameters larger than eight inches.

All pitot-static tubes were commercial tubes manufactured by Dwyer Instruments Incorporated in accordance with ASME standards. Tests were conducted to determine the degree of variation of flow measurements using the purchased pitot-static probes. A sharp edged orifice flow meter and a stagnation tube made from a hypodermic needle were used to measure mass flow rate in a pipe with a two inch inside diameter. The pitot-static tube was then used to measure the same mass flow rate. Agreement between the pitot-static tube and stagnation tube was within one-half of a percent. The orifice flow meter and pitot-static tube had a one and nine tenths percent variation in flow rate. The precise discharge coefficient for the orifice meter was not known. At this point, it was assumed that flow measuring procedures with pitot-static tubes could accomplish the accuracy needed in this study. Periodic checks were made to be sure the static pressure holes and total pressure hole did not become clogged.

The procedure to measure air flow using a pitot-static tube first required a twenty point velocity traverse (see Ref. 13) with the tube to determine the centerline coefficient for that section. The mean velocity was then determined by the product of the centerline coefficient and centerline velocity. Traverses were made possible by attaching pitot-static tubes to clamps that could be slid in the horizontal and vertical planes on rails rigidly mounted to fixed stands. Tubes were allowed to enter the duct work through holes in the duct walls. To assure symmetrical velocity profiles, pitot-static tubes were placed at least ten diameters downstream from flow disturbances (see Ref. 13). Careful checks were made to assure the pressure sensing probes remained parallel with the walls of the duct as recommended in Reference 22. During regular data collection, the sensing probes remained stationary at the centerline of the duct.

All pressure measurements were made by commercial manometers. Five inclined manometers and one U-tube manometer were required with the proper scale range and readability selected for each pressure reading. Velocity pressures for the branch take-off and main upstream were measured with Ellison inclined manometers, both of which had zero to three inch scale ranges, one-hundredth of an inch of water scale divisions, and readability to one-hundredth of an

inch of water. The velocity pressure downstream was measured with a Meriam manometer having a zero to six inch scale range, a scale division of five-hundredths of an inch of water, and readability to two-hundredths of an inch of water. This manometer was eventually exchanged for a more precise Meriam manometer which could be read to one-hundredth of an inch of water. Static pressure drops from the branch to downstream and upstream to downstream were measured with Meriam inclined manometers with a zero to twelve inch scale range, two-hundredths of an inch of water scale divisions, and readability to one-hundredth of an inch of water. The static gauge pressure was measured at the downstream station by a U-tube manometer with readability to five-hundredths of an inch of water. This satisfied the accuracy needed for static gauge pressure measurement because this pressure was added to the ambient barometric pressure which had a magnitude several thousand times the readability of the U-tube manometer. The degree of readability was determined by comparing pressure readings from the different manometers to a Meriam micromanometer which could be read to one-thousandth of an inch of water.

A standard sling psychrometer was used to measure the dry-bulb and wet-bulb temperatures which had a readability of one half a degree fahrenheit.

3.5 Experimental Procedure

The six manometers mentioned in the previous section were connected to pitot-static tubes as shown in Figure 3-3. Inclined manometers were first leveled and zeroed. The fan was allowed to run for several minutes before data collection to assure steady flow. Dry-bulb and wet-bulb temperatures were taken at the main upstream inlet. The ambient barometric pressure was measured with a nearby barometer. Additional temperature and barometer readings were taken periodically depending on how rapidly ambient conditions changed for that particular time of day. Frequent checks were also made against possible leaks in tubing and manometer fittings.

Flow rates were controlled by the volume dampers and fan speed. All manometers showed quick response to flow changes and stabilized completely within one minute. Some fluctuations did occur in the branch velocity pressure at high branch flow rates. The fluctuations were attributed to flow resonances and could not be eliminated. Uncertainties due to fluctuations were seen to be approximately one percent of the velocity head. The uncertainty analysis discussed in Appendix E showed that the possible error in the final fitting loss coefficient due to flow fluctuations was usually less than one and a half percent. A precaution

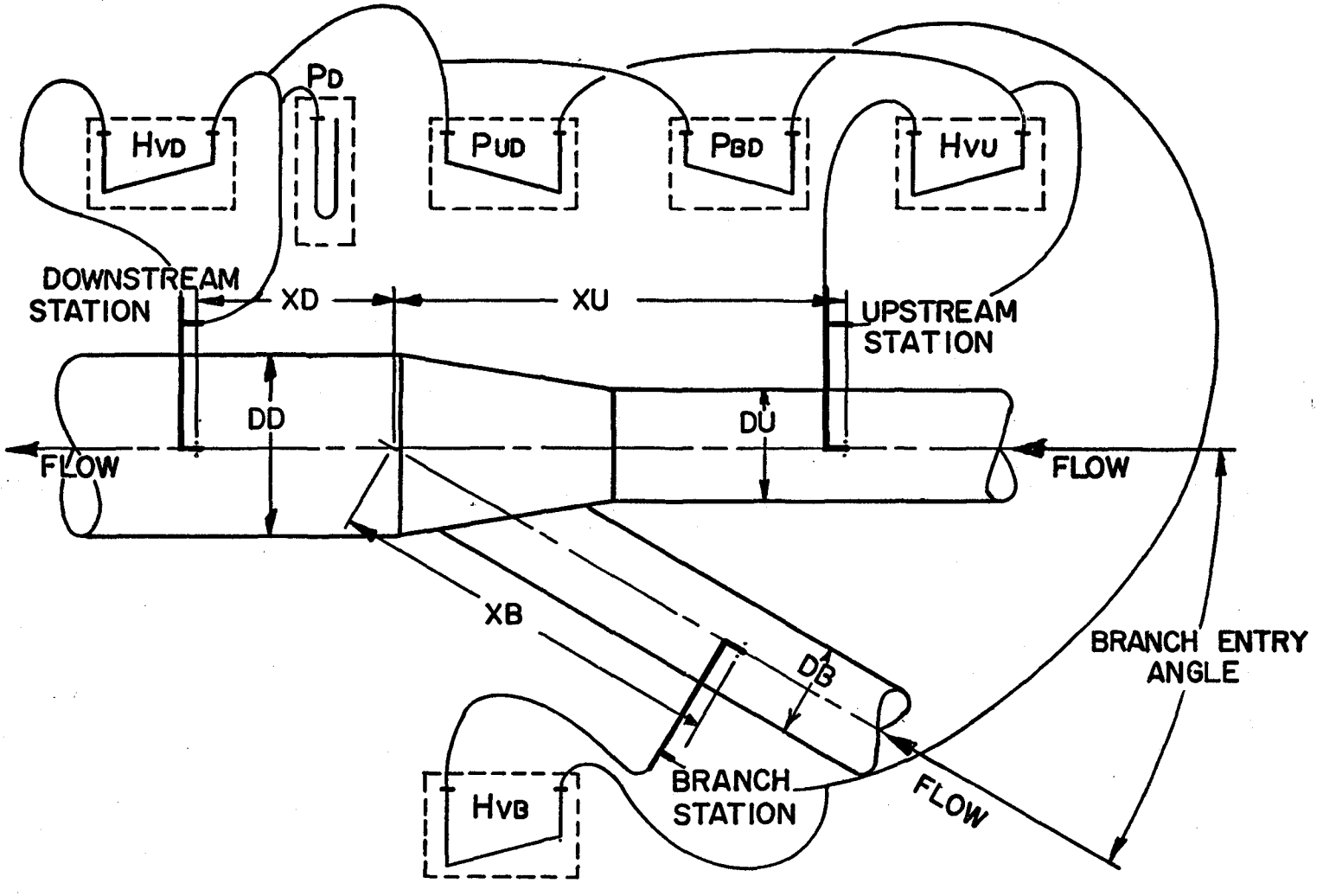

FIGURE 3-3 SCHEMATIC DIAGRAM OF TEST SECTION

against misread manometers required two people to simultaneously collect the same data and compare results after each data point. Approximately thirty data points were taken per fitting to cover the branch and main upstream velocities and velocity ratios previously set forth.

Distances between the static pressure holes in the test probes and the center of the fitting were measured. The friction pressure drop between the pitot-static tube and fitting could then be determined by the equations presented in Appendix C and subtracted from the measured pressure drop to standardize loss coefficient information on a no length basis.

A complete list of raw data collected is tabulated in Appendix D of Reference 19. This data was reduced by an IBM 370/165 computer using the equations in Section 3.2 and reduced results are also listed in Appendix D of Reference 19.

3.6 Discussion of Data

Results for the thirty-three different fittings studied are in graphical form and presented in Appendix A. Two plots are given for each fitting, one for the branch loss coefficient defined in equation 2.1 and the other for the main loss coefficient defined in equation 2.2. Both loss coefficients are plotted against the ratio of branch volume flow to the upstream volume flow.

An important consideration in experimental work is to know the reliability of the results. Error in the results is the sum of fixed error and random error. Fixed error occurs from a miscalibration of a measuring instrument. Random error is the noise or fluctuation of a reading.

Attempts to eliminate fixed error were made by checking manometer calibrations against a precision micromanometer and taking the utmost care in referencing zero pressure readings. Random error was reduced by requiring two persons to read each pressure reading and estimate an average pressure where fluctuations occurred. This also eliminated bias in data which sometimes results from only one person collecting data.

The major precaution to assure that the curve drawn through the data points represented the true curve was simply to run enough data points per fitting that the general trends were undoubtedly defined. Prediction of the maximum random error was made by the uncertainty analysis (see Ref. 6) in Appendix E. Although this error varied for different flow conditions, it normally stayed around ± 7 percent for the branch loss coefficient and ± 10 percent for the main loss coefficient at the higher volume flow ratios. The scatter band was roughly ± 3 percent for the branch loss coefficient and ± 4 percent for the main loss coefficient at the higher volume flow ratios.

Data reproducibility was checked by conducting tests on two fittings which had previously been studied. The first fitting was a fitting investigated by Sepsy-Lauvray (see Ref. 18) and the second fitting was an arbitrarily chosen fitting previously studied in this investigation. Agreement between Sepsy-Lauvray's branch and main loss coefficient values and the values of the reproducibility check were within 4 percent. The test performed on the fitting which had previously been studied in this investigation gave branch loss coefficient values within the originally observed ± 3 percent scatter band and main loss coefficient values within the ± 4 percent scatter band seen in the original test for this fitting. At this point, the experimental loss coefficient results were felt completely reliable within the precision needed for duct work design.

CHAPTER IV

ANALYTICAL PROGRAM

4.1 Introduction

As mentioned in Chapter II, the analytical approach taken in this investigation was to empirically fit theoretical equations to correspond with the experimental data. The correction factors which were added to the theoretical values of the branch and main loss coefficients were placed in terms of Q_b/Q_u, A_b/A_d, A_u/A_d, and branch angle. It was also observed that correction factors were dependent on the downstream diameter for fittings with branch angles of ninety degrees.

A general system boundary energy and mass balance was first applied to a fitting. Although it was found that this energy balance approach did not yield useful equations for calculating the branch and main loss coefficients, the analysis did produce results which revealed an interesting phenomenon within fittings depending on the downstream diameter and branch angle. The theoretical energy-mass balance analysis and the results of this analysis are presented in this chapter.

The principle of conservation of mass and momentum was then applied at the system boundaries. This momentum

expression was manipulated into two dimensionless forms to describe the branch and main loss coefficients. Certain minor terms in these theoretical loss coefficient equations were dropped so that all terms could be arranged as factors of Q_b/Q_u, A_b/A_d, A_u/A_d, and/or branch angle. The remaining terms in the theoretical branch and main loss coefficient equations gave numerical values in the range of the experimental data. Empirical correction factors were then determined for particular fitting geometries. An in-depth discussion of the analytical investigation is given in this chapter.

4.2 Conservation of Mass and Energy

The assumptions used in the energy-mass balance analysis were: (1) no change in potential energy; (2) no heat transfer; (3) steady flow; (4) no mechanical work done on the system; (5) incompressible gas; (6) perfect gas; and (7) constant specific heats. The energy balance reduced to an expression stating that the flux of internal and kinetic energy plus the flow work at the branch and upstream sections equals the flux of internal and kinetic energy plus flow work at the downstream section. The mathematical expression for the energy balance was

$$m_b\left(u_b + \frac{V_b^2}{2} + \frac{P_b}{\rho}\right) + m_u\left(u_u + \frac{V_u^2}{2} + \frac{P_u}{\rho}\right) = m_d\left(u_d + \frac{V_d^2}{2} + \frac{P_d}{\rho}\right) \qquad 4.1$$

Using the definition of enthalpy ($h \triangleq u + \frac{P}{\rho}$) and conservation of mass ($m_b + m_u = m_d$), the energy-mass balance relation took the form

$$m_b(h_b - h_d) + m_b\left(\frac{V_b^2 - V_d^2}{2}\right) + m_u(h_u - h_d) + m_u\left(\frac{V_u^2 - V_d^2}{2}\right) = 0 \qquad 4.2$$

For a perfect gas,

$$h_u - h_d = C_p(T_u - T_d)$$

$$h_b - h_d = C_p(T_b - T_d)$$

$$T_b = \frac{P_b}{\rho R}$$

$$T_u = \frac{P_u}{\rho R}$$

$$T_d = \frac{P_d}{\rho R}$$

$$R = C_p - C_v$$

$$\gamma = \frac{C_p}{C_v} = 1.4$$

These relations were substituted into equation 4.2 and the new expression was written as equation 4.3

$$\frac{m_b}{\rho}\frac{\gamma}{\gamma-1}(P_b - P_d) + m_b\left(\frac{V_b^2 - V_d^2}{2}\right) + \frac{m_u}{\rho}\frac{\gamma}{\gamma-1}(P_u - P_d) + m_u\left(\frac{V_u^2 - V_d^2}{2}\right) = 0 \qquad 4.3$$

Substituting the expressions

$$m_b = \rho A_b V_b$$

$$m_u = \rho A_u V_u$$

$$Q_b = A_b V_b$$

$$Q_u = A_u V_u$$

$$Q_d = A_d V_d$$

and $$H_{vd} = \frac{\rho V_d^2}{2}$$

into equation 4.3 and making the proper manipulations, a dimensionless energy-mass balance expression was formed and given by equation 4.4.

$$\frac{\gamma}{\gamma-1}\left(\frac{P_u-P_d}{H_{vd}}\right)+\left(\left(\frac{A_d}{A_u}\frac{Q_u}{Q_d}\right)^2-1.0\right)+\frac{Q_b}{Q_u}\left(\frac{\gamma}{\gamma-1}\right)\left(\frac{P_b-P_d}{H_{vd}}\right)+\frac{Q_b}{Q_u}\left(\left(\frac{A_d}{A_b}\frac{Q_b}{Q_d}\right)^2-1.0\right)=0 \qquad 4.4$$

Breaking the definition of branch and main loss coefficient into velocity heads, static pressures, volume flow ratios, and area ratios gave

$$CB = \frac{H_{vb}-H_{vd}}{H_{vd}}+\frac{P_b-P_d}{H_{vd}} = \left(\frac{A_d}{A_b}\frac{Q_b}{Q_d}\right)^2+\frac{P_b-P_d}{H_{vd}}-1.0 \qquad 4.5$$

$$CM = \frac{H_{vu}-H_{vd}}{H_{vd}}+\frac{P_u-P_d}{H_{vd}} = \left(\frac{A_d}{A_u}\frac{Q_u}{Q_d}\right)^2+\frac{P_u-P_d}{H_{vd}}-1.0 \qquad 4.6$$

Observing equations 4.4, 4.5, and 4.6, it was seen that the equations could be combined and the $\frac{P_b-P_d}{H_{vd}}$ and $\frac{P_u-P_d}{H_{vd}}$ terms could be eliminated. From continuity, equations

$Q_b/Q_d = \frac{Q_b/Q_u}{(1.0+Q_b/Q_u)}$ and $Q_u/Q_d = \frac{1.0}{(1.0+Q_b/Q_u)}$ allowed equation 4.4 to be rearranged and CB expressed in terms of CM,

Q_b/Q_u, A_b/A_d, A_u/A_d and γ. The equation for CB was

$$CB = \frac{\gamma-1}{\gamma}\frac{1.0+Q_b/Q_u}{Q_b/Q_u}-\frac{1.0+CM}{Q_b/Q_u}+\frac{(A_d/A_u)^2+(A_d/A_b)^2\ (Q_b/Q_u)^3}{\gamma(Q_b/Q_u)(1.0+Q_b/Q_u)^2}-1.0 \qquad 4.7$$

The significance of having CB as a function of CM, Q_b/Q_u, A_b/A_d, A_u/A_d, and γ was that by empirically determining CM, a theoretical value of CB could be calculated. It was originally felt that the theoretical value of CB should be reliable because the energy-mass balance relation (equation 4.1) was based on a conservative set of assumptions.

Accuracy of the theoretical equation for CB was studied by substituting experimental values of CM, Q_b/Q_u, A_b/A_d, and A_u/A_d into equation 4.7 and comparing the theoretical and experimental values of CB. Although the assumptions used in the energy-mass balance were felt conservative enough to yield accurate values of CB, the actual case implied that the mathematical model in this theoretical investigation was not reliable. Definite trends of inaccuracy were attributed to the branch angle and the downstream diameter for branch angles equal to ninety degrees. Deviations between experimental and theoretical values of CB were relatively small for fittings with thirty degree branch angles. Deviations were definitely greater for fittings with forty-five degree branch angles than for

those with thirty degree branch angles. A substantial loss in accuracy was observed for fittings with ninety degree branch angles. Also, inaccuracy was distinctly greater for ninety degree fittings with downstream diameters less than ten inches than for ninety degree fittings with downstream diameters of ten inches or greater.

The most reasonable explanation for the decrease in accuracy with an increase in branch angle was that turbulence within the fitting was increased with increasing branch angle. The turbulence converted the kinetic energy of the flowing fluid into thermal energy by viscous dissipation of flow eddies. This phenomenon was felt to have caused a heat transfer from the fitting to the ambient which was equal to the order of magnitude of the drop in enthalpy plus kinetic energy flux between inlet and exit conditions. The significant decrease in accuracy for ninety degree fittings with downstream diameters less than ten inches was attributed to an effect produced by a lip formed in the fabrication of the branch tap to main fitting body connection (a detailed description of this lip is given in Section 5.2 under Effect of the Branch Tap Entrance). It was felt this connection had a more significant effect on turbulence for fittings with downstream diameters less than ten inches because the lip required in the fabrication

of the branch tap to main fitting body connection was closer to the size of the downstream flow area than the lip in fittings with ten inch or greater downstream diameters. The proposed reasons for inaccuracy of the energy-mass balance equation could not be proven with the test facility used in this investigation, but the phenomenon was further confirmed by the trends of the theoretical equations derived on a conservation of mass and momentum basis.

4.3 Conservation of Mass and Momentum

A system boundary was described around a fitting which cut through the branch, upstream, and downstream sections perpendicular to the flow. For this steady flow analysis, the sum of the forces and momentum flux in the main stream direction were equated to zero. Force contributions in the general case were attributed to the pressure forces, wall friction, and pressure gradients within the branch tap. The wall friction was not included because the loss coefficients were to be standardized on a no-length basis. Pressure gradient effects in the branch tap were dropped because the resultant force from such a gradient in the mainstream direction appeared to be small. Momentum fluxes were described by the mass flow rate times the velocity component

in the mainstream direction at a cross-section. The general momentum balance equation was

$$P_u A_u + P_b A_b \cos\theta + m_u V_u + m_b V_b \cos\theta = P_d A_d + m_d V_d \qquad 4.8$$

Dividing equation 4.8 by $V_d^2 A_d$ and substituting $m=\rho VA$ for the branch, upstream, and downstream mass flow rates gave

$$\frac{P_d}{V_d^2}+\rho=\frac{P_u}{V_d^2}\frac{A_u}{A_d}+\frac{P_b}{V_d^2}\frac{A_b}{A_d}\cos\theta + \rho\frac{A_u}{A_d}\frac{V_u^2}{V_d^2} +\rho\frac{A_b}{A_d}\left(\frac{V_b}{V_d}\right)^2\cos\theta \qquad 4.9$$

Substituting the downstream velocity head expression in for the downstream velocity ($V_d^2 = 2H_{vd}/\rho$), knowing $Q = VA$, and multiplying equation 4.9 by $2/\rho$ gave

$$\frac{P_u}{H_{vd}}\frac{A_u}{A_d} + \frac{P_d}{H_{vd}}\frac{A_b}{A_d}\cos\theta+2\frac{A_d}{A_u}\left(\frac{Q_u}{Q_d}\right)^2+2\frac{A_d}{A_b}\left(\frac{Q_b}{Q_d}\right)^2\cos\theta- \frac{P_d}{H_{vd}} - 2 = 0 \qquad 4.10$$

Making several manipulations on equation 4.10 and combining with equations 4.5 and 4.6 gave theoretical expressions for the branch and main loss coefficients (equations 4.11 and 4.12 respectively).

$$CB=1.0+\left(\frac{Q_b}{Q_d}\frac{A_d}{A_b}\right)^2-2\frac{A_d}{A_u}\left(\frac{Q_u}{Q_d}\right)^2-2\frac{A_d}{A_b}\left(\frac{Q_b}{Q_d}\right)^2\cos\theta-\frac{P_b}{H_{vd}}\left(\frac{A_b}{A_d}\cos\theta-1.0\right)-\frac{P_u}{H_{vd}}\frac{A_u}{A_d} \qquad 4.11$$

$$CM=1.0+\left(\frac{Qu}{Qd}\frac{Ad}{Au}\right)^2-2\frac{Ad}{Au}\left(\frac{Qu}{Qd}\right)^2-2\frac{Ad}{Ab}\left(\frac{Qb}{Qd}\right)^2\cos\theta-\frac{Pu}{Hvd}\left(\frac{Au}{Ad}-1.0\right)-\frac{Pb}{Hvd}\frac{Ab}{Ad}\cos\theta \qquad 4.12$$

In duct design work, pressure data is useful only in a pressure drop or pressure increase form. Since branch and upstream static pressure terms appeared in equations 4.11 and 4.12, CB and CM could not be expressed solely in terms of Q_b/Q_u, A_b/A_d, A_u/A_d, and branch angle unless these pressure terms were related by general empirical expressions or the pressure terms were dropped from the equations. The experimental data was used to attempt to correlate the terms containing P_b and P_u, but no apparent correlations were observed.

It was felt the last two terms of equations 4.11 and 4.12 should be dropped so that CB and CM would be in terms of only useful parameters. These simplified theoretical equations were designated by CB_t and CM_t and were given by equations 4.13 and 4.14 respectively.

$$CB_t = 1.0 + \left(\frac{Ad}{Ab}\frac{Qb}{Qd}\right)^2 - 2\frac{Ad}{Au}\left(\frac{Qu}{Qd}\right)^2 - 2\frac{Ad}{Ab}\left(\frac{Qb}{Qd}\right)^2\cos\theta \qquad 4.13$$

$$CM_t = 1.0 + \left(\frac{Ad}{Au}\frac{Qu}{Qd}\right)^2 - 2\frac{Ad}{Au}\left(\frac{Qu}{Qd}\right)^2 - 2\frac{Ad}{Ab}\left(\frac{Qb}{Qd}\right)^2\cos\theta \qquad 4.14$$

Substitution of CB (equation 4.5) and CM (equation 4.6) into equations 4.13 and 4.14 for CB_t and CM_t gave

$$\frac{P_b-P_d}{H_{vd}} - 1.0 = 1.0 - 2\frac{A_d}{A_u}\left(\frac{Q_u}{Q_d}\right)^2 - 2\frac{A_d}{A_b}\left(\frac{Q_b}{Q_d}\right)^2\cos\theta \qquad 4.15$$

$$\frac{P_u-P_d}{H_{vd}} - 1.0 = 1.0 - 2\frac{A_d}{A_u}\left(\frac{Q_u}{Q_d}\right)^2 - 2\frac{A_d}{A_b}\left(\frac{Q_b}{Q_d}\right)^2\cos\theta \qquad 4.16$$

and subtracting equation 4.16 from 4.15 gave

$$\frac{P_b-P_d}{H_{vd}} - \frac{P_u-P_d}{H_{vd}} = 0 \qquad \text{or}$$

$$P_b = P_u$$

Thus, simply dropping the static pressure terms from equations 4.11 and 4.12 implied the static pressure of the branch section equals the static pressure of the upstream section. The experimental data was used to compare values of P_b and P_u for different fittings and different flow conditions. For each of the fittings in the experimental investigation, deviations between P_b and P_u were small only for branch to upstream velocity ratios near one, and at branch velocities around 1000 feet per minute. Since the velocity ratios reached six and the branch velocities reached 6000 feet per minute, the condition $P_b = P_u$ was not satisfied for the general case. Nevertheless, CB_t and CM_t

were used as first approximations to determine the branch and main loss coefficients.

4.4 Correction Terms

4.4.1 Introduction

The branch and main loss coefficient analytical expressions were

$$CB = CB_t + \Delta CB \qquad 4.17$$

$$CM = CM_t + \Delta CM \qquad 4.18$$

where CB_t and CM_t were evaluated theoretically by equations 4.13 and 4.14 respectively, and ΔCB and ΔCM were evaluated by pure empirical expressions depending on the branch angle and downstream diameter for fittings with ninety degree branch angles. Correction factors ΔCB and ΔCM were determined by plotting the difference between the experimental and theoretical values of CB and CM against various combinations of flow ratios and area ratios.

It was observed that the reliability of the empirical correlations for ΔCB and ΔCM were consistent with the trends of accuracy in the theoretical energy-mass balance equation. These trends implied that ΔCB and ΔCM gave better correlations for thirty degree branch angles than for forty-five degree branch angles, and forty-five degree

branch angles gave better correlations than fittings with ninety degree branch angles. Also, fittings with ninety degree branch angles showed better correlation for downstream diameters greater than or equal to ten inches than those with downstream diameters less than ten inches. With the exception of ΔCM for fittings with thirty degree branch angles, correlations were not well defined. General expressions for ΔCB and ΔCM required lengthy trial-and-error attempts at combining parameters to satisfy all cases covered in the experimental investigation. Although the analytical expressions lacked accuracy in some cases, it was felt that these equations could be used in design work to give fairly reliable loss coefficients. The evaluation of ΔCB and ΔCM follows in this chapter and a comparison between analytical work in this investigation and similar works by other authors is found in Chapter V. Comparison between the analytical expressions and experimental results is found in Appendix A.

4.4.2 ΔCM for Thirty Degree Branch Angles

Good correlation was observed between ΔCM and CM_t (equation 4.14) for fittings with thirty degree branch angles. ΔCM appeared to represent a parabola, and using the method of least squares, a second degree curve was fit

to ΔCM versus CM_t. The empirical equation for ΔCM was

$$\Delta CM = 0.0556\ CM_t^2 - 0.0106\ CM_t - 0.116 \qquad 4.19$$

4.4.3 ΔCM for Forty-Five Degree Branch Angles

Fair correlation was observed between ΔCM and CM_t (equation 4.14) for fittings with forty-five degree branch angles. Similar trends of ΔCM appeared for forty-five and thirty degree branch angles, except the ΔCM parabola for forty-five degree branch angles tended to be shifted in the ΔCM direction as a linear function of A_u/A_d. The empirical equation fit to ΔCM versus CM_t and A_u/A_d was

$$\Delta CM = 0.096\ CM_t^2 - 0.41\ A_u/A_d + 0.109 \qquad 4.20$$

4.4.4 ΔCB for Thirty Degree Branch Angles

Although a general correlation of ΔCB for fittings with thirty degree branch angles was not obvious, ΔCB was observed to be a linear function of Q_b/Q_u for fixed A_b/A_d and A_u/A_d. Various combinations and arrangements of Q_b/Q_u, A_b/A_d, and A_u/A_d were tried and the most appropriate form of ΔCB was

$$\Delta CB = \beta_1\ Q_b/Q_u + \beta_0 \qquad 4.21$$

where, $A_r = \frac{A_b/A_d}{A_u/A_d} (A_b/A_d + A_u/A_d)$

$$\beta_1 = \frac{0.0111}{A_r - 0.462} \text{ for } A_r \geq 0.56$$

$$\beta_1 = -2.71\ A_r + 1.635 \text{ for } A_r < 0.56$$

$$\beta_0 = -1.694\ A_u/A_d + 1.172$$

4.4.5 ΔCB for Forty-Five Degree Branch Angles

Correlations of ΔCB for fittings with forty-five degree branch angles gave trends of correlation similar to those of the thirty degree branch angle case. ΔCB was described by the following combination of parameters:

$$\Delta CB = \beta_3 \frac{A_u/A_d}{A_b/A_d} Q_b/Q_u + \beta_2 \qquad 4.22$$

where, $A_{r1} = \frac{A_b}{A_d} (A_b/A_d + A_u/A_d)$

$$\beta_3 = -2.15\ A_{r1} + 0.838 \quad \text{for } A_{r1} \leq 0.36$$

$$\beta_3 = -0.118\ A_{r1} + 0.10 \quad \text{for } A_{r1} > 0.36$$

$$\beta_2 = 0.55 \quad \text{for } A_u/A_d < 0.6$$

$$\beta_2 = -0.03 \quad \text{for } A_u/A_d \geq 0.6.$$

4.4.6 ΔCB for Ninety Degree Branch Angles and Downstream Diameters ≥ Ten Inches

Plots of ΔCB versus V_b/V_u ($V_b/V_u = \frac{A_u/A_d}{A_b/A_d} Q_b/Q_u$) at fixed A_b/A_d and A_u/A_d for ninety degree branch angles showed a grouping of curves for downstream diameters greater than or equal to ten inches. ΔCB for downstream diameters greater than or equal to ten inches was

$$\Delta CB = \frac{6.61}{\frac{A_u/A_d}{A_b/A_d}\frac{Q_b}{Q_u}+2.78} + 0.178\frac{A_u/A_d}{A_b/A_d}\frac{Q_b}{Q_u}\left(\frac{A_b}{A_d}+\frac{A_u}{A_d}-1.0\right) - 0.089\left(\frac{A_b}{A_d}+\frac{A_u}{A_d}\right) - 1.91 \qquad 4.23$$

4.4.7 ΔCB for Ninety Degree Branch Angles and Downstream Diameters < Ten Inches

Plots of ΔCB versus V_b/V_u for ninety degree branch angles and downstream diameters less than ten inches showed considerable deviations between curves of fixed A_b/A_d and A_u/A_d. Curve-fitting procedures similar to those applied to ΔCB for thirty and forty-five degree branch angles were used for this ninety degree case and ΔCB was found to be described by

$$\Delta CB = \beta_5 \frac{A_u/A_d}{A_b/A_d} Q_b/Q_u + \beta_4 \qquad 4.24$$

where, $A_{r1} = A_b/A_d\ (A_b/A_d + A_u/A_d)$

$\beta_5 = -1.483\ A_{r1} + 0.544$ for $A_{r1} < 0.4$

$$\beta_5 = -0.133\ A_{r1} + 0.003 \quad \text{for } A_{r1} \geq 0.4$$

$$\beta_4 = -0.912\ A_u/A_d + 0.845$$

4.4.8 ΔCM for Ninety Degree Branch Angles and Downstream Diameters ≥ Ten Inches

ΔCM was plotted against V_b/V_u for fittings with ninety degree branch angles, and a distinction was observed between curves for downstream diameters greater than or equal to ten inches and curves for downstream diameters less than ten inches for fixed A_b/A_d and A_u/A_d. For the entire range of downstream diameters investigated, ΔCM showed poor correlation against all combinations of parameters tried. Although empirical expressions were obtained for ΔCM, the reliability of these equations was felt questionable. ΔCM for fittings with ninety degree branch angles and downstream diameters greater than or equal to ten inches was related by

$$\Delta CM = 0.554\ \frac{A_u/A_d}{A_b/A_d}\ \frac{Q_b}{Q_u}\left(\frac{A_b}{A_d} + \frac{A_u}{A_d}\right)^2 - 1.508\ \frac{A_u/A_d}{A_b/A_d}\ \frac{Q_b}{Q_u}\left(\frac{A_b}{A_d} + \frac{A_u}{A_d}\right)$$

$$+ 0.971\ \frac{A_u/A_d}{A_b/A_d}\ \frac{Q_b}{Q_u} - 0.15 \qquad 4.25$$

4.4.9 ΔCM for Ninety Degree Branch Angles and Downstream Diameters < Ten Inches

As mentioned in section 4.4.8, ΔCM for ninety degree branch angles gave poor correlation. It was also observed that as the downstream diameter decreased, the trends of ΔCM became less defined. ΔCM for downstream diameters less than ten inches could be represented only by a rough approximation equation. For some combinations of A_b/A_d and A_u/A_d, the equation for ΔCM described curves that tended to diverge from the experimental data at low and high branch to upstream volume flow ratios. It was felt that the curves used in design work would be more reliable if extrapolations were made from analytical curves described over the range of Q_b/Q_u from 0.6 to 2.4 than for establishing the curves over the entire range of Q_b/Q_u by the analytical expressions. Therefore, the generalized main loss coefficient curves in Appendix D for fittings with ninety degree branch angles and downstream diameters less than ten inches were based on analytical equations for Q_b/Q_u from 0.6 to 2.4 and were linear extrapolations for $Q_b/Q_u < 0.6$ and $Q_b/Q_u > 2.4$. This analytical expression for ΔCM was

$$\Delta CM = 0.308 \frac{A_u/A_d}{A_b/A_d} \frac{Q_b}{Q_u}\left(\frac{A_b}{A_d} + \frac{A_u}{A_d}\right)^2 - 0.913 \frac{A_u/A_d}{A_b/A_d} \frac{Q_b}{Q_u}\left(\frac{A_b}{A_d} + \frac{A_u}{A_d}\right)$$

$$+ 0.628 \frac{A_u/A_d}{A_b/A_d} \frac{Q_b}{Q_u} - 0.417 \left(\frac{A_b}{A_d} + \frac{A_u}{A_d}\right) + C \qquad 4.26$$

where, $C = 0.53$ for $(A_b/A_d + A_u/A_d) \geq 1.2$

$C = 0.735$ for $(A_b/A_d + A_u/A_d) < 1.2$

4.4.10 Summary of Analytical Equations

The branch and main loss coefficients were described by equations 4.17 and 4.18. These equations were

$$CB = CB_t + \Delta CB \qquad 4.17$$

$$CM = CM_t + \Delta CM \qquad 4.18$$

where CB_t and CM_t were evaluated by equations 4.13 and 4.14 respectively for all A_b/A_d, A_u/A_d, and all branch angles. Table 4-1 lists the equation numbers pertaining to ΔCB and ΔCM for different branch angles and specifies the reliability restrictions based on comparison between the analytical equations and the experimental data.

TABLE 4-1

EQUATION NUMBERS FOR ΔCB AND ΔCM

θ	ΔCB	ΔCM	Reliability Restrictions
30	4.21	4.19	
45	4.22	4.20	
90	4.23	4.25	ΔCB and ΔCM only for the downstream diameters $\geq$ 10 inches
90	4.24	4.26	ΔCB and ΔCM only for the downstream diameters < 10 inches, ΔCM only for $0.6 \leq Q_b/Q_u \leq 2.4$

CHAPTER V

DISCUSSION OF ANALYTICAL RESULTS

5.1 Introduction

Accuracy of the semi-empirical equations in Chapter IV was observed to be dependent primarily on the branch angle and downstream diameter. The diameter dependence was contributed to manufacturing inconsistencies in the lip formed at the branch tap entrance. It was noted that effects from deviations in the fabrication of this lip became suppressed for ten inch or greater downstream diameters. The effects of a lip at the branch tap entrance were also felt to accent losses for increasing branch angle. Verification and discussion of the branch tap entrance effect and comparison of the analytical equations with other sources of information is presented in this chapter.

5.2 Effect of the Branch Tap Entrance

Standard manufacturing techniques of divided flow fittings cover three basic types of branch tap entrances. Choice of the type of entrance is determined by the size of the fitting body, style of the fitting body, and branch angle. These three branch tap entrance categories are depicted by Figures 5-1, 5-2, and 5-3. Generally, the rolled

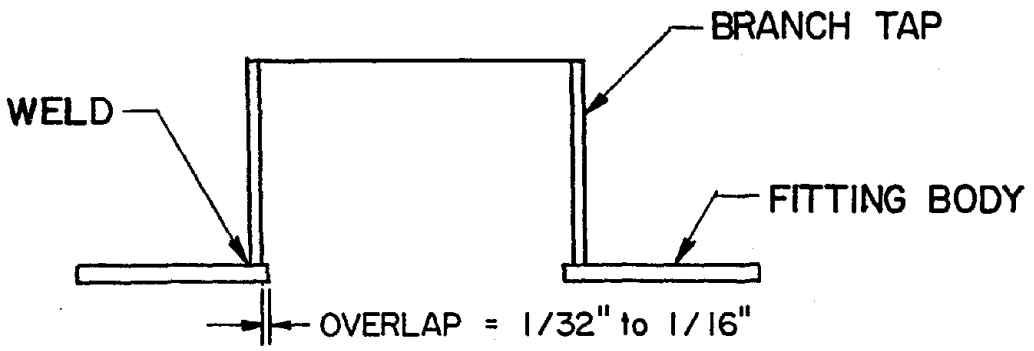

FIGURE 5-1; SHARP EDGE ENTRANCE.

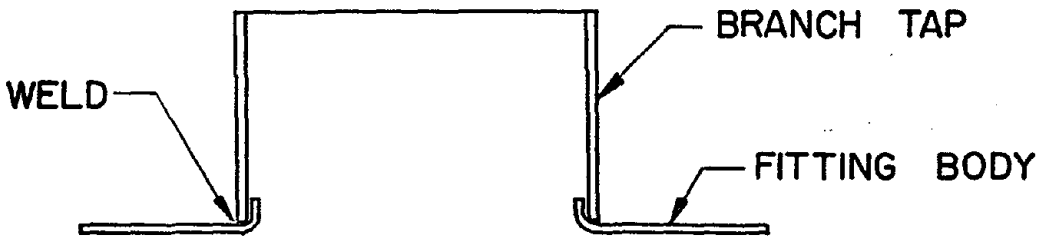

FIGURE 5-2; ROLLED EDGE ENTRANCE.

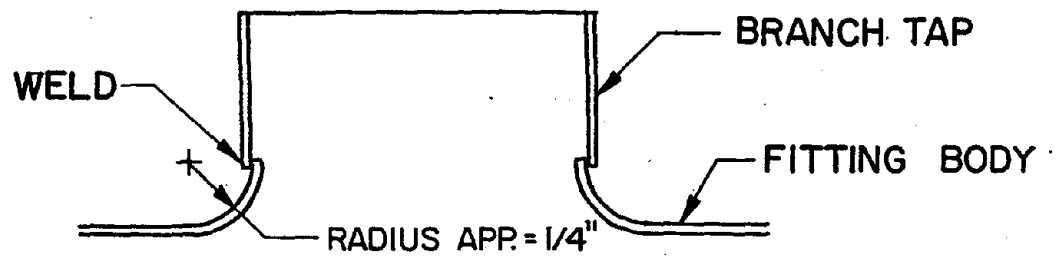

FIGURE 5-3; ROUND EDGE ENTRANCE.

edge entrance (Figure 5-2) was used in the fittings for this investigation, although some of the fittings which had small branch diameters and small tapered fitting bodies did not allow construction of the rolled edge entrance and required use of the sharp edge entrance (Figure 5-1). This rolled edge entrance was formed simply by rolling an overlapping portion of the fitting body into the inner periphery of the branch tap. Also, fittings with constant main stream diameters and ninety degree branch angles employed the round edge entrance (Figure 5-3) which had a large radius compared to the radius of the rolled edge. Even though the type of entrance varied between fittings, it was felt that data should be established for fittings made within the limits of production techniques and not for laboratory controlled fittings.

An experimental investigation was conducted to determine the degree of variation in the branch and main loss coefficients due to the branch tap entrance effect. Two fittings were chosen which originally had sharp edge entrances. One fitting had a three inch diameter branch, three inch diameter upstream, four inch diameter downstream, and a forty-five degree branch angle; and the other fitting had a three inch diameter branch, four inch diameter upstream, six inch diameter downstream, and a ninety degree

branch angle. Standard loss coefficient tests were first performed on each fitting. The branch tap entrance on both fittings were then machined to form an approximate three-sixteenths inch radius edge. Standard tests were again performed on both fittings and the branch and main loss coefficient plots for the sharp edge and round edge cases were compared. Figures 5-4, 5-5, 5-6, and 5-7 are loss coefficient comparison graphs which show data points for the sharp edge and round edge entrances and the curve of the analytical equation for each of the fittings. Deviations in the loss coefficients between the sharp edge and round edge cases ranged between twenty and thirty percent. Although the two fittings used in the experiment typically did not have round edge entrances, the investigation did show the significance of variation in the branch tap entrance on the branch and main loss coefficients.

5.3 Comparison of Analytical Equations with Experimental Data

Figures A-1 through A-66 in Appendix A compare the experimental data with the semi-empirical branch and main loss coefficient equations. Each dashed curve represents the analytically determined branch or main loss coefficient and the solid line represents the curve drawn through the experimental data points. The semi-empirical loss

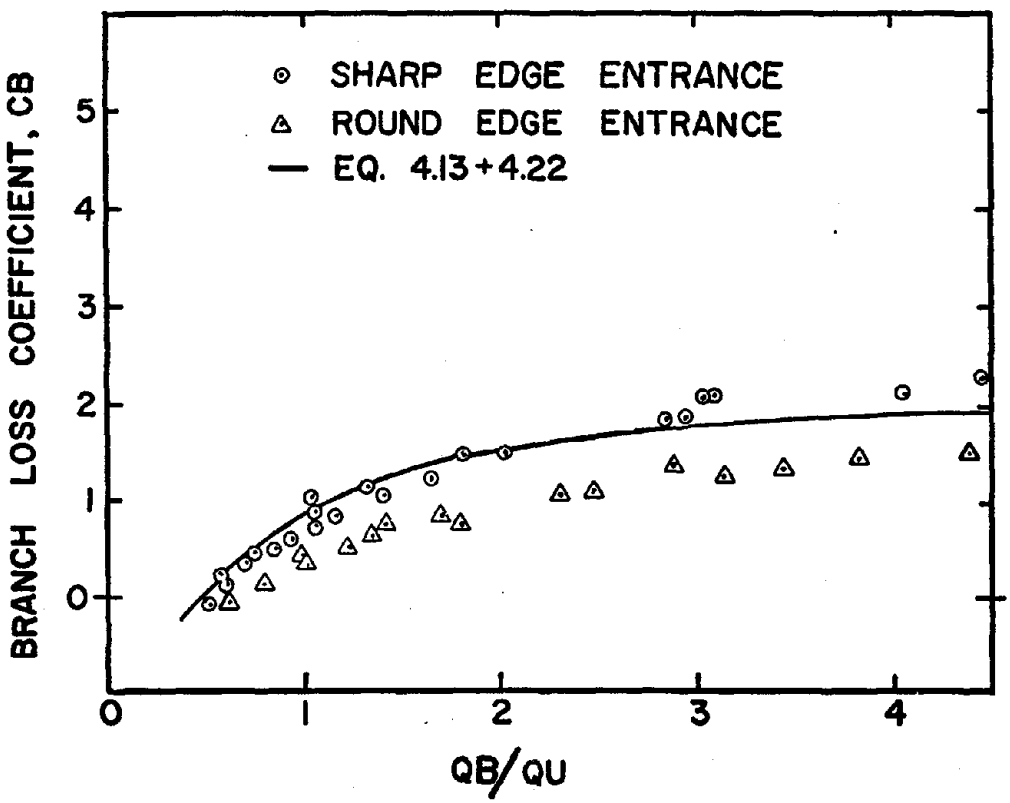

FIGURE 5-4; BRANCH ANGLE=45°, DB=3", DU=3", DD=4"; EFFECT OF THE BRANCH TAP ENTRANCE.

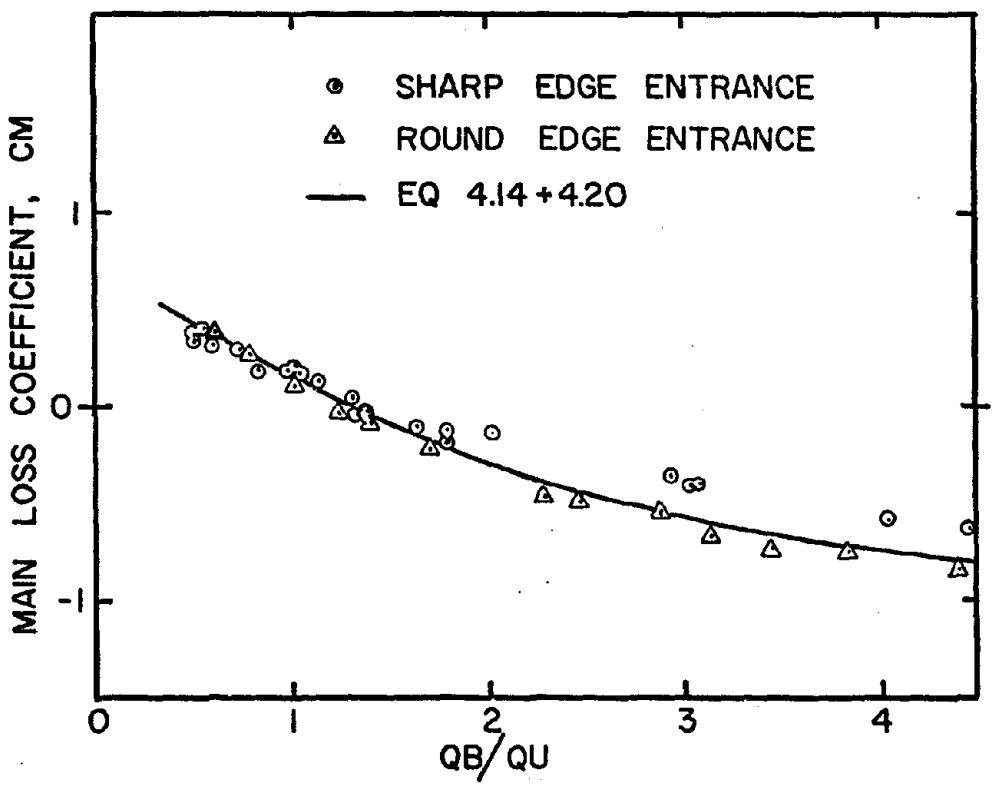

FIGURE 5-5; BRANCH ANGLE=45°, DB=3", DU=3", DD=4"; EFFECT OF THE BRANCH TAP ENTRANCE.

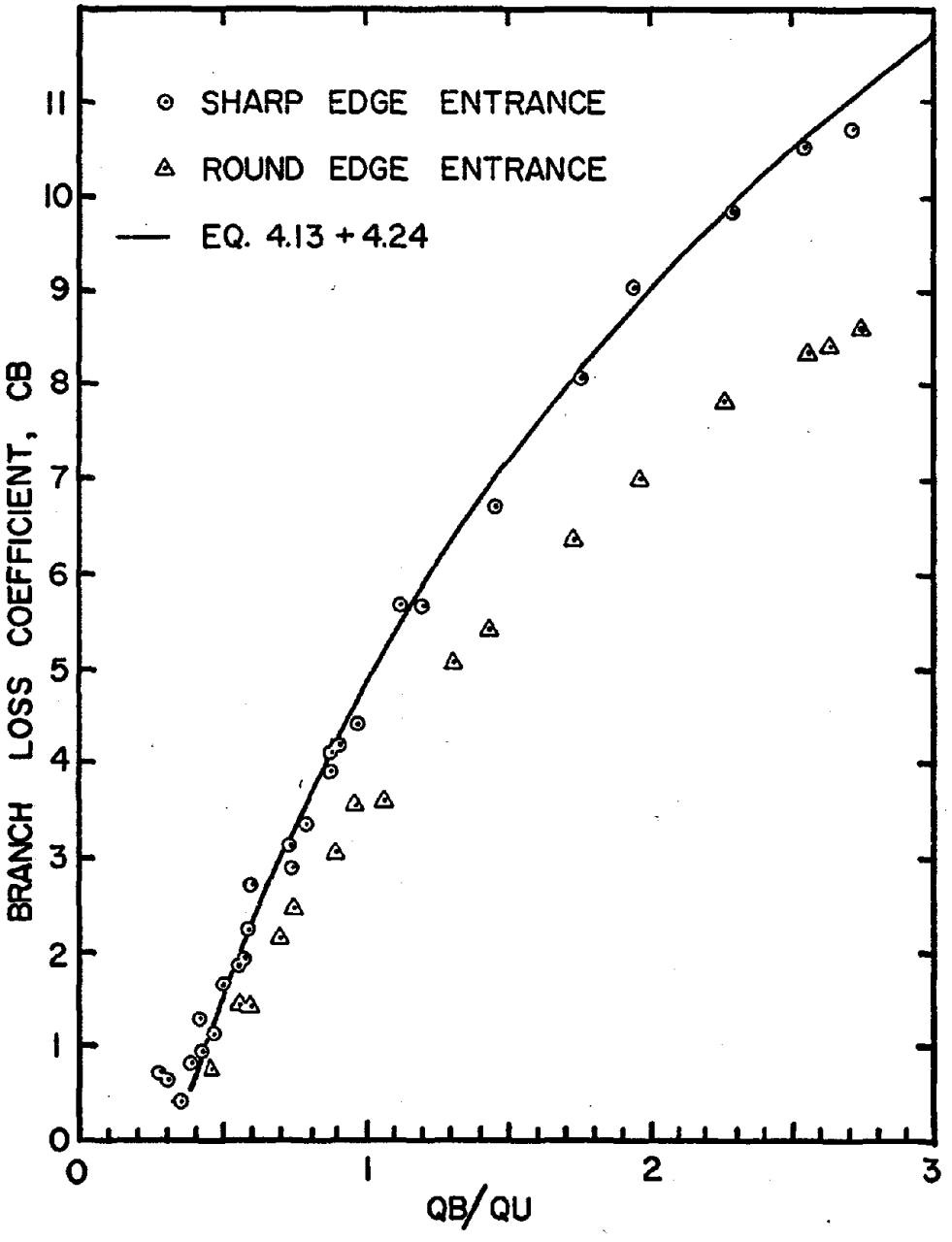

FIGURE 5-6; BRANCH ANGLE = 90°, DB=3", DU=4", DD=6"; EFFECT OF THE BRANCH TAP ENTRANCE.

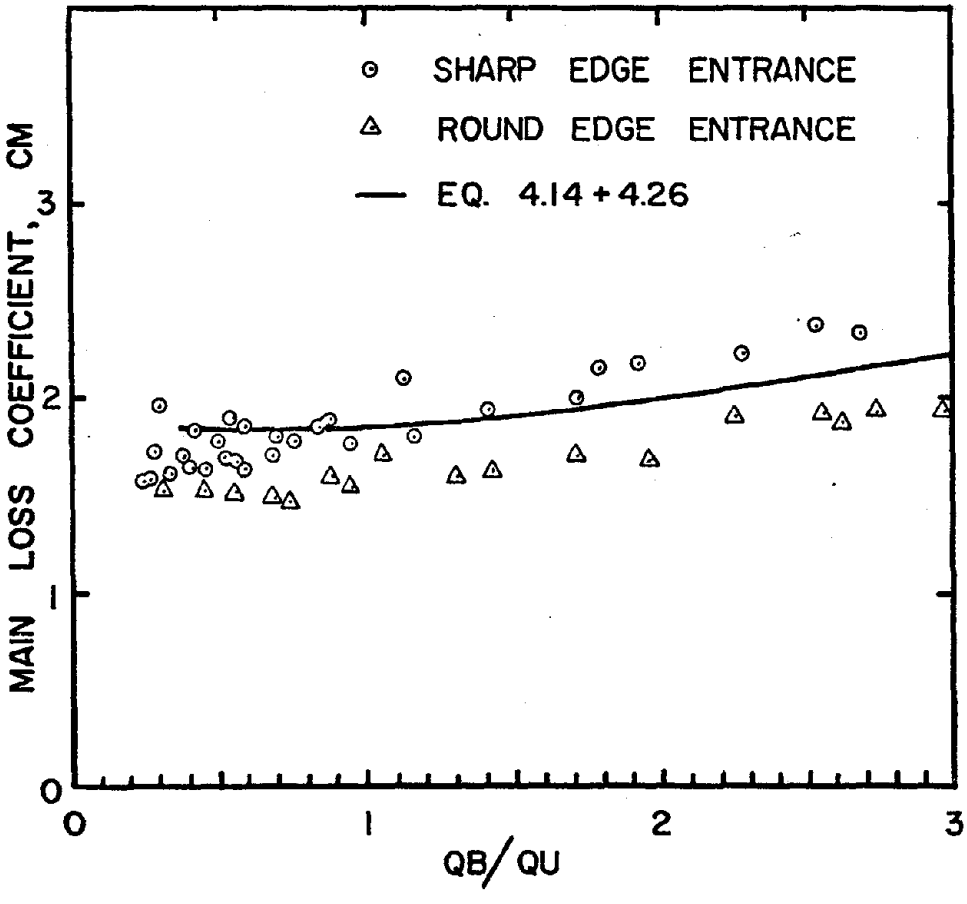

FIGURE 5-7; BRANCH ANGLE = 90°, DB=3", DU=4", DD=6"; EFFECT OF THE BRANCH TAP ENTRANCE.

coefficient values were calculated by equations 4.17 and 4.18 where the correction factor equation numbers are listed in Table 4-1 corresponding to particular fitting geometries.

With the exception of main loss coefficients for fittings with ninety degree branch angles, the analytical equations showed close agreement with the experimental data. As mentioned in sections 4.4.8 and 4.4.9, correction factors could not be correlated accurately for main loss coefficients when the branch angle was ninety degrees.

A recent experimental investigation by Sepsy-Lauvray (Ref. 18) included several converging flow fittings of the type applicable to the analytical equations. Their data for four fittings is compared with the analytical equations in Figures 5-8 through 5-15. Figures 5-8 and 5-9 show loss coefficient data from Sepsy-Lauvray's work, Springman's work (Ref. 21), the experimental portion of this investigation, and the semi-empirical equations for $A_b/A_d = 0.562$, $A_u/A_d = 1.00$, and branch angle = 45 degrees. The fittings studied by Sepsy-Lauvray and Springman in Figures 5-8 and 5-9 had six inch branch diameters, eight inch upstream and downstream diameters, and forty-five degree branch angles. It was noted that only the branch loss coefficient could be extracted from Springman's data. The experimental data in Figures 5-8 and 5-9 for this investigation was collected

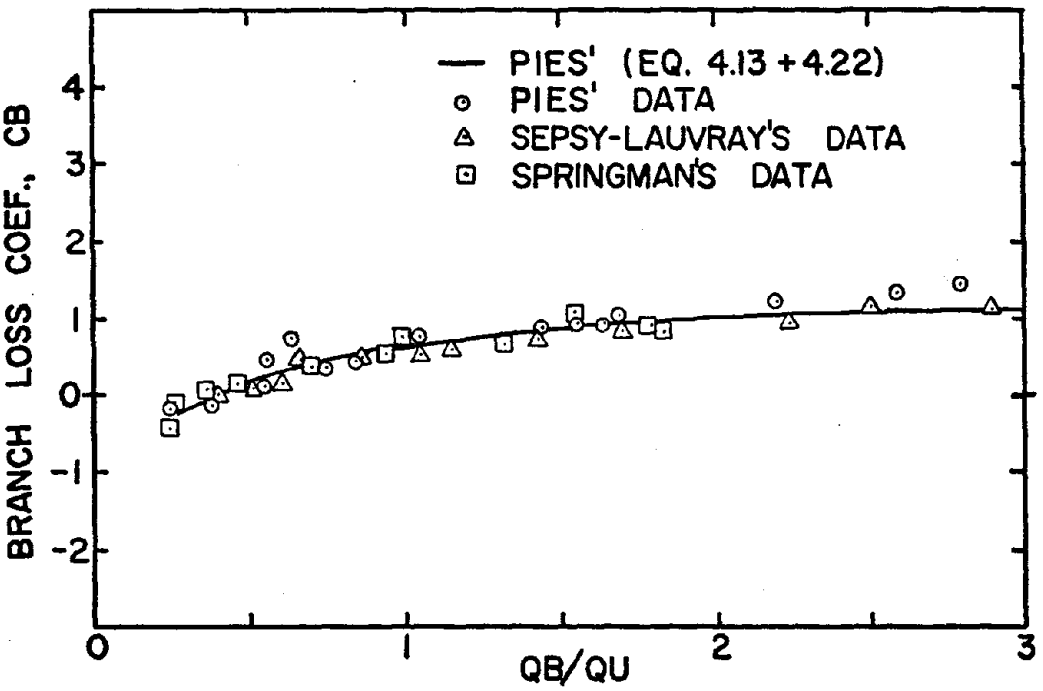

FIGURE 5-8; BRANCH ANGLE=45°, AB/AD=0.562; AU/AD=1.00, COMPARISON OF PIES', SPRINGMAN'S, AND SEPSY-LAUVRAY'S DATA.

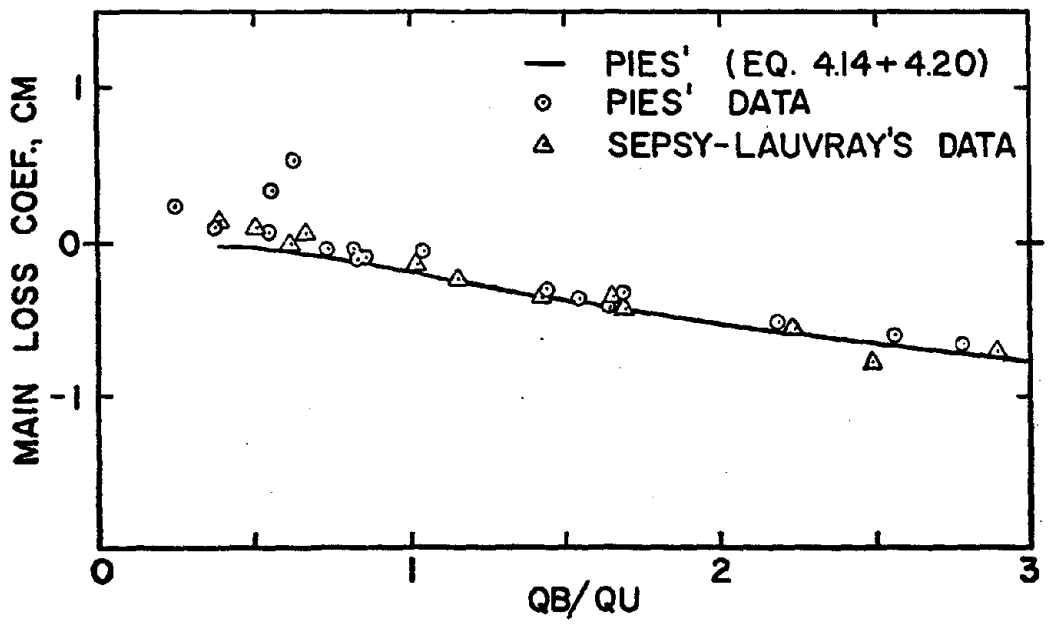

FIGURE 5-9; BRANCH ANGLE=45°, AB/AD=0.562, AU/AD=1.00, COMPARISON OF PIES' AND SEPSY-LAUVRAY'S DATA.

from a fitting with a four inch branch diameter, six inch upstream and downstream diameter, and a forty-five degree branch angle. Good agreement was observed between the analytical curves and experimental data in Figures 5-8 and 5-9.

Comparisons were made in Figures 5-10 through 5-15 between analytical loss coefficient values and Sepsy-Lauvray's data for three fittings which had four inch branch diameters, six inch upstream diameters, and eight inch downstream diameters. The branch angles for these three fittings investigated by Sepsy-Lauvray were thirty, forty-five, and ninety degrees. Excellent agreement was observed between data and analytical values for the thirty degree branch angle fitting (Figures 5-10 and 5-11), although deviations increased for the forty-five and ninety degree fittings (Figures 5-12, 5-13, 5-14, and 5-15).

Sepsy-Lauvray also investigated fittings with branch angles of fifteen and sixty degrees. Analytical branch and main loss coefficients (equations 4.17 and 4.18) were evaluated for branch angle equal fifteen degrees and correction factors from equations 4.21 and 4.19. These values were compared with Sepsy-Lauvray's data for the fifteen degree branch angle fitting, but agreement was not felt close enough to deduce that the analytical expressions were valid for fifteen degree branch angles. The same check was made

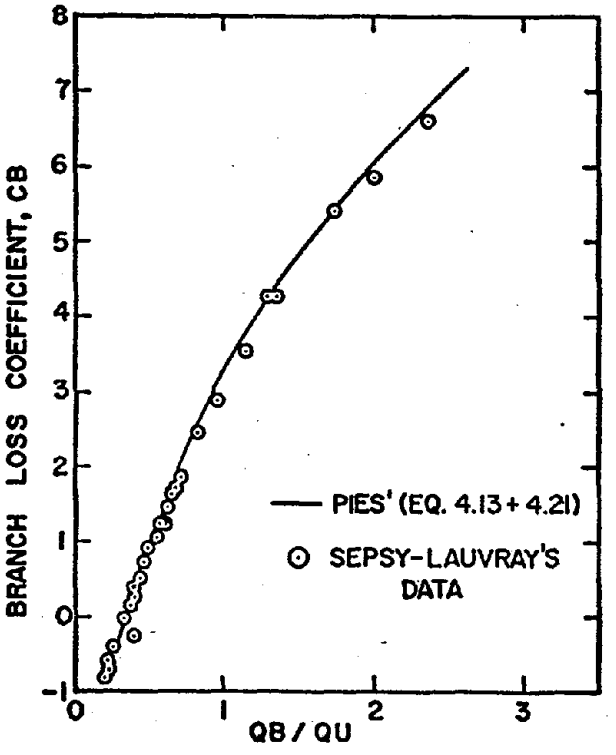

FIGURE 5-10; BRANCH ANGLE = 30°, AB / AD = 0.25, AU / AD = 0.562; COMPARISON OF ANALYTICAL EQUATION WITH SEPSY-LAUVRAY'S DATA.

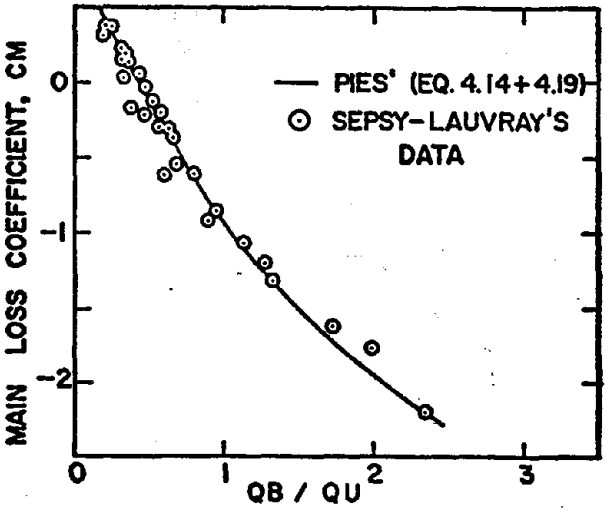

FIGURE 5-11; BRANCH ANGLE = 30°, AB / AD = 0.25, AU / AD = 0.562; COMPARISON OF ANALYTICAL EQUATION WITH SEPSY-LAUVRAY'S DATA.

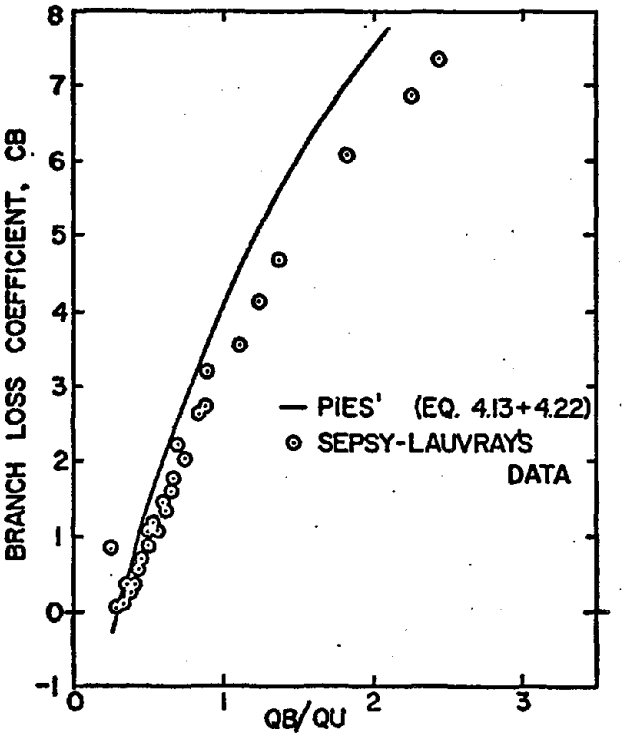

FIGURE 5-12; BRANCH ANGLE = 45°, AB/AD=0.25, AU/AD=0.562; COMPARISON OF ANALYTICAL EQUATION WITH SEPSY-LAUVRAY'S DATA.

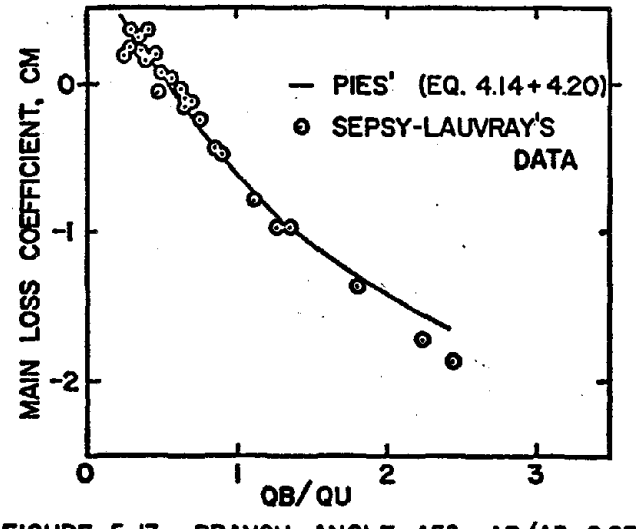

FIGURE 5-13; BRANCH ANGLE=45°, AB/AD=0.25, AU/AD=0.562; COMPARISON OF ANALYTICAL EQUATIONS WITH SEPSY-LAUVRAY'S DATA.

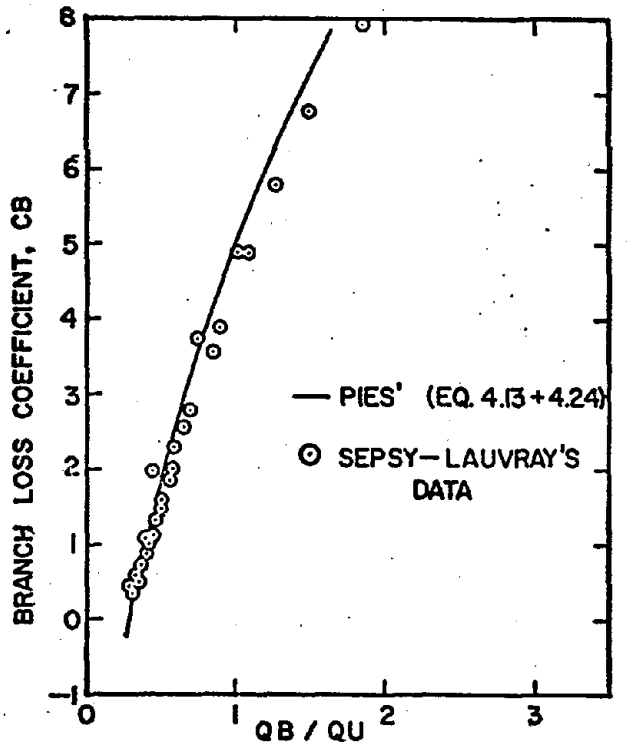

FIGURE 5-14; BRANCH ANGLE=90°, AB/AD=0.25, AU/AD=0.562; COMPARISON OF ANALYTICAL EQUATION WITH SEPSY-LAUVRAY'S DATA.

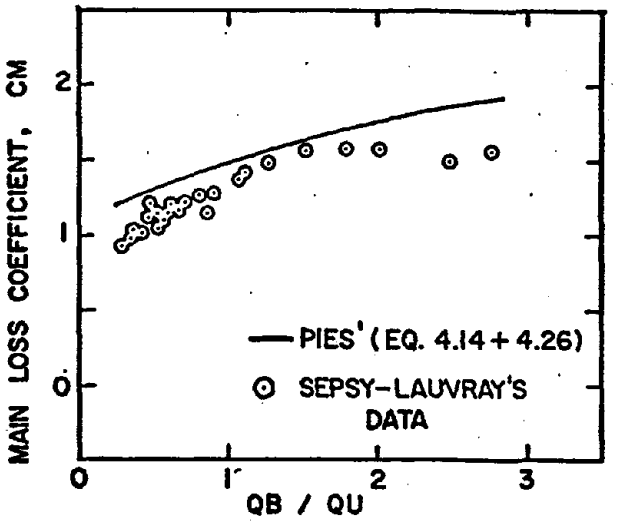

FIGURE 5-15; BRANCH ANGLE=90°, AB/AD=0.25, AU/AD=0.562; COMPARISON OF ANALYTICAL EQUATION WITH SEPSY—LAUVRAY'S DATA.

between the analytical equations (using correction factors from equations 4.22 and 4.20) and Sepsy-Lauvray's data for the sixty degree branch angle fitting. Significant deviations were also observed for this sixty degree branch angle case. It was felt the analytical expressions should not be used for branch angles other than thirty, forty-five, or ninety degrees.

Pioneering work in pressure losses for converging flow fittings was conducted by Petermann (Ref. 14) and Vogel (Ref. 23) at the University of Münich in Germany. Both investigations used small diameter flanged fittings and water flow. Analytical curves are compared with data in Figures 5-16 and 5-17 for Petermann's data and in Figures 5-18 and 5-19 for Vogel's data. The solid curves in Figures 5-18 and 5-19 are for downstream diameters greater than or equal to ten inches and the dashed curves are for downstream diameters less than ten inches. Although Petermann's and Vogel's data did not agree with the analytical values, the general trends between the curves were consistent.

5.4 Comparison with Analytical Work from Other Sources

Three previous analytical studies were conducted to determine branch and main loss coefficients for converging flow fittings. Behls-Brown (Ref. 4) made a purely empirical analysis of fittings with constant mainstream diameters and

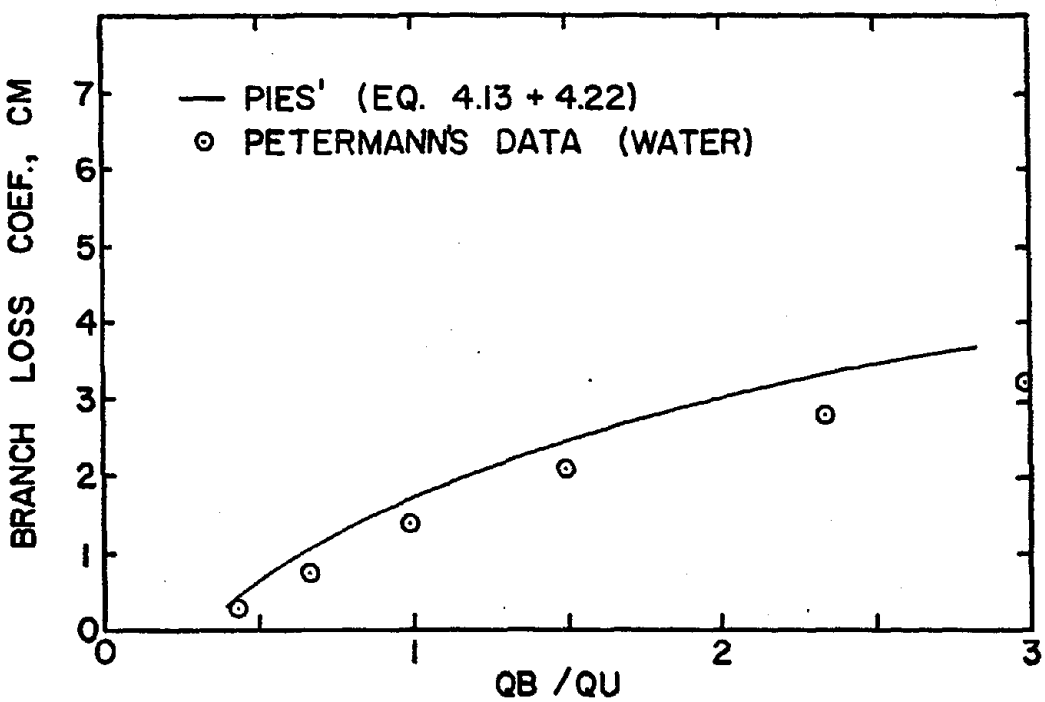

FIGURE 5-16; BRANCH ANGLE = 45°, AB /AD = 0.338, AU/AD = 1.00; COMPARISON WITH PETERMANN'S DATA.

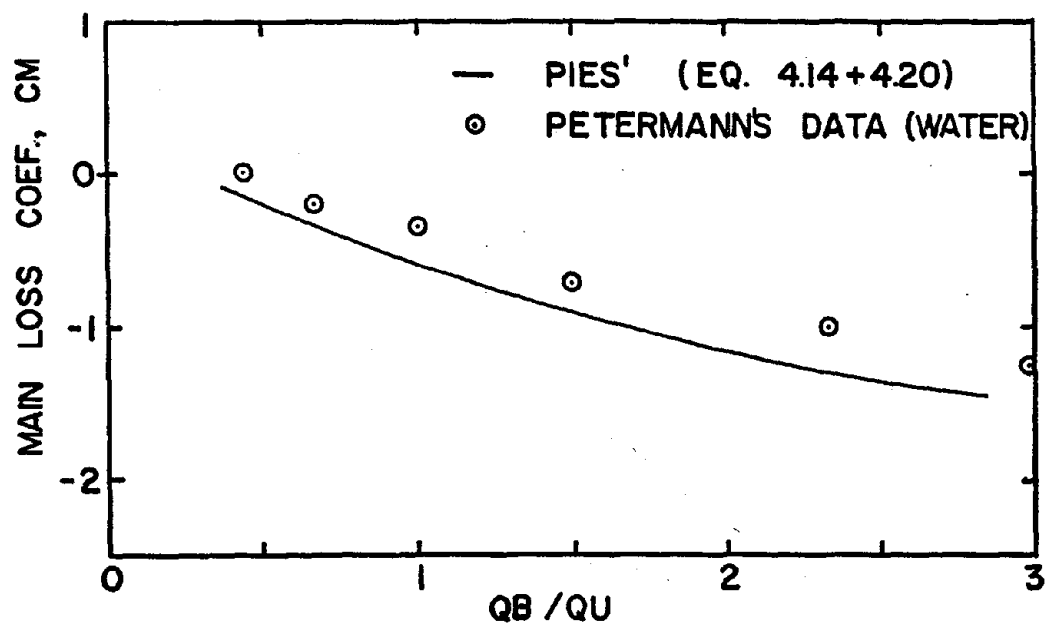

FIGURE 5-17; BRANCH ANGLE = 45°, AB/AD=0.338, AU/AD=1.00; COMPARISON WITH PETERMANN'S DATA.

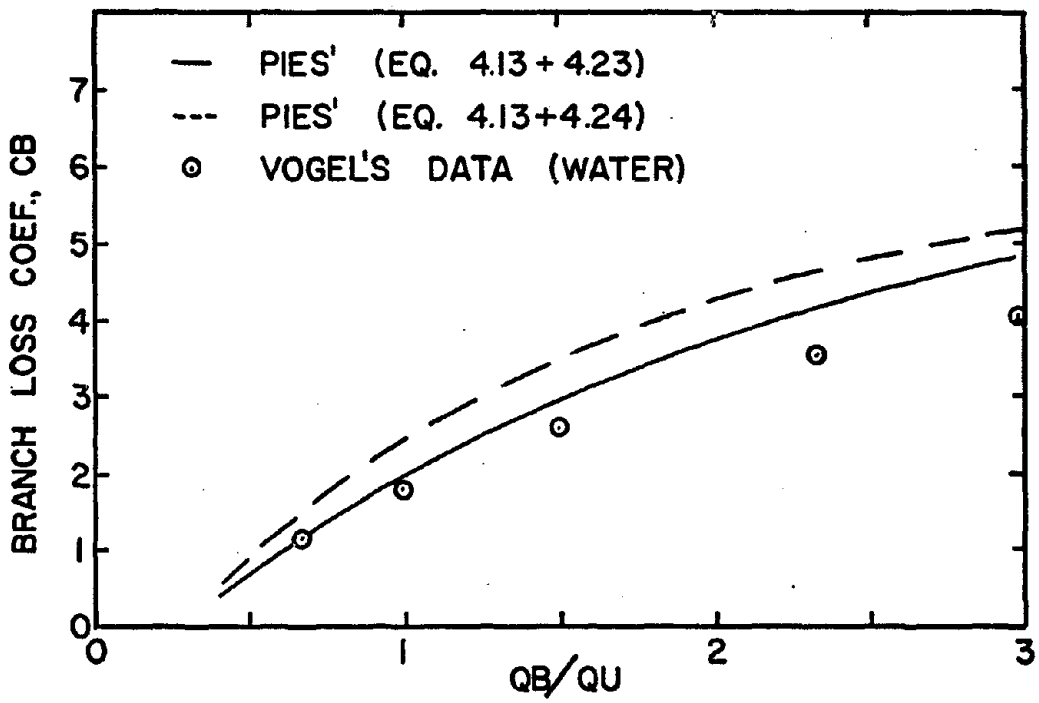

FIGURE 5-18; BRANCH ANGLE=90°, AB/AD=0.338, AU/AD=1.00; COMPARISON WITH VOGEL'S DATA.

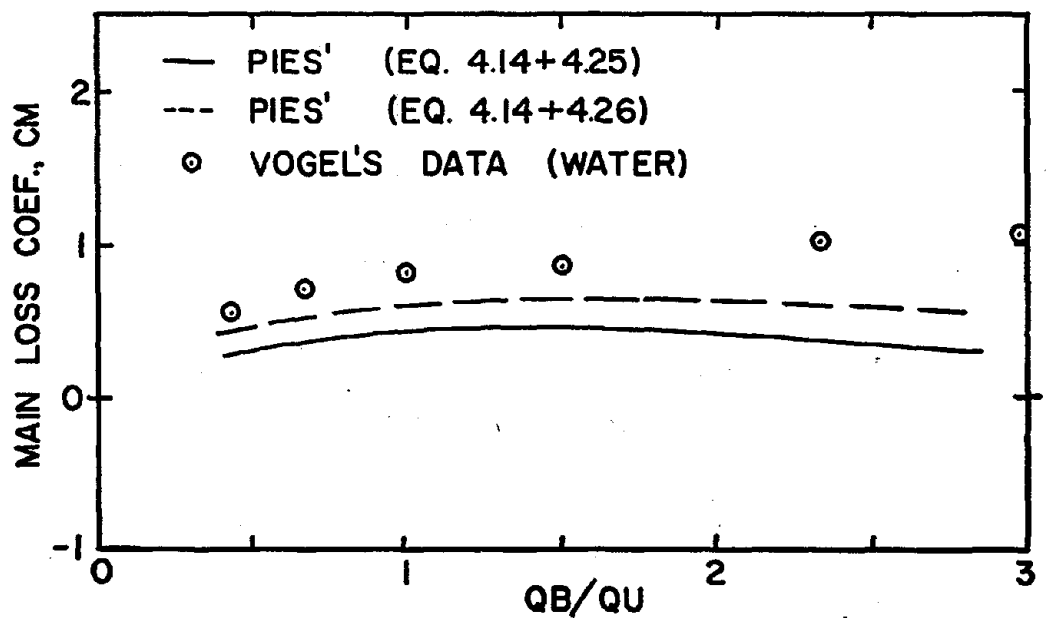

FIGURE 5-19; BRANCH ANGLE=90°, AB/AD=0.338, AU/AD=1.00; COMPARISON WITH VOGEL'S DATA.

forty-five degree branch angles. The expressions determined by Behls-Brown were

$$CB = 1.0276\sqrt{\frac{A_b}{A_d}} - 0.3405\sqrt{\frac{A_d}{A_b}}\,\frac{Q_b/Q_u}{1.0 + Q_b/Q_u} + \left(\frac{A_d}{A_b}\right)^2\left(\frac{Q_b/Q_u}{1.0 + Q_b/Q_u}\right)^2 - 1.0 \qquad 5.1$$

and

$$CM = \left[-1.461\left(\frac{A_d}{A_b}\right)^{0.9306}\right]\left\{1.0 - \frac{0.3015}{(A_d/A_b)^{0.6566}} - \frac{A_d/A_u}{1.0+Q_b/Q_u}\right\}^2 + 0.5978 - 0.5926\left(1.0 - \frac{0.3015}{(A_d/A_b)^{0.6566}}\right) \qquad 5.2$$

Ashley (Ref. 1) analyzed converging flow fittings with constant mainstream diameters by a purely theoretical approach. Assumptions in Ashley's model were: the branch and upstream static pressures were equal; potential flow existed; and branch flow entered the mainstream at an effective angle less than the actual branch angle; and the model was only valid for $V_b/V_u \leq 1.0$. The equations became involved and the branch and main loss coefficients could not be expressed explicitly. Although Ashley's assumptions were supported by the discussion in section 4.3, the information was felt limited since the theoretical model became inaccurate for $V_b/Vu > 1.0$.

The Handbook of Hydraulic Resistance (Ref. 10) presented semi-empirical loss coefficient equations for converging flow fittings. Although the original derivation of these equations was not available, it was noted that the form of the theoretical expressions in the Handbook of Hydraulic Resistance were the same as CB_t (eq. 4.13) and CM_t (eq. 4.14). It appeared the empirical corrections of CB_t and CM_t in the Handbook of Hydraulic Resistance were far too simplified when compared with the experimental data in Appendix A.

A particular case was chosen which could be applied to the analytical studies of Behls-Brown, Ashley, the Handbook of Hydraulic Resistance, and this investigation. For the case selected, $A_b/A_d = 0.3$, $A_u/A_d = 1.00$, and the branch angle = 45 degrees. Branch and main loss coefficient curves are compared in Figures 5-20 and 5-21 for these four analytical works. All branch loss coefficient curves tended to group together at low Q_b/Q_u, although Ashley's and the Handbook of Hydraulic Resistance's curves tended to drop below the curves of Behls-Brown and this investigation as Q_b/Q_u increased. It was felt that the decrease in the two curves was attributed to the unreliable assumption in the Ashley and Handbook of Hydraulic Resistance equations which required $P_b = P_u$. The trends of the main loss coefficient

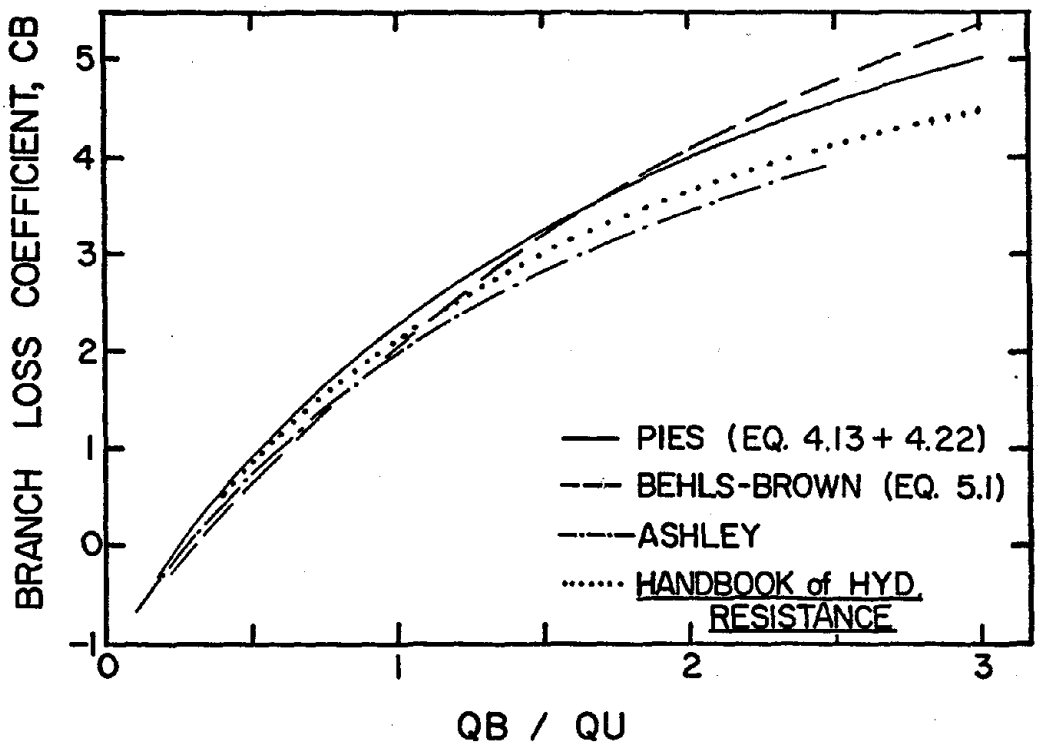

FIGURE 5-20; BRANCH ANGLE = 45°, AB / AD = 0.3
AU/AD = 1.00; COMPARISON OF ANALYTICAL EQUATIONS.

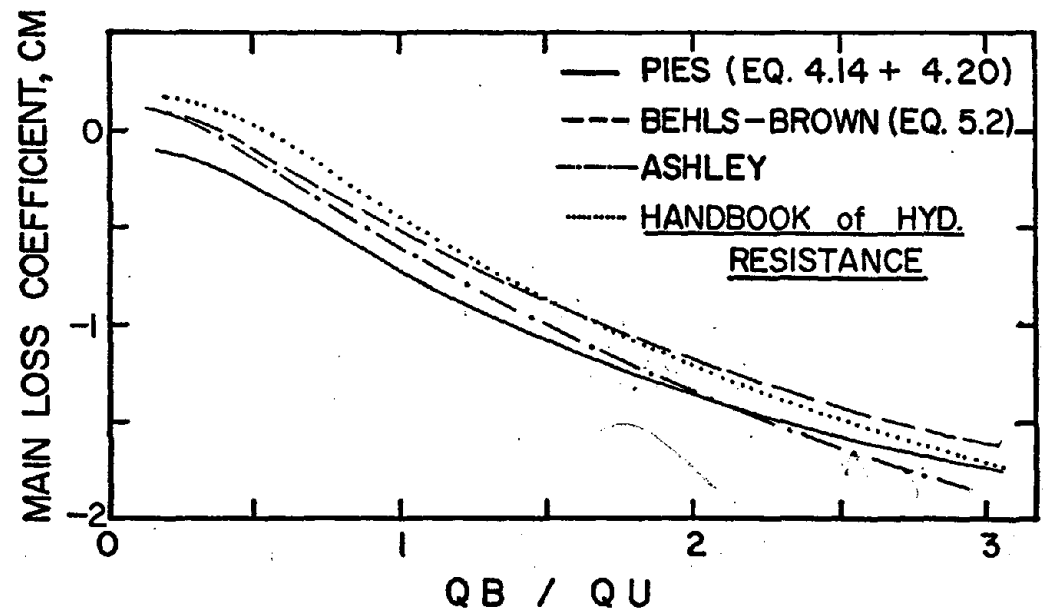

FIGURE 5-21; BRANCH ANGLE = 45°, AB / AD = 0.3
AU / AD = 1.00; COMPARISON OF ANALYTICAL EQUATIONS.

curves were the same for the four analytical studies, but no grouping between curves was observed.

5.5 Reliability of the Analytical Equations

It was not felt appropriate to simply specify one uncertainty tolerance limit on the branch and main loss coefficients for the general case. Reliability was observed to depend on A_b/A_d, A_u/A_d, branch angle, Q_b/Q_u, and downstream diameter. When correlating the correction terms in section 4.4, accuracy was seen to decrease as the values of A_b/A_d and A_u/A_d decreased; accuracy decreased for increased branch angle; accuracy decreased for $Q_b/Q_u < 0.4$ and $Q_b/Q_u > 6.0$; and accuracy decreased for the downstream diameter less than ten inches although this decrease in accuracy was not necessarily proportional to the diameter. Nevertheless, the analytical equations were felt to give loss coefficients within roughly five to twenty percent of the actual values for production fittings.

One of the main sources of possible inaccuracy between loss coefficient values from the semi-empirical equations of this study and the actual values from a randomly chosen production line fitting could be attributed to inconsistencies in the fabrication of the branch tap entrance. Since the fittings used in the experimental investigation had branch tap entrances standard for that particular fitting geometry, the semi-empirical equations were felt to be representative of design data for the nominal production fitting.

CHAPTER VI

CONCLUSIONS AND RECOMMENDATIONS

6.1 Introduction

The experimental investigation showed that the branch and main loss coefficients (defined by equations 2.1 and 2.2, respectively) correlated with good agreement when plotted against the ratio of branch to upstream volume flow rate.

It was observed that no simple generalized plots could be constructed directly from the experimental loss coefficient curves. Analytical expressions must be derived which would allow evaluation of the branch and main loss coefficients for all fittings commonly used in industrial exhaust ventilation systems. The semi-empirical loss coefficient equations were found to be functions of Q_b/Q_u, A_b/A_d, A_u/A_d, branch angle, and downstream diameter. These analytical expressions consisted of theoretical loss coefficients plus empirical correction terms. Although the correction terms were difficult to correlate, the final forms of the semi-empirical equations were felt to give reliable loss coefficient values for converging flow fittings used in the design field. Generalized curves are given in Appendix D for thirty, forty-five, and ninety degree branch angles over a wide range of A_b/A_d and A_u/A_d.

6.2 Conclusions

6.2.1 Branch Tap Entrance Effect on the Loss Coefficients

The three types of branch tap entrances (sharp, rolled, and round edge entrances) discussed in section 5.2 were shown to have a significant effect on the branch and main loss coefficients. The experiment mentioned in section 5.2 verified that a twenty to thirty percent deviation could occur in both loss coefficients between the sharp and round edge entrance cases.

6.2.2 Failure of the Simple Energy-Mass Balance Model

The energy-mass balance model in section 4.2 was based on setting the flux of internal and kinetic energy plus flow work at the branch and upstream cross-sections equal to the flux of internal and kinetic energy plus flow work at the downstream cross-section. This theoretical model was proven unreliable, and the only reason for its unreliability was attributed to heat transfer from the fitting to the ambient due to viscous dissipation of turbulent eddies as the branch flow enters the mainstream flow. Although such heat transfer was felt small, it was noted that energy drops or gains of the flow in the fitting were also small because there was no process within the fitting which could add energy to the flow such as mechanical work or a heat source.

6.2.3 Limitations on the Assumption $P_b = P_u$

Past authors have felt it reasonable to assume $P_b = P_u$ in converging flow fittings. The experimental portion of this investigation shows that the assumption $P_b = P_u$ becomes unreliable for branch to upstream velocity ratios greater than one and branch velocities greater than 1000 feet per minute.

6.2.4 Branch Angle Effect on the Semi-Empirical Correlations

Correction terms ΔCB and ΔCM become more difficult to correlate as the branch angle was increased. ΔCM for ninety degree branch angles could not be correlated accurately, although an empirical equation was determined to give approximate values of ΔCM.

Also, it was observed that the semi-empirical equations in this investigation were unreliable when used for branch angles other than thirty, forty-five, or ninety degrees, and new empirical correction terms would need to be determined for any additional branch angles not covered in this study.

6.2.5 Downstream Diameter Effect on the Semi-Empirical Correlations

For all branch angles, the comparison plots in Figures A-1 through A-66 showed the best agreement between experimental and analytical curves for downstream diameters greater than or equal to ten inches. It was felt that correlations became less accurate for downstream diameters less than ten inches because the physical dimensions of the branch tap entrance lip were significant compared to the dimensions of the fitting; whereas in the case of the ten inch or greater downstream diameter fitting, the inertia of the bulk flow was great enough to suppress the pressure losses from turbulence produced by the branch tap entrance lip. The diameter effect for ninety degree branch angles was predominant enough that the empirical correction terms for downstream diameters less than ten inches were distinct from the correction terms for ten inch or greater downstream diameters.

6.2.6 Comparison Between Analytical Equations and Other Sources

In all cases, the curves of the analytical equations followed the same trends as the data from other authors. With the exception of Petermann's (Ref. 14) and Vogel's (Ref. 23) data, analytical branch and main loss coefficient

values showed close agreement with the data from the other investigators. Deviations between the data of Petermann and Vogel and the analytical equations were attributed to the downstream diameter effect mentioned in section 6.2.5 (all downstream diameters were approximately two inches) and possibly a Reynolds number effect. The downstream Reynolds numbers ranged from 40,000 to 700,000 (well within the turbulent region) for the experimental portion of this investigation, but since Petermann and Vogel used water and small diameter pipes to determine their loss coefficients, it was questioned that the data might have been collected at low enough Reynolds numbers to allow the viscosity of the water to have significant influence on the loss coefficients.

6.2.7 Effects on the Loss Coefficient for Variable A_b/A_d and A_u/A_d

Observation of the generalized curves in Appendix D showed the following: the branch loss coefficient increased for decreasing A_b/A_d and/or increasing A_u/A_d for all branch angles; the main loss coefficient increased for increasing A_b/A_d and/or decreasing A_u/A_d for thirty and forty-five degree branch angles; and the main loss coefficient followed no definite trends for variable A_b/A_d and/or A_u/A_d for ninety degree branch angles.

6.2.8 Diffuser Losses for Tapered Fitting Bodies

Although total pressure losses due to the diffuser effect in the mainstream for tapered fitting bodies were intrinsic in the empirical correction factor ΔCM, the magnitude of the diffuser loss coefficient for each fitting investigated was compared with the value of the main loss coefficient. The diffuser loss coefficient was dependent on the degree of fitting body taper and was evaluated by an empirical expression found in Reference 10. For all fittings studied, the diffuser loss coefficient usually was less than one percent of the main loss coefficient. Thus, it was felt total pressure losses due to the taper of fitting bodies was small compared to the other sources of pressure loss in the fitting.

6.3 Negative Loss Coefficient

The concept of a negative loss coefficient might seem unfeasible because this would imply a total pressure increase in the direction of flow and a violation of conservation of energy. However, occurrence of a negative branch loss coefficient is seen when the upstream flow rate is high enough compared to the branch flow rate that the upstream flow can add sufficient energy to the flow between the branch and downstream to cause an increase in total pressure. The same argument holds for a negative main loss coefficient where the branch flow rate is great enough compared to the

upstream flow rate that the branch flow adds sufficient energy to the mainstream flow to cause an increase in total pressure between the upstream and downstream. This explanation of the negative loss coefficient phenomenon is consistent with similar arguments posed by Sepsy-Lauvray (Ref. 18), Behls-Brown (Ref. 4), and the Handbook of Hydraulic Resistance (Ref. 10).

6.4 Recommendations

6.4.1 Better Main Loss Coefficient Correlations for Ninety Degree Branch Angle Fittings

Empirical correction terms for CM for ninety degree branch angle fittings were determined in sections 4.4.8 and 4.4.9, where it was mentioned that, at best, only approximate correction terms could be correlated. It is felt that the semi-empirical main loss coefficient equations for ninety degree branch angles are accurate enough for design work, although more precise correlations would be desirable.

6.4.2 Overall Performance Coefficient

In the duct design field, the performance of such fittings as elbows or transitions is determined by the value of the loss coefficient. Since converging flow fittings require two loss coefficients, the overall efficiency of a converging flow fitting relative to the overall efficiency of another converging flow fitting is not clearly defined

by simply comparing the branch or main loss coefficient graphs. In fact, at the present time there is no way to rate the overall efficiency of converging flow fittings. There is a definite need to define an overall performance parameter for converging flow fittings. Although time did not allow the author to thoroughly investigate the definition of such an overall performance parameter, the author intuitively felt this parameter might be some factor of CB + CM. Several plots were constructed and CB + CM was observed to correlate against Q_b/Q_u.

The author suggests further investigation in defining an overall performance parameter should include attempts at correlating the following forms:

$$\frac{CB + CM}{Q_b/Q_u}\ ,\ \frac{CB + CM}{V_b/V_u}\ ,\ \frac{CB + CM}{\ln(Q_b/Q_u)},\ \text{or}\ \frac{CB + CM}{\ln(V_b/V_u)}\ .$$

It is warned that a simple correlation of one of these forms does not necessarily mean a universal overall efficiency parameter has been found. For the aid of future investigators in converging flow fittings, tabulated raw and reduced data for this investigation can be found in Reference 19, and tabulated raw and reduced data for additional fittings can be found in Reference 18.

LIST OF REFERENCES

1. Ashley, C.M., "Performance Analysis of Return Air Duct Branch Inlet Fittings." ASHRAE Transactions. 1971.

2. Ashley, C.M., Gilman, S.F., and Church, R.A., "Branch Fitting Performance at High Air Velocity." ASHRAE Transactions. Vol. 62, 1956, pp. 279-294.

3. ASHRAE Handbook of Fundamentals. 1972. New York: American Society of Heating, Refrigerating and Air-Conditioning Engineers, Inc.

4. Behls, H.F., Brown, W.K. Jr., "Pressure Loss Coefficients for the 45-Degree Return Air Tee." First Symposium on Use of Computers for Environmental Engineering Related to Buildings. Building Science Series 39, Oct. 1971, pp. 375-384. Washington, D.C.: National Bureau of Standards.

5. Dillis, C.C., Nye, E.P., Thermal Engineering. 1969. Scranton Pa.: International Textbook Company.

6. Doebelin, E.O., Measurement Systems: Application and Design. 1966. New York: McGraw-Hill.

7. Engineering Bulletin, Machine-Formed Branch Fittings. March 7, 1969. Westerville, Ohio: United Sheet Metal of United McGill Corporation.

8. Engineering Design Manual, Round Duct Section. 1970. Westerville, Ohio: United Sheet Metal of United McGill Corporation.

9. Haerter, A.A., "Flow Distribution and Pressure Change Along Slotted or Branched Ducts." ASHRAE Transactions. Vol. 69, 1963, pp. 124-137.

10. Handbook of Hydraulic Resistance. 1966. Jerusalem, Israel: Israel Program for Scientific Translations, Ltd.

11. Hays, F.C., Konzo, S., "Investigation of Air Flow in Branch Take-Offs with the Use of a Water Table." ASHRAE Transactions. No. 2124, 1969, pp. 210-221.

12. Healy, J.H., Patterson, M.N. and Brown, E.J., "Pressure Losses through Fittings Used in Return Air Duct Systems." ASHRAE Transactions. May, 1962, pp. 70-76.

13. Industrial Ventilation, A Manual of Recommended Practice. 1968. Lansing Michigan: American Conference of Governmental Industrial Hygienists.

14. Petermann, F., "Der Verlust in schiefwickligen Rohrverzweigungen." Mitteilunger des Hydraulischen Institute der Technischen Hochschule, München. Heft 3, 1929, pp. 98-117.

15. Reynolds, W.C., Thermodynamics. 1968. New York: McGraw-Hill.

16. Sepsy, C.F., "Static and Total Pressure Measurement." News in Engineering. Nov., 1959.

17. Sepsy, C.F., Knotts, R.E., "The Effect of Branch Spacing on the Loss Coefficient of Divided Flow Fittings." ASHRAE Transactions. No. 2228. 1972.

18. Sepsy, C.F., Lauvray, T.L., An Experimental Study of the Pressure Losses in Converging Flow Fittings Used in Exhaust Systems. Phase Report Number One. (Contract No. HSM 099-71-28 with the National Institute for Occupational Safety and Health, H.E.W.). The Ohio State Research Foundation. Dec., 1971.

19. Sepsy, C.F., Pies, D.B., An Experimental Study of the Pressure Losses in Converging Flow Fittings Used in Exhaust Systems. Phase Report Number Two. (Contract No. HSM 099-71-28 with the National Institute for Occupational Safety and Health, H.E.W.). The Ohio State Research Foundation. June, 1972.

20. Shapiro, A.H., The Dynamics and Thermodynamics of Compressible Flow. 1953. New York: Ronald Press.

21. Springman, R.A., A Study of the Effect of Branch Spacing on the Pressure Loss Coefficient for Converging Flow Fittings in Exhaust Systems. Master's Thesis. The Ohio State University. 1972.

22. Streeter, V.L., Handbook of Fluid Dynamics. 1961. New York: McGraw Hill.

23. Vogel, G., "Untersuchungen über den Verlust in rechtwinkligen Rohrverzweigungen." Mitteilungen des Hydraulischen Instituts der Technischen Hochschule, München. Heft 1, 1926, pp. 75-90.

APPENDIXES

APPENDIX A

COMPARISON OF ANALYTICAL AND EXPERIMENTAL RESULTS

Plots of the semi-empirical branch and main loss coefficient equations are compared with the experimental curves in Figures A-1 through A-66. Each dashed curve represents the semi-empirically determined branch or main loss coefficient and the solid line represents the curve drawn through the experimental data points. The semi-empirical branch and main loss coefficients were evaluated by equations 4.17 and 4.18. These equations were

$$CB = CB_t + \Delta CB \qquad 4.17$$

$$CM = CM_t + \Delta CM \qquad 4.18$$

where CB_t and CM_t were evaluated by equations 4.13 and 4.14 respectively for all A_b/A_d, A_u/A_d, and all branch angles. Table 4-1 lists the equation numbers pertaining to ΔCB and ΔCM for different branch angles and specifies the reliability restrictions based on comparison between the analytical equations and the experimental data. Actual data points for each fitting are also shown.

The schematic drawing on each plot gives the take-off diameters and branch angle for the different fittings. Identification codes for each fitting (for example, L-IRT-AA

corresponding to Figure A-1) are helpful in referencing material throughout the Appendixes for a particular fitting. The first two parts of the code (L-IRT) are fitting description codes, and the last part (AA) identifies an individual fitting. A list of all fitting descriptions and codes is given in Appendix B.

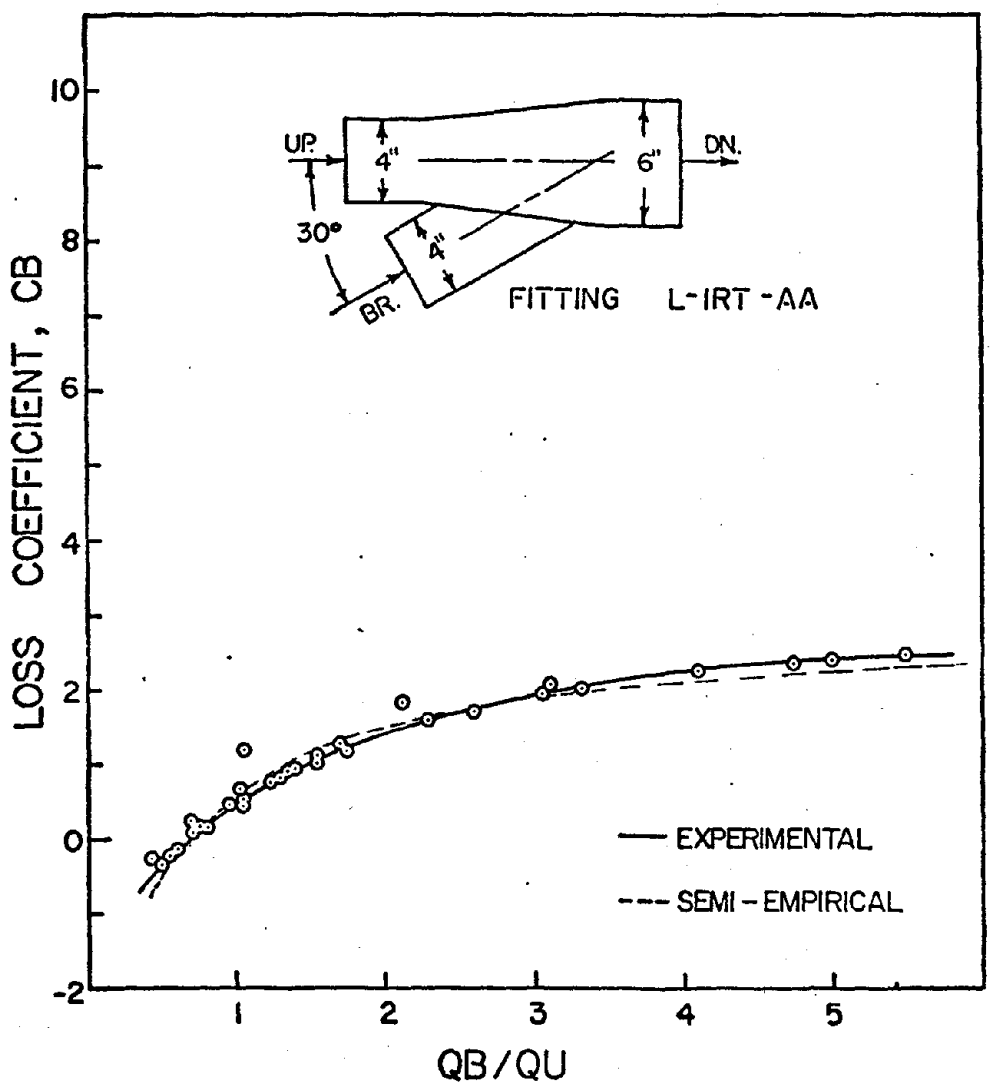

FIGURE A-1 BRANCH LOSS COEFFICIENT VS. THE RATIO OF BRANCH VOLUME FLOW TO THE UPSTREAM VOLUME FLOW

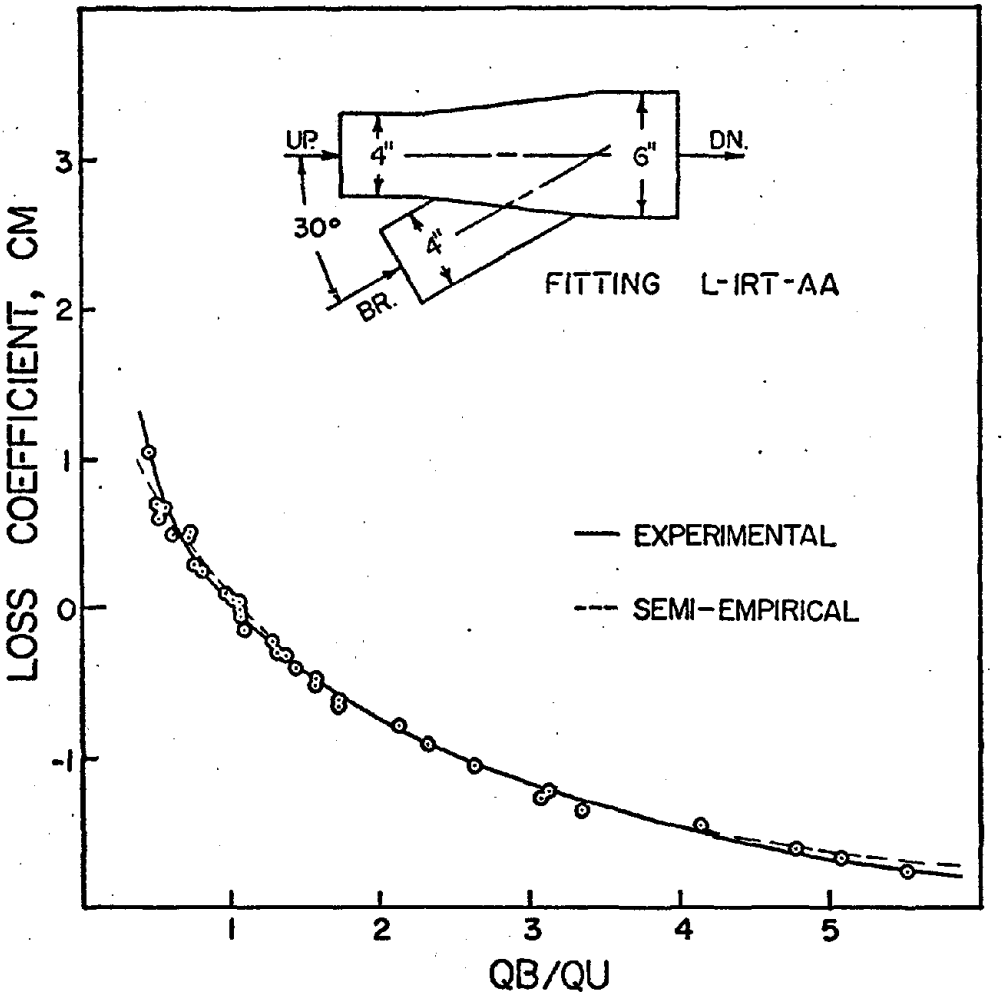

FIGURE A-2 MAIN LOSS COEFFICIENT VS. THE RATIO OF BRANCH VOLUME FLOW TO THE UPSTREAM VOLUME FLOW

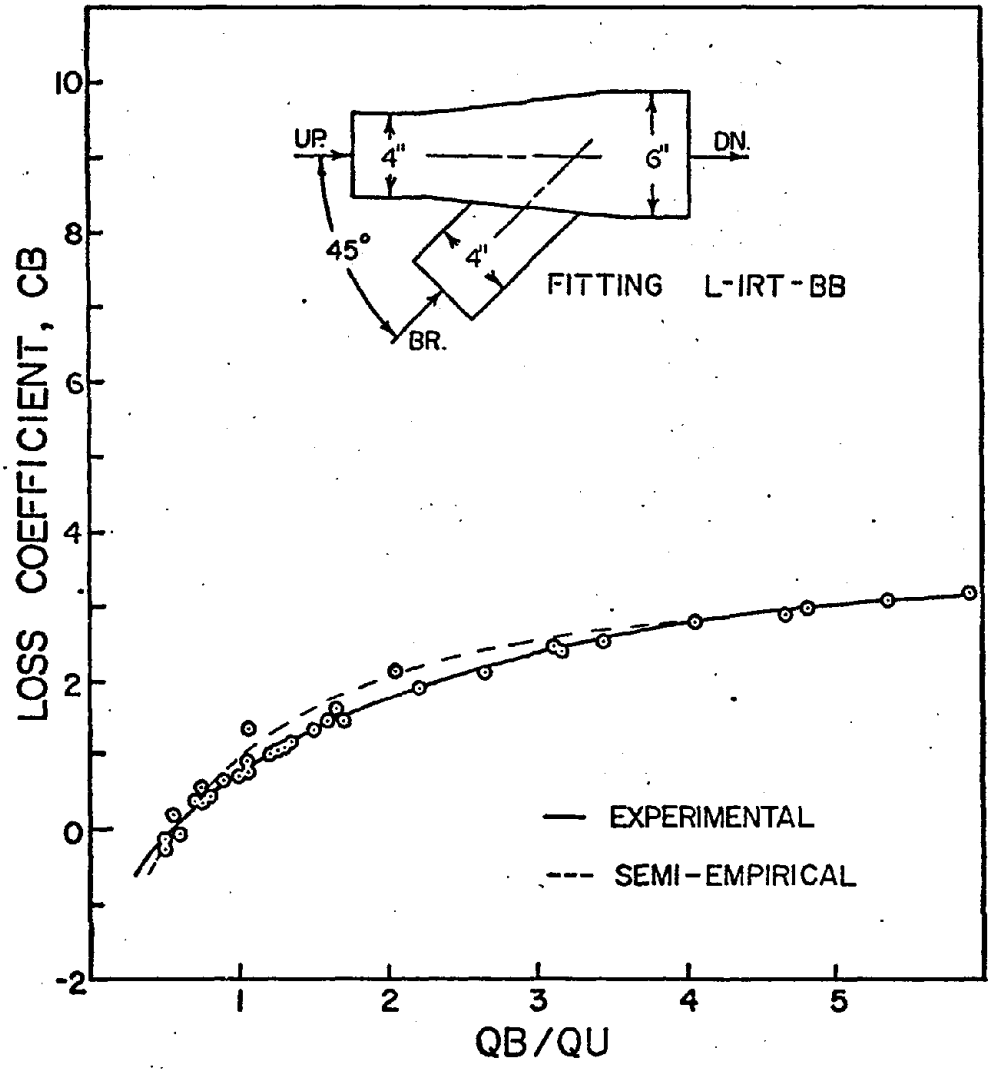

FIGURE A-3 BRANCH LOSS COEFFICIENT VS. THE RATIO OF BRANCH VOLUME FLOW TO THE UPSTREAM VOLUME FLOW

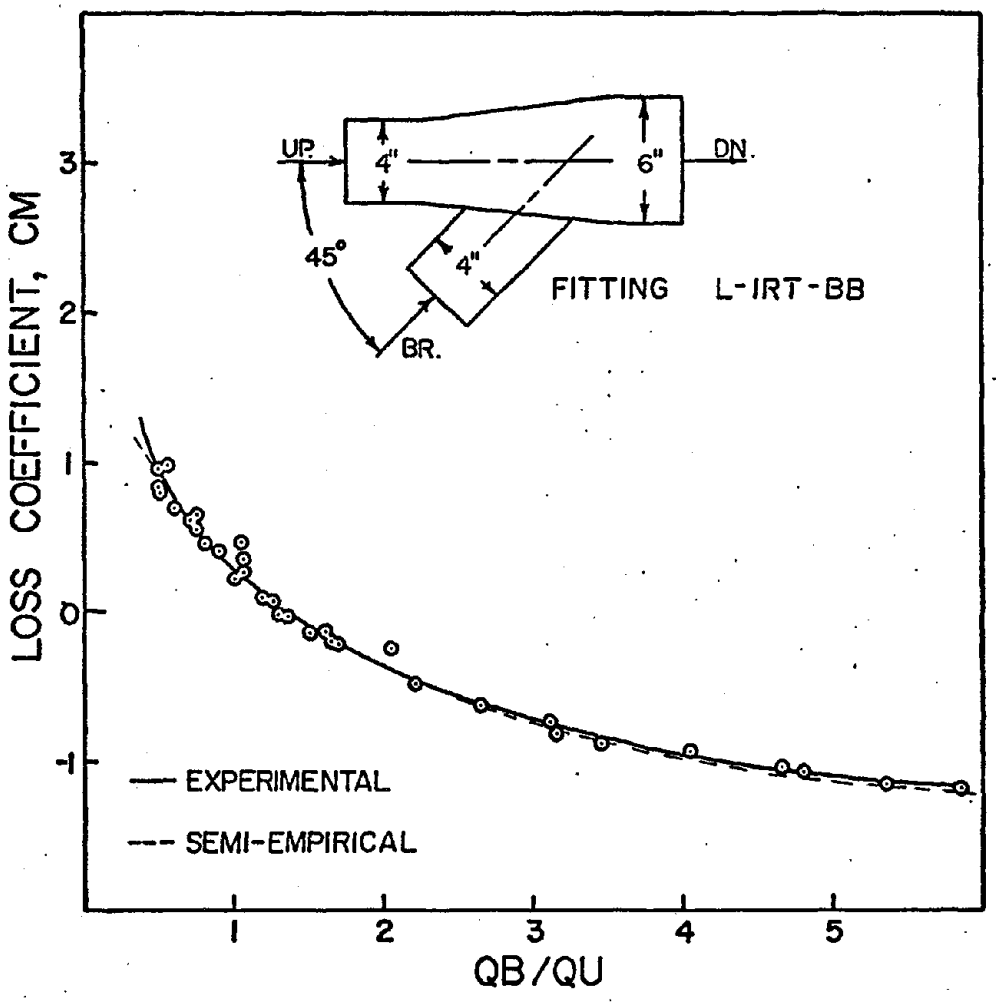

FIGURE A-4 MAIN LOSS COEFFICIENT VS. THE RATIO OF BRANCH VOLUME FLOW TO THE UPSTREAM VOLUME FLOW .

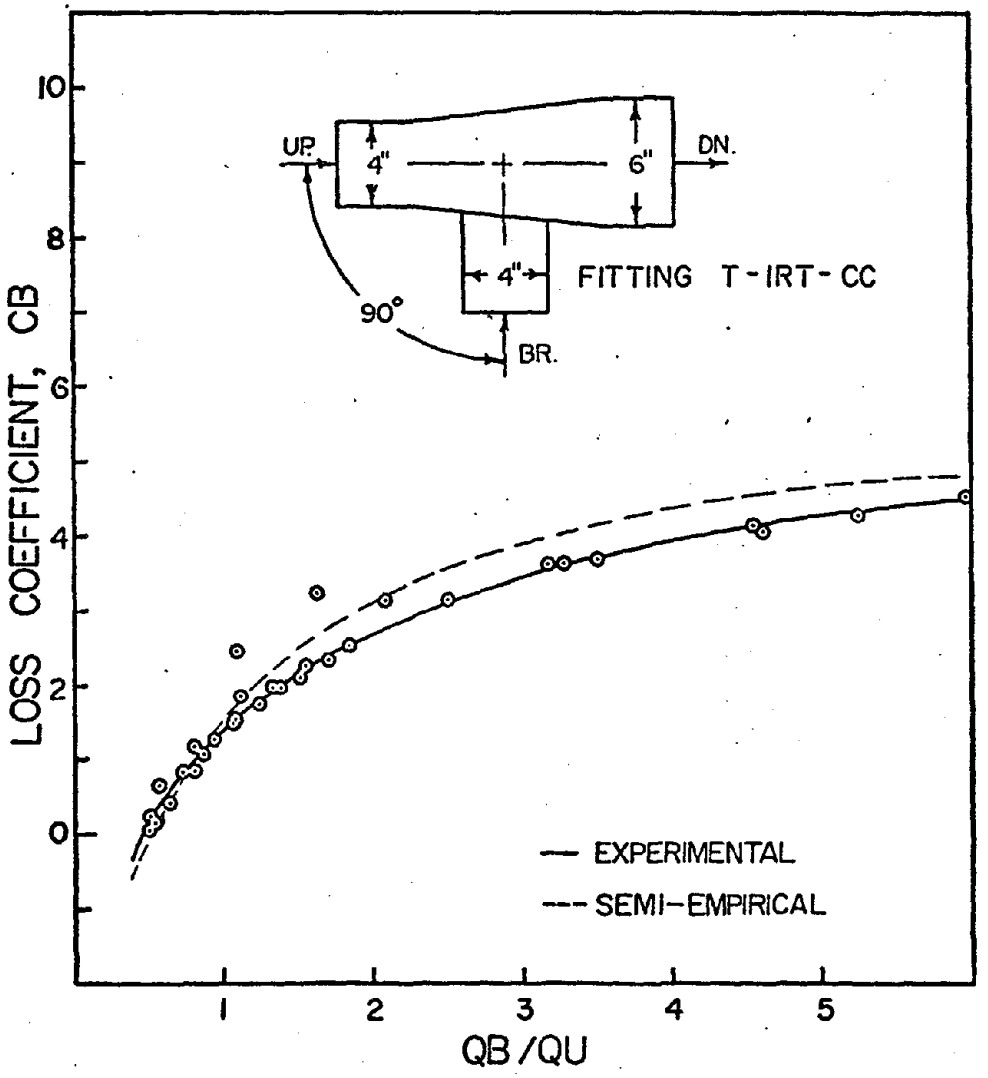

FIGURE A-5 BRANCH LOSS COEFFICIENT VS. THE RATIO OF BRANCH VOLUME FLOW TO THE UPSTREAM VOLUME FLOW

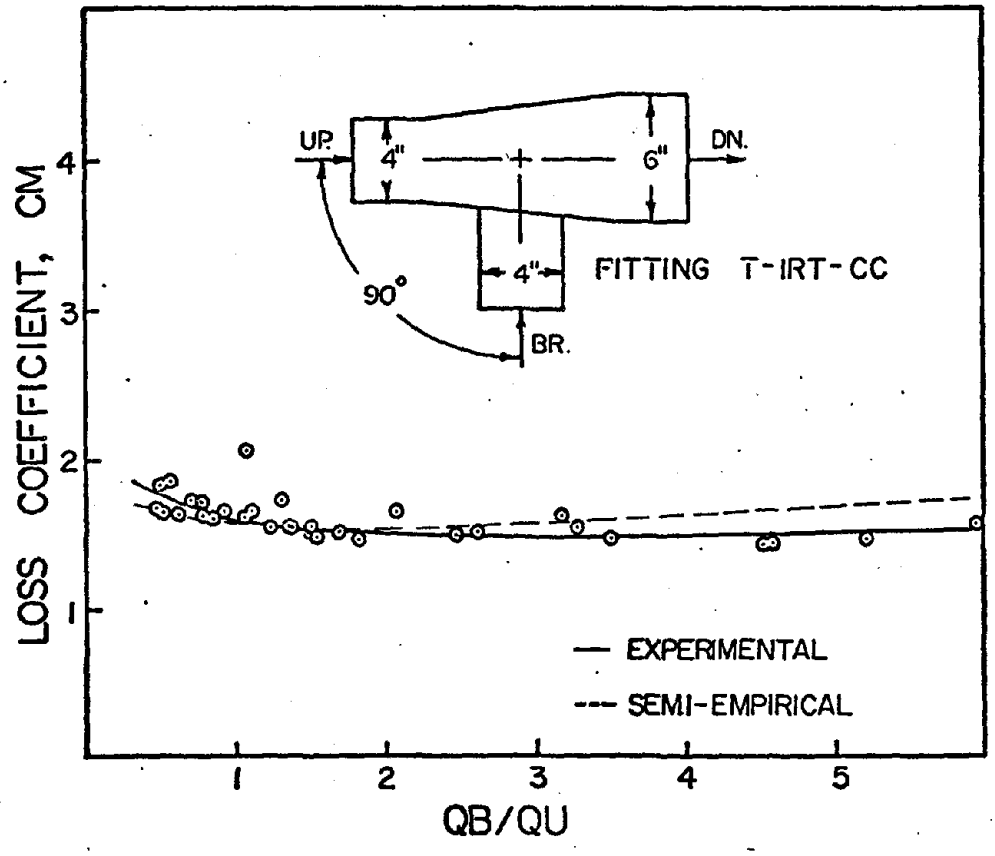

FIGURE A-6 MAIN LOSS COEFFICIENT VS. THE RATIO OF BRANCH VOLUME FLOW TO THE UPSTREAM VOLUME FLOW

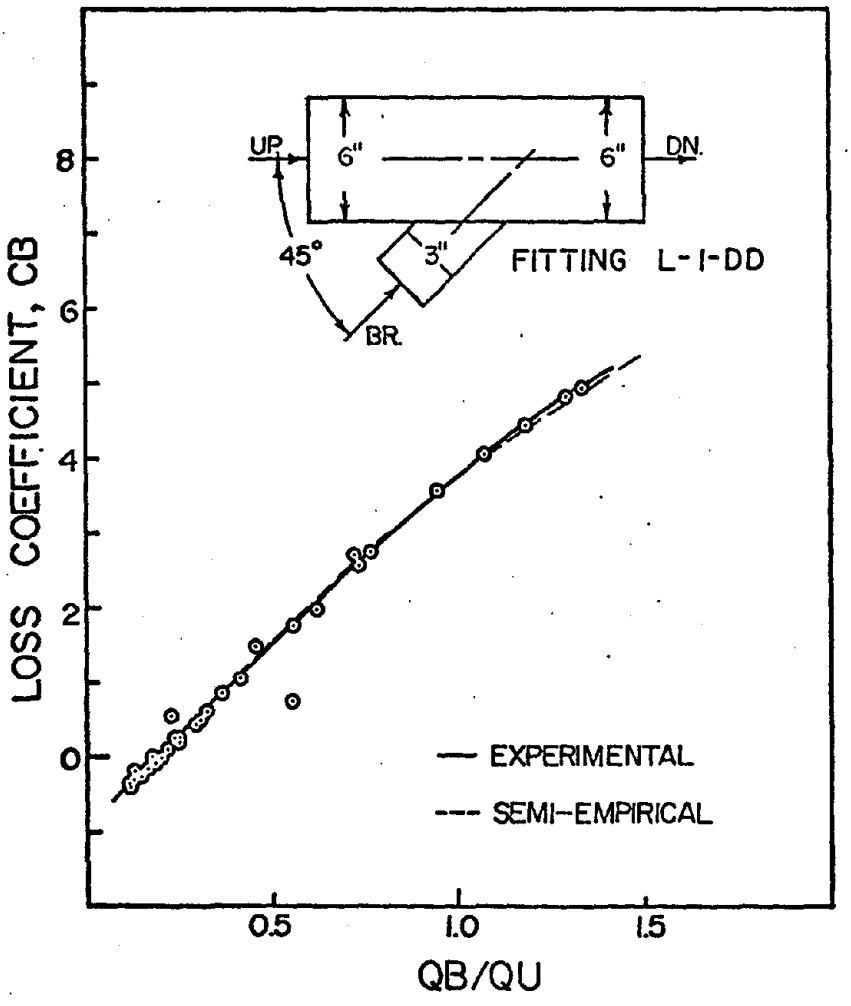

FIGURE A-7 BRANCH LOSS COEFFICIENT VS. THE RATIO OF BRANCH VOLUME FLOW TO THE UPSTREAM VOLUME FLOW

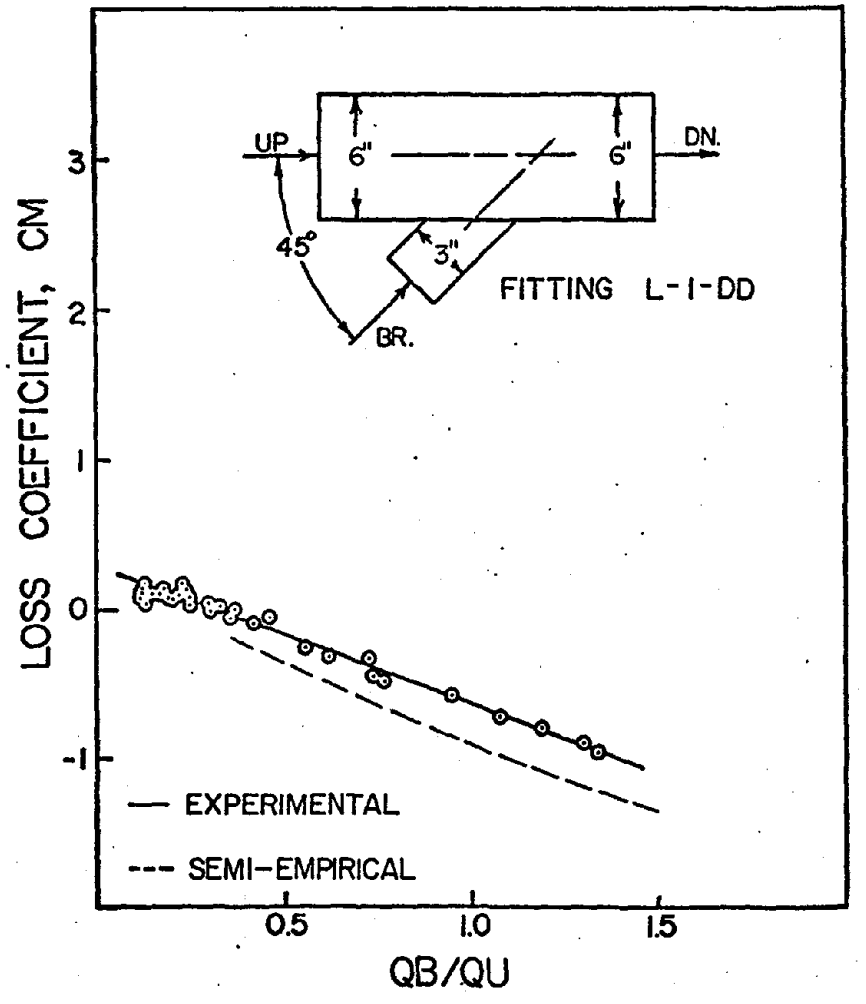

FIGURE A-8 MAIN LOSS COEFFICIENT VS. THE RATIO OF BRANCH VOLUME FLOW TO THE UPSTREAM VOLUME FLOW

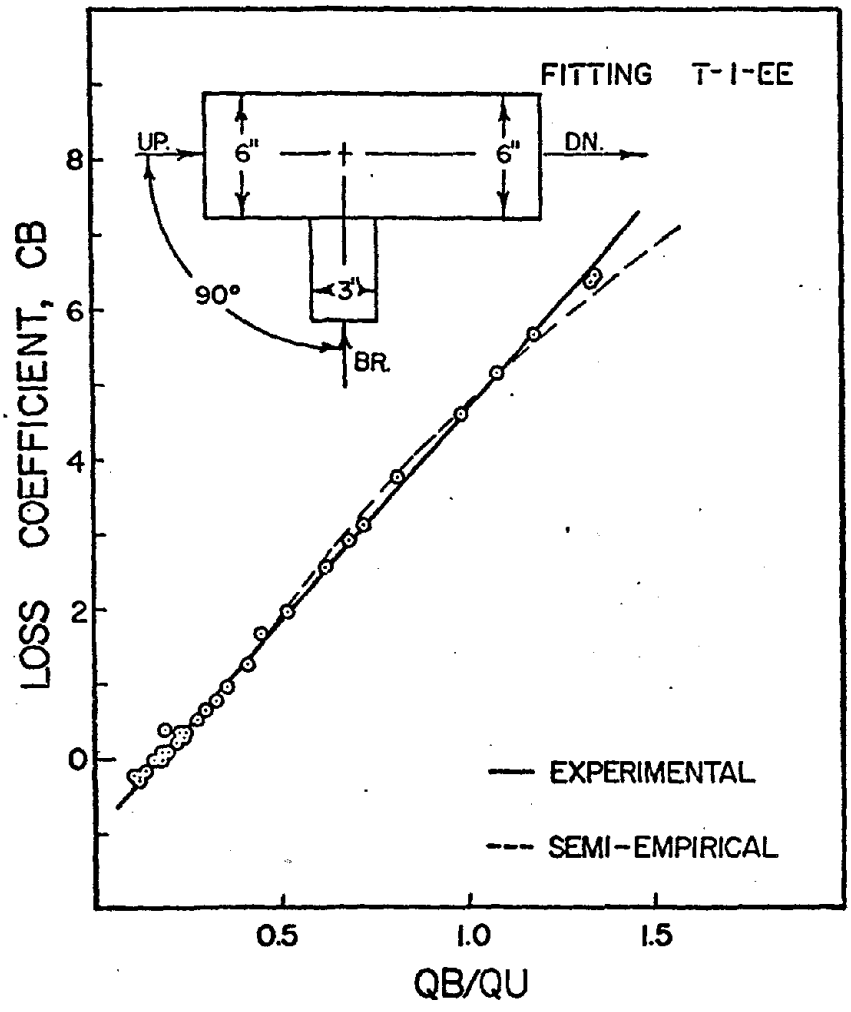

FIGURE A-9 BRANCH LOSS COEFFICIENT VS. THE RATIO OF BRANCH VOLUME FLOW TO UPSTREAM VOLUME FLOW

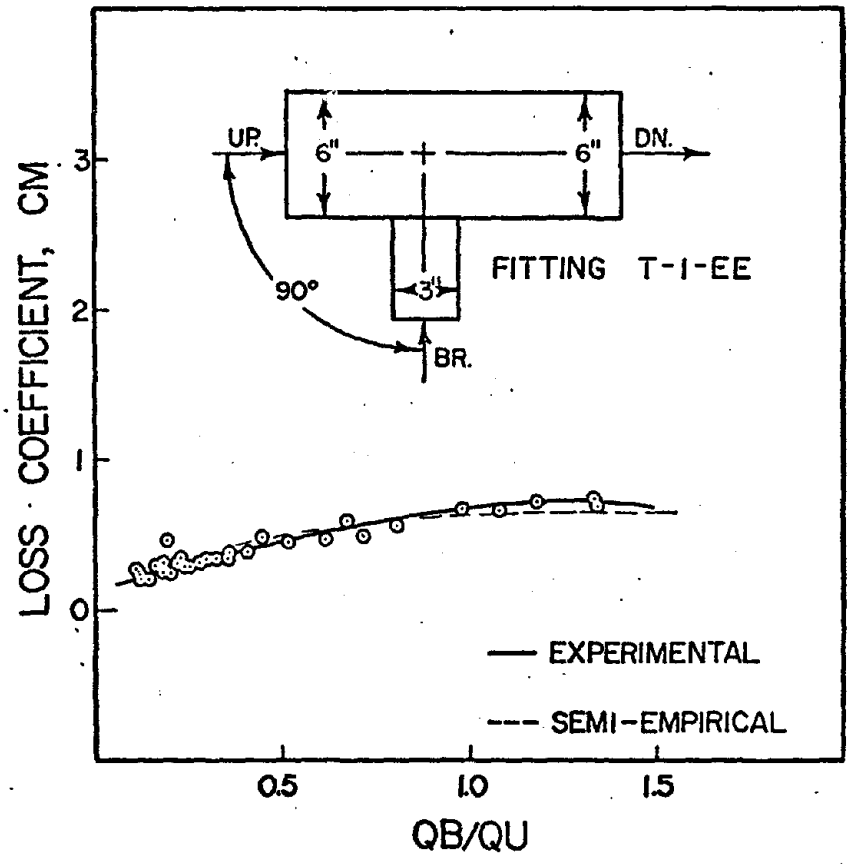

FIGURE A-10 MAIN LOSS COEFFICIENT VS. THE RATIO OF BRANCH VOLUME FLOW TO THE UPSTREAM VOLUME FLOW

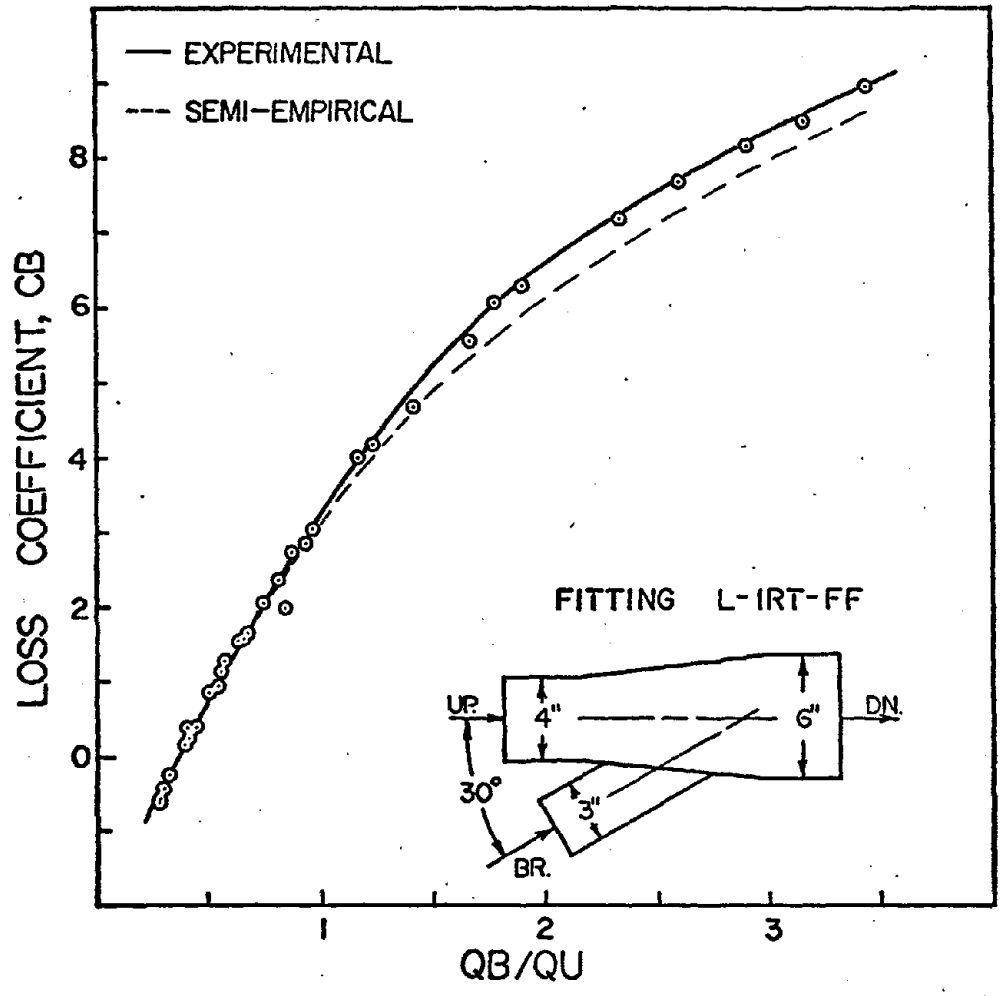

FIGURE A-11 BRANCH LOSS COEFFICIENT VS. THE RATIO OF BRANCH VOLUME FLOW TO THE UPSTREAM VOLUME FLOW

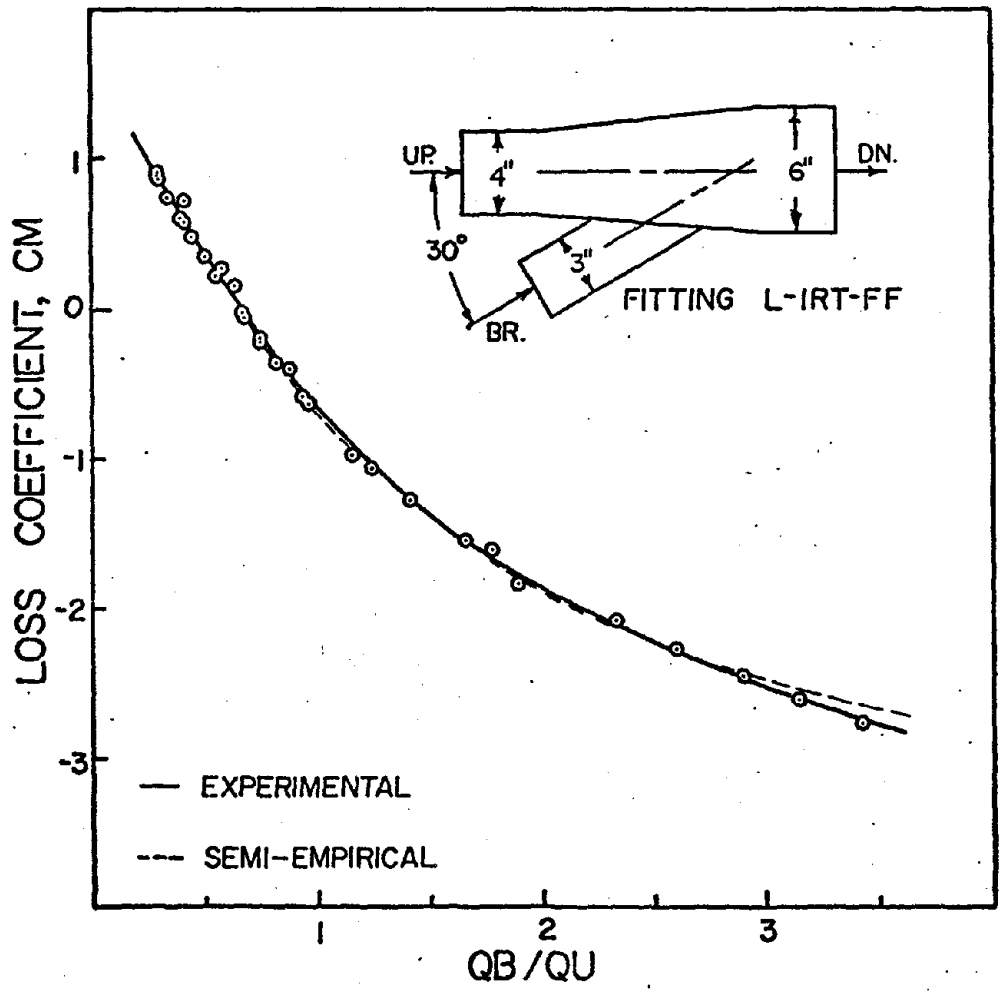

FIGURE A-12 MAIN LOSS COEFFICIENT VS. THE RATIO OF BRANCH VOLUME FLOW TO THE UPSTREAM VOLUME FLOW

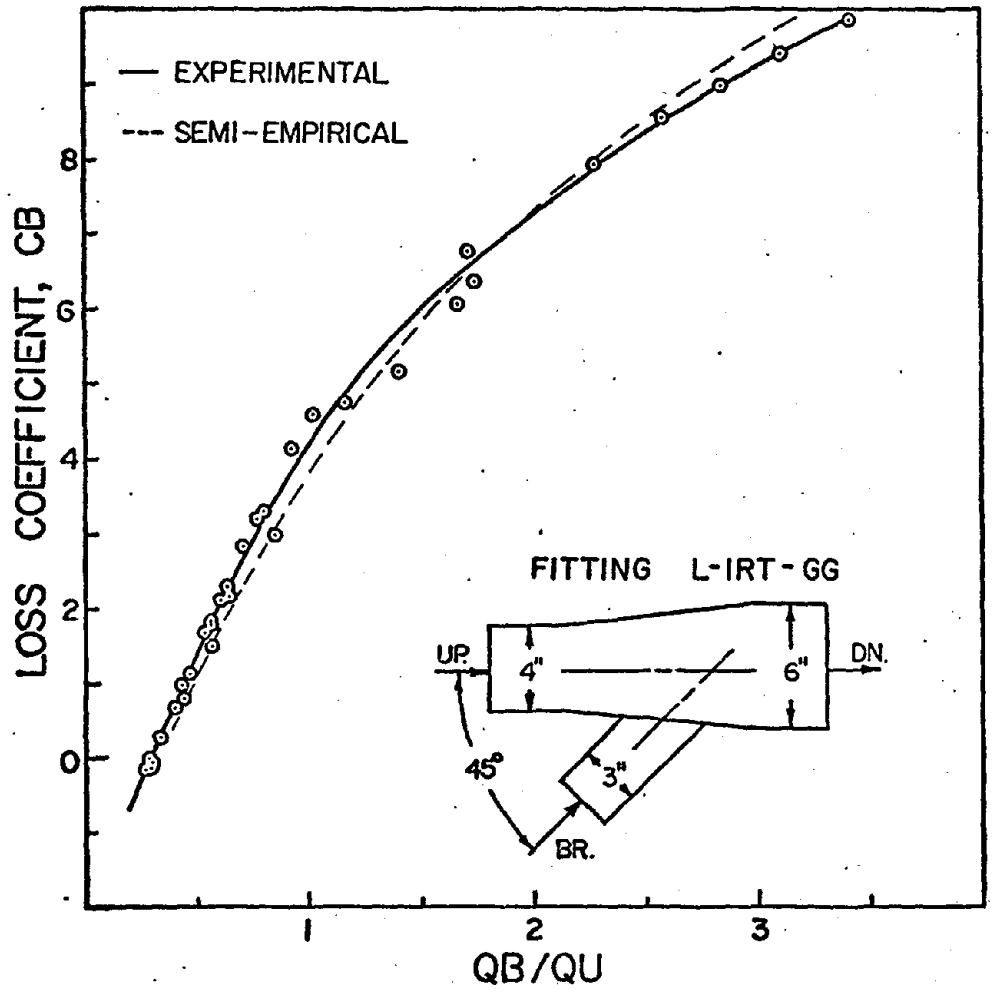

FIGURE A-13 BRANCH LOSS COEFFICIENT VS. THE RATIO OF BRANCH VOLUME FLOW TO THE UPSTREAM VOLUME FLOW

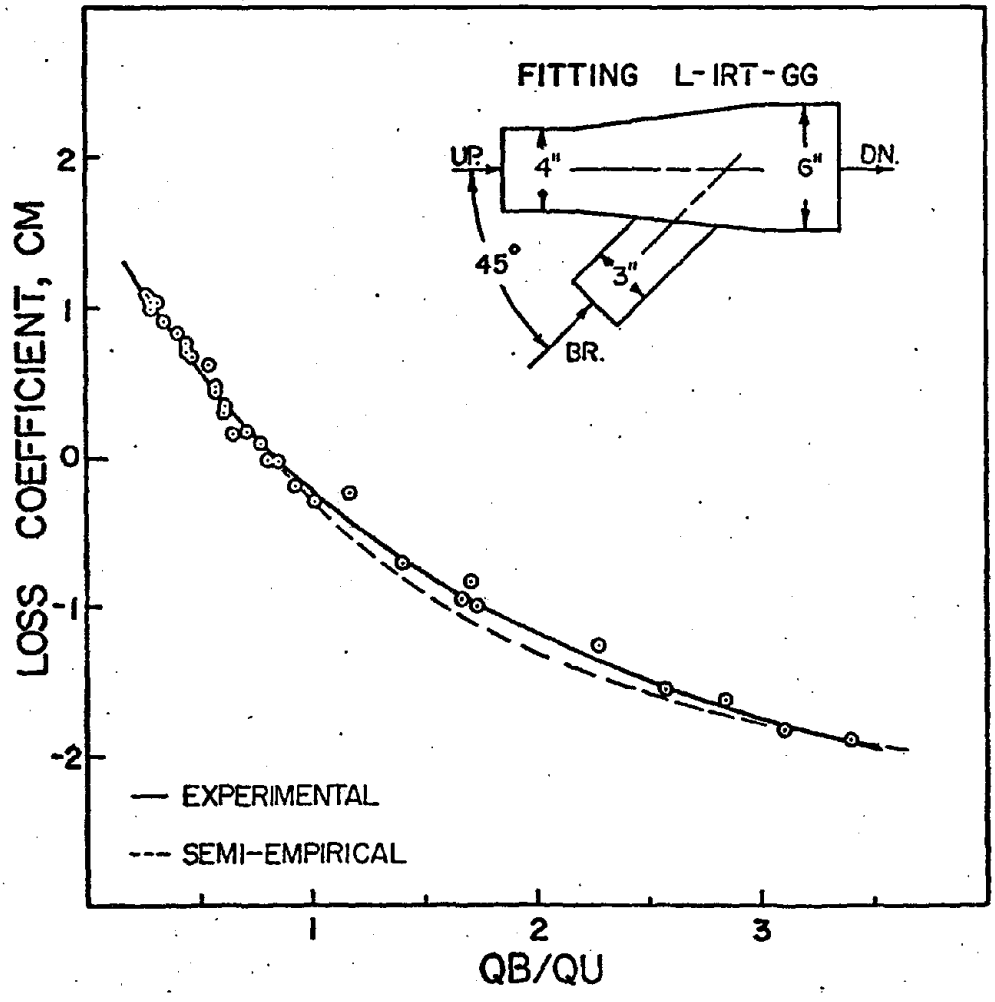

FIGURE A-14 MAIN LOSS COEFFICIENT VS. THE RATIO OF THE BRANCH VOLUME FLOW TO THE UPSTREAM VOLUME FLOW

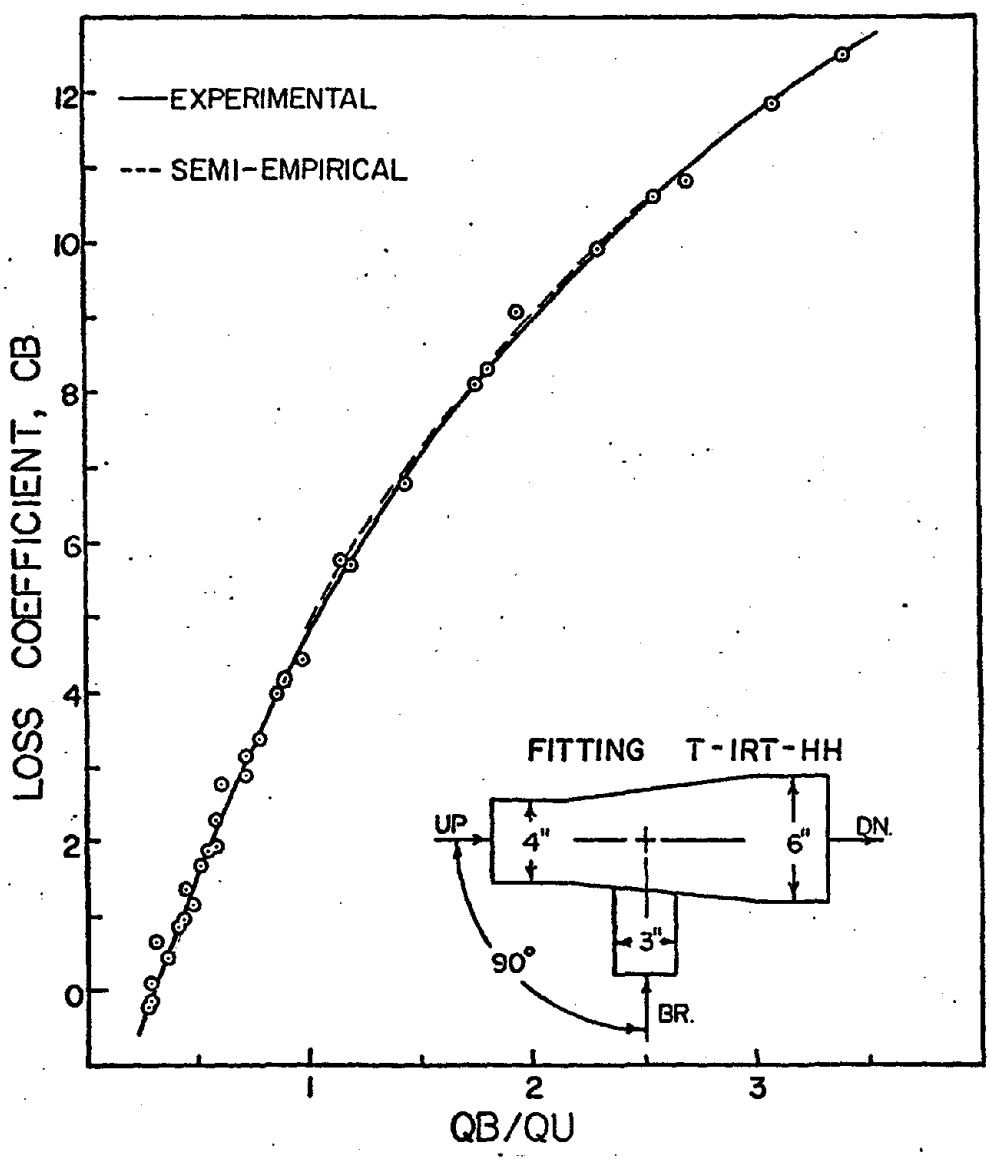

FIGURE A-15 BRANCH LOSS COEFFICIENT VS. THE RATIO OF BRANCH VOLUME FLOW TO THE UPSTREAM VOLUME FLOW

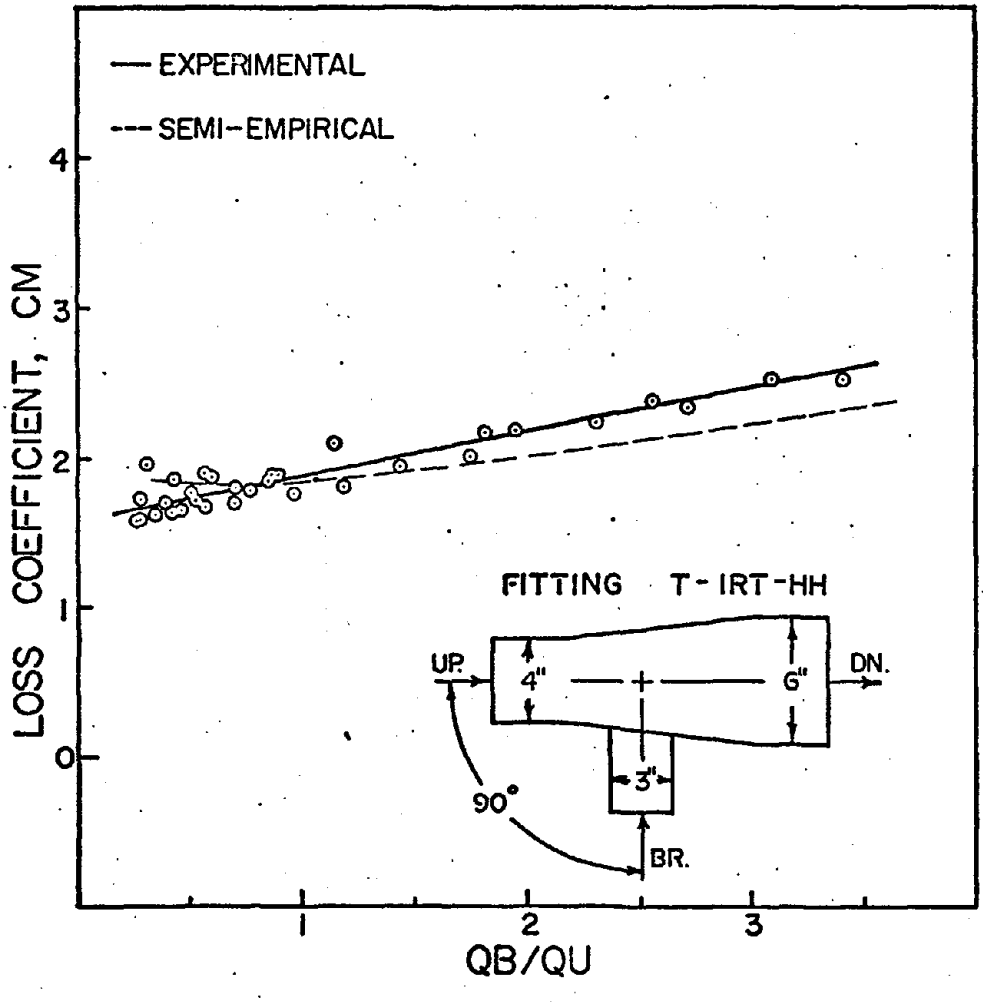

FIGURE A-16 MAIN LOSS COEFFICIENT VS. THE RATIO OF BRANCH VOLUME FLOW TO THE UPSTREAM VOLUME FLOW

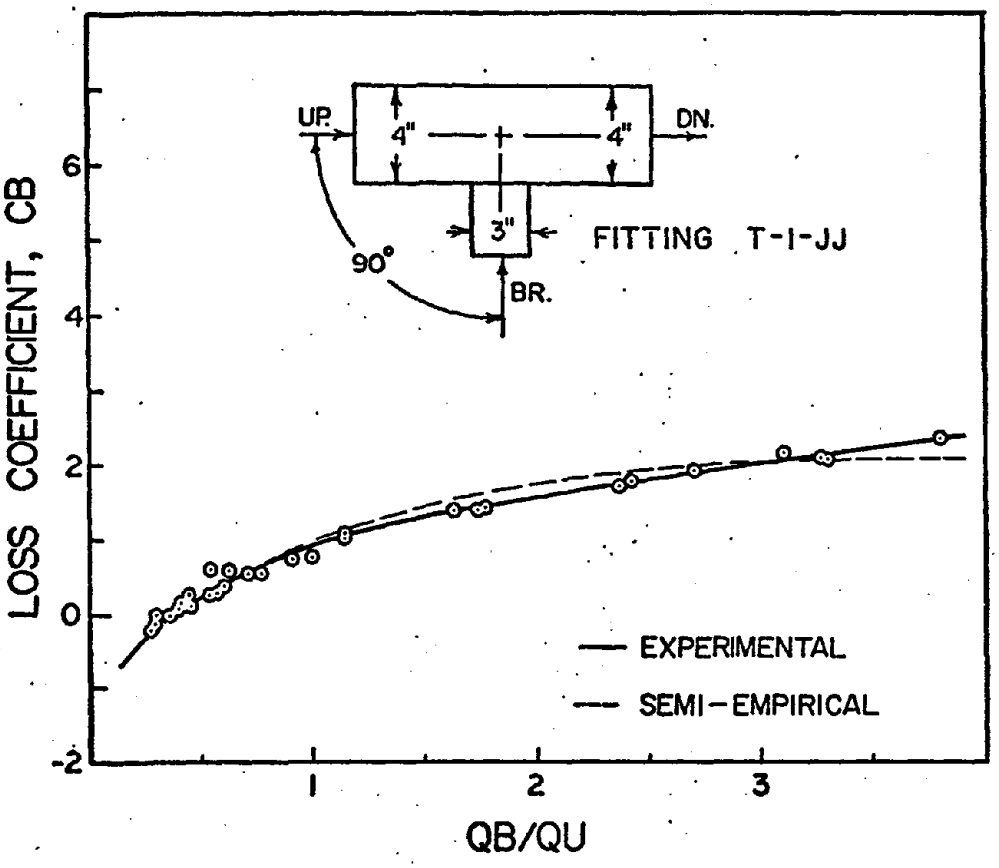

FIGURE A-17 BRANCH LOSS COEFFICIENT VS. THE RATIO OF BRANCH VOLUME FLOW TO THE UPSTREAM VOLUME FLOW

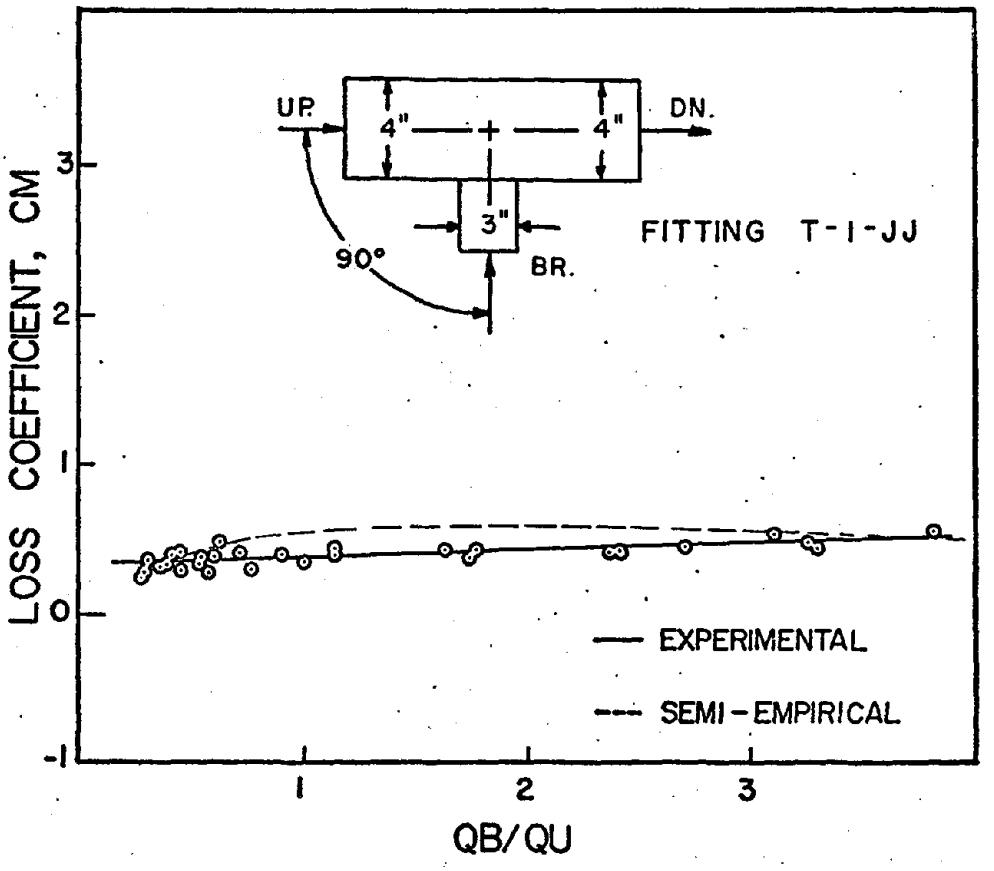

FIGURE A-18 MAIN LOSS COEFFICIENT VS. THE RATIO OF BRANCH VOLUME FLOW TO THE UPSTREAM VOLUME FLOW

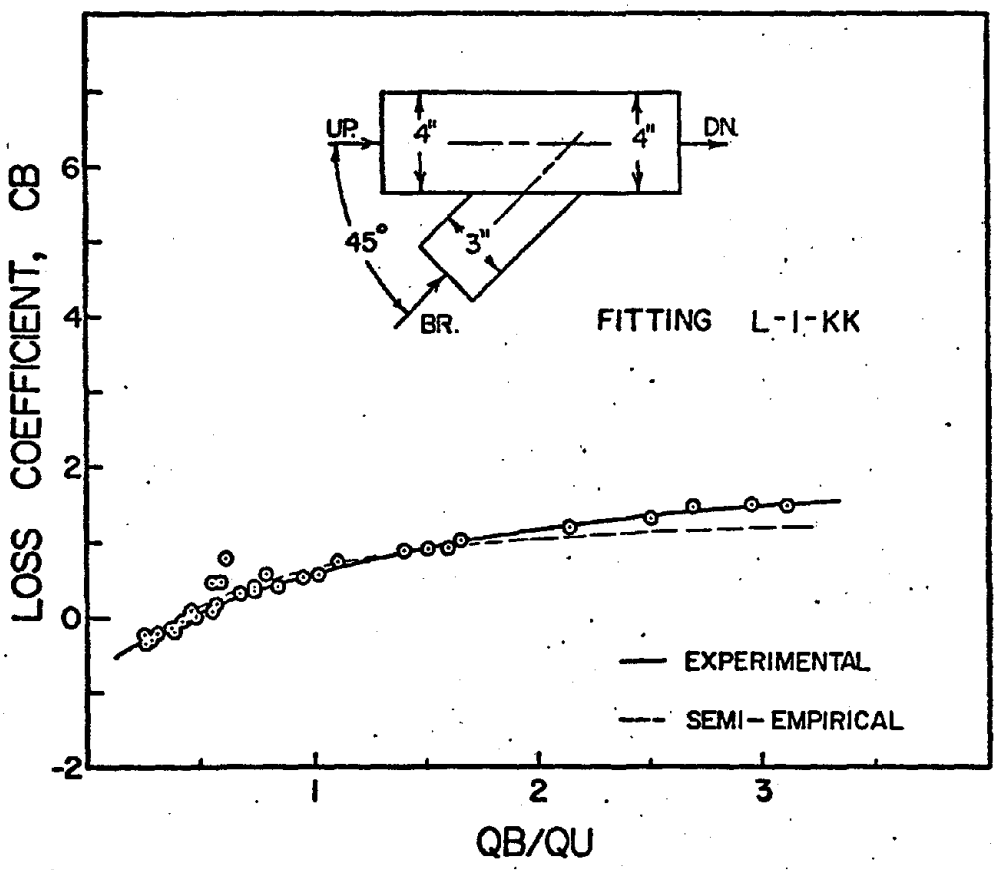

FIGURE A-19 BRANCH LOSS COEFFICIENT VS. THE RATIO OF BRANCH VOLUME FLOW TO THE UPSTREAM VOLUME FLOW

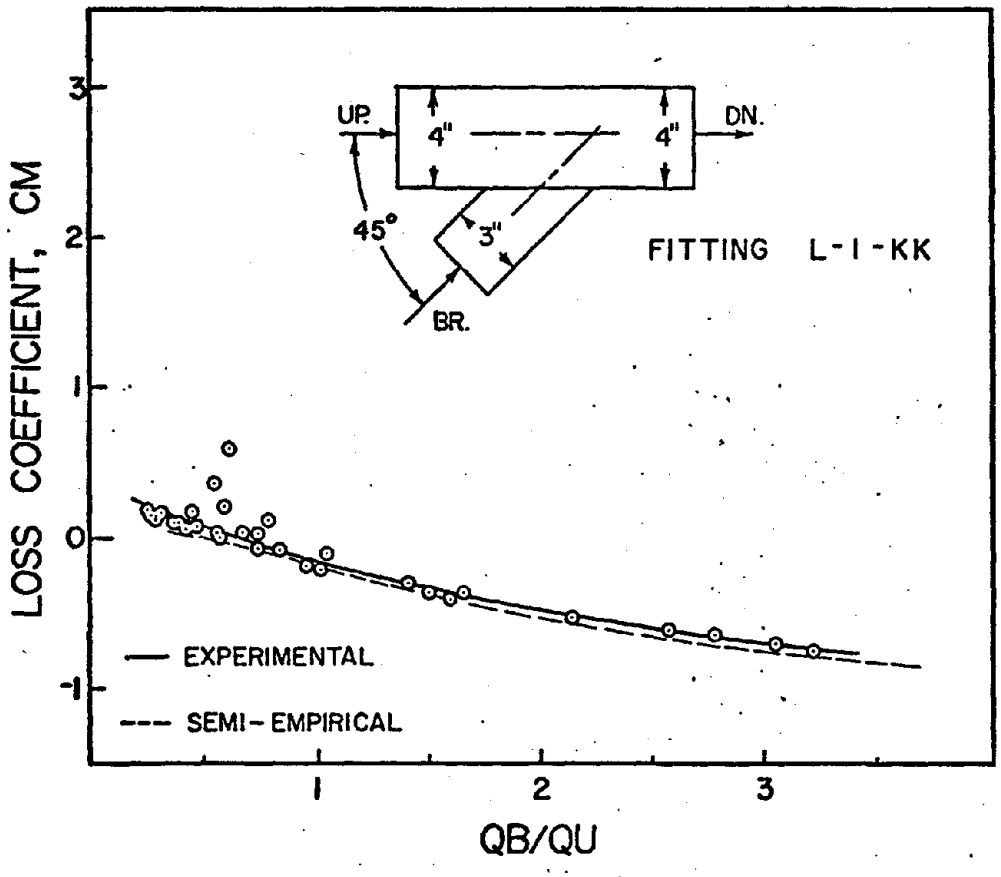

FIGURE A-20 MAIN LOSS COEFFICIENT VS. THE RATIO OF BRANCH VOLUME FLOW TO THE UPSTREAM VOLUME FLOW.

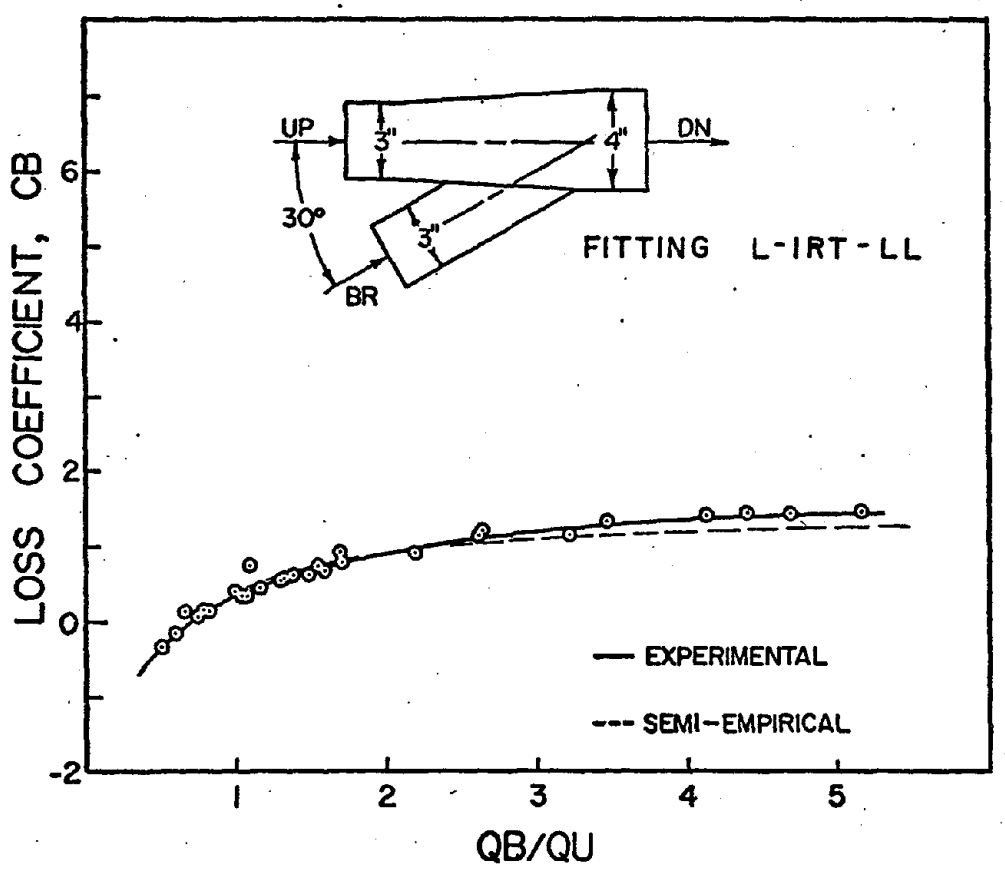

FIGURE A-21 BRANCH LOSS COEFFICIENT VS. THE RATIO OF BRANCH VOLUME FLOW TO THE UPSTREAM VOLUME FLOW

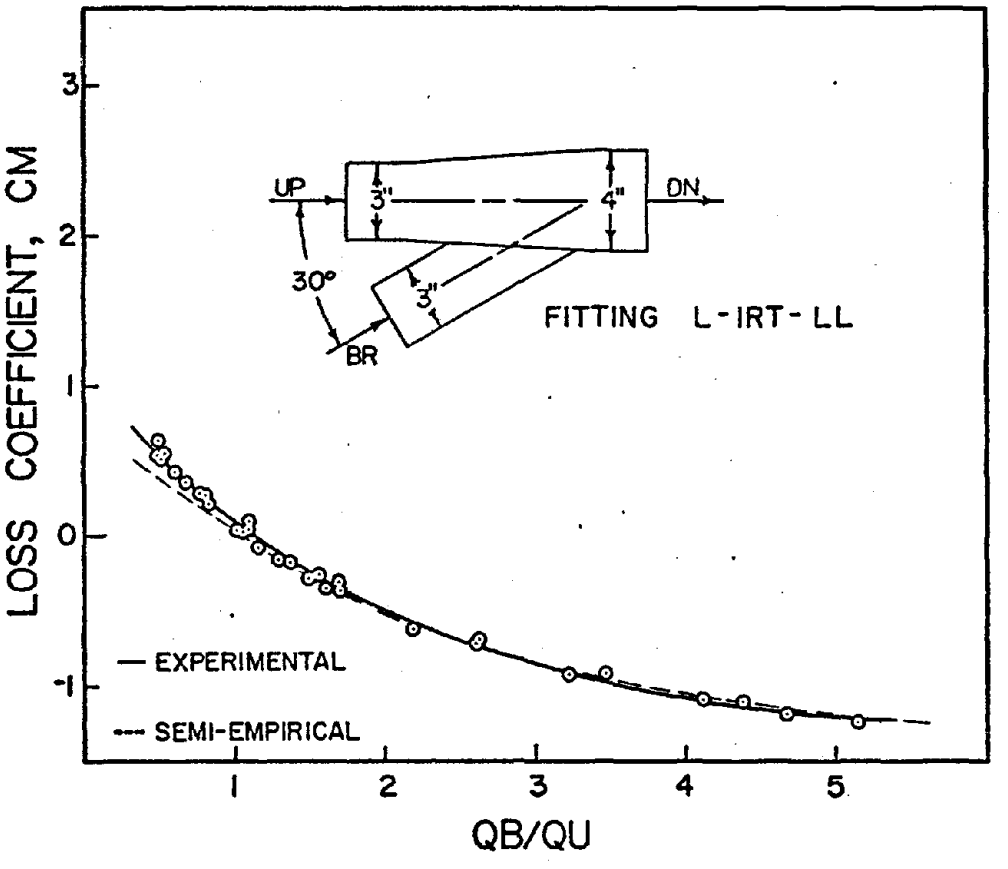

FIGURE A-22 MAIN LOSS COEFFICIENT VS. THE RATIO OF BRANCH VOLUME FLOW TO THE UPSTREAM VOLUME FLOW.

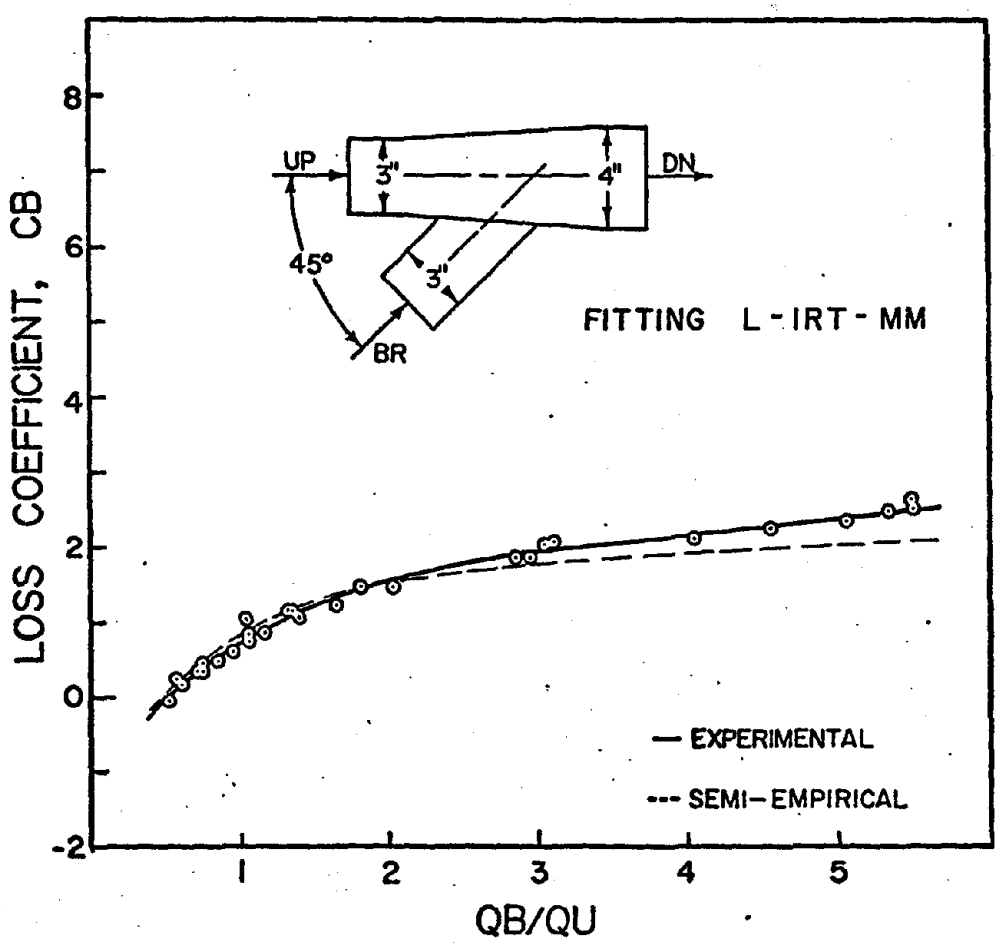

FIGURE A-23 BRANCH LOSS COEFFICIENT VS. THE RATIO OF BRANCH VOLUME FLOW TO THE UPSTREAM VOLUME FLOW

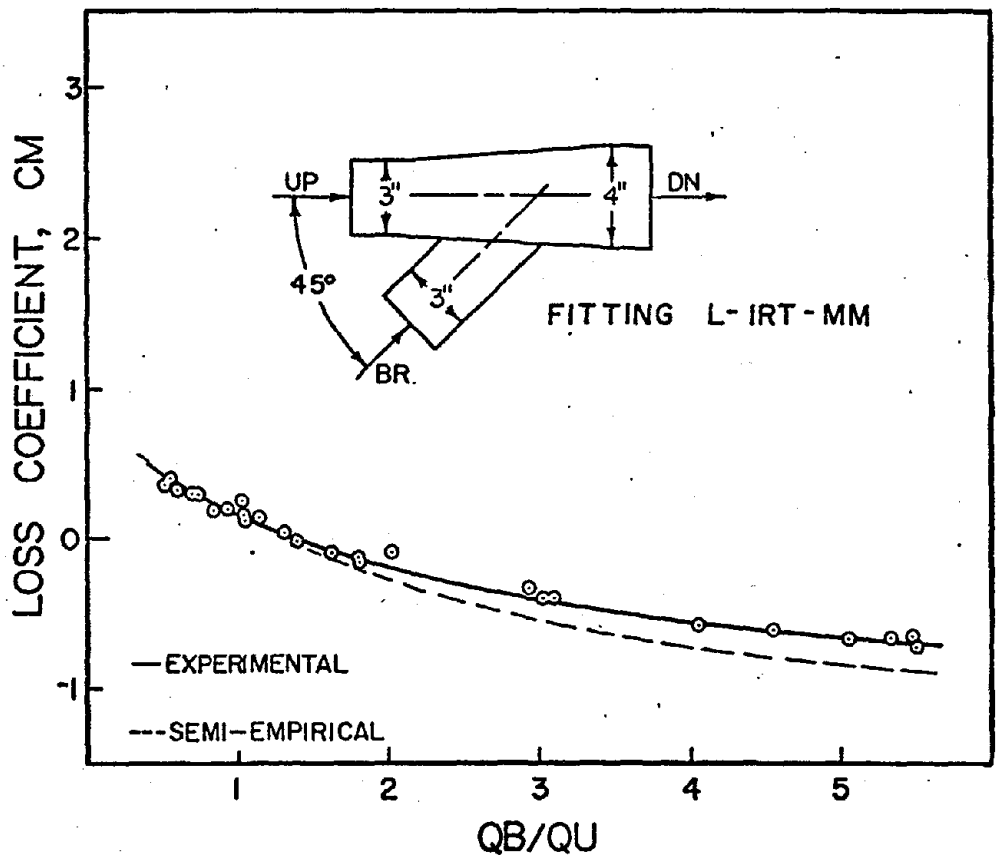

FIGURE A-24 MAIN LOSS COEFFICIENT VS. THE RATIO OF BRANCH VOLUME FLOW TO THE UPSTREAM VOLUME FLOW

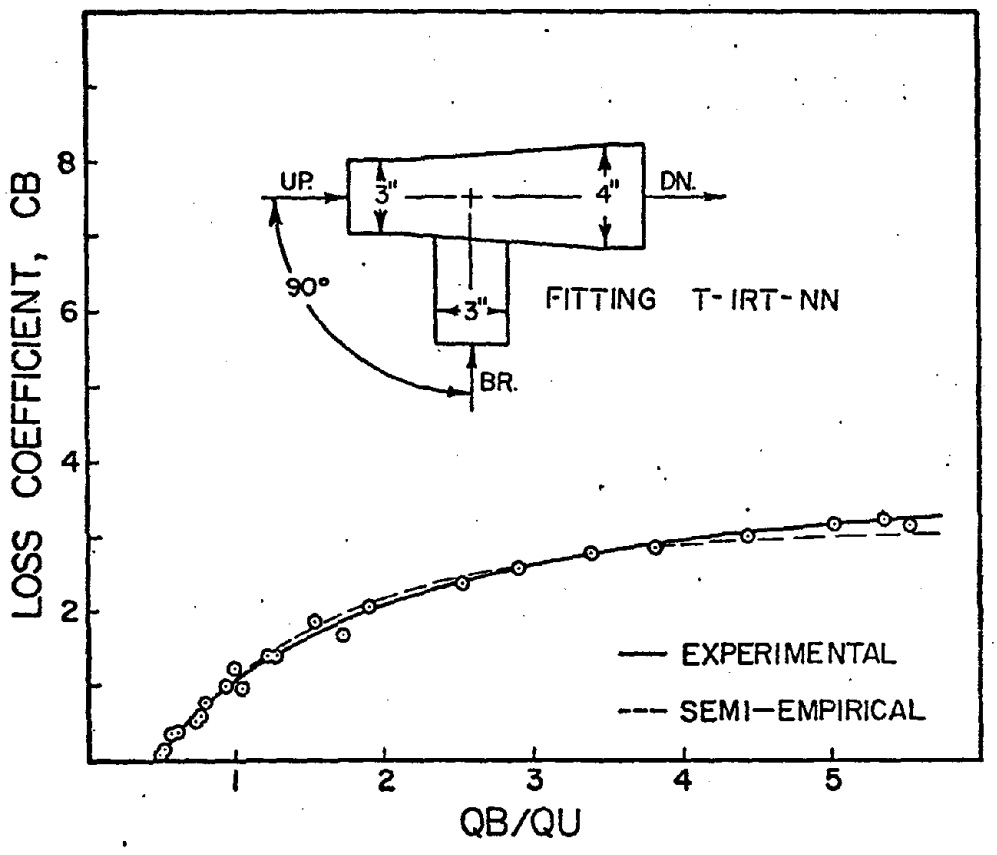

FIGURE A-25 BRANCH LOSS COEFFICIENT VS. THE RATIO OF BRANCH VOLUME FLOW TO THE UPSTREAM VOLUME FLOW

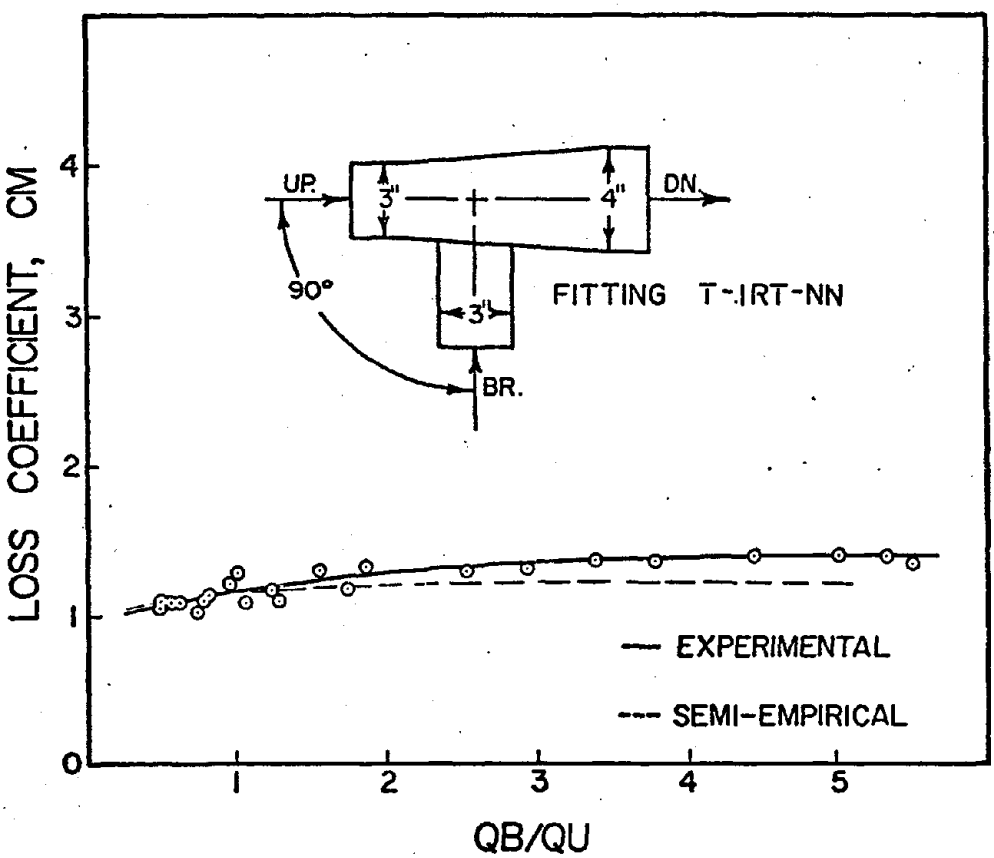

FIGURE A-26 MAIN LOSS COEFFICIENT VS. THE RATIO OF THE BRANCH VOLUME FLOW TO THE UPSTREAM VOLUME FLOW

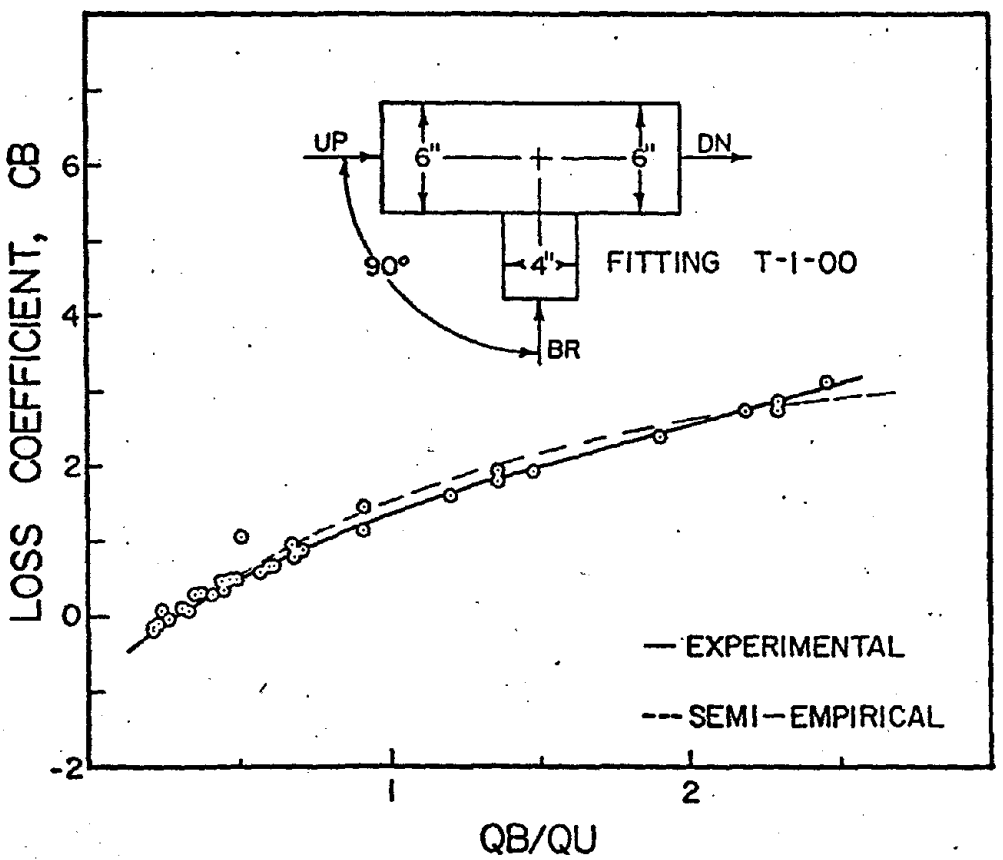

FIGURE A-27 BRANCH LOSS COEFFICIENT VS. THE RATIO OF BRANCH VOLUME FLOW TO THE UPSTREAM VOLUME FLOW

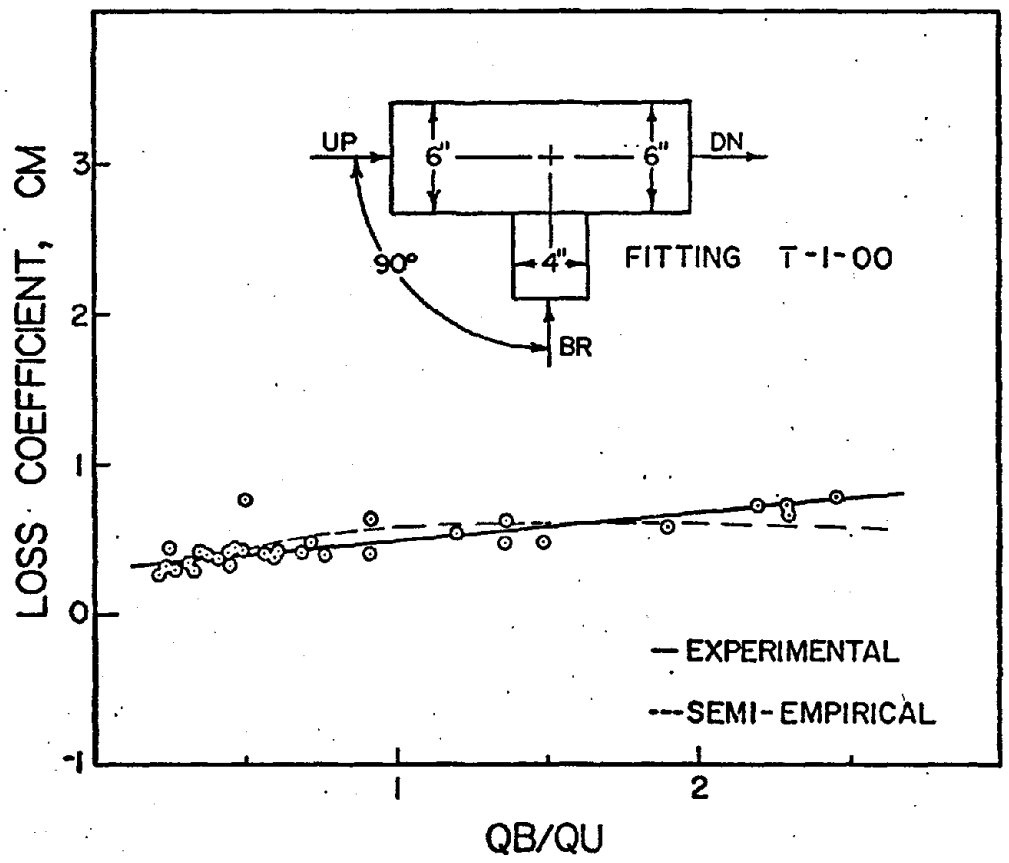

FIGURE A-28 MAIN LOSS COEFFICIENT VS. THE RATIO OF BRANCH VOLUME FLOW TO THE UPSTREAM VOLUME FLOW

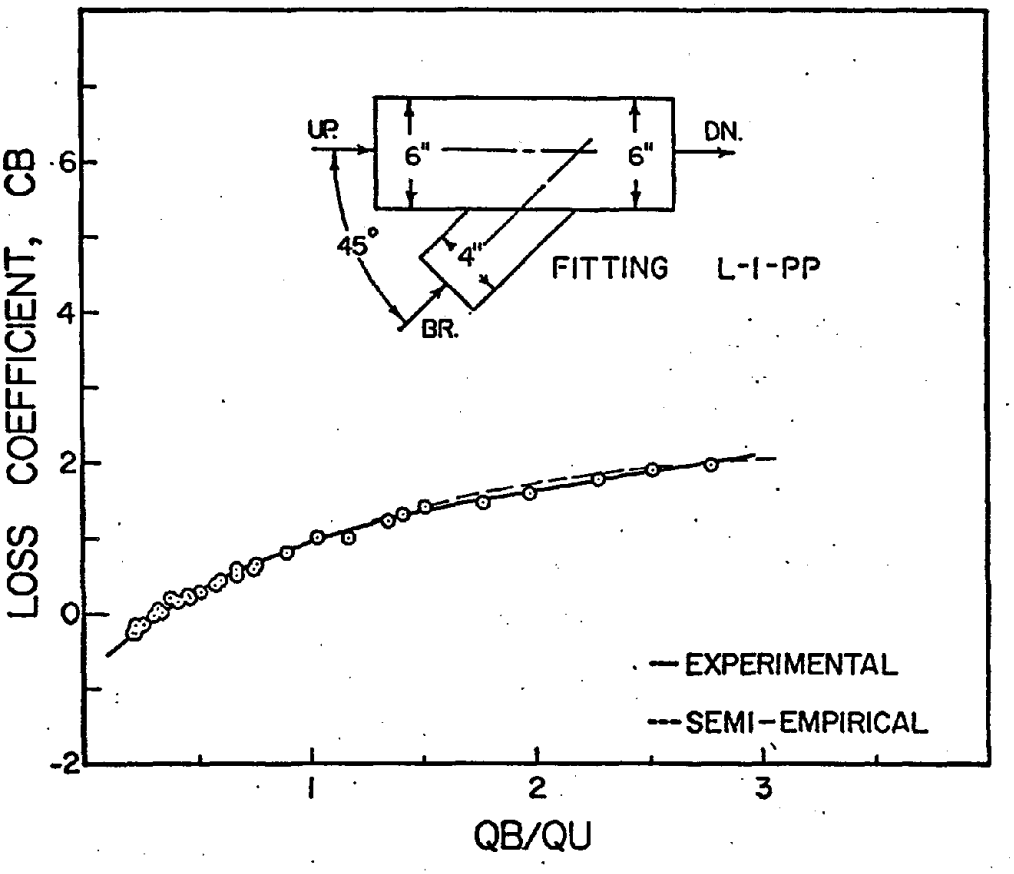

FIGURE A-29 BRANCH LOSS COEFFICIENT VS. THE RATIO OF THE BRANCH VOLUME FLOW TO THE UPSTREAM VOLUME FLOW

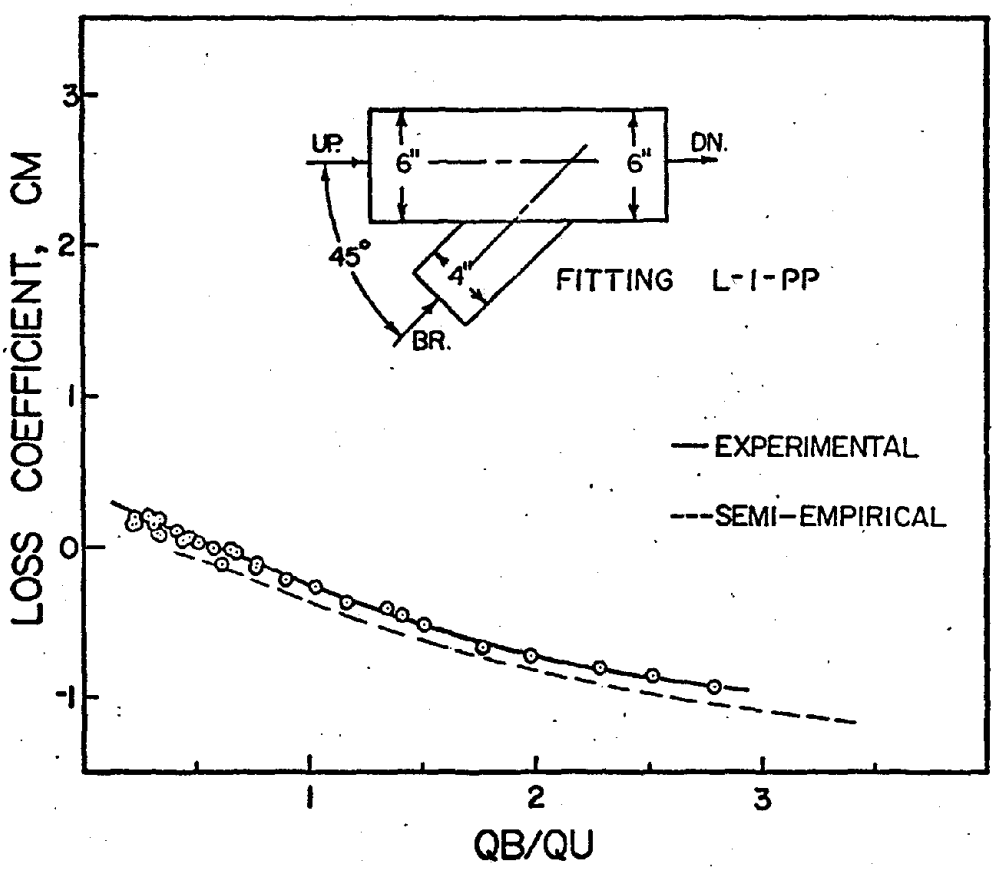

FIGURE A-30 MAIN LOSS COEFFICIENT VS. THE RATIO OF THE BRANCH VOLUME FLOW TO THE UPSTREAM VOLUME FLOW

12/

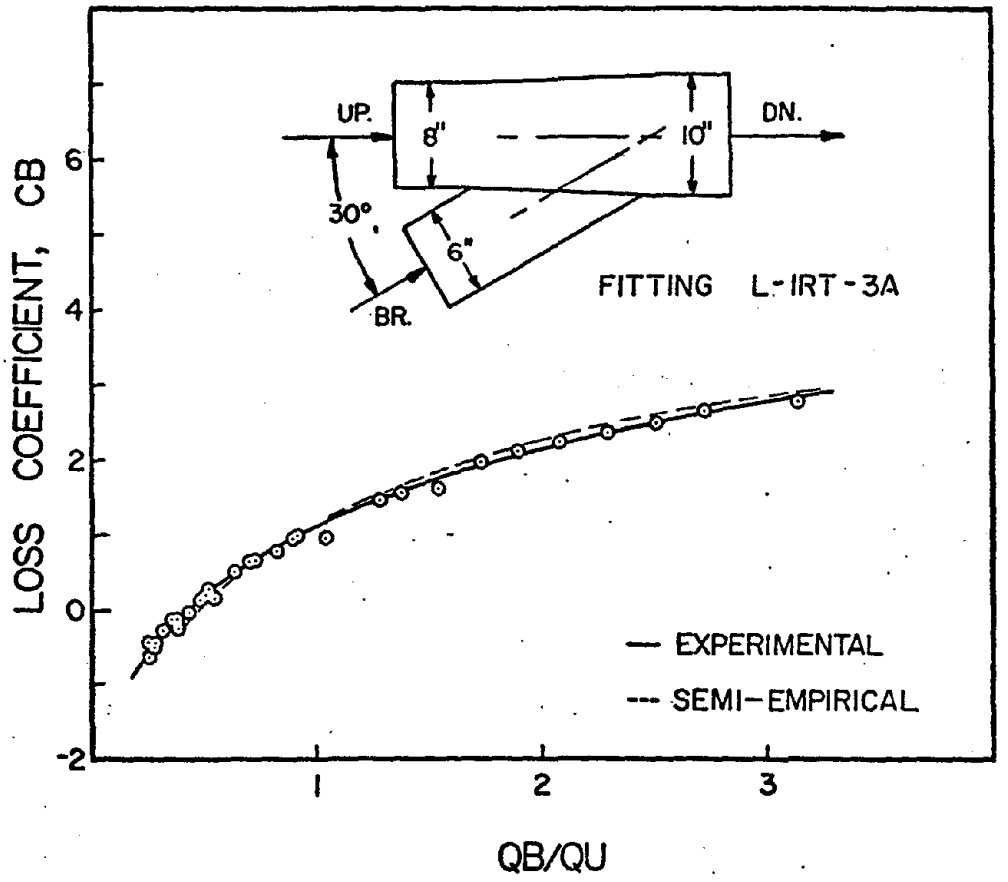

FIGURE A-31 BRANCH LOSS COEFFICIENT VS. THE RATIO OF BRANCH VOLUME FLOW TO UPSTREAM VOLUME FLOW

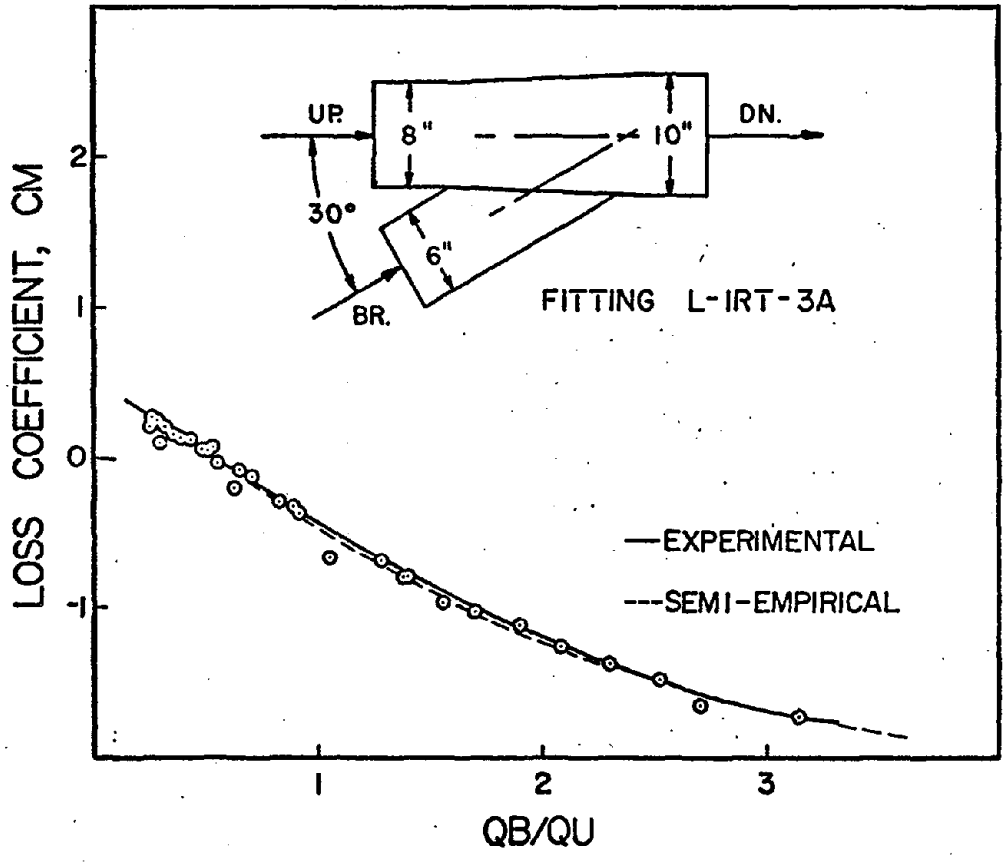

FIGURE A-32 MAIN LOSS COEFFICIENT VS. THE RATIO OF BRANCH VOLUME FLOW TO THE UPSTREAM VOLUME FLOW

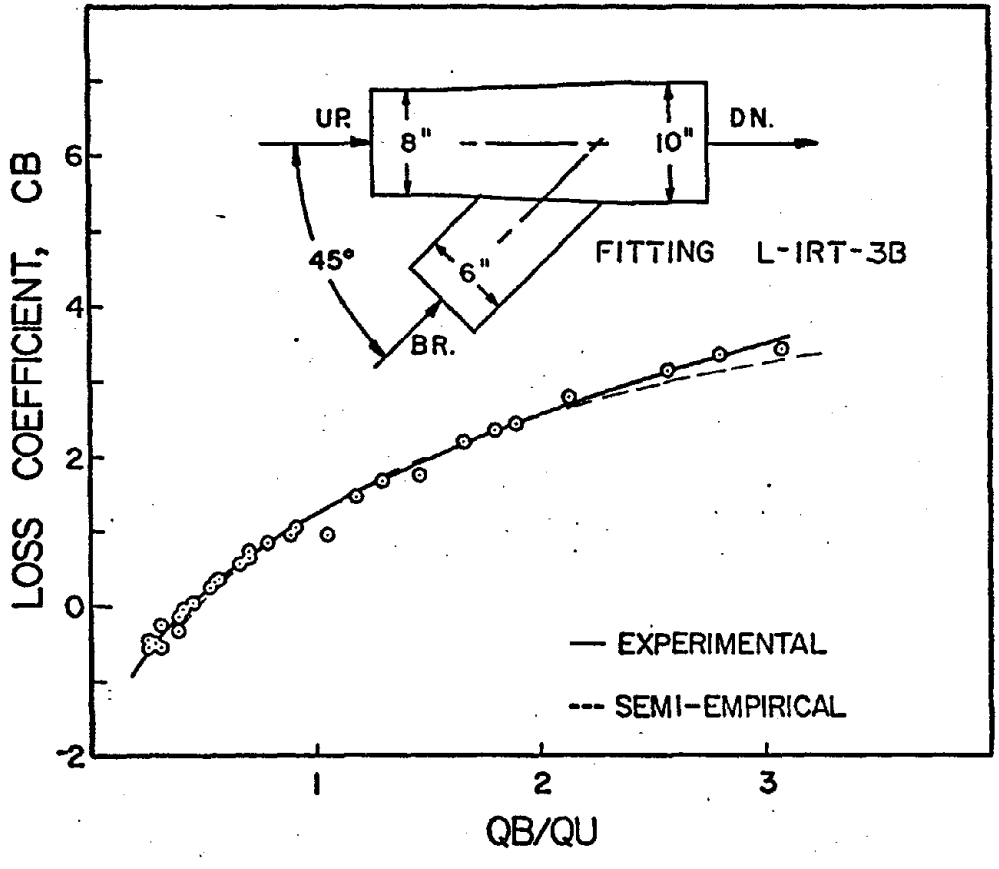

FIGURE A-33 BRANCH LOSS COEFFICIENT VS. THE RATIO OF BRANCH VOLUME FLOW TO THE UPSTREAM VOLUME FLOW

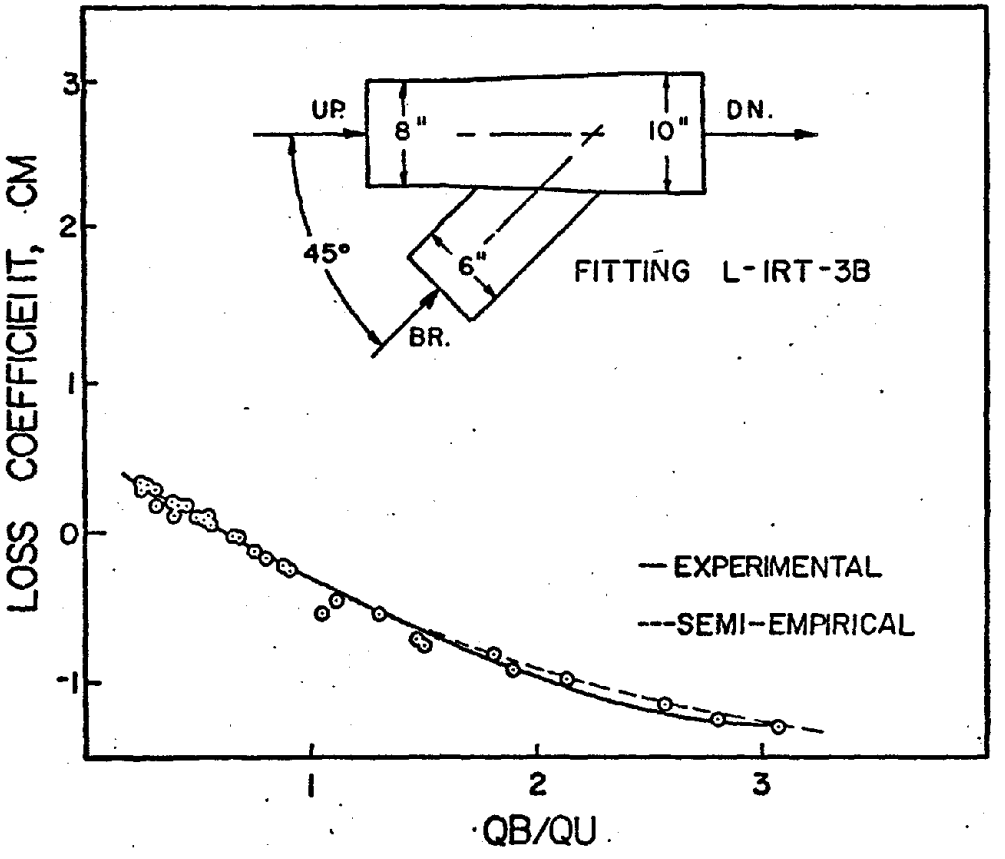

FIGURE A-34 MAIN LOSS COEFFICIENT VS. THE RATIO OF BRANCH VOLUME FLOW TO THE UPSTREAM VOLUME FLOW

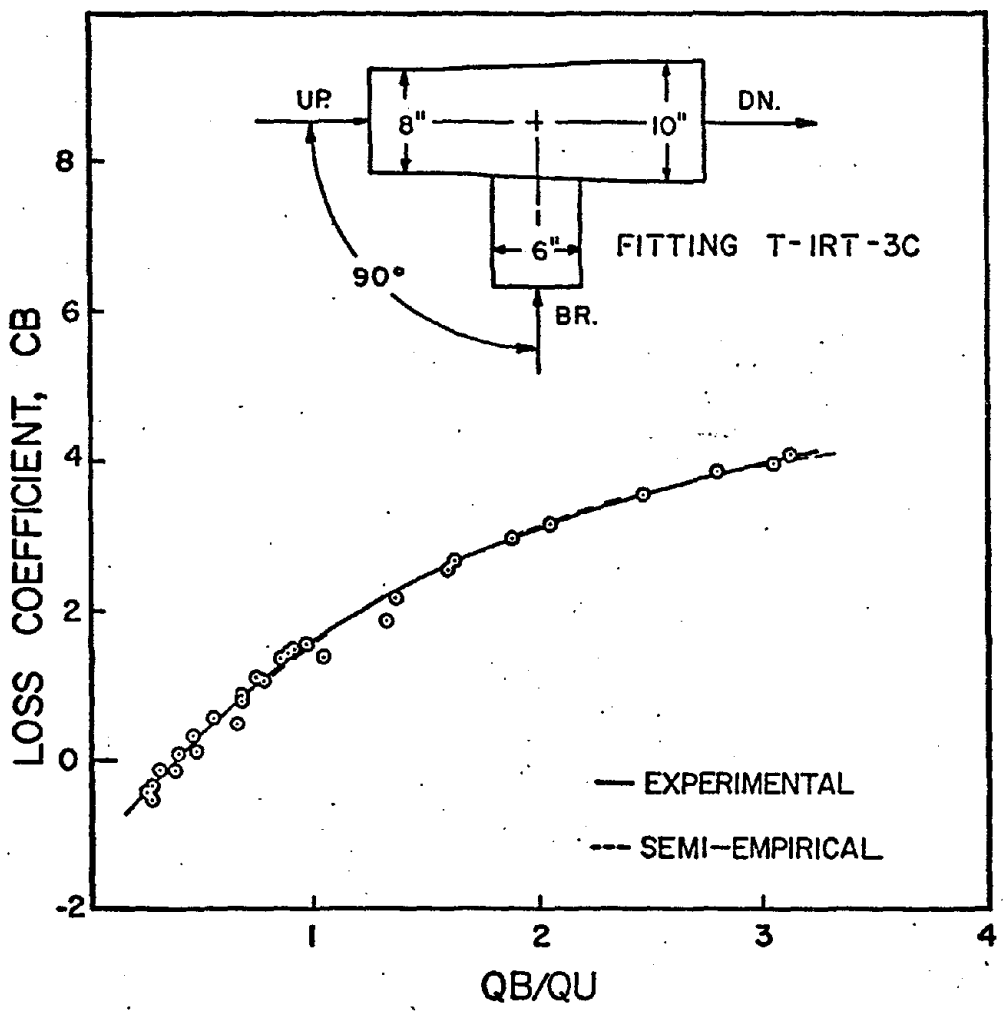

FIGURE A-35 BRANCH LOSS COEFFICIENT VS. THE RATIO OF BRANCH VOLUME FLOW TO THE UPSTREAM VOLUME FLOW

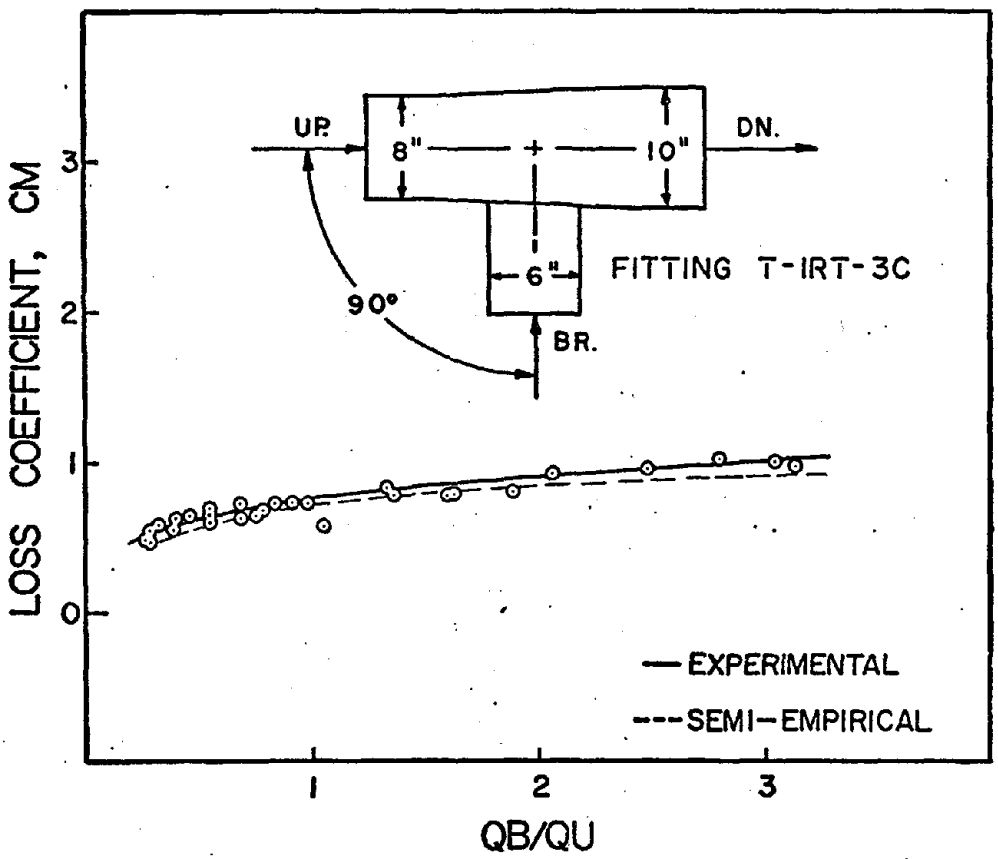

FIGURE A-36 MAIN LOSS COEFFICIENT VS. THE RATIO OF BRANCH VOLUME FLOW TO THE UPSTREAM VOLUME FLOW

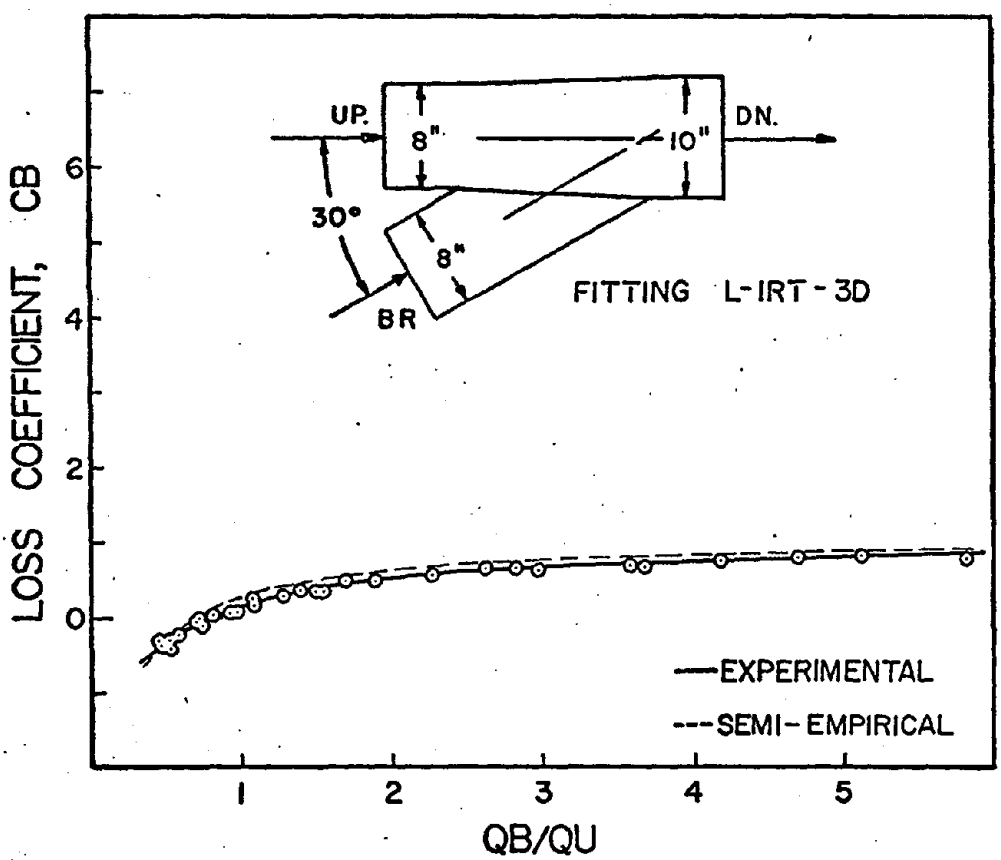

FIGURE A-37 BRANCH LOSS COEFFICIENT VS. THE RATIO OF BRANCH VOLUME FLOW TO THE UPSTREAM VOLUME FLOW

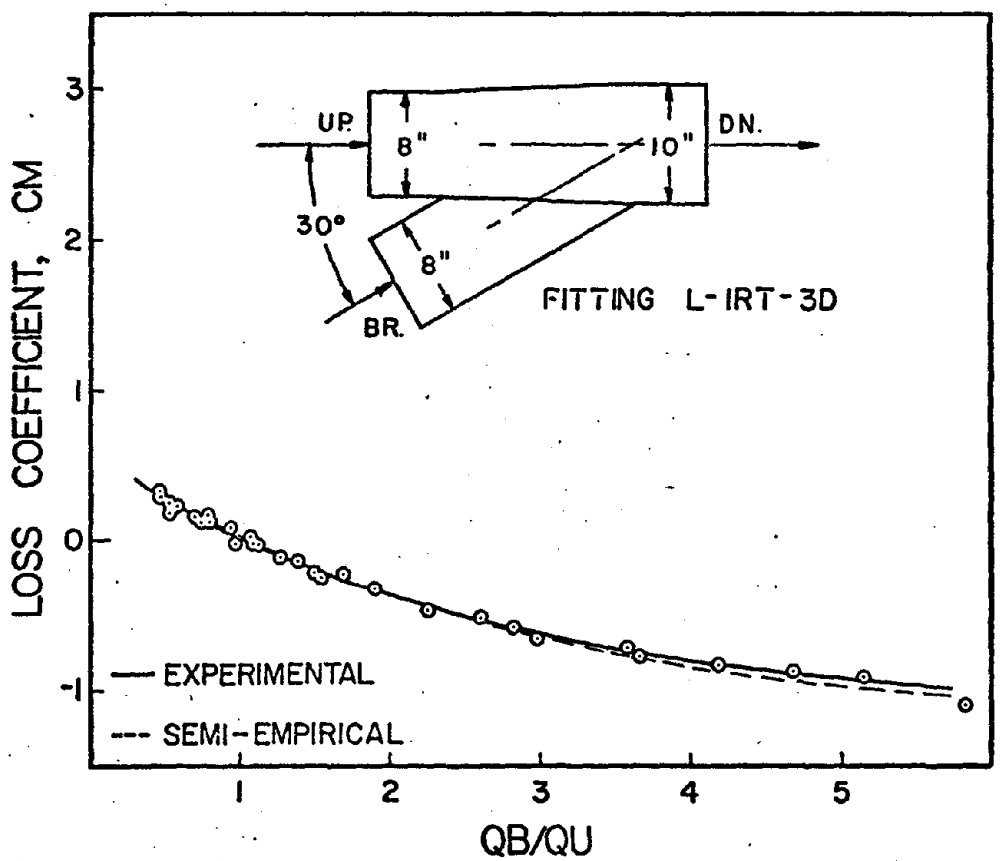

FIGURE A-38 MAIN LOSS COEFFICIENT VS. THE RATIO OF BRANCH VOLUME FLOW TO THE UPSTREAM VOLUME FLOW

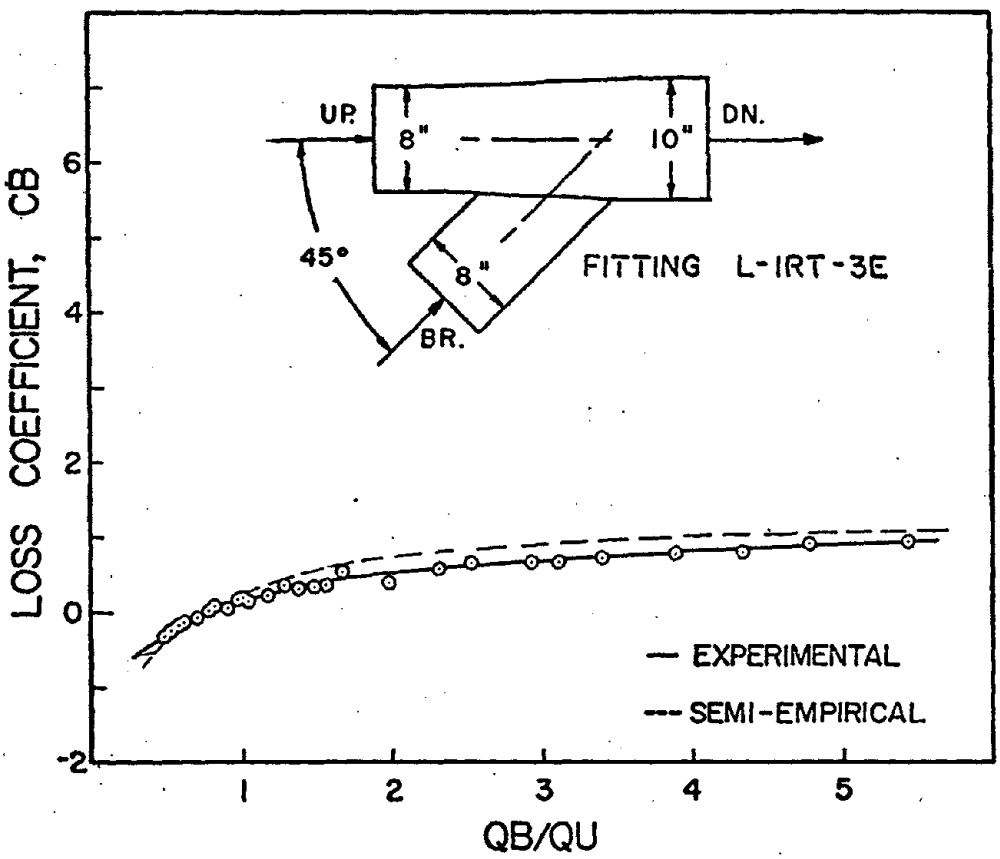

FIGURE A-39 BRANCH LOSS COEFFICIENT VS. THE RATIO OF BRANCH VOLUME FLOW TO THE UPSTREAM VOLUME FLOW

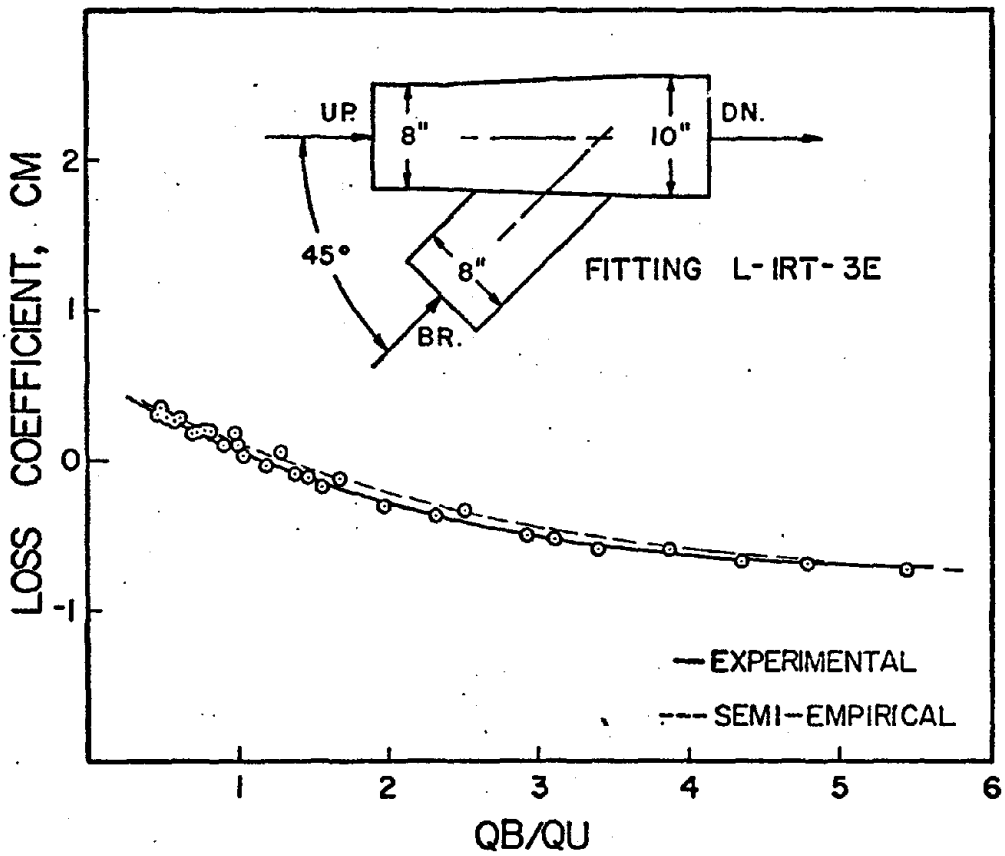

FIGURE A-40 MAIN LOSS COEFFICIENT VS. THE RATIO OF BRANCH VOLUME FLOW TO THE UPSTREAM VOLUME FLOW

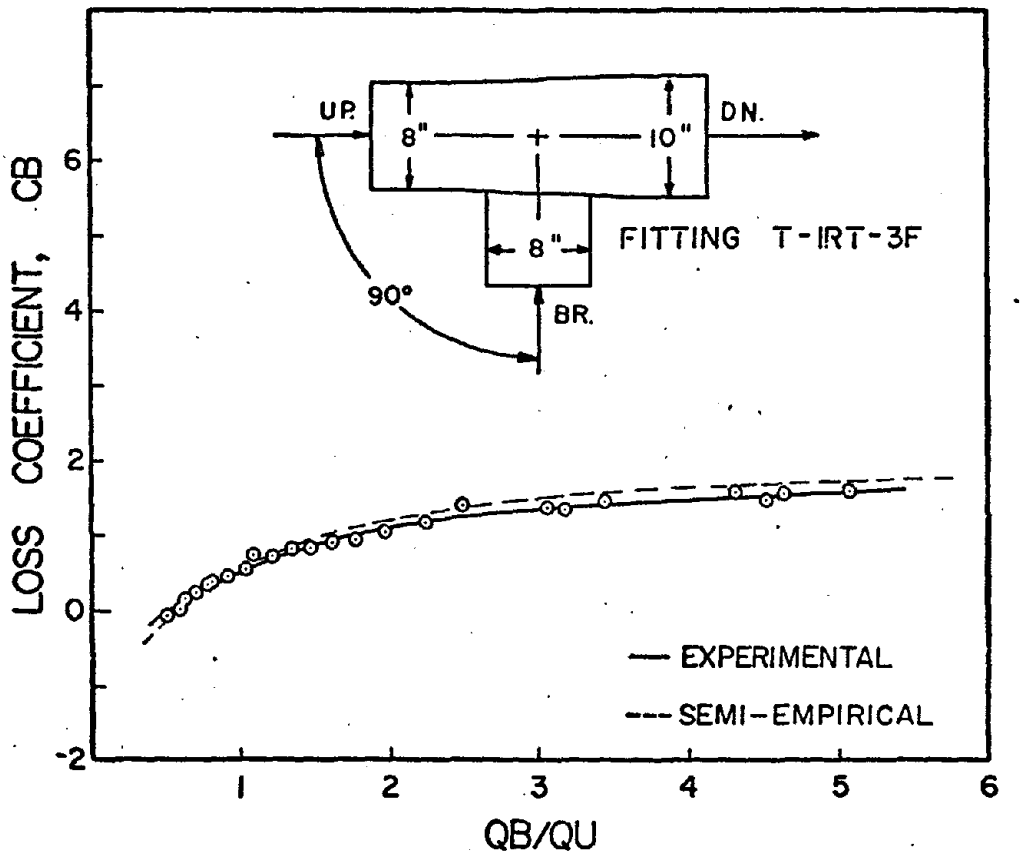

FIGURE A-41 BRANCH LOSS COEFFICIENT VS. THE RATIO OF BRANCH VOLUME FLOW TO THE UPSTREAM VOLUME FLOW

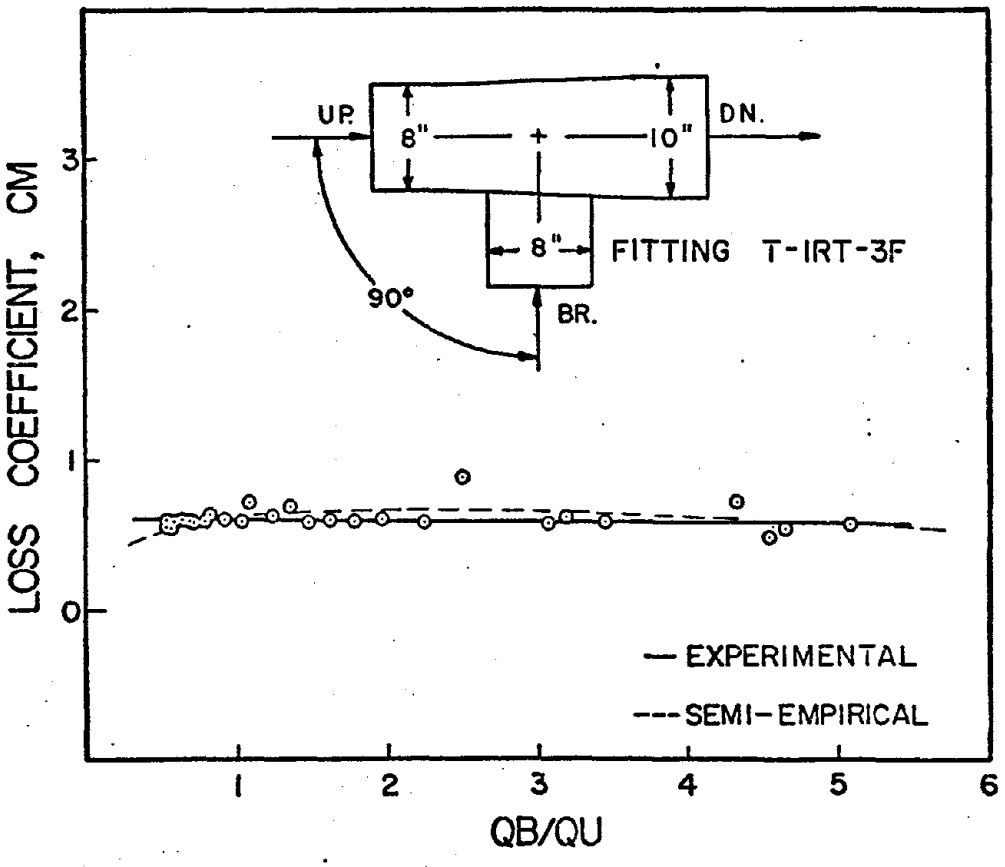

FIGURE A-42 MAIN LOSS COEFFICIENT VS. THE RATIO OF BRANCH VOLUME FLOW TO THE UPSTREAM VOLUME FLOW

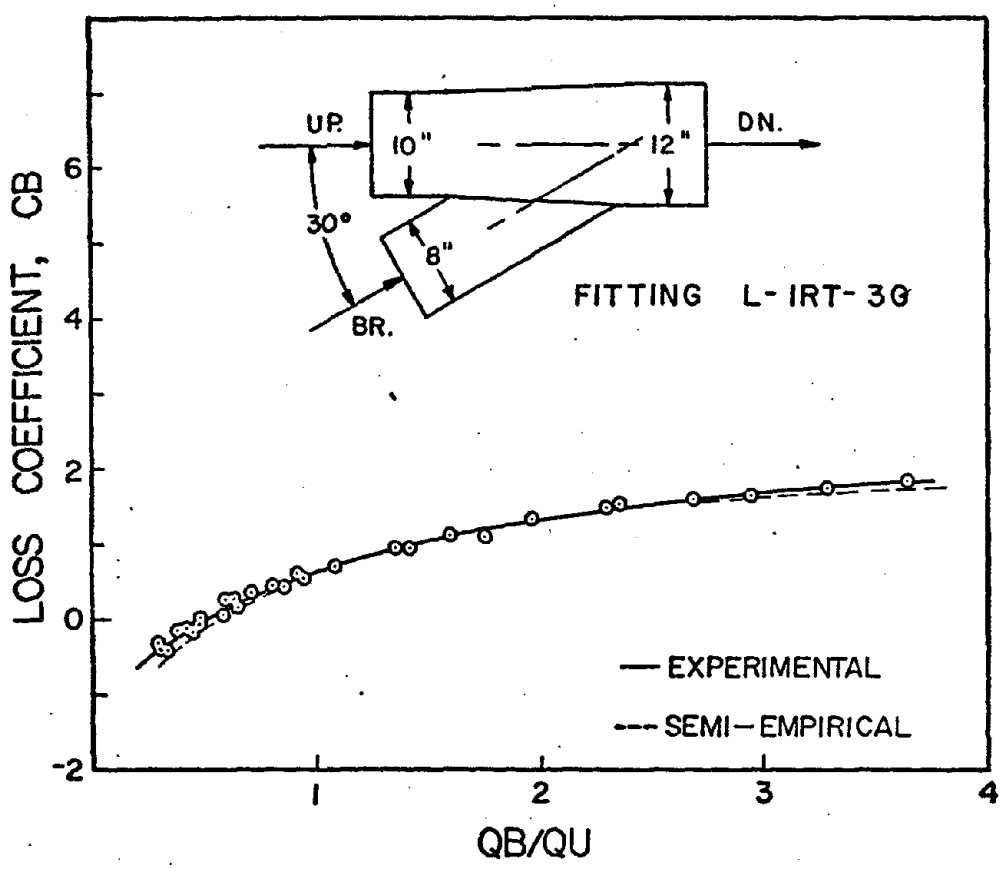

FIGURE A-43 BRANCH LOSS COEFFICIENT VS. THE RATIO OF BRANCH VOLUME FLOW TO THE UPSTREAM VOLUME FLOW

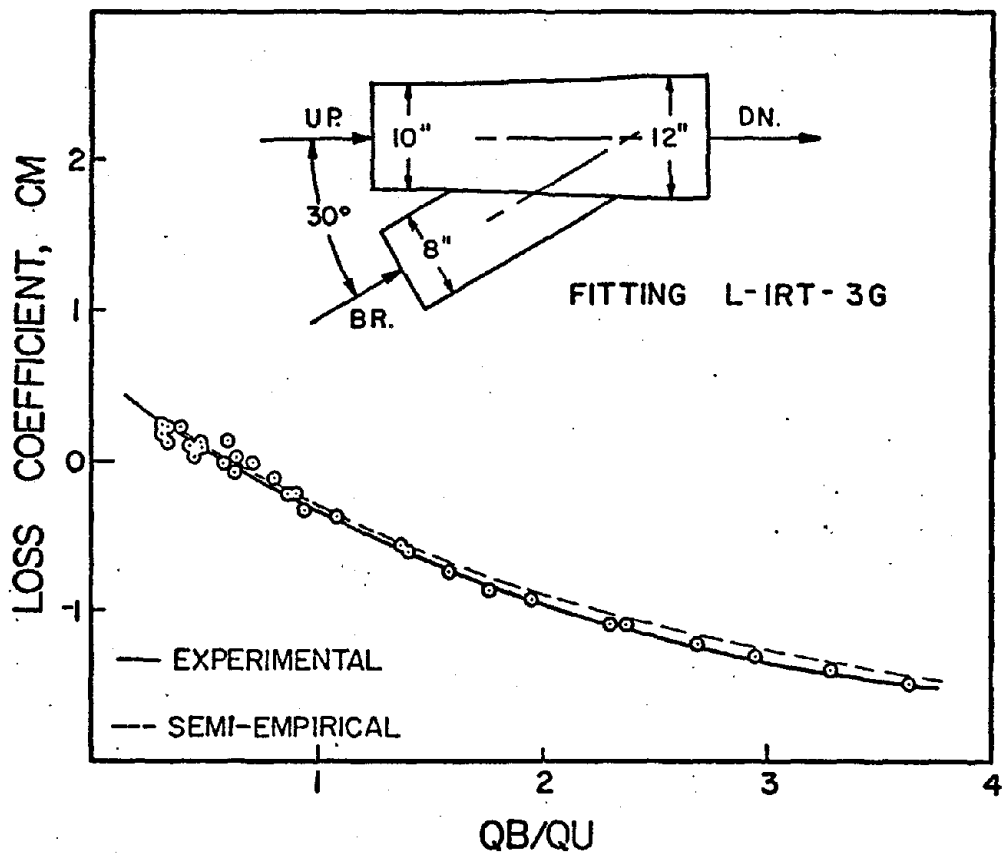

FIGURE A-44 MAIN LOSS COEFFICIENT VS. THE RATIO OF BRANCH VOLUME FLOW TO THE UPSTREAM VOLUME FLOW

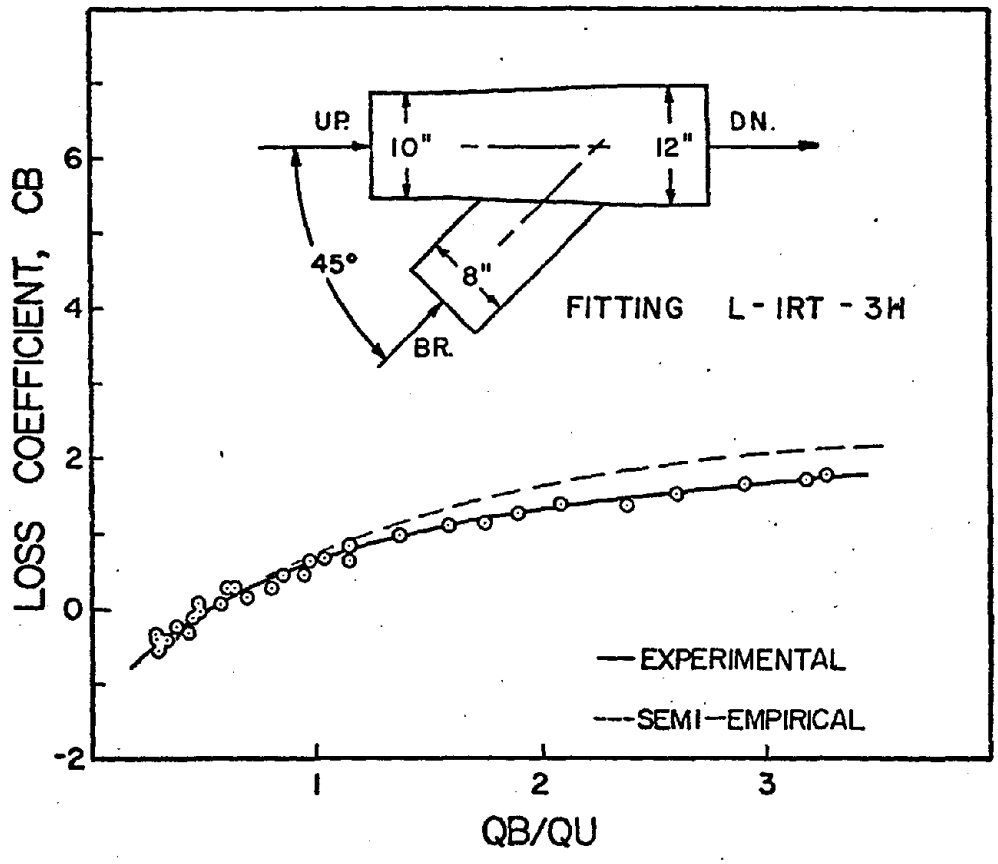

FIGURE A-45 BRANCH LOSS COEFFICIENT VS. THE RATIO OF BRANCH VOLUME FLOW TO THE UPSTREAM VOLUME FLOW

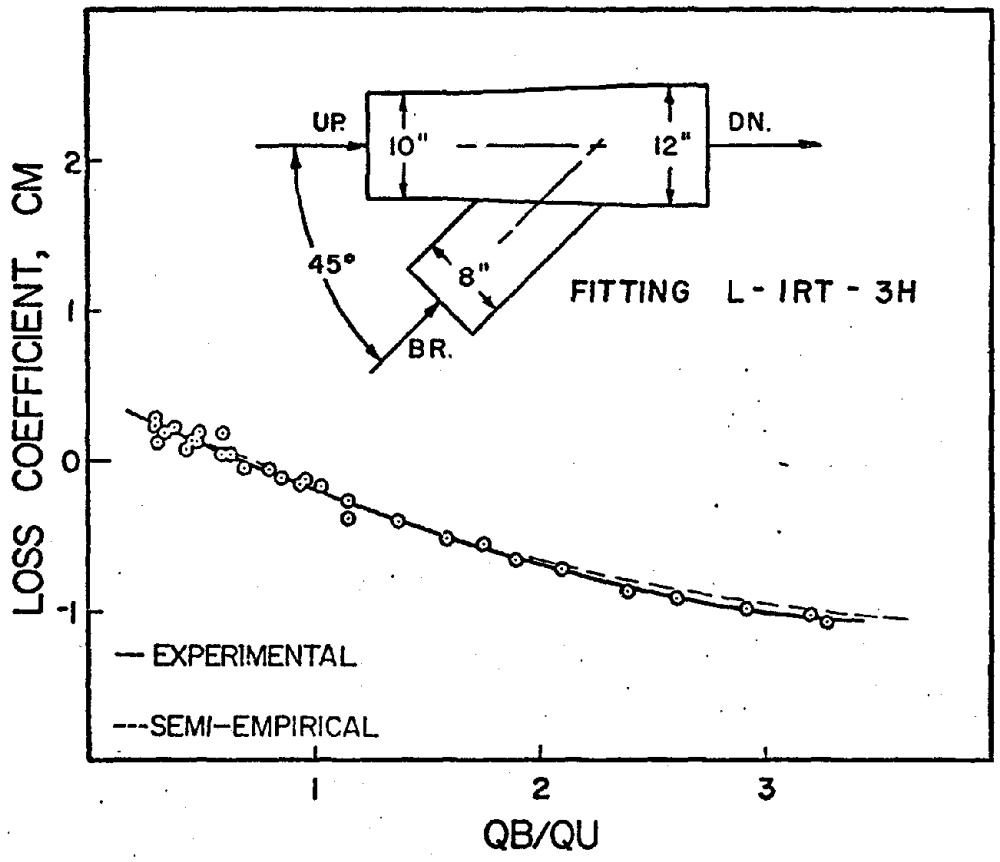

FIGURE A-46 MAIN LOSS COEFFICIENT VS. THE RATIO OF BRANCH VOLUME FLOW TO THE UPSTREAM VOLUME FLOW

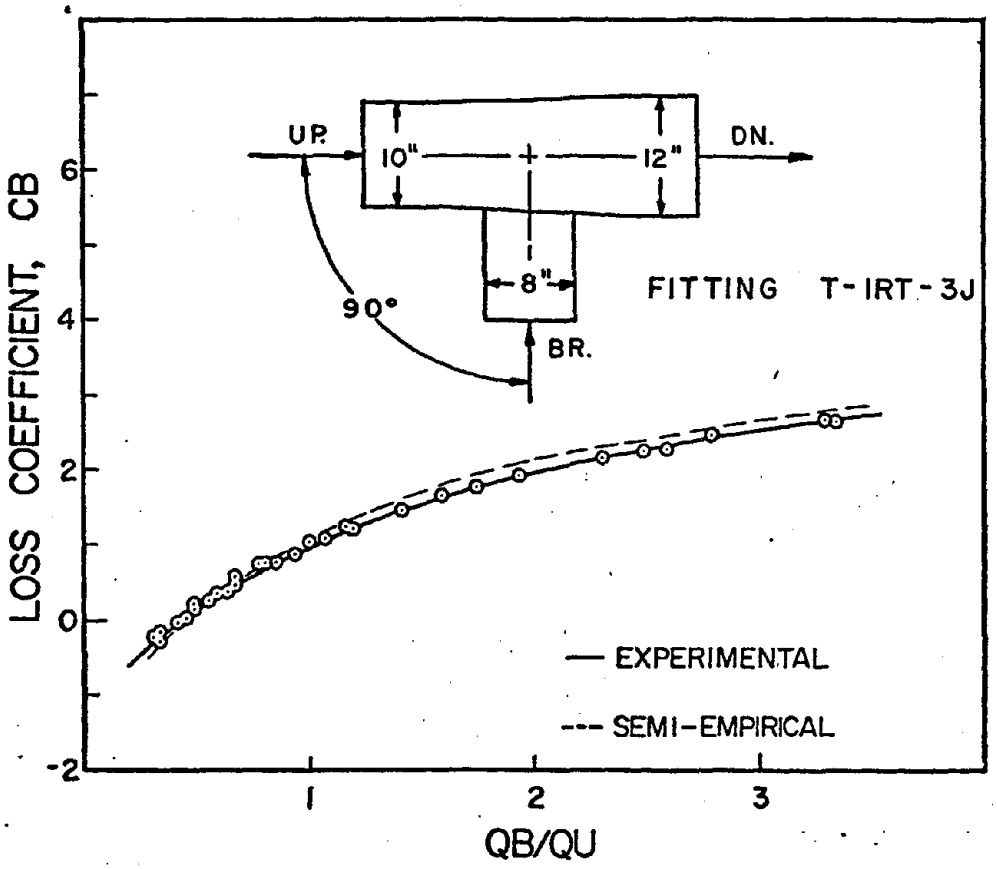

FIGURE A-47 BRANCH LOSS COEFFICIENT VS. THE RATIO OF BRANCH VOLUME FLOW TO THE UPSTREAM VOLUME FLOW

14

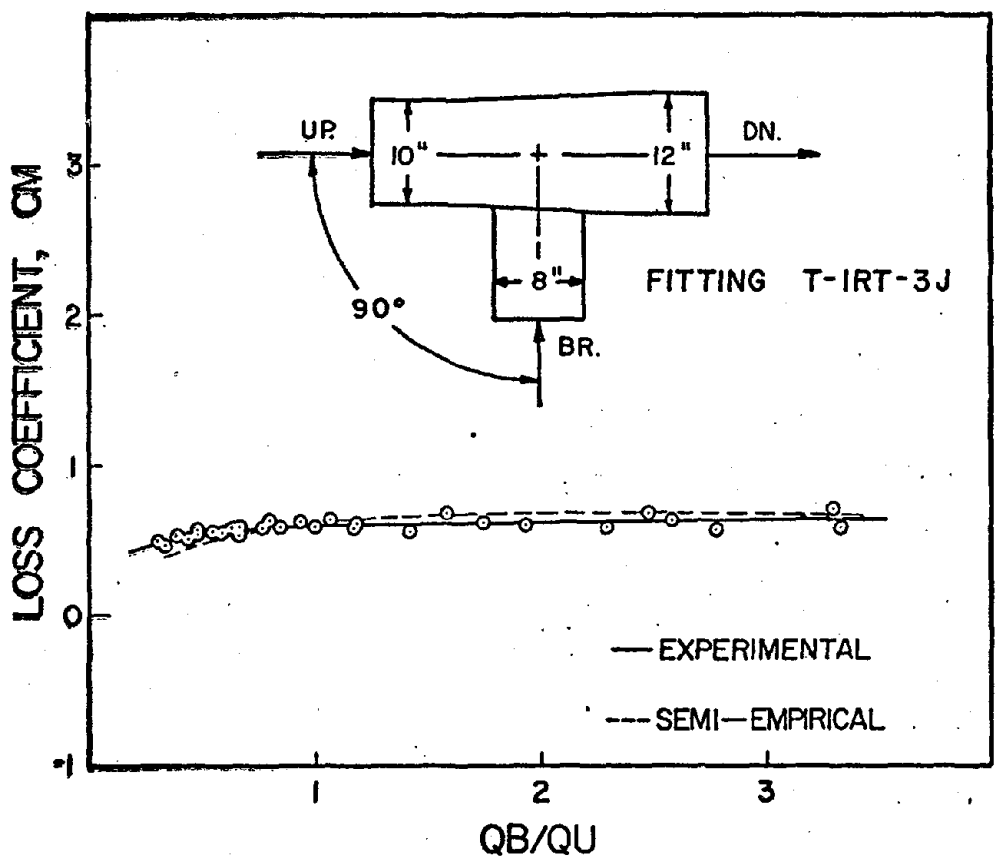

FIGURE A-48 MAIN LOSS COEFFICIENT VS. THE RATIO OF BRANCH VOLUME FLOW TO THE UPSTREAM VOLUME FLOW

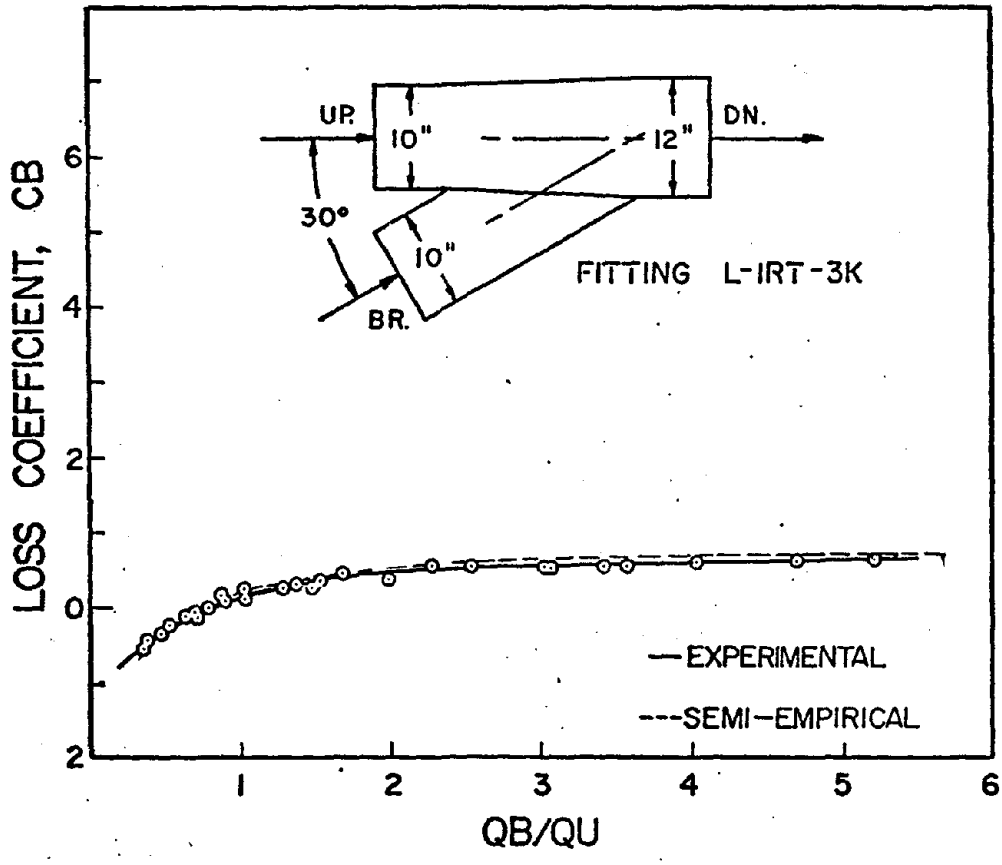

FIGURE A-49 BRANCH LOSS COEFFICIENT VS. THE RATIO OF BRANCH VOLUME FLOW TO THE UPSTREAM VOLUME FLOW

14

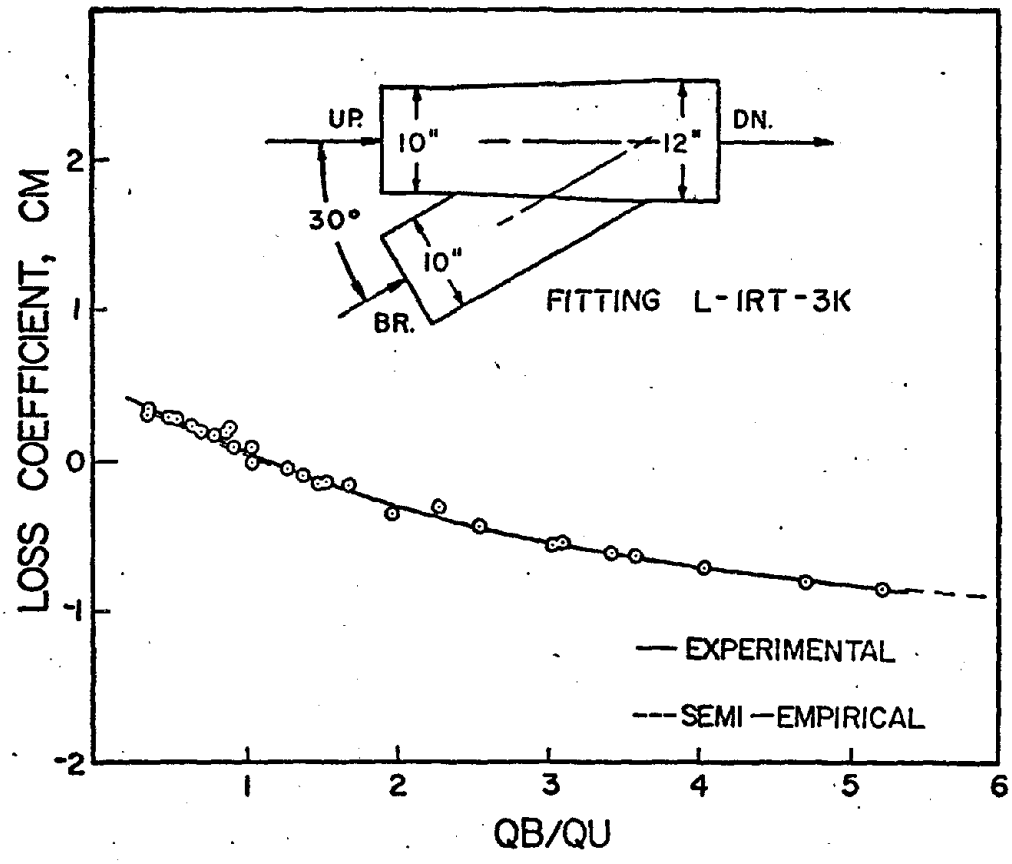

FIGURE A-50 MAIN LOSS COEFFICIENT VS. THE RATIO OF BRANCH VOLUME FLOW TO THE UPSTREAM VOLUME FLOW

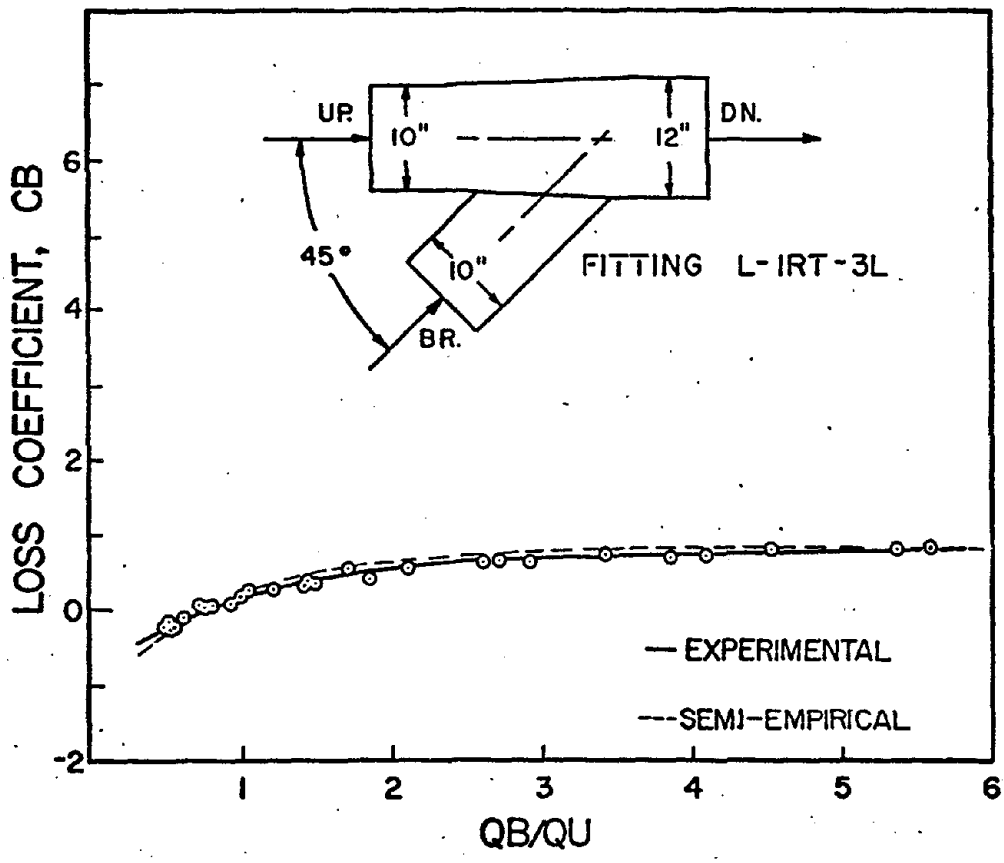

FIGURE A-51 BRANCH LOSS COEFFICIENT VS. THE RATIO OF BRANCH VOLUME FLOW TO THE UPSTREAM VOLUME FLOW

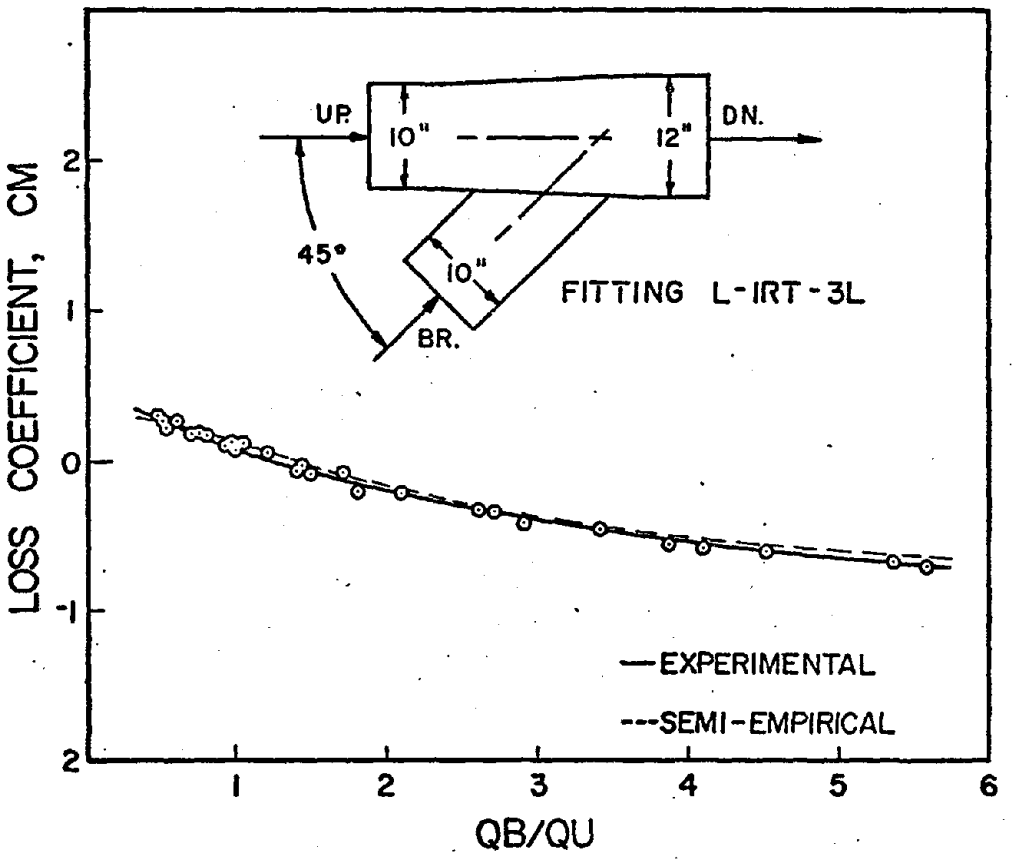

FIGURE A-52 MAIN LOSS COEFFICIENT VS. THE RATIO OF BRANCH VOLUME FLOW TO THE UPSTREAM VOLUME FLOW

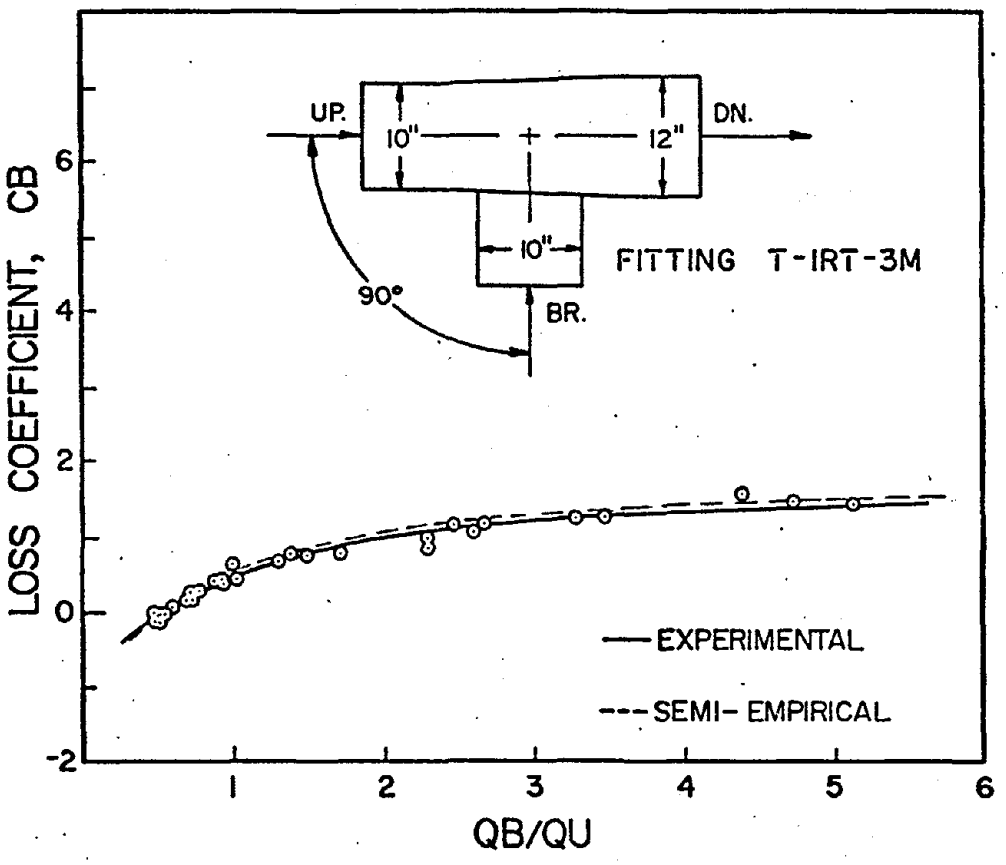

FIGURE A-53 BRANCH LOSS COEFFICIENT VS. THE RATIO OF BRANCH VOLUME FLOW TO THE UPSTREAM VOLUME FLOW

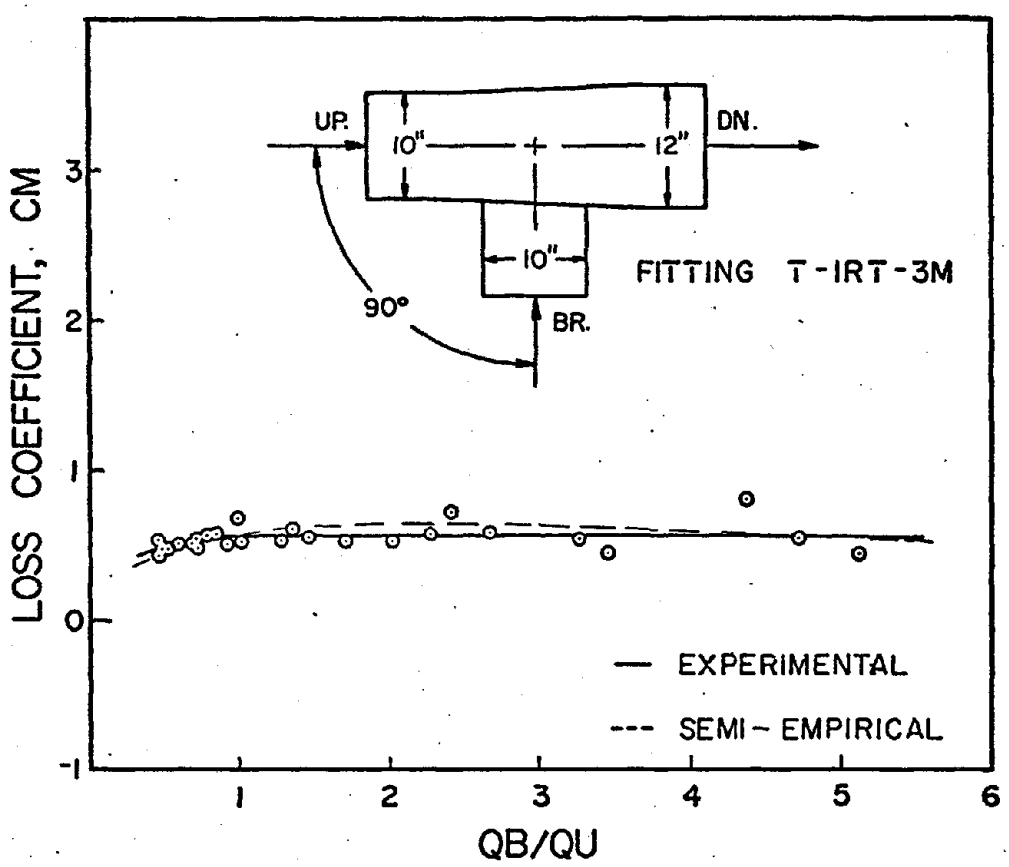

FIGURE A-54 MAIN LOSS COEFFICIENT VS. THE RATIO OF BRANCH VOLUME FLOW TO THE UPSTREAM VOLUME FLOW

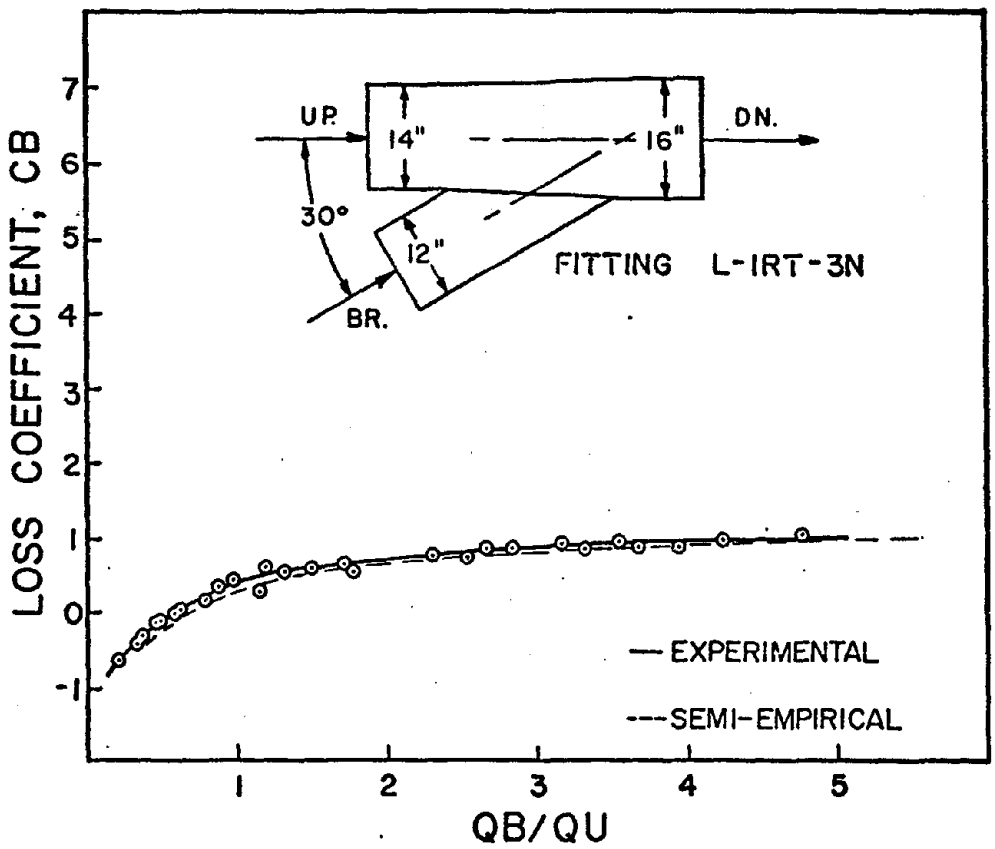

FIGURE A-55 BRANCH LOSS COEFFICIENT VS. THE RATIO OF BRANCH VOLUME FLOW TO THE UPSTREAM VOLUME FLOW.

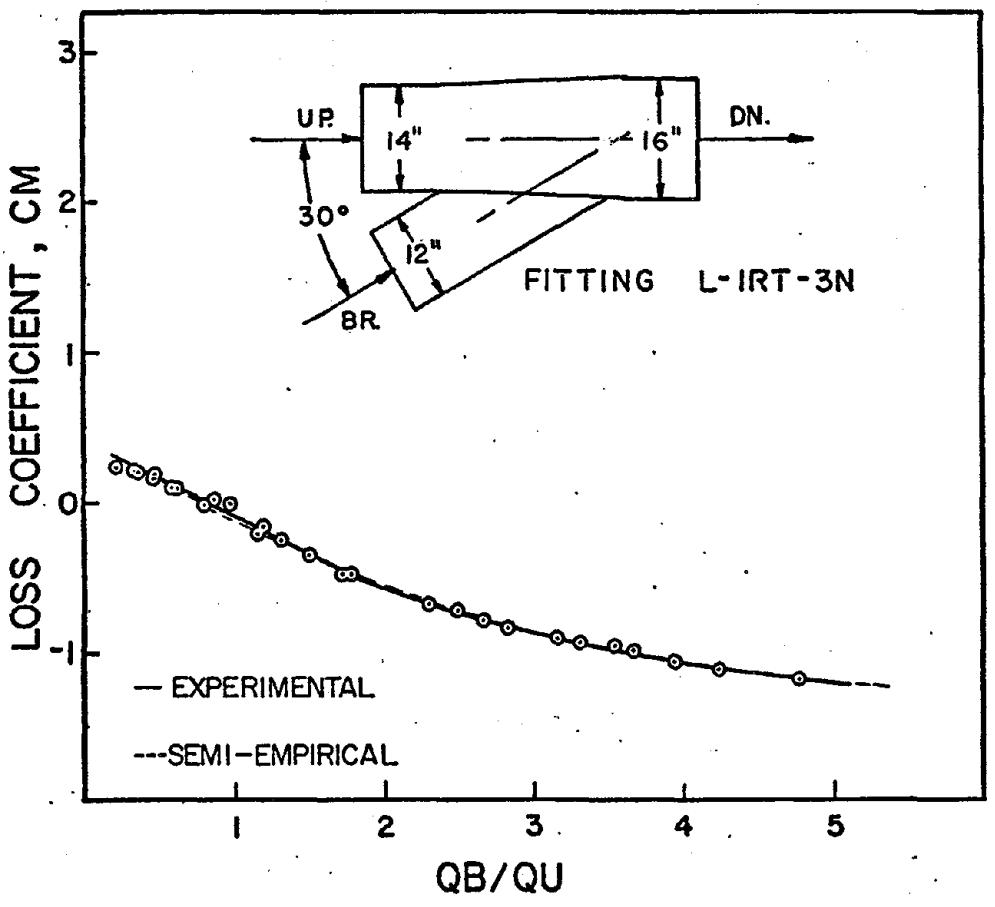

FIGURE A-56 MAIN LOSS COEFFICIENT VS. THE RATIO OF BRANCH VOLUME FLOW TO THE UPSTREAM VOLUME FLOW

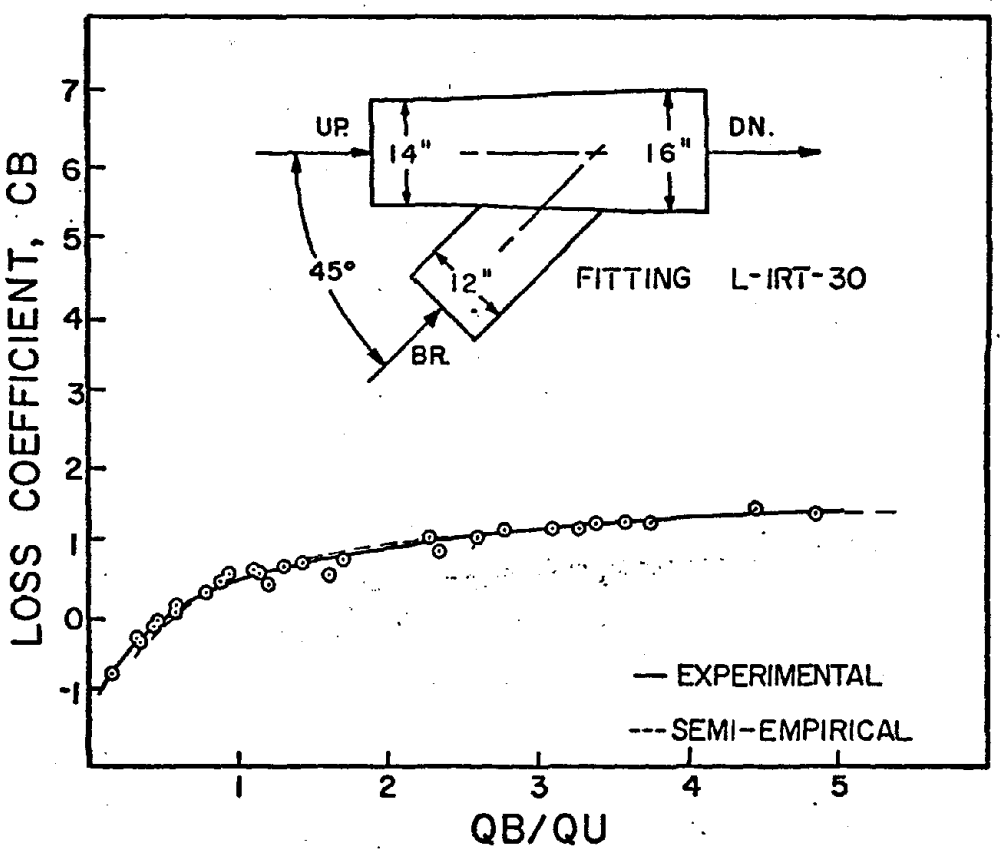

FIGURE A-57 BRANCH LOSS COEFFICIENT VS. THE RATIO OF BRANCH VOLUME FLOW TO THE UPSTREAM VOLUME FLOW

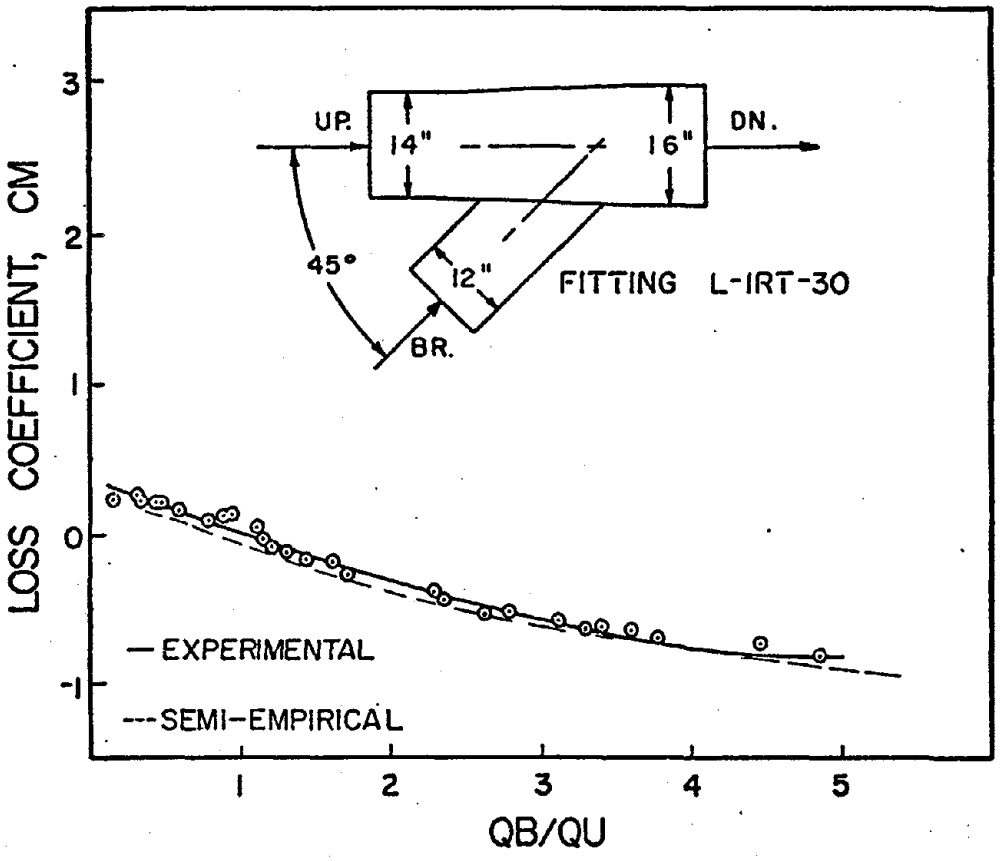

FIGURE A-58 MAIN LOSS COEFFICIENT VS. THE RATIO OF BRANCH VOLUME FLOW TO THE UPSTREAM VOLUME FLOW

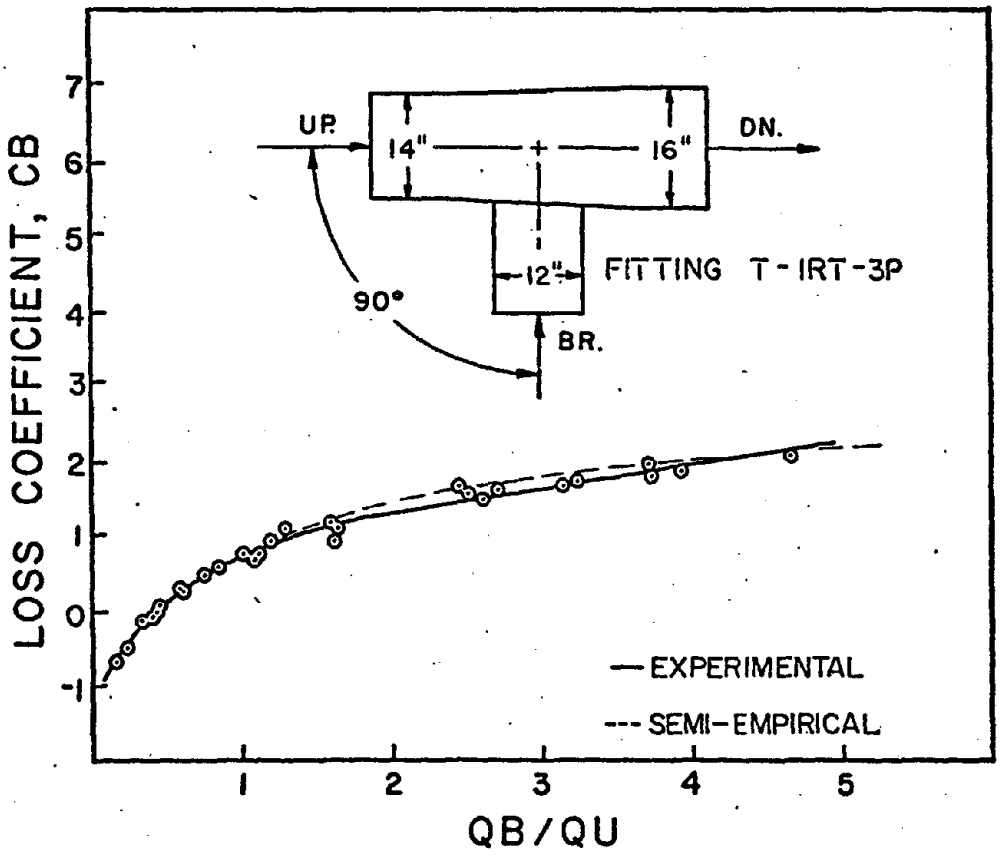

FIGURE A-59 BRANCH LOSS COEFFICIENT VS. THE RATIO OF THE BRANCH VOLUME FLOW TO THE UPSTREAM VOLUME FLOW

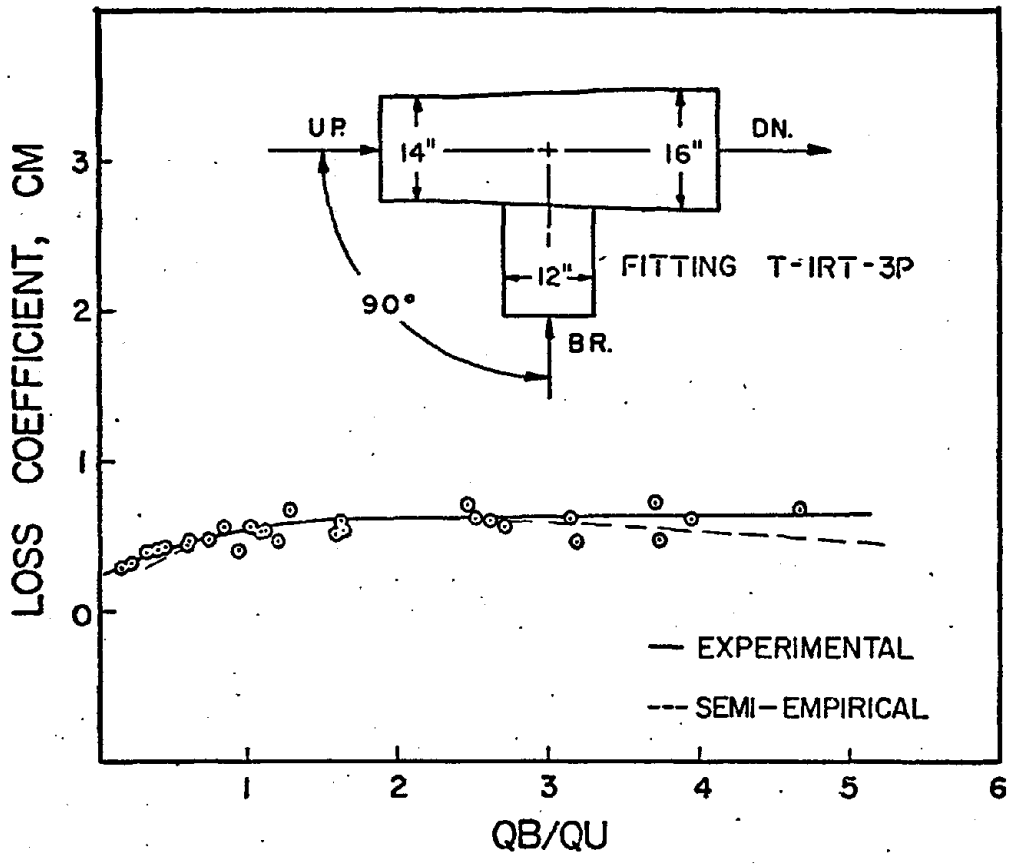

FIGURE A-60 MAIN LOSS COEFFICIENT VS. THE RATIO OF BRANCH VOLUME FLOW TO THE UPSTREAM VOLUME FLOW

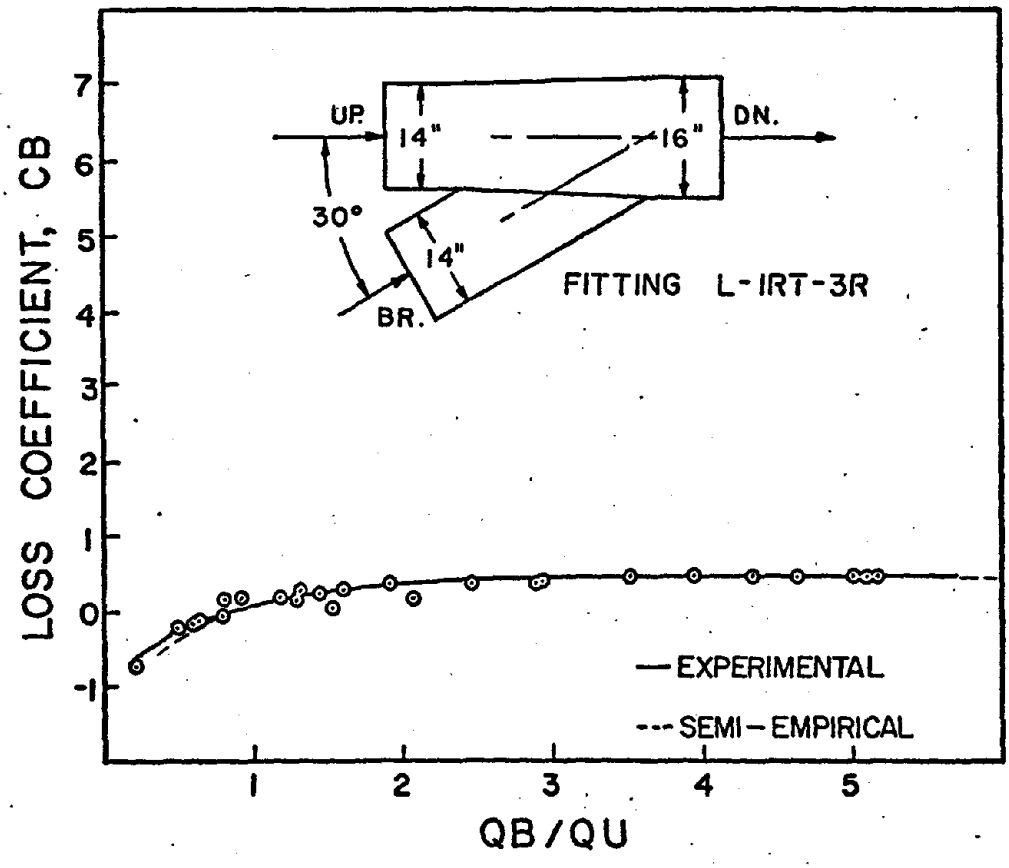

FIGURE A-61 BRANCH LOSS COEFFICIENT VS. THE RATIO OF THE BRANCH VOLUME FLOW TO THE UPSTREAM VOLUME FLOW

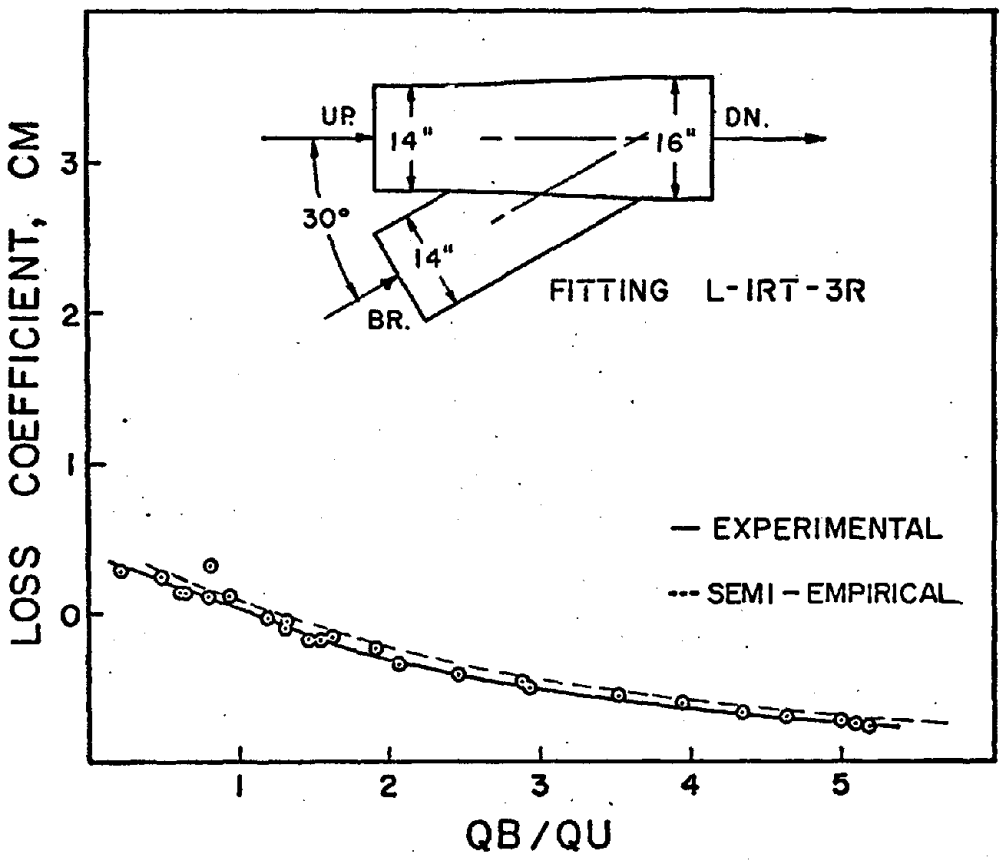

FIGURE A-62 MAIN LOSS COEFFICIENT VS. THE RATIO OF BRANCH VOLUME FLOW TO THE UPSTREAM VOLUME FLOW

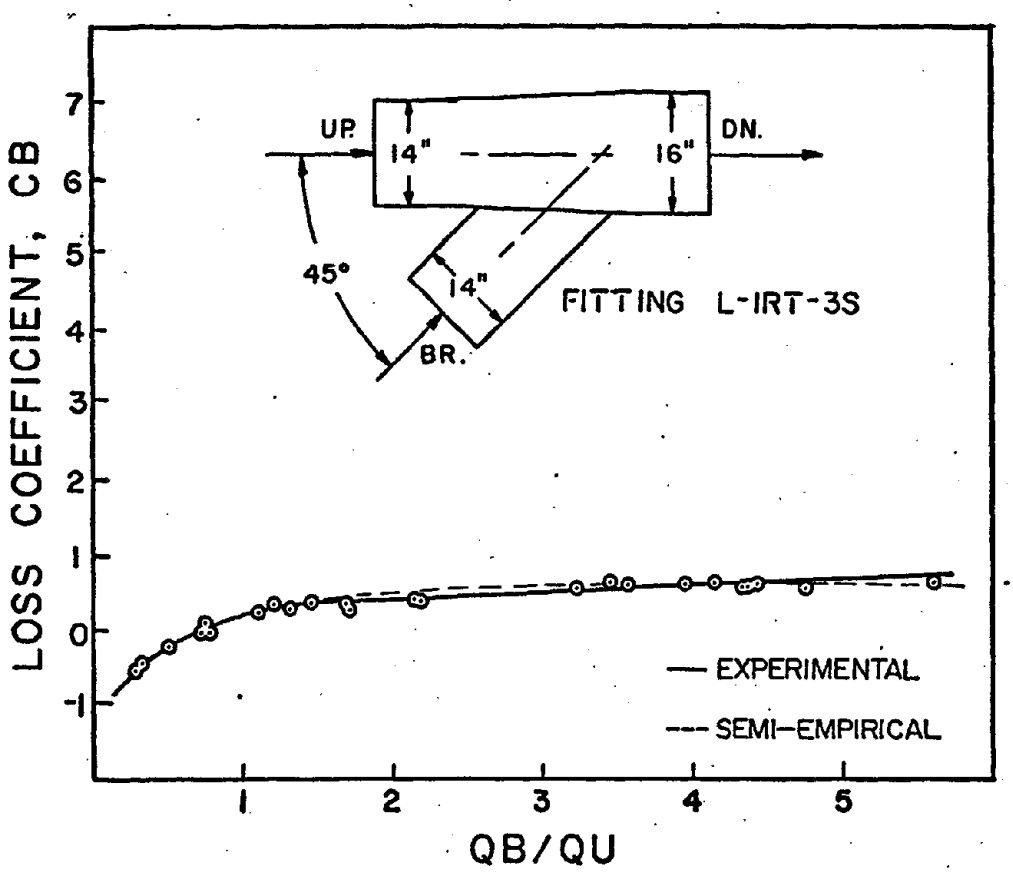

FIGURE A-63 BRANCH LOSS COEFFICIENT VS. THE RATIO OF BRANCH VOLUME FLOW TO THE UPSTREAM VOLUME FLOW

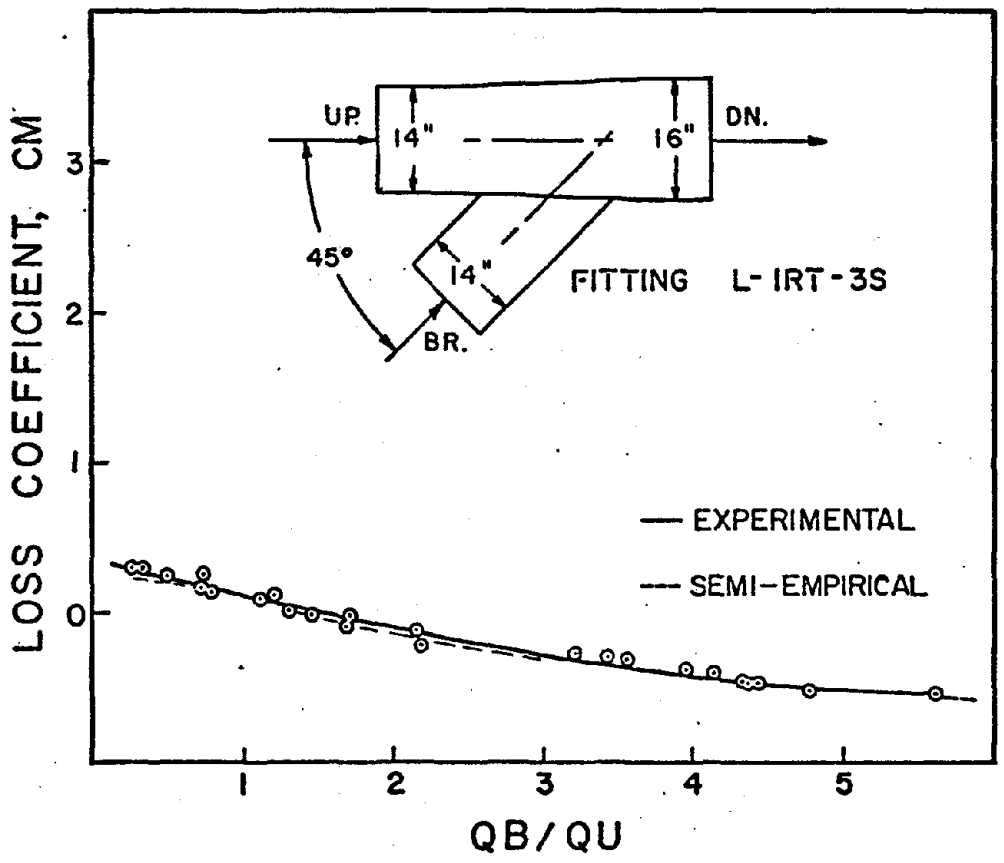

FIGURE A-64 MAIN LOSS COEFFICIENT VS. THE RATIO OF BRANCH VOLUME FLOW TO THE UPSTREAM VOLUME FLOW

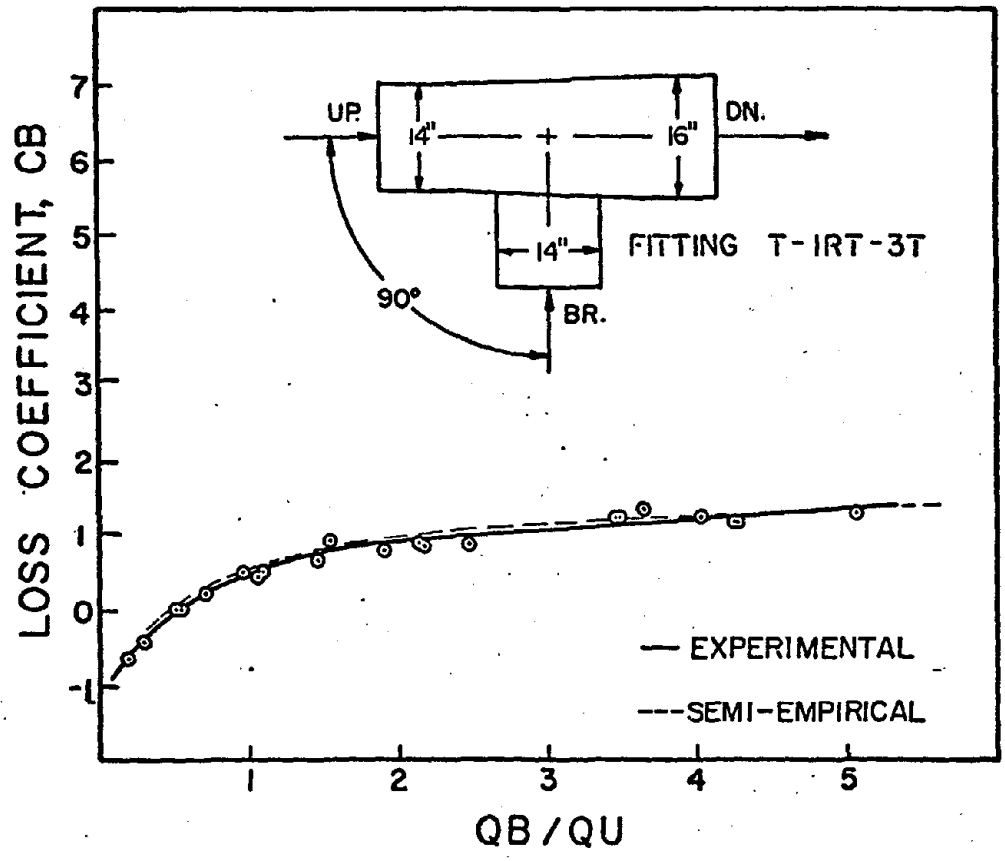

FIGURE A-65 BRANCH LOSS COEFFICIENT VS. THE RATIO OF BRANCH VOLUME FLOW TO THE UPSTREAM VOLUME FLOW

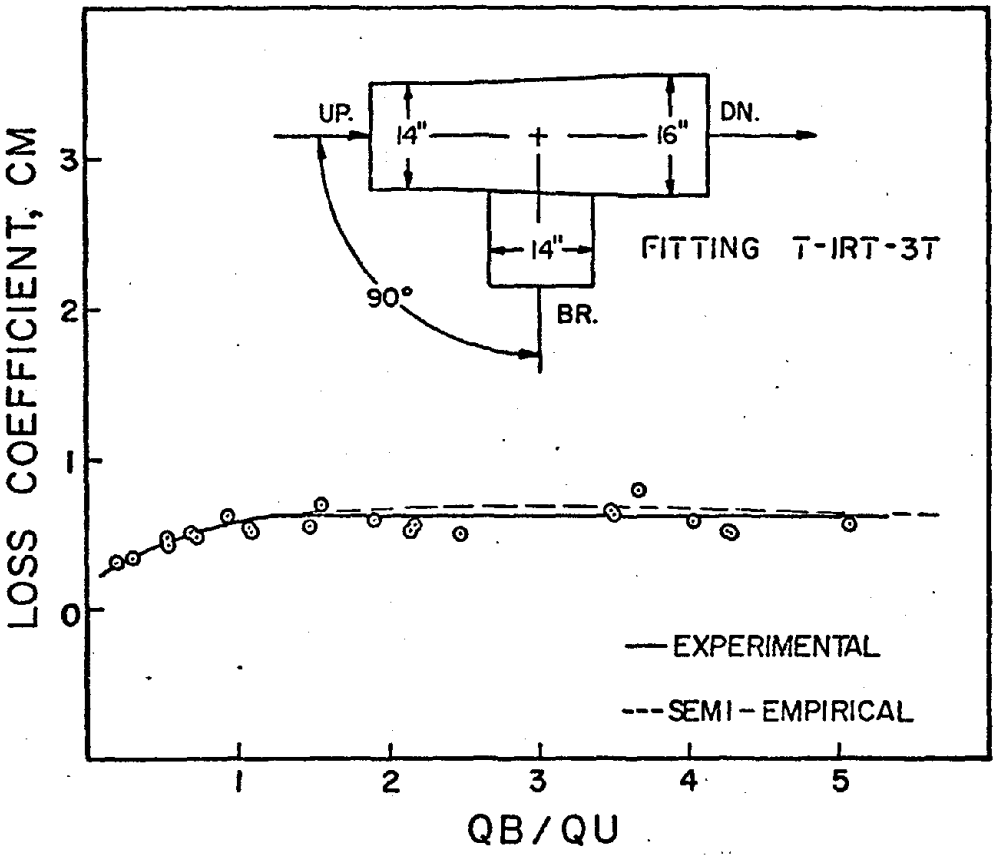

FIGURE A-66 MAIN LOSS COEFFICIENT VS. THE RATIO OF THE BRANCH VOLUME FLOW TO THE UPSTREAM VOLUME FLOW

APPENDIX B

DESCRIPTION OF FITTINGS

Figures B-1 through B-33 depict the thirty-three fittings used in the experimental investigation. A list of fitting dimensions is presented in Table B-1.

The joint between the branch tap and main fitting body corresponded to the sharp edge entrance, rolled edge entrance, or round edge entrance. Each of these type entrances is described in Section 5.2. Even though variations occurred between the branch tap entrances, it was felt important not to modify the manufactured entrance to comply with a standard type entrance. Using stock branch tap entrances assured that results were representative of production fittings used in practice and not in controlled laboratory conditions.

TABLE B-1

FITTING DIMENSIONS

Fitting Ident. Code	Drawing and Picture Figure	Branch Inside Dia., Inches	Upstream Inside Dia., Inches	Downstream Inside Dia., Inches	Branch Entry Angle, Deg.
L-1RT-AA	B-1	4	4	6	30
L-1RT-BB	B-2	4	4	6	45
T-1RT-CC	B-3	4	4	6	90
L-1-DD	B-4	3	6	6	45
T-1-EE	B-5	3	6	6	90
L-1RT-FF	B-6	3	4	6	30
L-1RT-GG	B-7	3	4	6	45
T-1RT-HH	B-8	3	4	6	90
T-1-JJ	B-9	3	4	4	90
L-1-KK	B-10	3	4	4	45
L-1RT-LL	B-11	3	3	4	30
L-1RT-MM	B-12	3	3	4	45
T-1RT-NN	B-13	3	3	4	90
T-1-00	B-14	4	6	6	90
L-1-PP	B-15	4	6	6	45
L-1RT-3A	B-16	6	8	10	30
L-1RT-3B	B-17	6	8	10	45
T-1RT-3C	B-18	6	8	10	90
L-1RT-3D	B-19	8	8	10	30

TABLE B-1 (CONT'D.)

FITTING DIMENSIONS

Fitting Ident. Code	Drawing and Picture Figure	Branch Inside Dia., Inches	Upstream Inside Dia., Inches	Downstream Inside Dia., Inches	Branch Entry Angle, Deg.
L-1RT-3E	B-20	8	8	10	45
T-1RT-3F	B-21	8	8	10	90
L-1RT-3G	B-22	8	10	12	30
L-1RT-3H	B-23	8	10	12	45
T-1RT-3J	B-24	8	10	12	90
L-1RT-3K	B-25	10	10	12	30
L-1RT-3L	B-26	10	10	12	45
T-1RT-3M	B-27	10	10	12	90
L-1RT-3N	B-28	12	14	16	30
L-1RT-3O	B-29	12	14	16	45
T-1RT-3P	B-30	12	14	16	90
L-1RT-3R	B-31	14	14	16	30
L-1RT-3S	B-32	14	14	16	45
T-1RT-3T	B-33	14	14	16	90

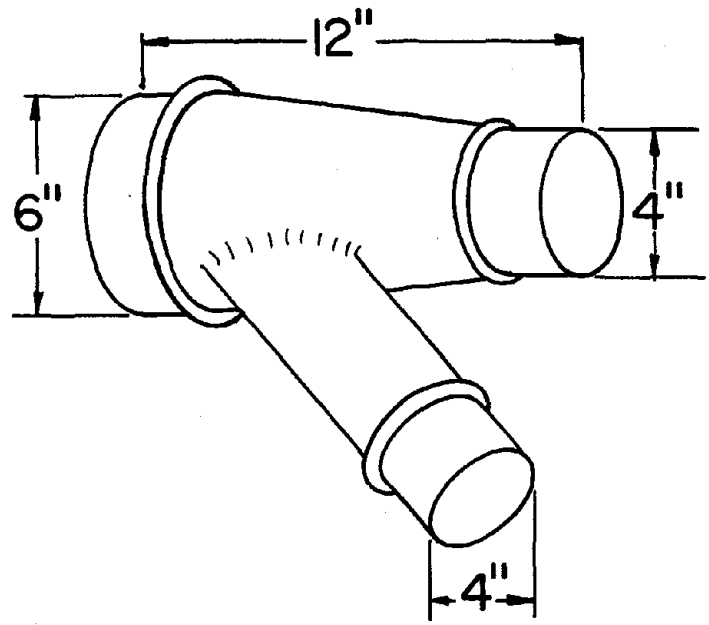

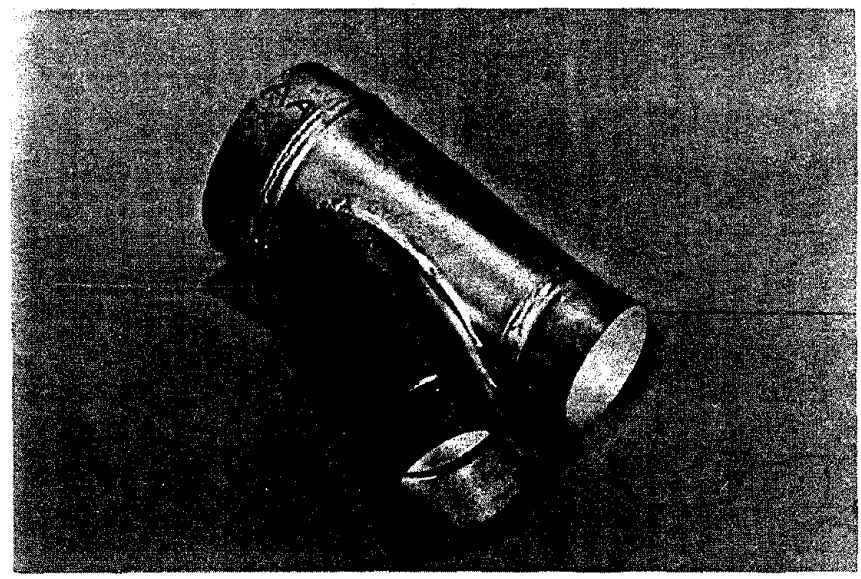

FIGURE B-1 FITTING L-IRT-AA

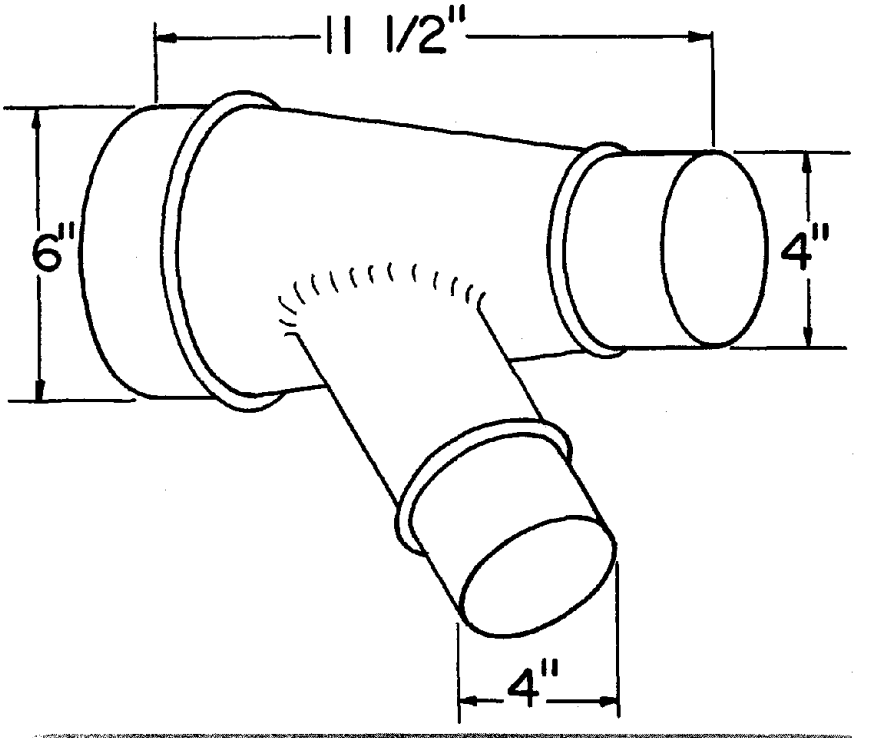

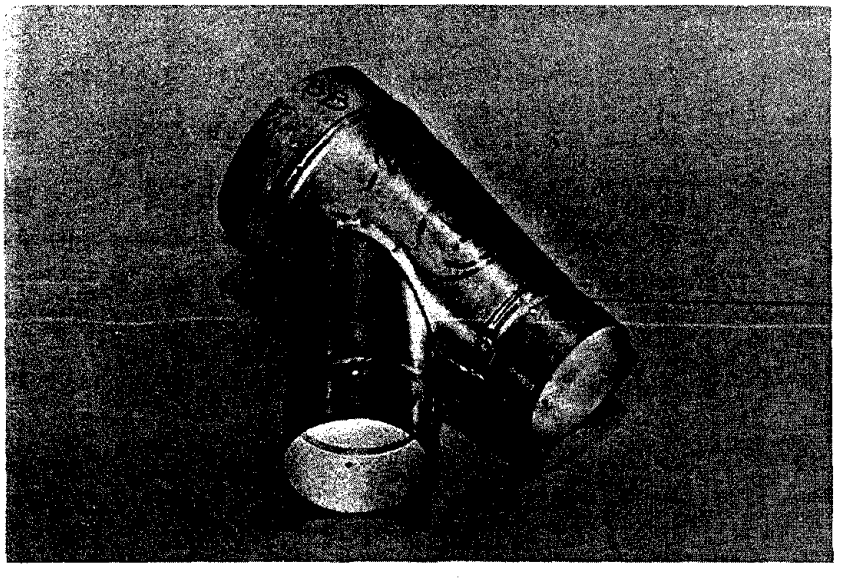

FIGURE B-2 FITTING L-IRT-BB

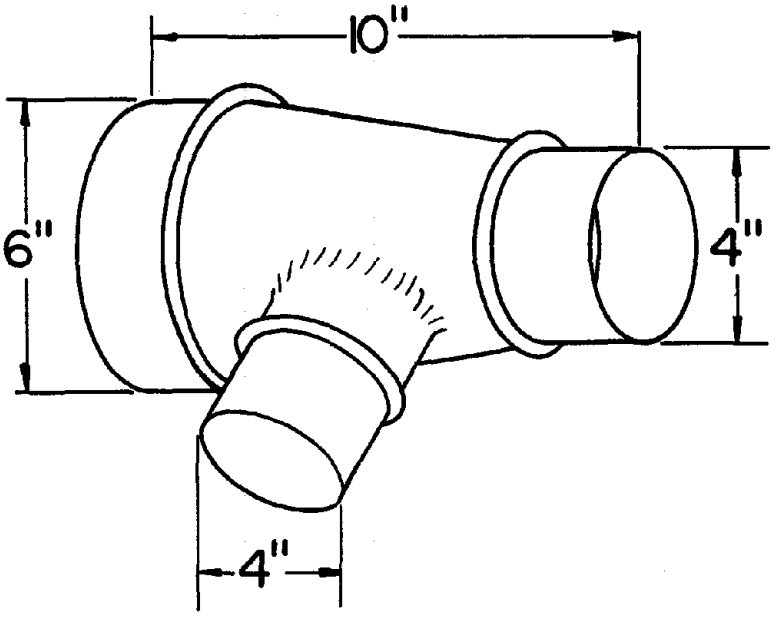

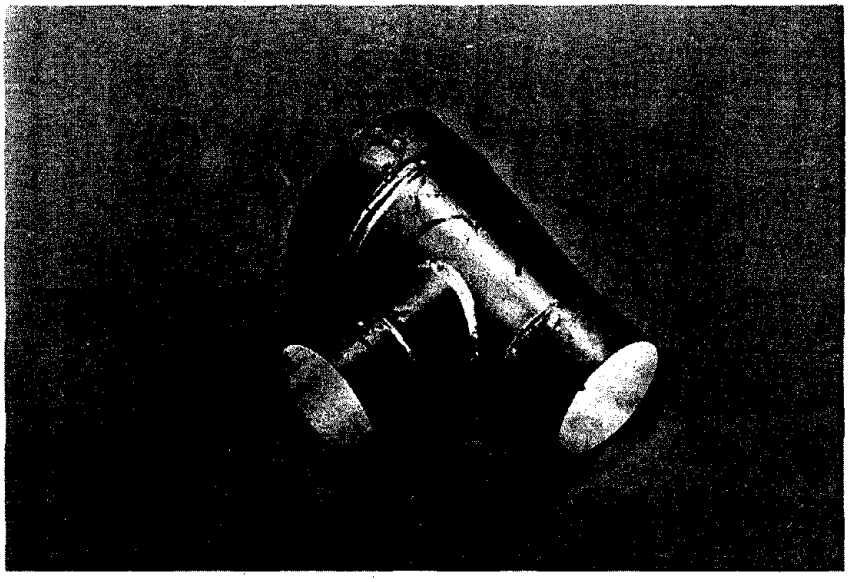

FIGURE B-3 FITTING T-IRT-CC

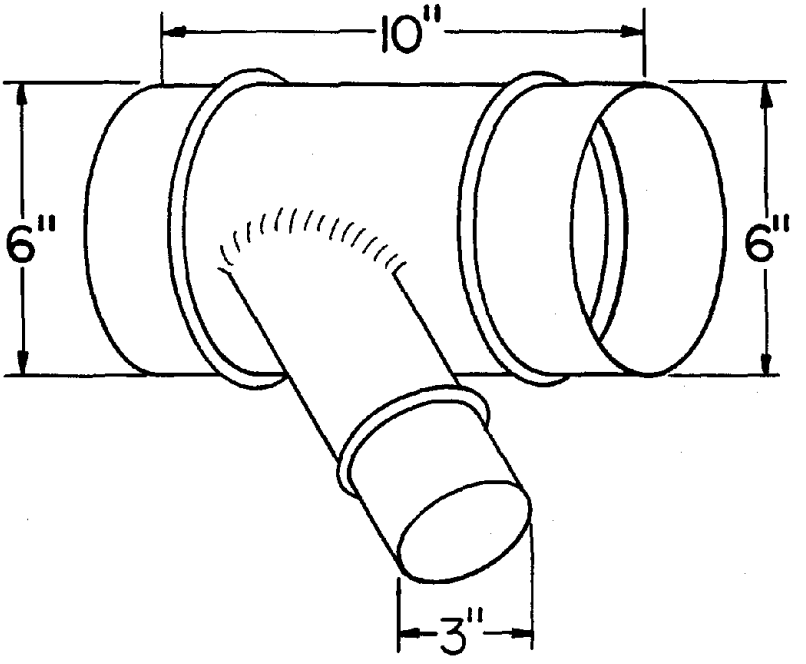

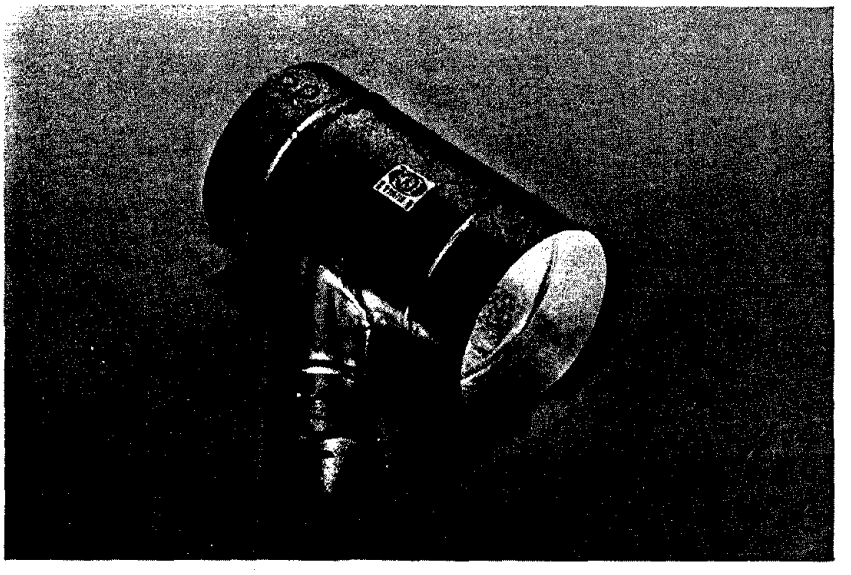

FIGURE B-4 FITTING L-1-DD

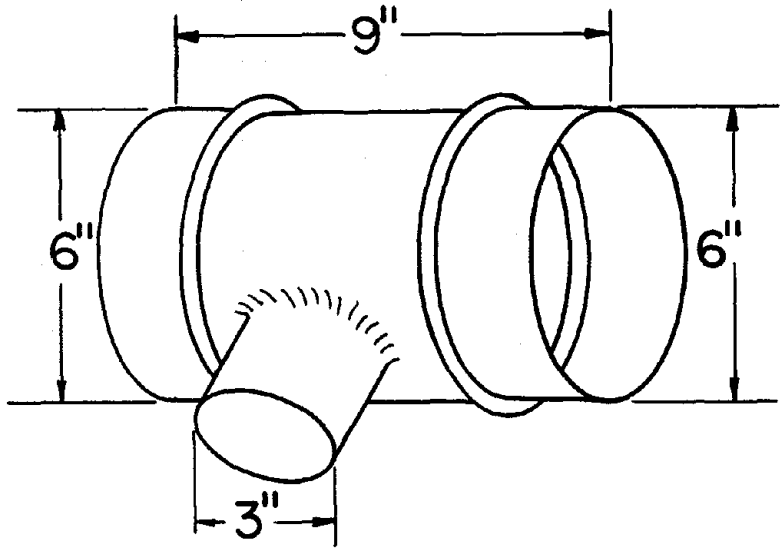

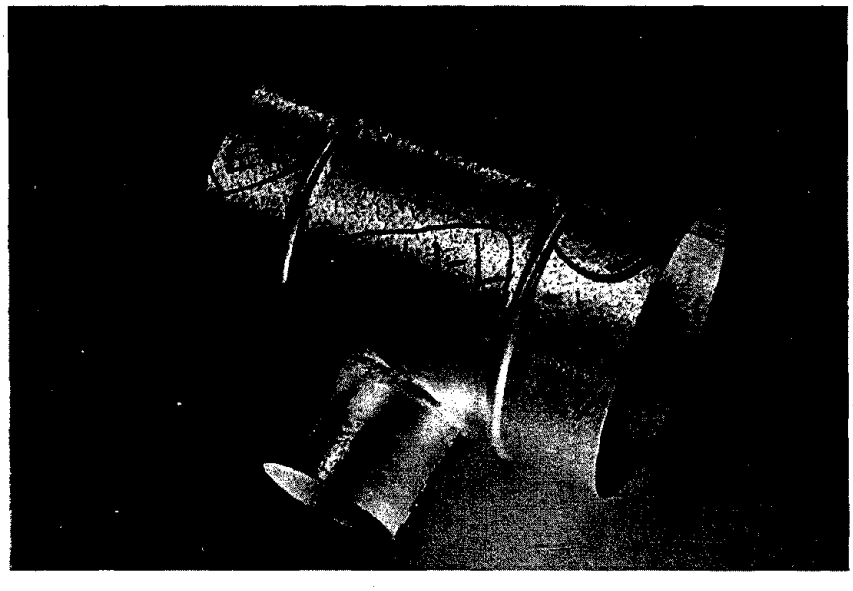

FIGURE B-5 FITTING T-1-EE

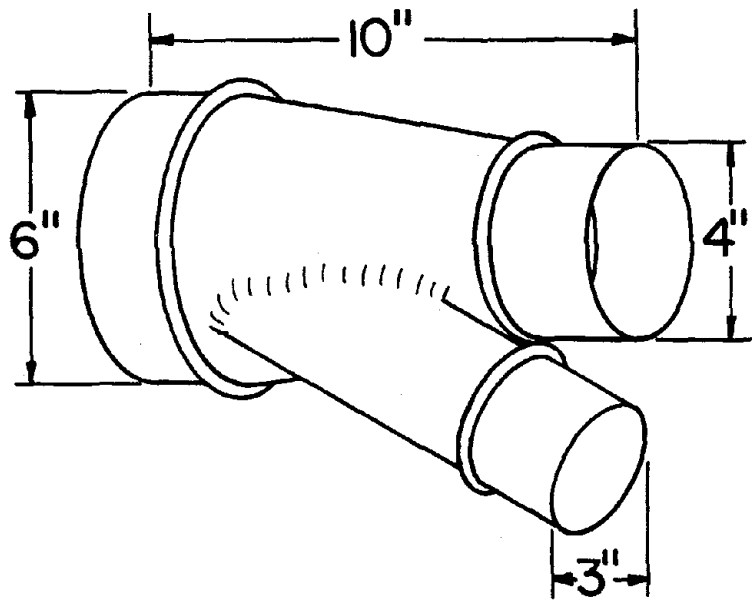

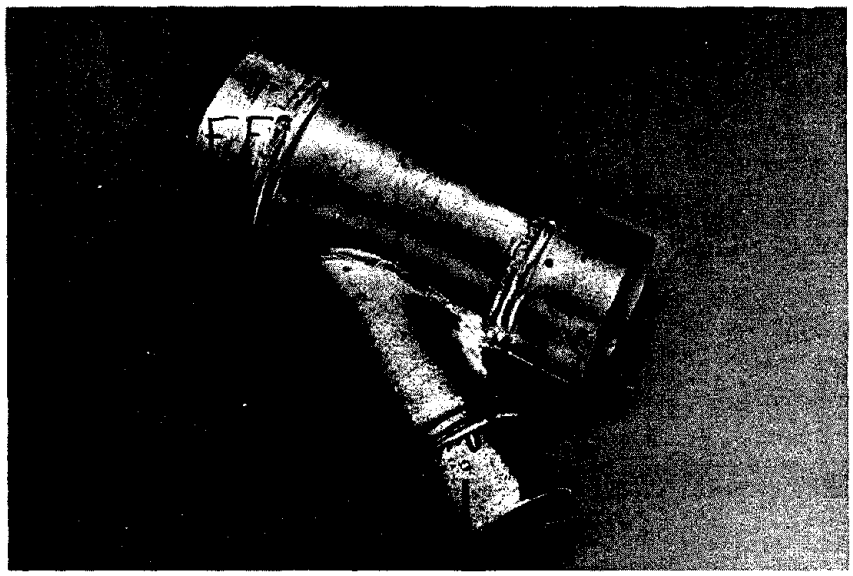

FIGURE B-6 FITTING L-IRT-FF

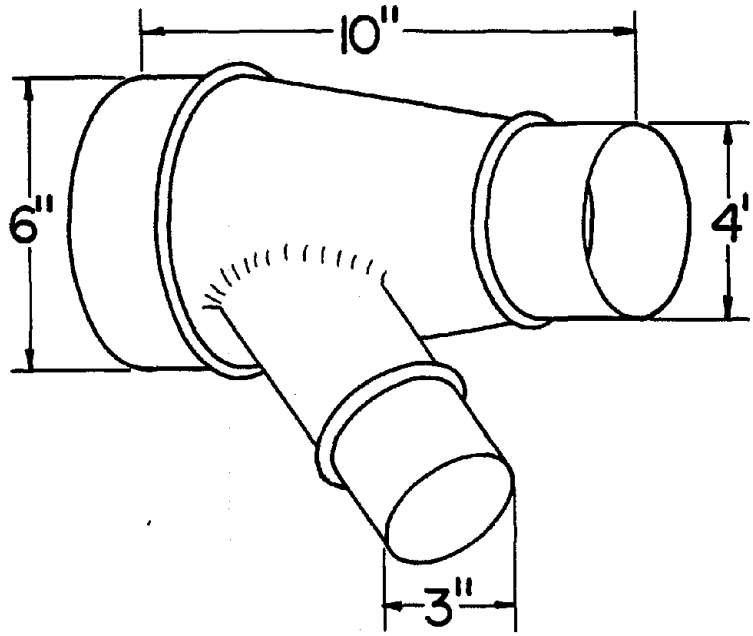

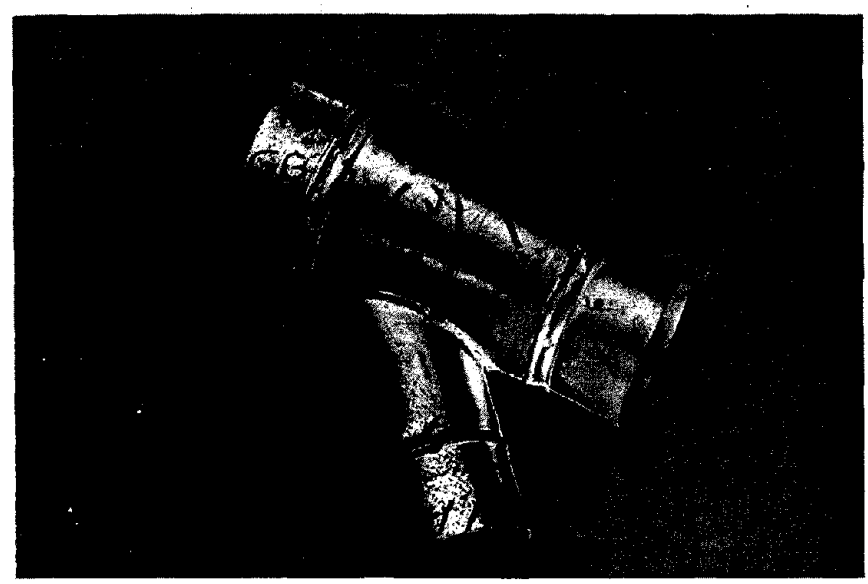

FIGURE B-7 FITTING L-IRT-GG

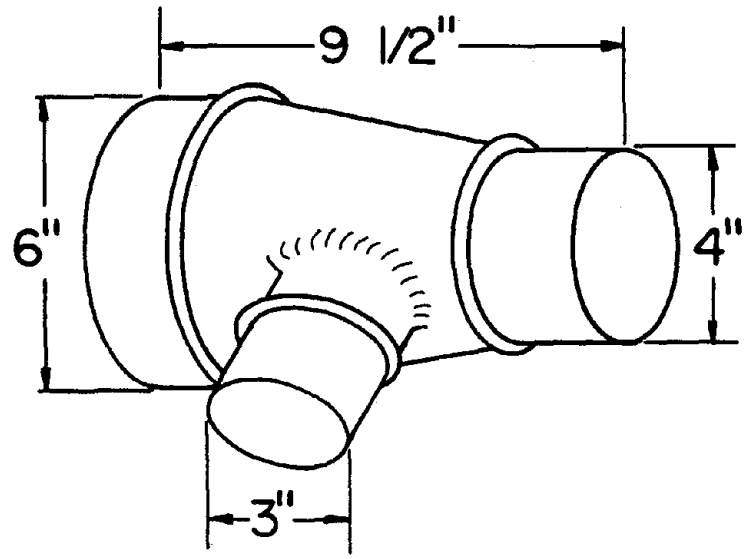

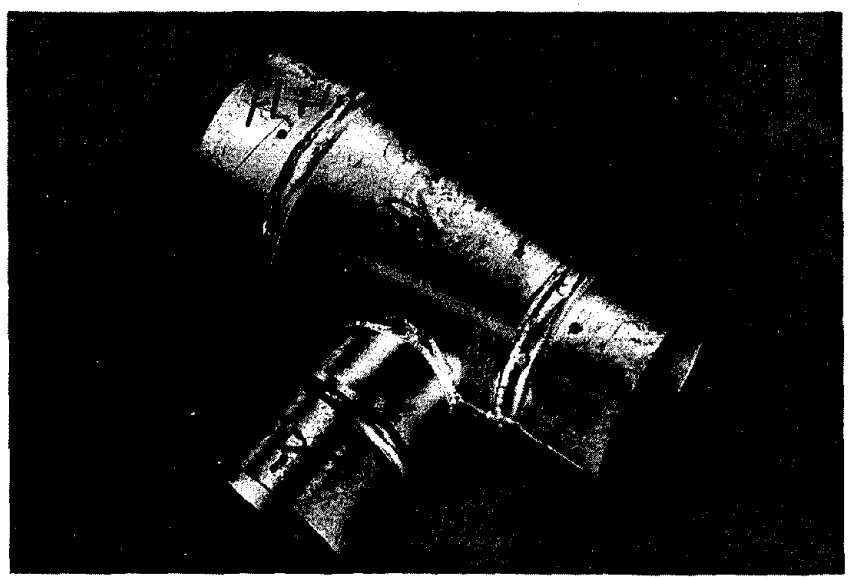

FIGURE B-8 FITTING T-IRT-HH

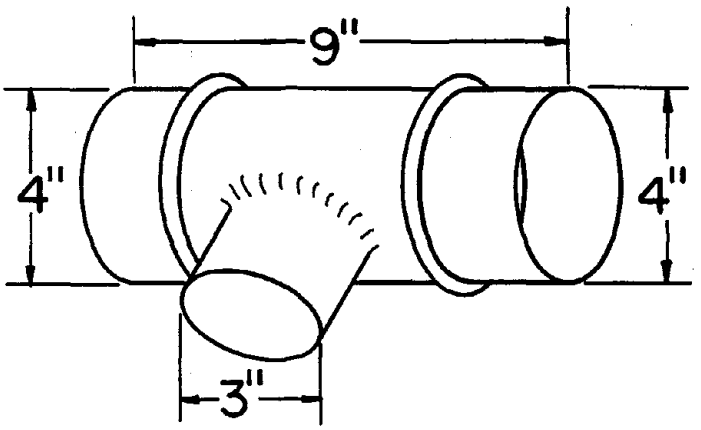

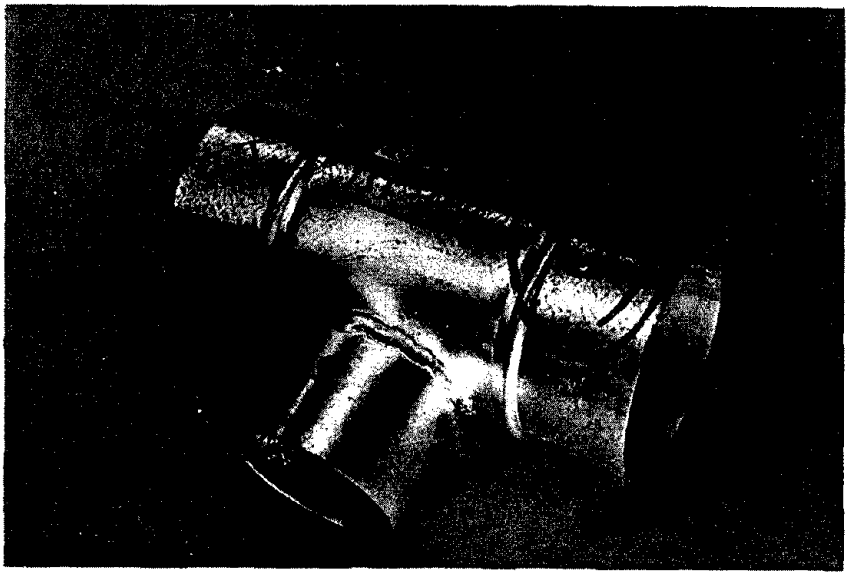

FIGURE B-9 FITTING T-1-JJ

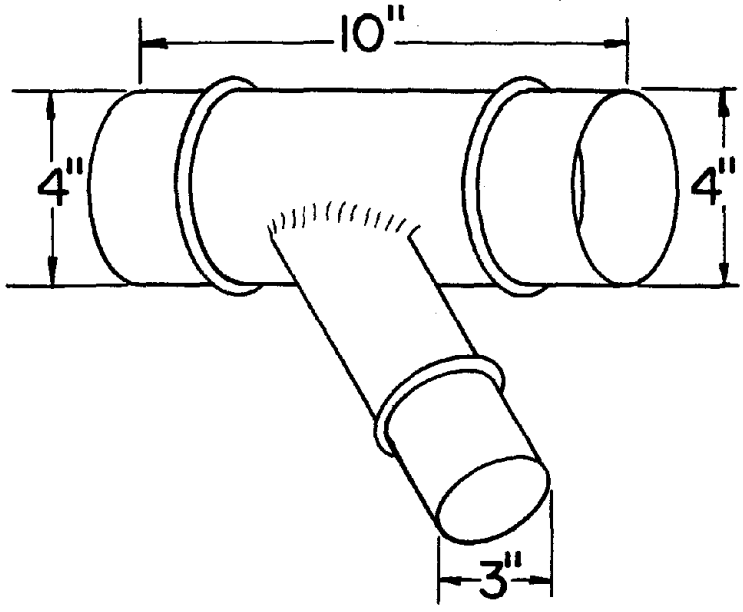

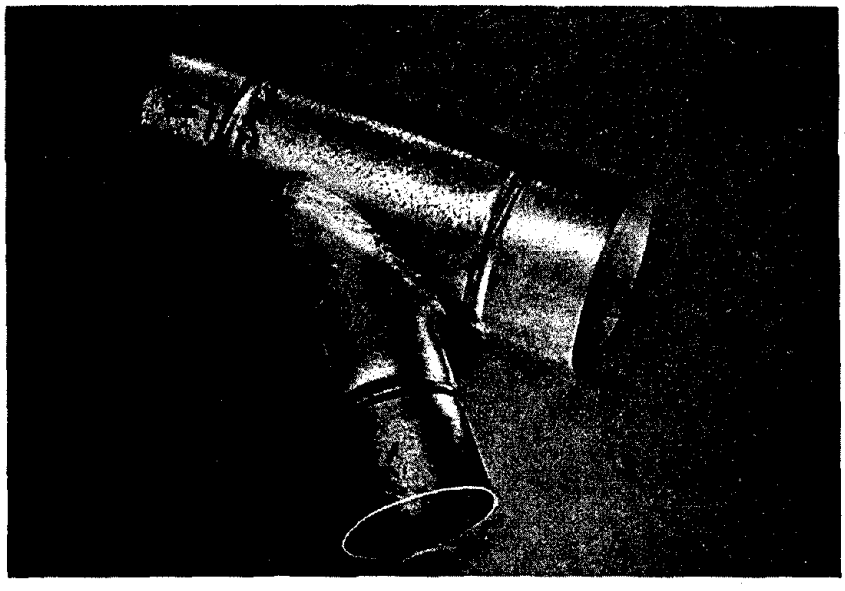

FIGURE B-10 FITTING L-1-KK

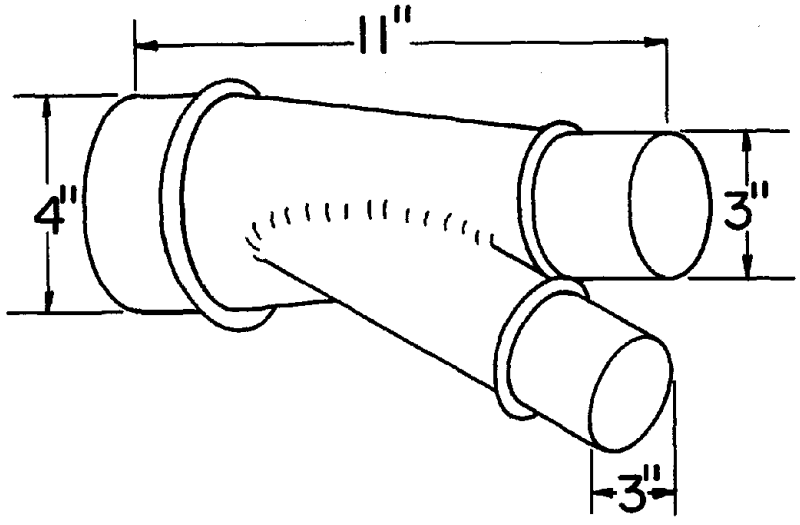

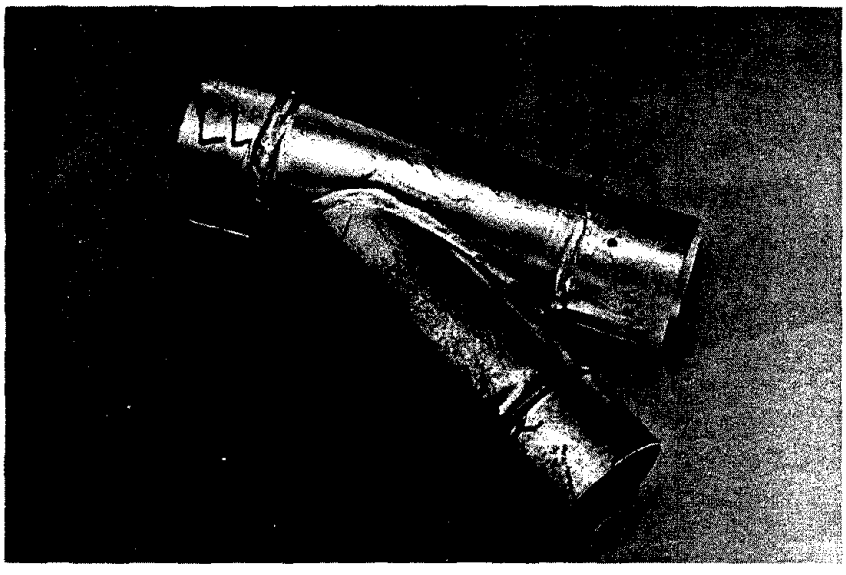

FIGURE B-11 FITTING L-IRT-LL

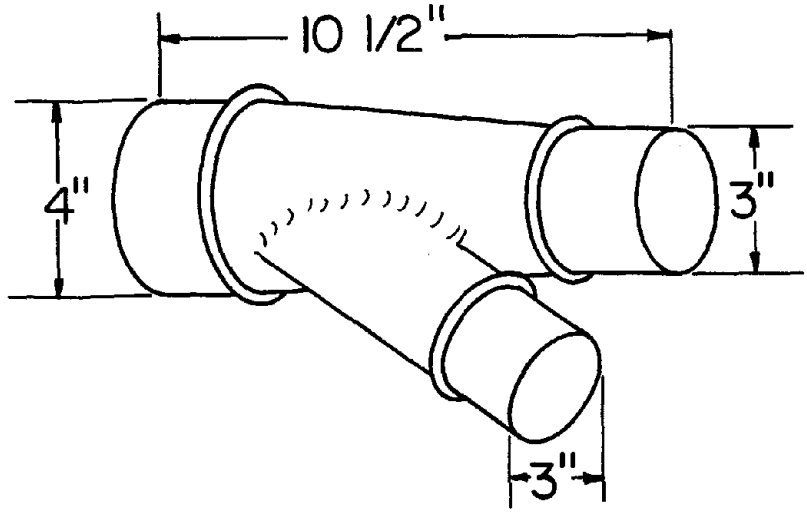

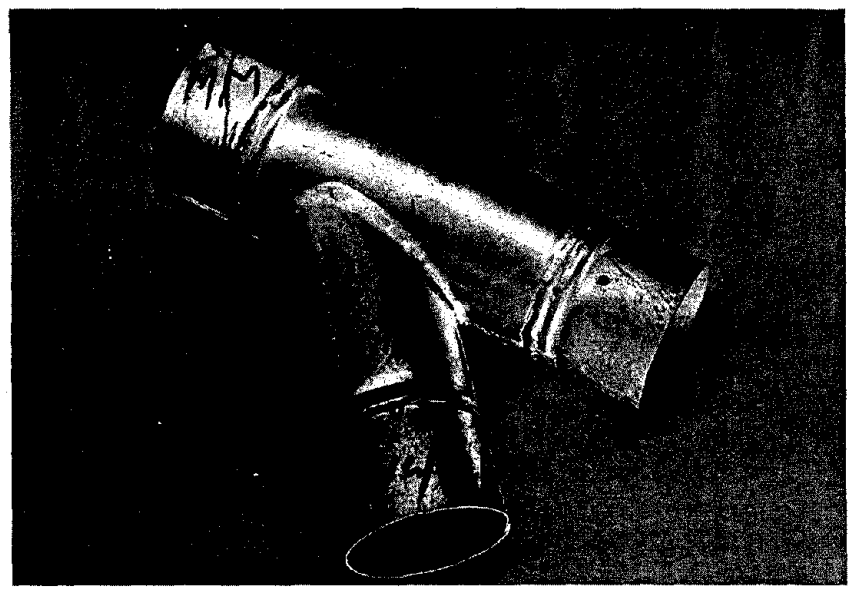

FIGURE B-12 FITTING L-IRT-MM

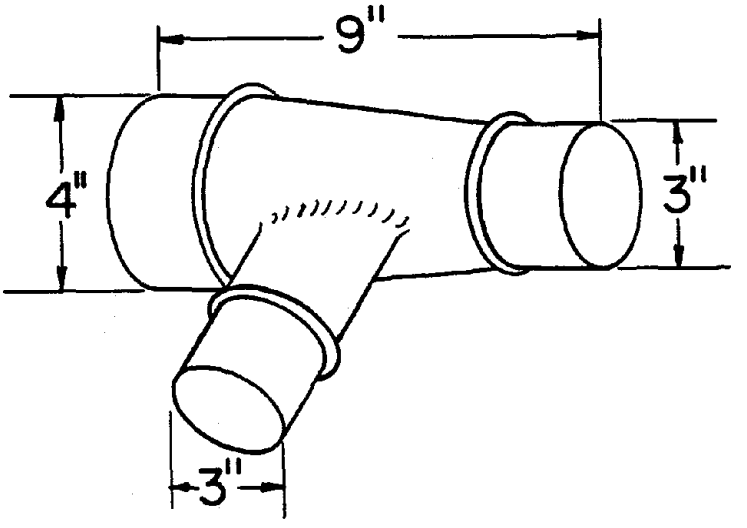

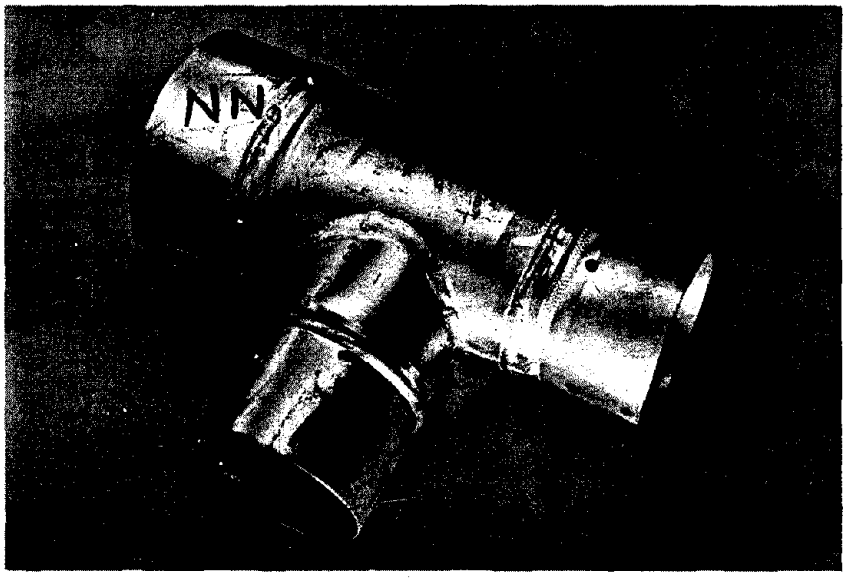

FIGURE B-13 FITTING T-IRT-NN

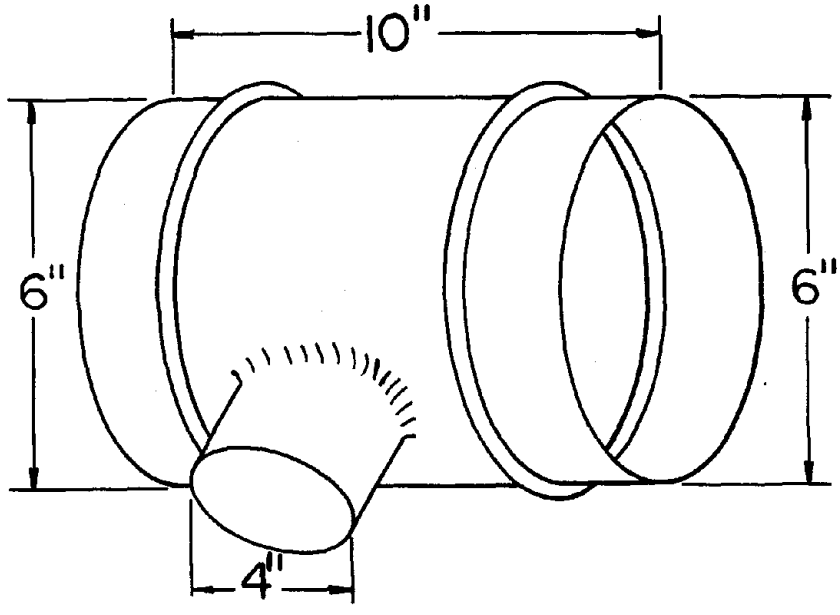

FIGURE B-14 FITTING T-1-00

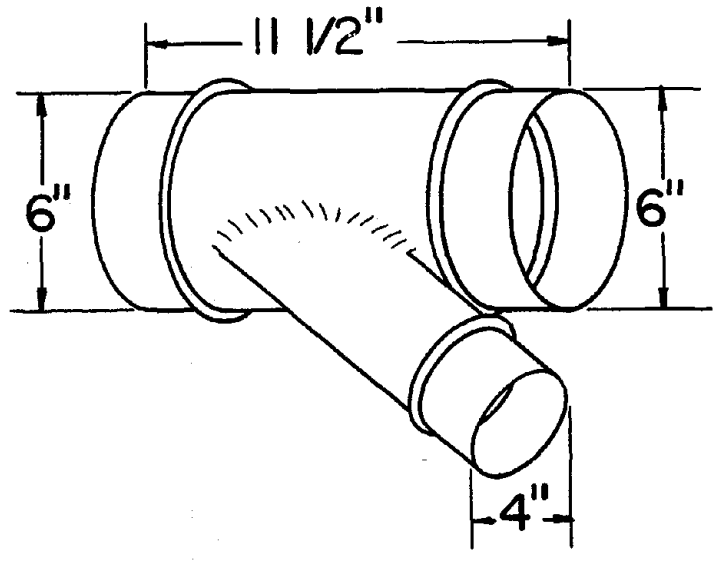

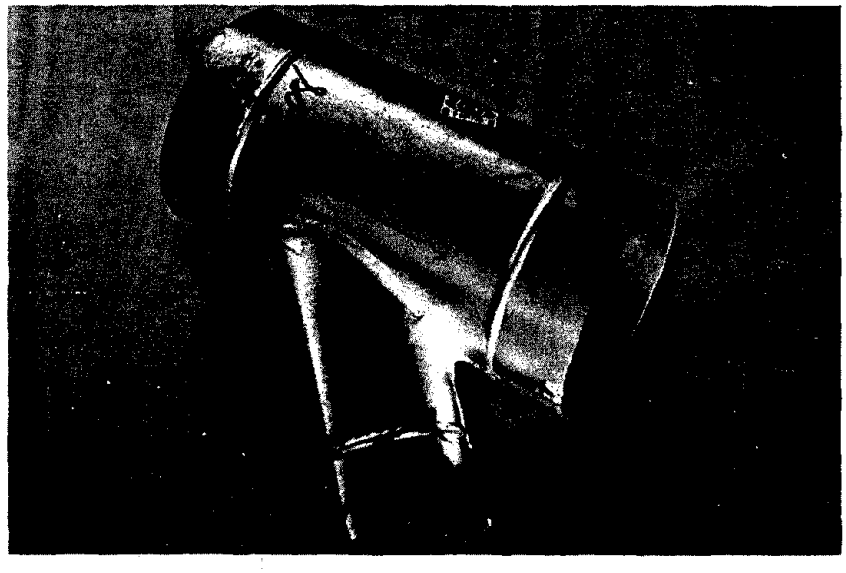

FIGURE B-15 FITTING L-1-PP

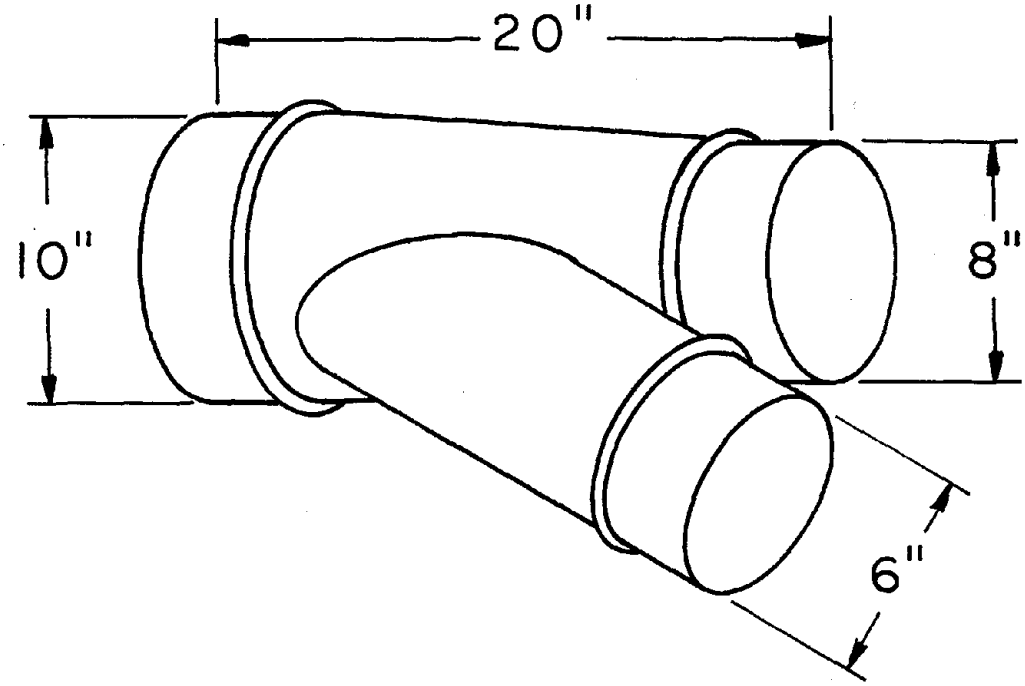

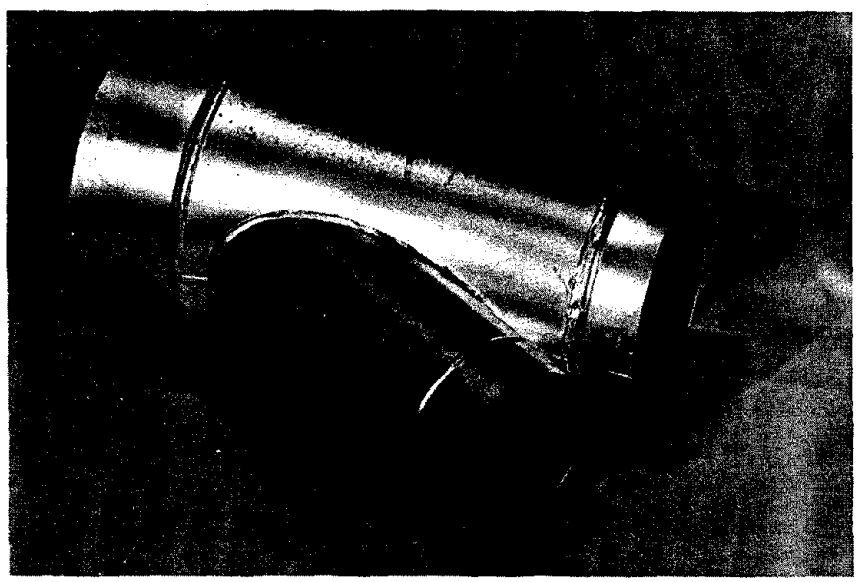

FIGURE B-16 FITTING L-IRT-3A

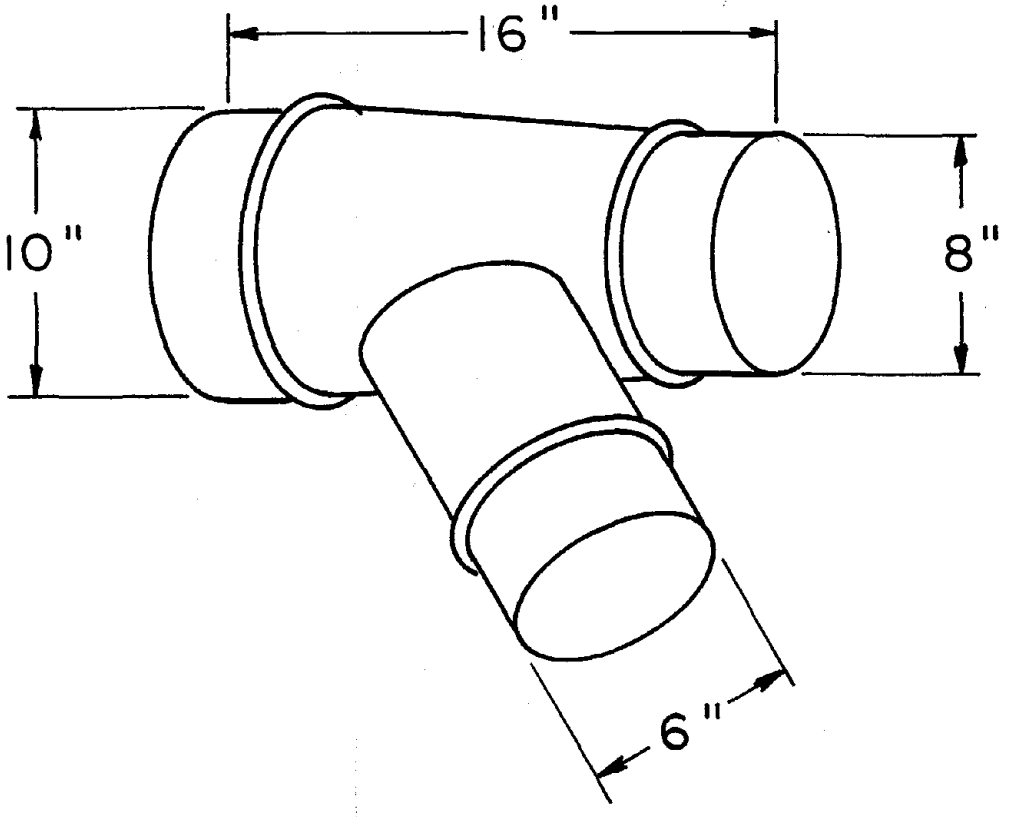

FIGURE B-17 FITTING L-IRT-3B

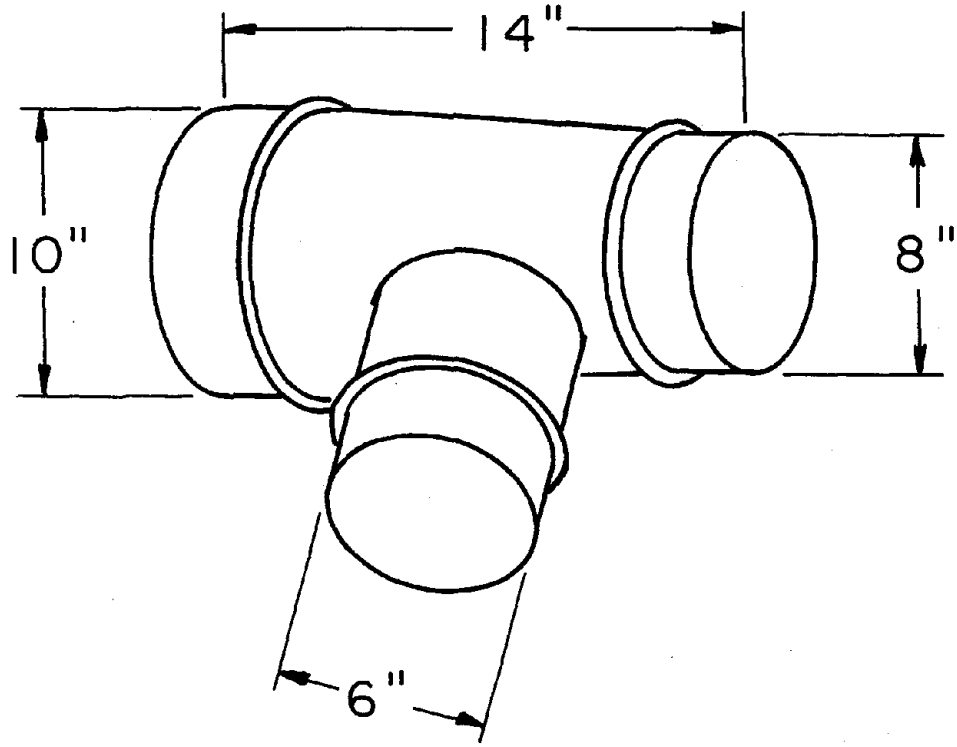

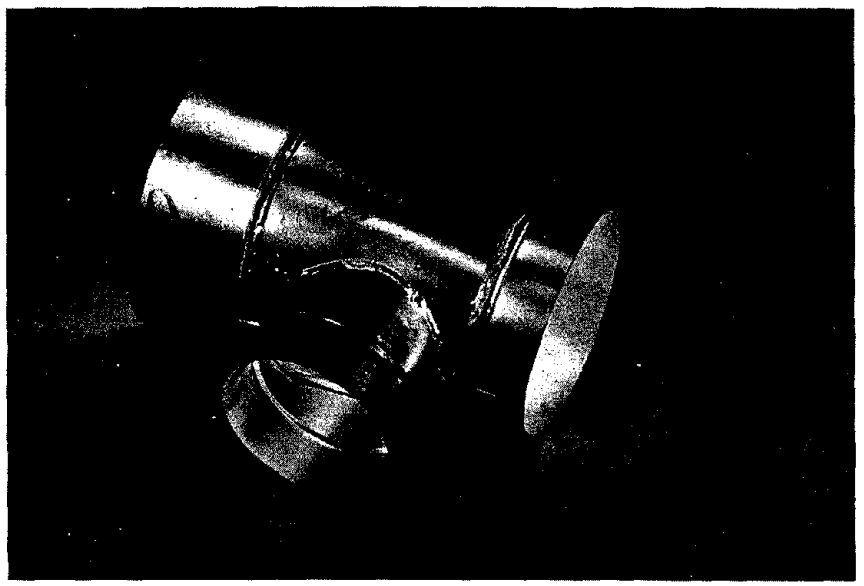

FIGURE B-18 FITTING T-IRT-3C

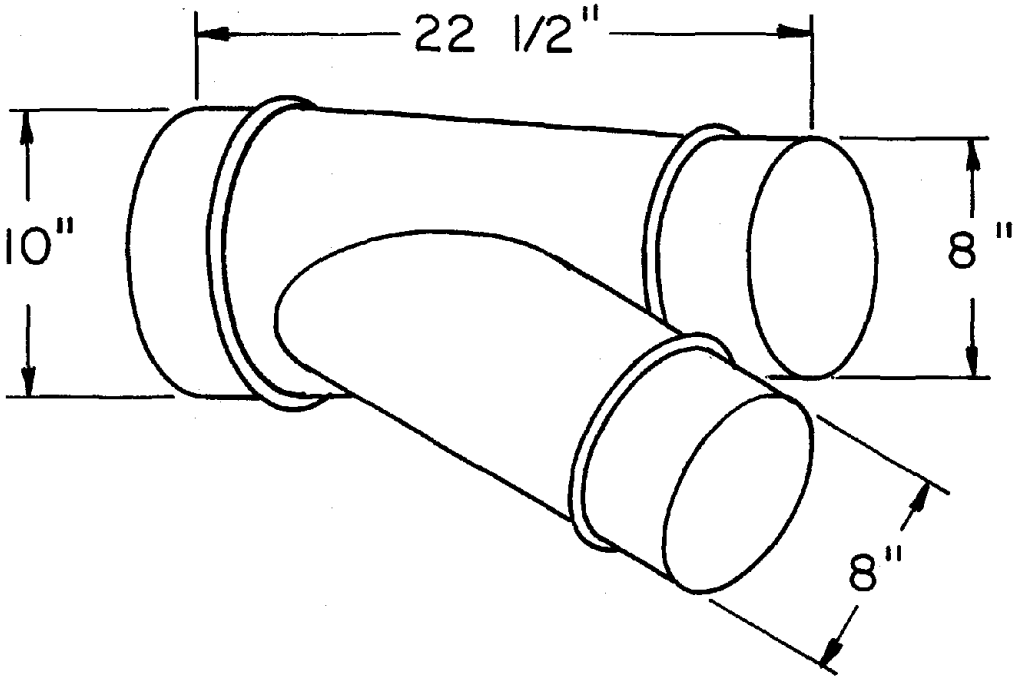

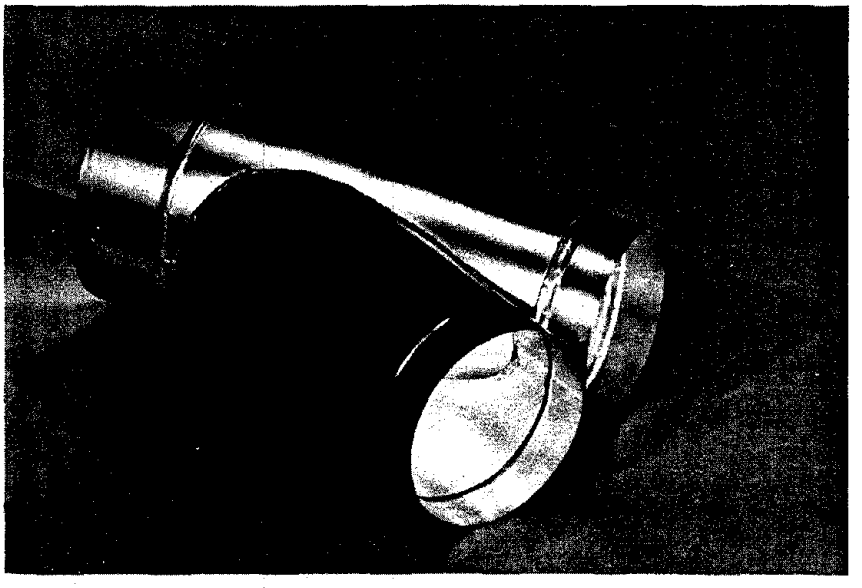

FIGURE B-19 FITTING L-IRT-3D

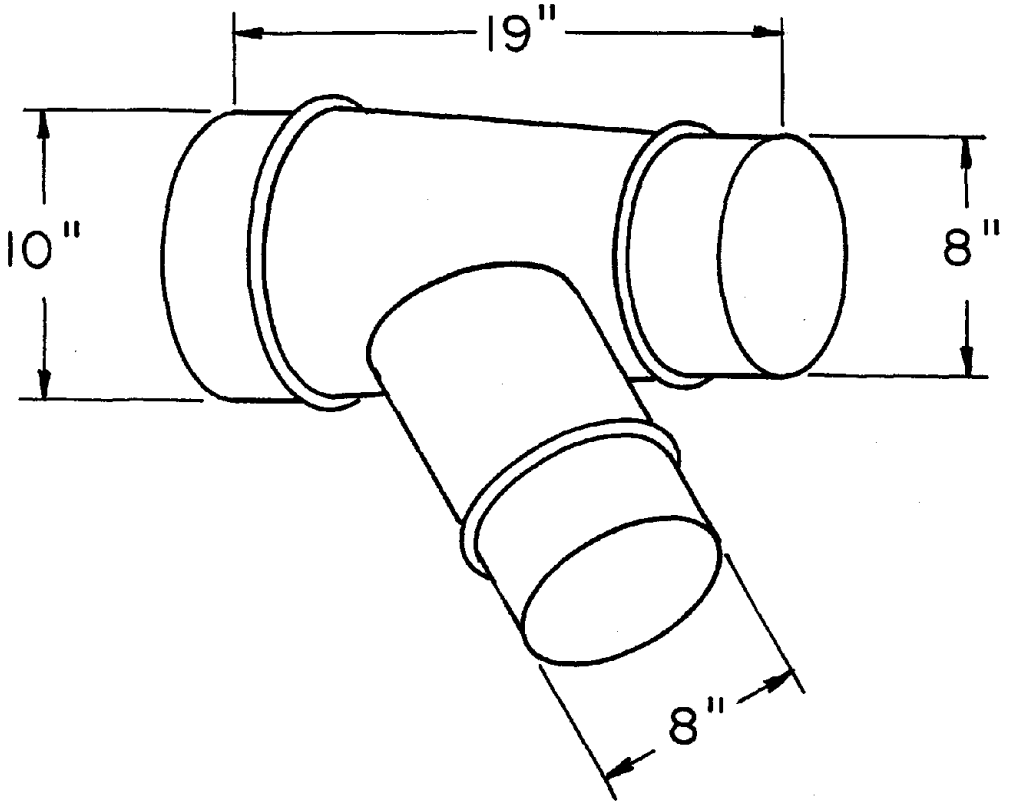

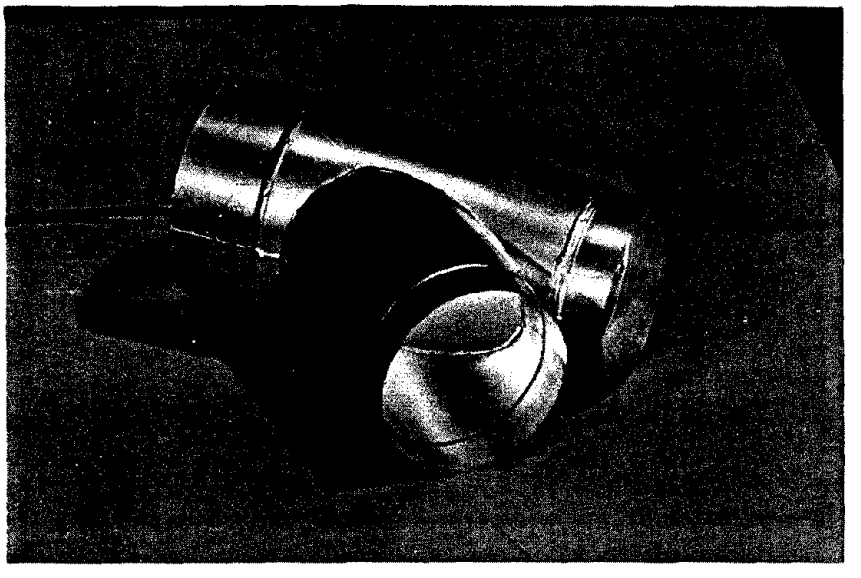

FIGURE B-20 FITTING L-IRT-3E

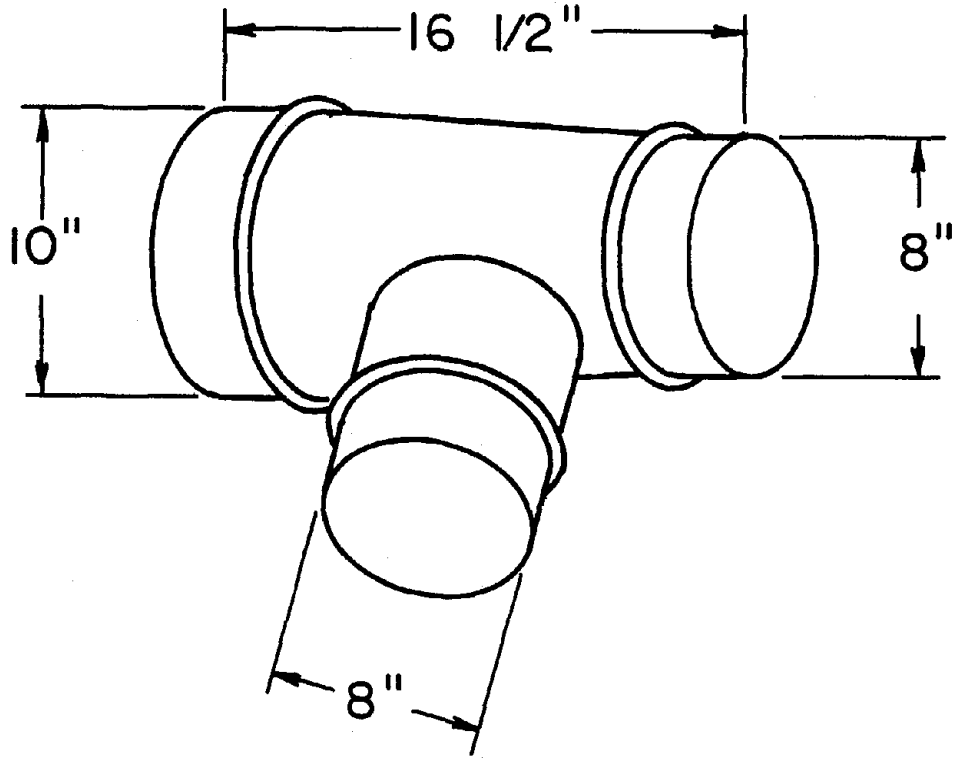

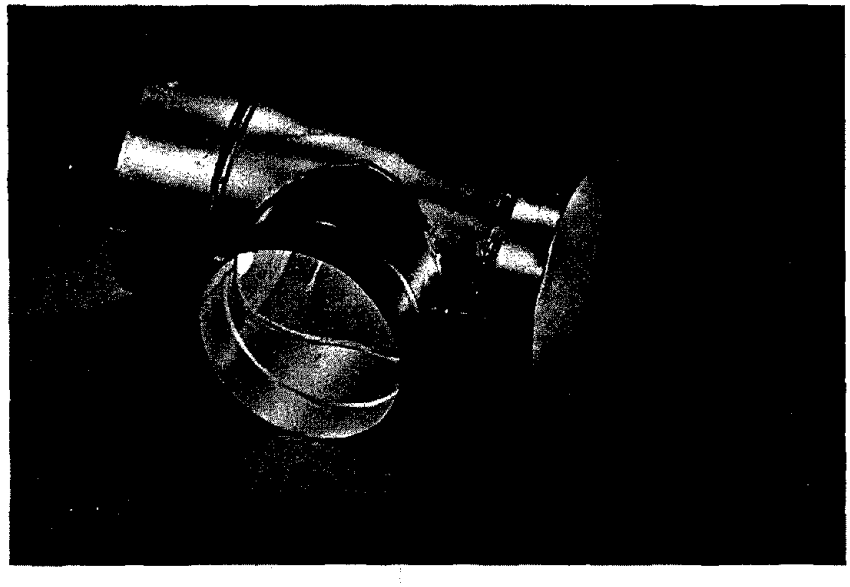

FIGURE B-21 FITTING T-IRT-3F

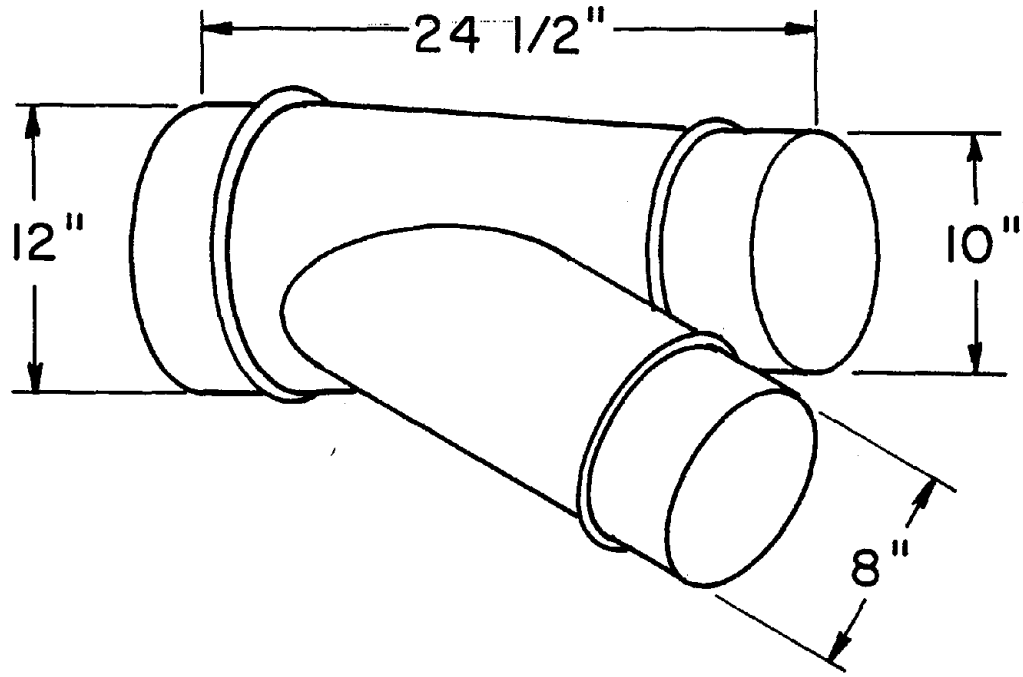

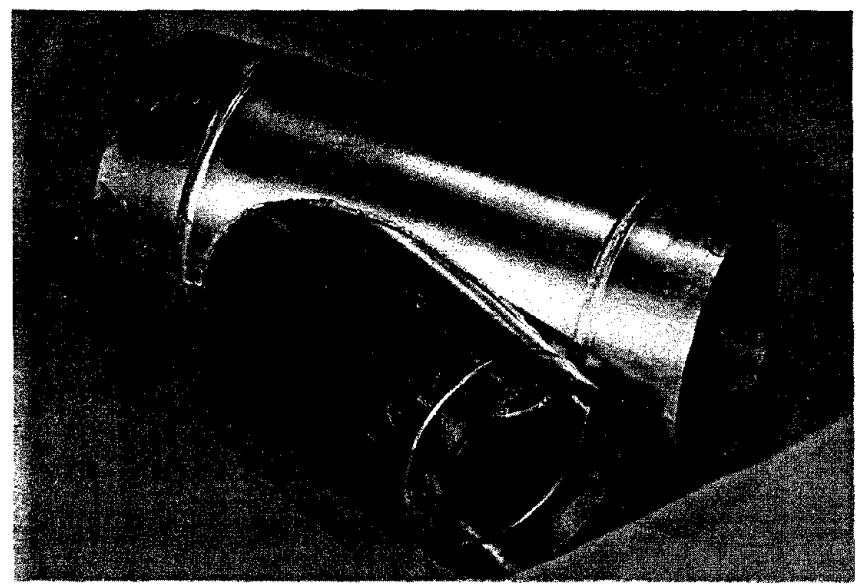

FIGURE B-22 FITTING L-IRT-3G

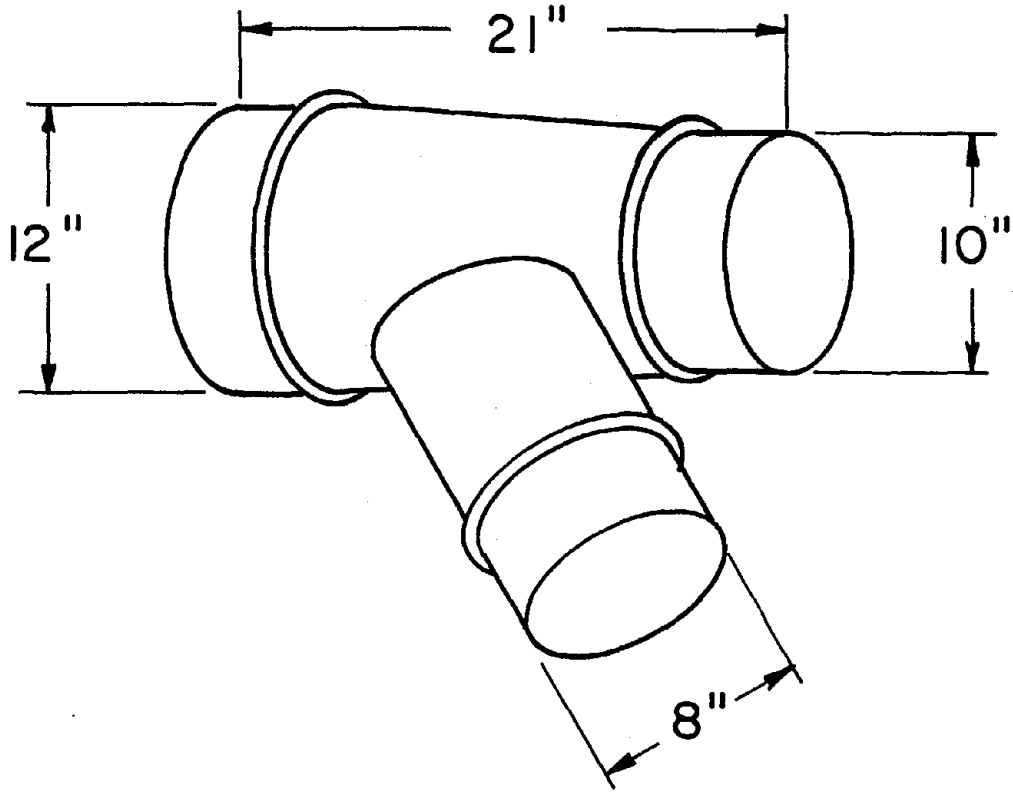

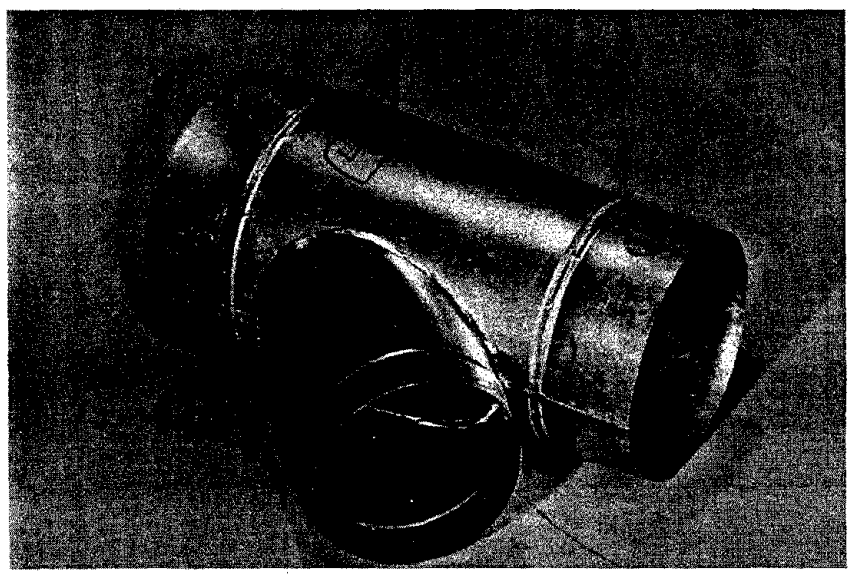

FIGURE B-23 FITTING L-IRT-3H

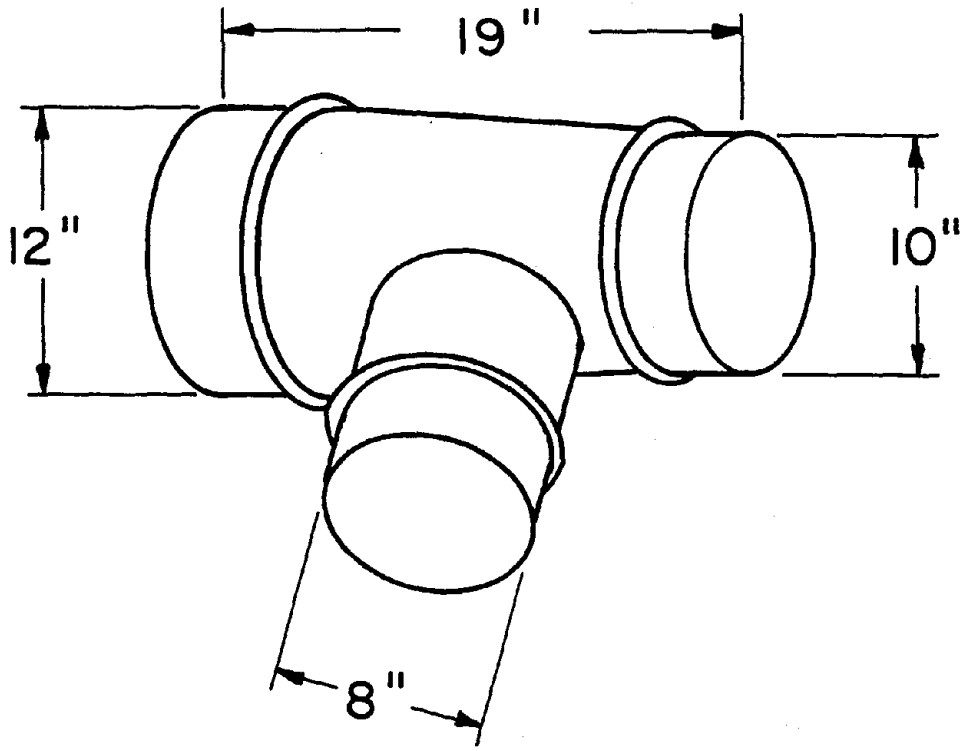

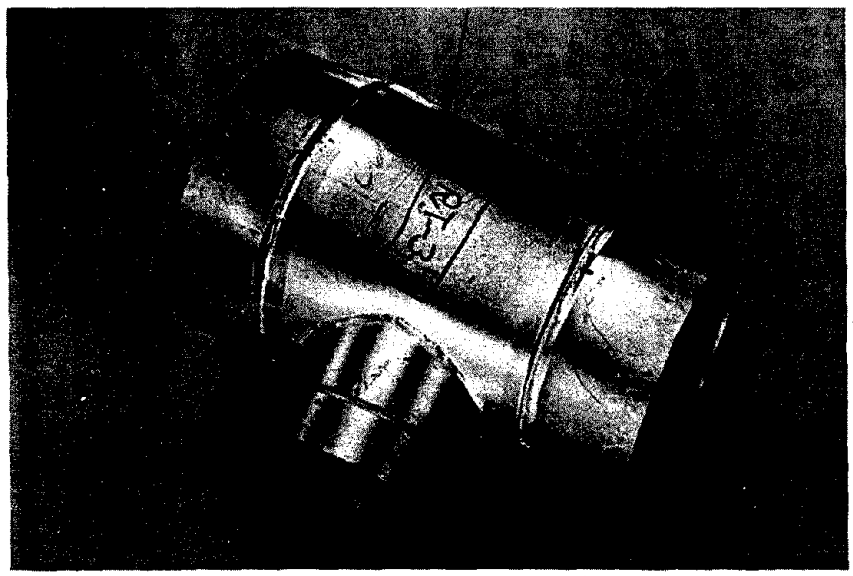

FIGURE B-24 FITTING T-IRT-3J

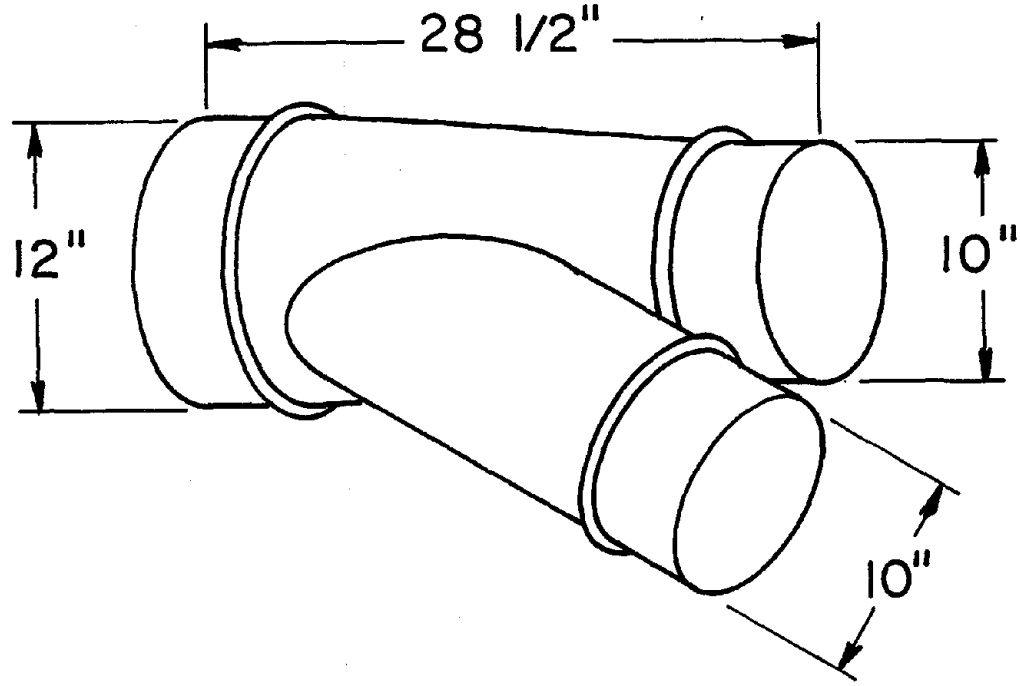

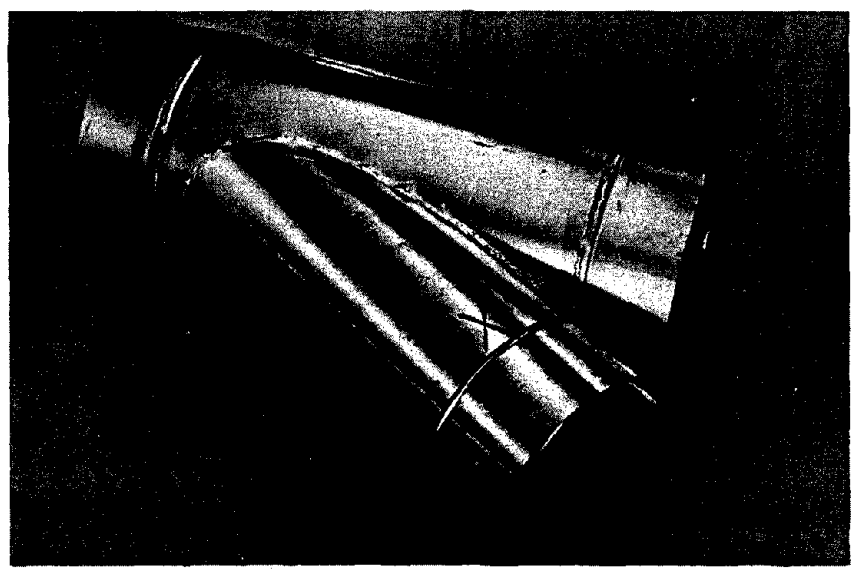

FIGURE B-25 FITTING L-IRT-3K

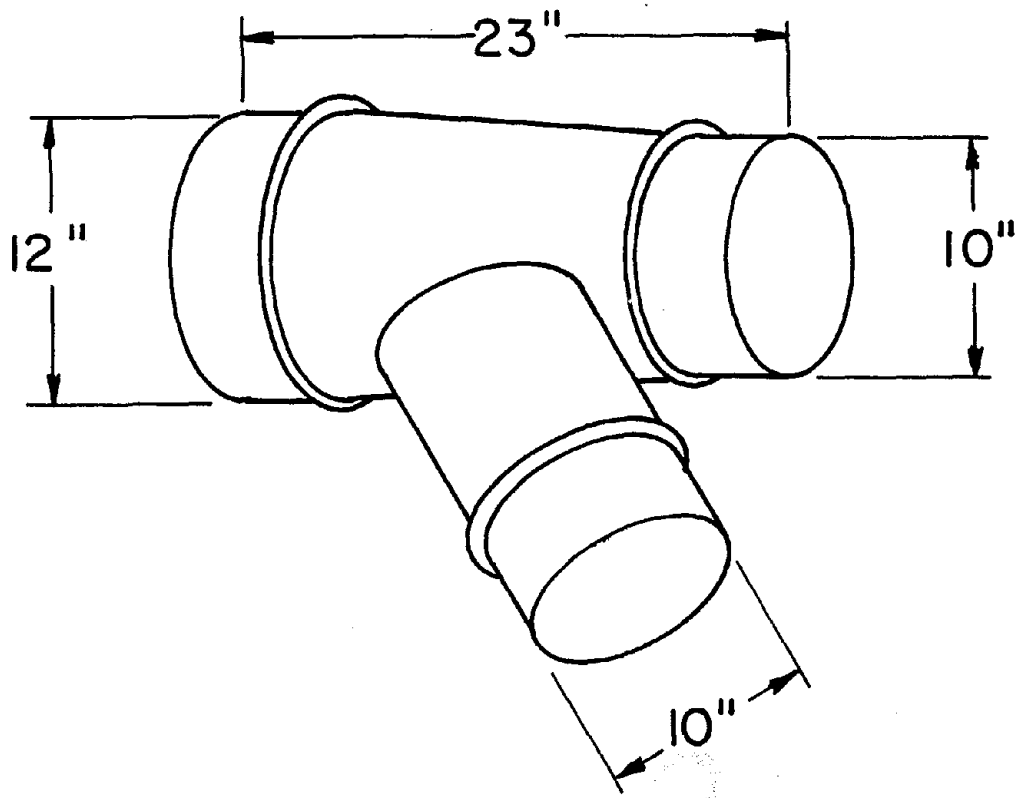

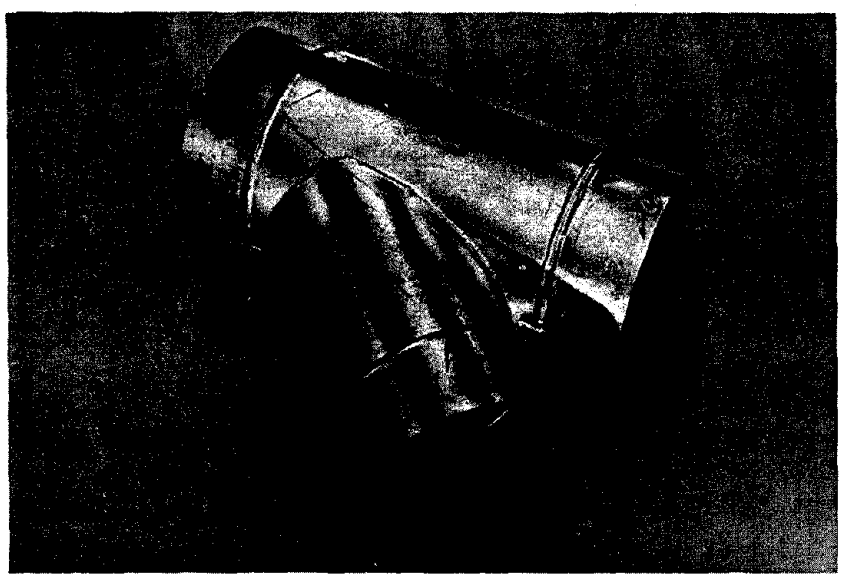

FIGURE B-26 FITTING L-IRT-3L

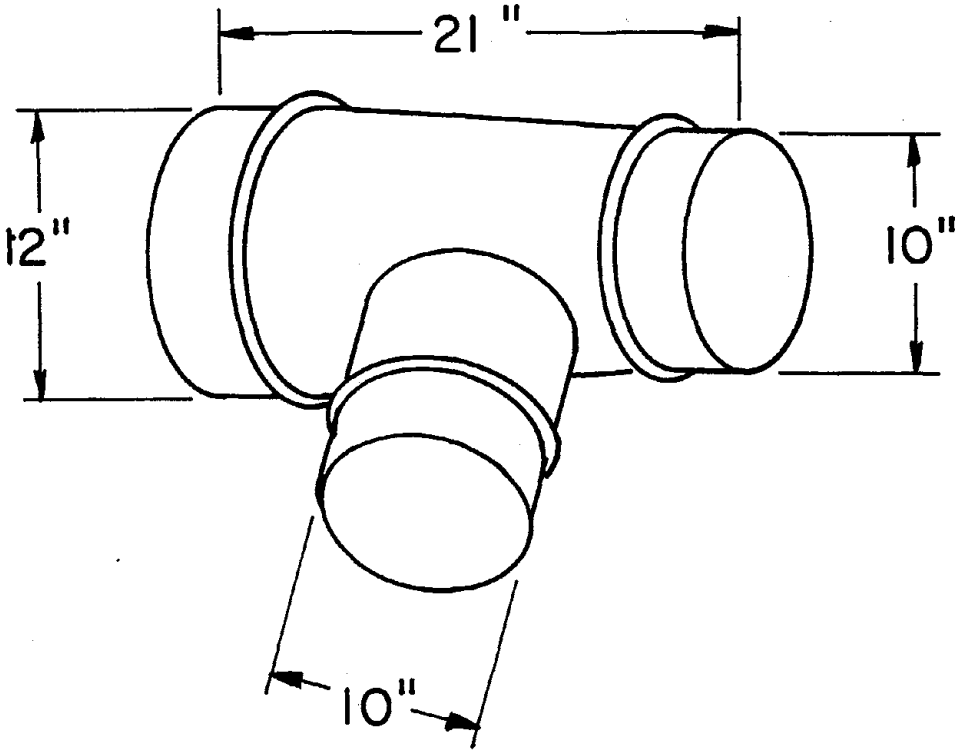

FIGURE B-27 FITTING T-IRT-3M

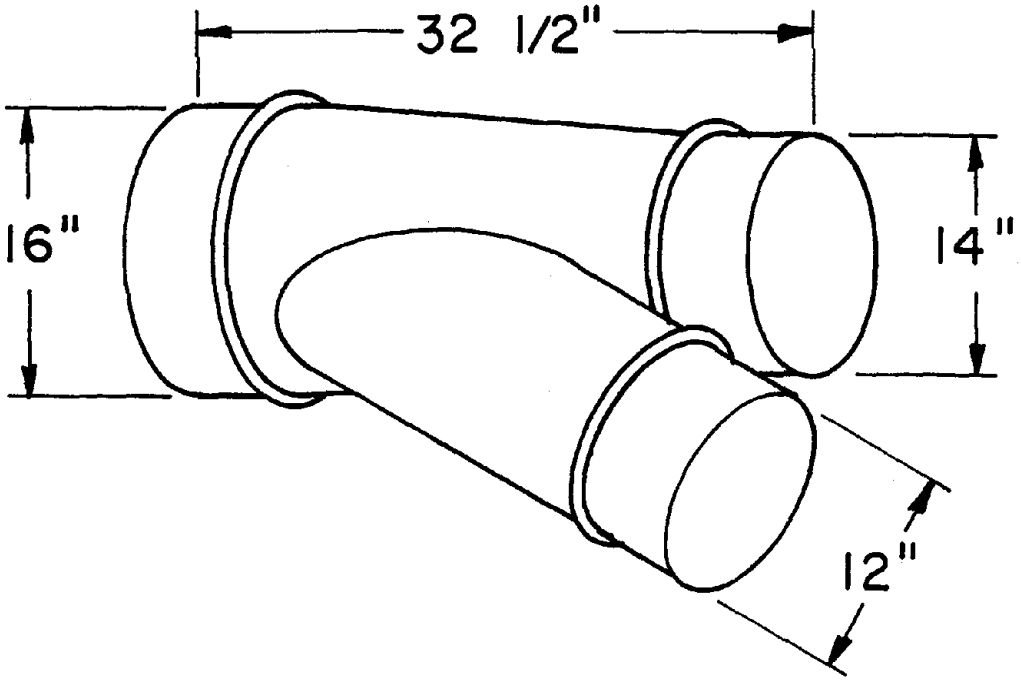

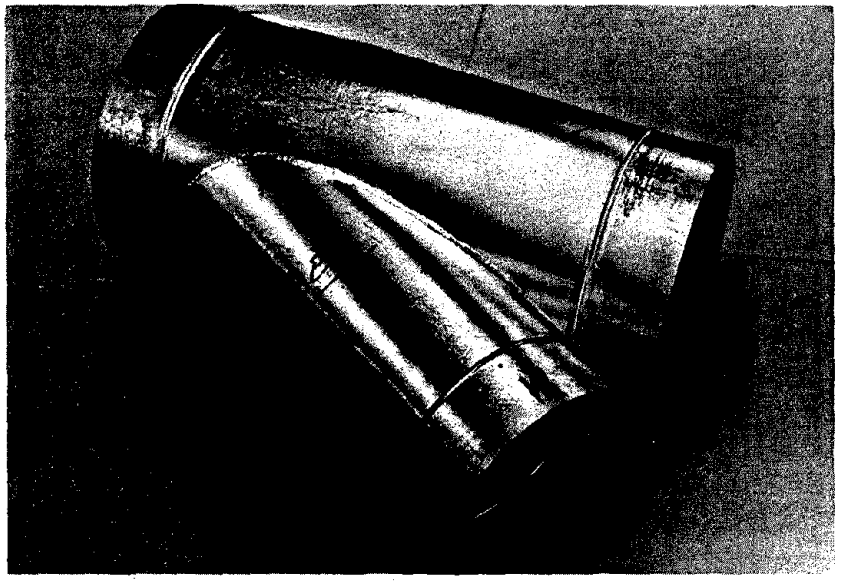

FIGURE B-28 FITTING L-IRT-3N

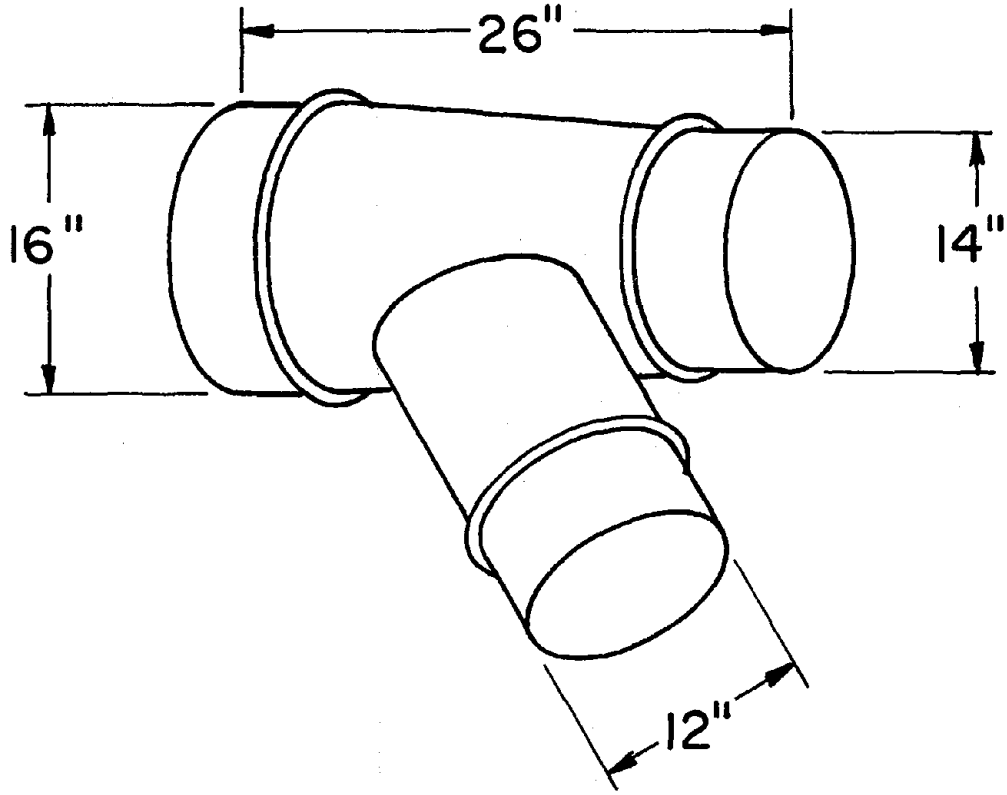

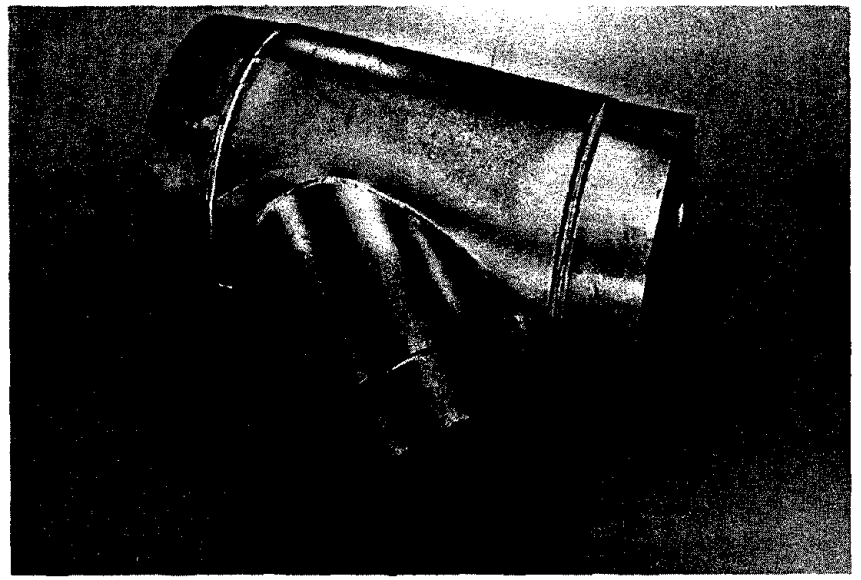

FIGURE B-29 FITTING L-IRT-30

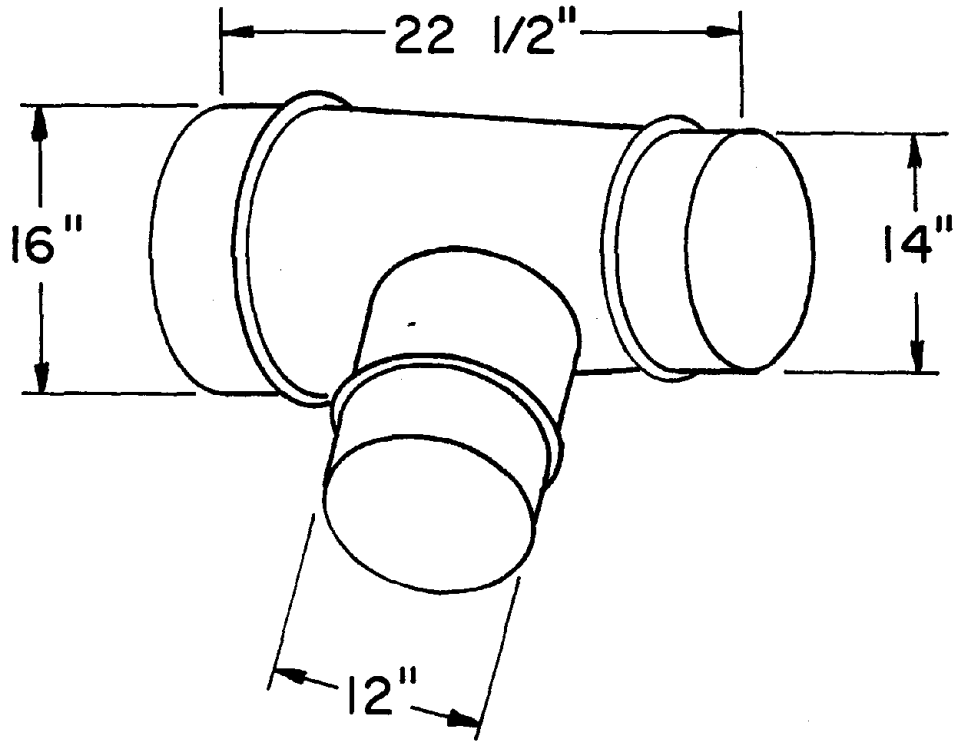

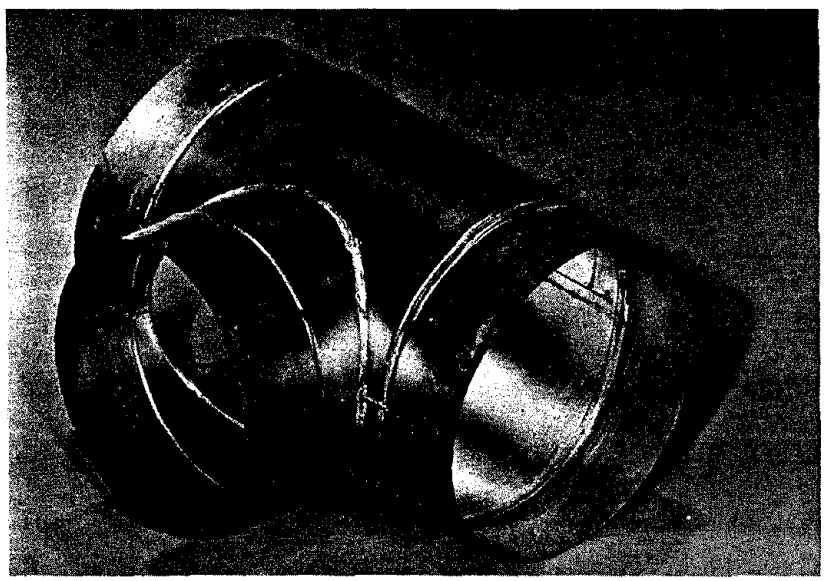

FIGURE B-30 FITTING T-IRT-3P

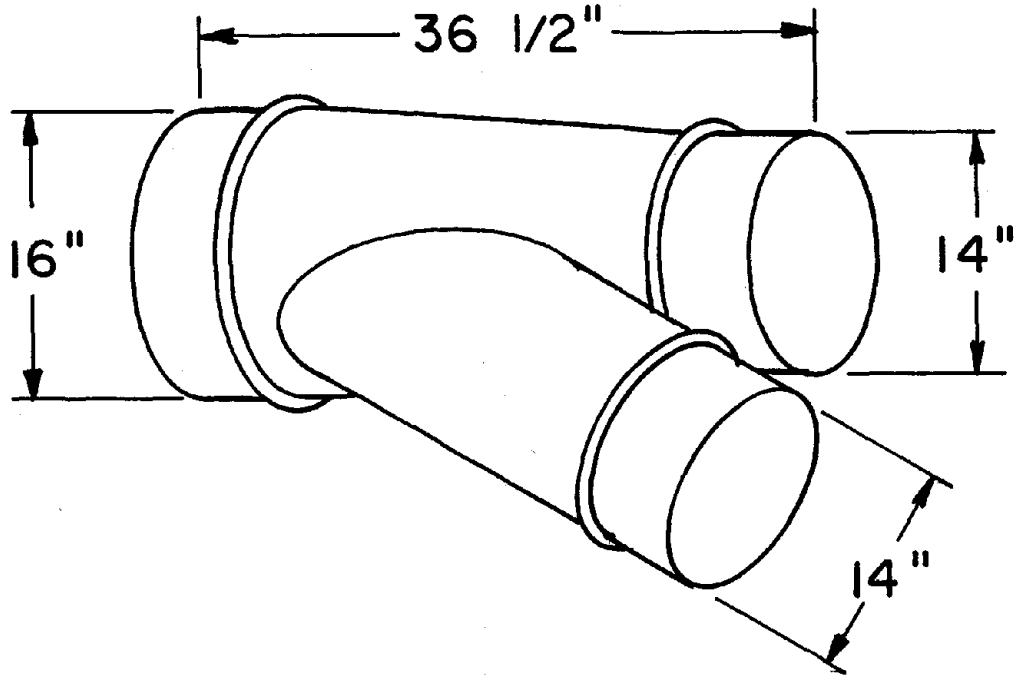

FIGURE B-31 FITTING L-IRT-3R

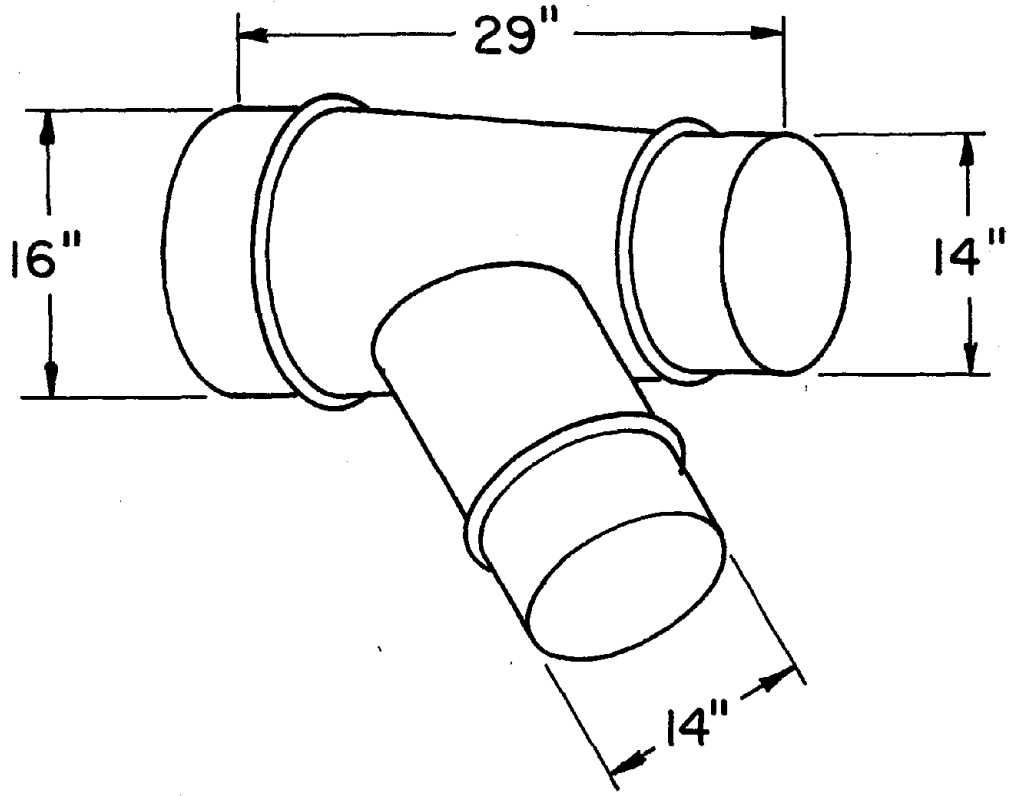

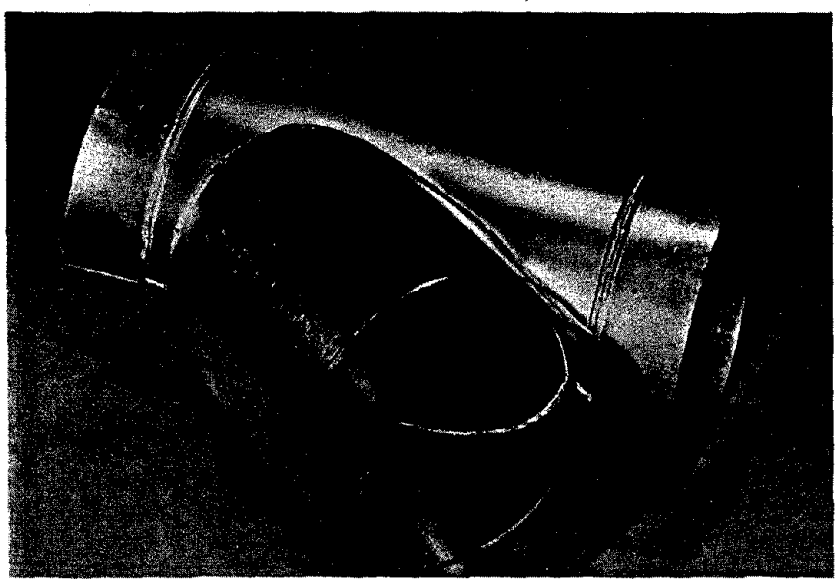

FIGURE B-32 FITTING L-IRT-3S

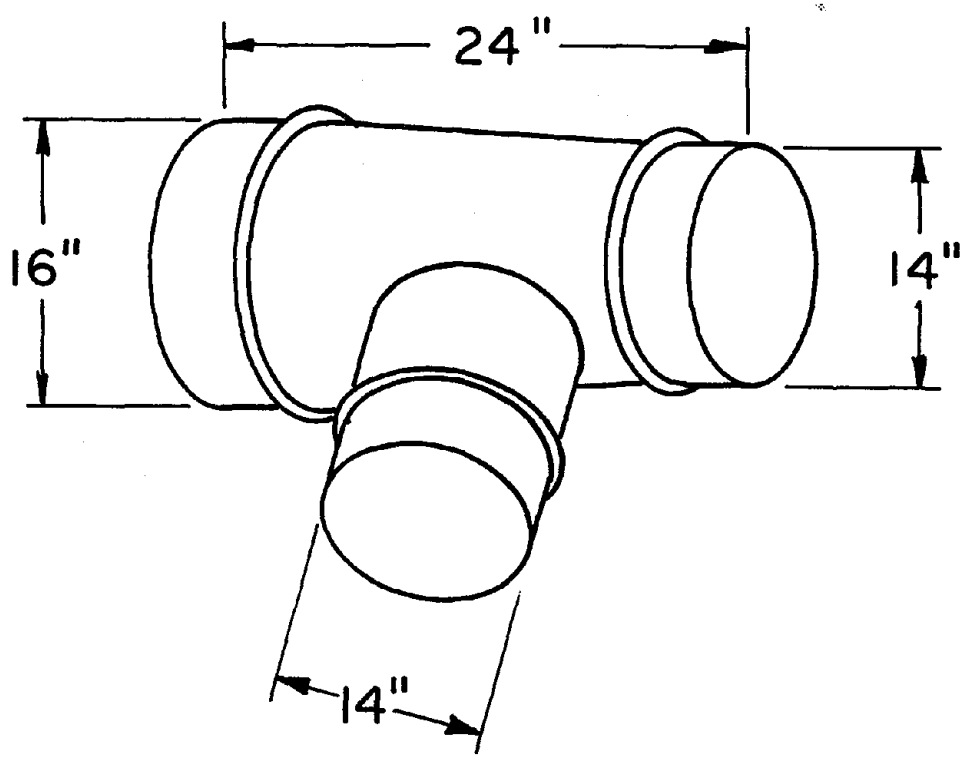

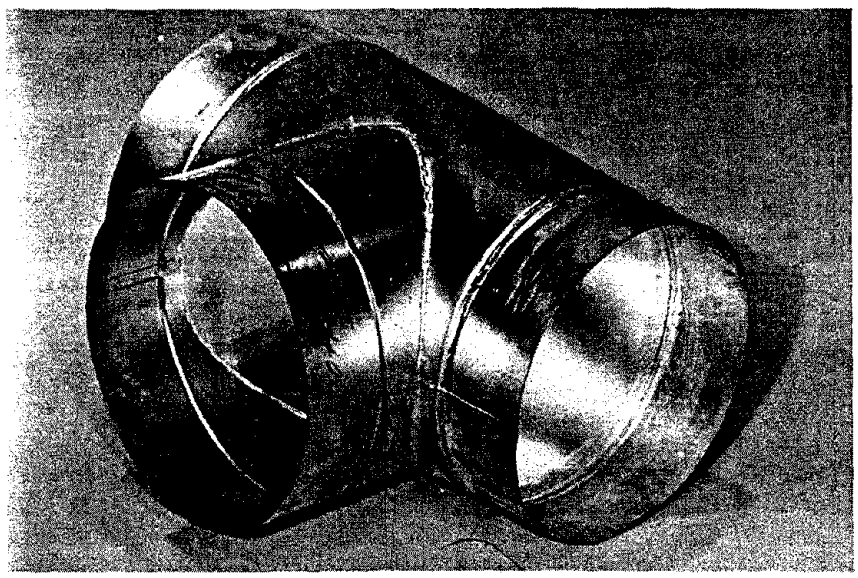

FIGURE B-33 FITTING T-IRT-3T

APPENDIX C

FRICTION LOSS

All results were standardized on a "no length" basis. This implies that the losses from the wall friction of the straight duct and fitting were subtracted from measured static pressure drops between two different sections. Friction loss in straight ducts can easily be determined by experiment, but the precise friction loss for taper fittings is quite difficult to predict. Since the length of the fittings were not much greater than the take-off diameters, it was assumed the wall friction between fitting entrances and the center of the fitting were the same as would correspond to a straight section with a diameter equal to the entrance diameter.

Present friction loss information was not used because recent changes in spiral duct fabrication procedures have resulted in a change in the friction factor. Experiments were conducted to measure losses for all diameters used in the fitting tests. Experimental procedures were the same as in Reference 18, and graphical results for 3, 10, 12, 14, and 16 inch diameter ducts are plotted in Figure C-1. Tests had already been conducted in Reference 18 for 4, 6, and 8 inch diameter ducts.

In order to most conveniently use friction loss results in computer computations, curve fitting procedures were used to determine equations which directly gave the pressure loss for any velocity and length of duct. These equations were made possible via a least squares fit OMNITAB "canned" program furnished by the Mechanical Engineering Department at The Ohio State University. All equations were sixth order polynomials and are listed in Fortran language in Table C-1.

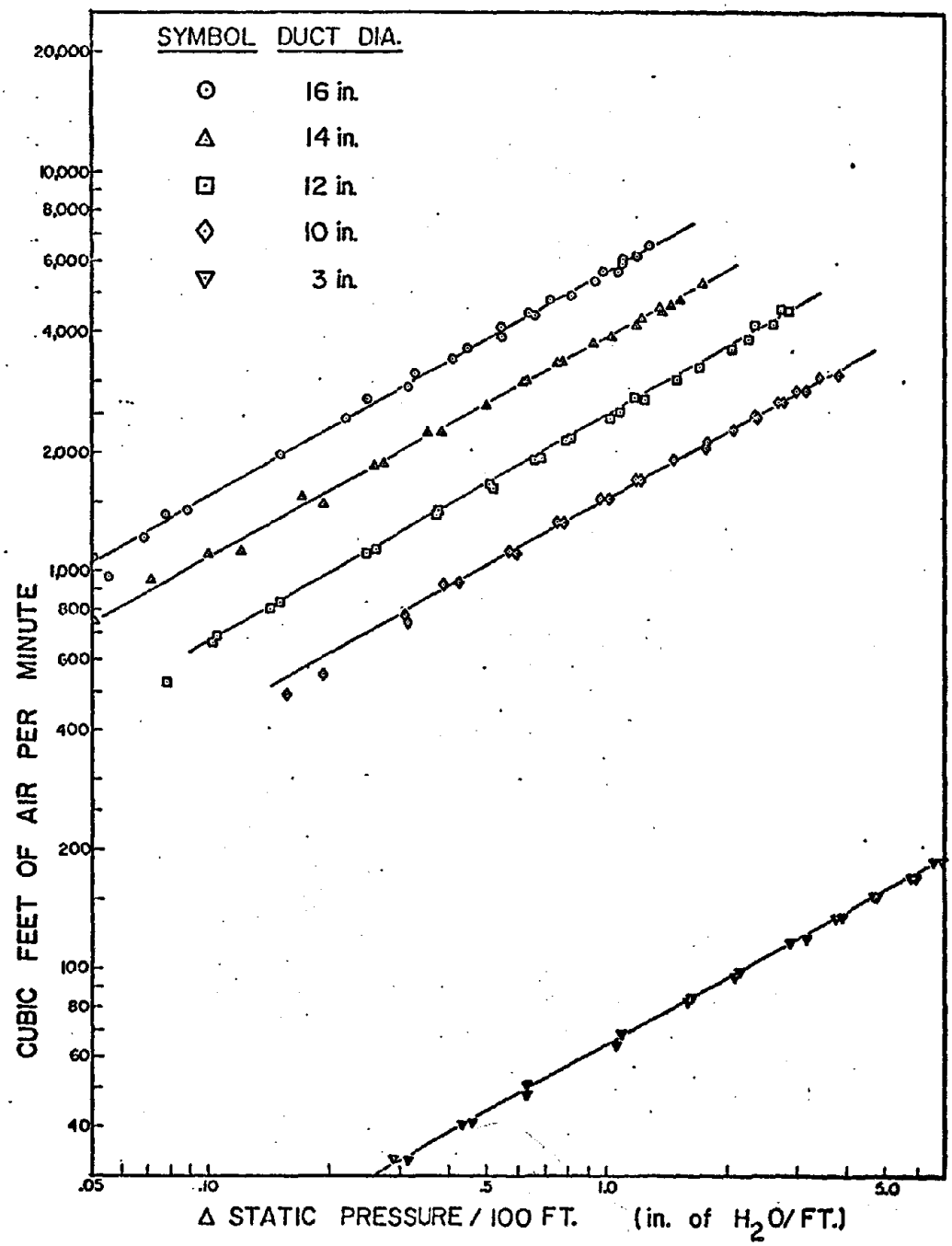

FIGURE C-1. VOLUME FLOW VS. FRICTION LOSS IN STRAIGHT DUCT.

TABLE C-1

FRICTION LOSS EQUATIONS

```
C     THREE INCH DIA BR
      DPFB = (5.681287 E-01 - 1.720752 E-03*VB + 2.672493 E-06*(VB**2)  BR3   1
     1     - 1.197475 E-09*(VB**3) + 3.150082 E-13*(VB**4) - 3.956586 E-1BR3   2
     27*(VB**5) + 1.866921 E-21*(VB**6))*(XB/100.)                     BR3   3
C     FOUR INCH DIA BR
      DPFB = (-.1457217E+01 + .4728083E-02*VB - .4922812E-05*(VB**2)    BR4   1
     1     + .2875454E-08*(VB**3) - .8177820E-12*(VB**4) + .1154929E-15* BR4   2
     2     (VB**5) - .6385938E-20*(VB**6))*(XB/100.)                   BR4   3
C     SIX INCH DIA BR
      DPFB = (.2812024E+0 - .7277231E-03*VB + .9753649E-06 *(VB**2)     BR6   1
     1     - .3645364E-09*(VB**3) + .8755344E-13*(VB**4) - .1015441E-16* BR6   2
     2     (VB**5) +.4454180E-21*(VB**6))*(XB/100.)                    BR6   3
C     EIGHT INCH DIA BR
      DPFB=(.9536024E+0-.2502983E-02*VB+.2744882E-05*(VB**2)            BR8   1
     1-.1254137E-08*(VB**3)+.3100551E-12*(VB**4)-.3800024E-16           BR8   2
     2*(VB**5)+.1829184E-20*(VB**6))*(XB/100.)                         BR8   3
C     TEN INCH DIA BR
      DPFB=(-7.566547E-01+2.074647E-03*VB-1.853260E-06*(VB**2)          BR10  1
     1+9.229926E-10*(VB**3)-2.254295E-13*(VB**4)+2.715945E-17           BR10  2
     2*(VB**5)-1.271218E-21*(VB**6))*(XB/100.)                         BR10  3
C     TWELVE INCH DIA BR
      DPFB=(4.428769E-01-1.302531E-03*VB+1.592866E-06*(VB**2)           BR12  1
     1-7.923484E-10*(VB**3)+2.126357E-13*(VB**4)-2.807806E-17           BR12  2
     2*(VB**5)+1.433924E-21*(VB**6))*(XB/100.)                         BR12  3
C     FOURTEEN INCH DIA BR
      DPFB=(-4.649544E-02+1.857951E-04*VB-1.666552E-07*(VB**2)          BR14  1
     1+1.865205E-10*(VB**3)-7.536571E-14*(VB**4)+1.429629E-17           BR14  2
     2*(VB**5)-1.034001E-21*(VB**6))*(XB/100.)                         BR14  3
C     THREE INCH DIA UP
      DPFU = (5.681287 E-01 - 1.720752 E-03*VU + 2.672493 E-06*(VU**2)  UP3   1
     1     - 1.197475 E-09*(VU**3) + 3.150082 E-13*(VU**4) - 3.956586. E-1UP3   2
     27*(VU**5) + 1.866921 E-21*(VU**6))*(XU/100.)                     UP3   3
C     FOUR INCH DIA UP
      DPFU = (-.1457217E+01 + .4728083E-02*VU - .4922812E-05*(VU**2)    UP4   1
     1     + .2875454E-08*(VU**3) - .8177820E-12*(VU**4) + .1154929E-15* UP4   2
     2     (VU**5) - .6385938E-20*(VU**6))*(XU/100.)                   UP4   3
C     SIX INCH DIA UP
      DPFU = (.2812024E+0 - .7277231E-03*VU + .9753649E-06 *(VU**2)     UP6   1
     1     - .3645364E-09*(VU**3) + .8755344E-13*(VU**4) - .1015441E-16* UP6   2
     2     (VU**5) +.4454180E-21*(VU**6))*(XU/100.)                    UP6   3
C     EIGHT INCH DIA UP
      DPFU=(.9536024E+0-.2502983E-02*VU+.2744882E-05*(VU**2)            UP8   1
     1-.1254137E-08*(VU**3)+.3100551E-12*(VU**4)-.3800024E-16           UP8   2
     2*(VU**5)+.1829184E-20*(VU**6))*(XU/100.)                         UP8   3
```

TABLE C-1 (CONT'D.)

FRICTION LOSS EQUATIONS

```
C     TEN INCH DIA  UP
      DPFU=(-7.566547E-01+2.074647E-03*VU-1.853260E-06*(VU**2)          UP10 1
     1+9.229926E-10*(VU**3)-2.254295E-13*(VU**4)+2.715945E-17           UP10 2
     2*(VU**5)-1.271218E-21*(VU**6))*(XU/100.)                          UP10 3
C     TWELVE INCH DIA UP
      DPFU=(4.428769E-01-1.302531E-03*VU+1.592866E-06*(VU**2)           UP12 1
     1-7.923484E-10*(VU**3)+2.126357E-13*(VU**4)-2.807806E-17           UP12 2
     2*(VU**5)+1.433924E-21*(VU**6))*(XU/100.)                          UP12 3
C     FOURTEEN INCH DIA UP
      DPFU=(-4.649544E-02+1.857951E-04*VU-1.666552E-07*(VU**2)          UP14 2
     1+1.869205E-10*(VU**3)-7.536571E-14*(VU**4)+1.439629E-17           UP14 2
     2*(VU**5)-1.034001E-21*(VU**6))*(XU/100.)                          UP14 3
C        FOUR INCH DIA DN
      DPFD = (-.1457217E+01 + .4728083E-02*VD - .4922812E-05*(VD**2)    DN4  1
     1     + .2875454E-08*(VD**3) - .8177820E-12*(VD**4) + .1154929E-15* DN4  2
     2     (VD**5) - .6385938E-20*(VD**6))*(XD/100.)                    DN4  3
C        SIX INCH DIA DN
      DPFD = (.2812024E+0 - .7277231E-03*VD + .9753449E-06 *(VD**2)     DN6  1
     1     - .3645364E-09*(VD**3) + .8755344E-13*(VD**4) - .1015441E-16* DN6  2
     2     (VD**5) +.4454180E-21*(VD**6))*(XD/100.)                     DN6  3
C     EIGHT INCH DIA DN
      DPFD=(.9536024E+0-.2602983E-02*VD+.2744882E-05*(VD**2)            DN8  1
     1-.1254137E-08*(VD**3)+.3100551E-12*(VD**4)-.3800024E-16           DN8  2
     2*(VD**5)+.1829184E-20*(VD**6))*(XD/100.)                          DN8  3
C     TEN INCH DIA DN
      DPFD=(-7.566547E-01+2.074647E-03*VD-1.853260E-06*(VD**2)          DN10 1
     1+9.229926E-10*(VD**3)-2.254295E-13*(VD**4)+2.715945E-17           DN10 2
     2*(VD**5)-1.271218E-21*(VD**6))*(XD/100.)                          DN10 3
C     TWELVE INCH DIA DN
      DPFD=(4.428769E-01-1.302531E-03*VD+1.592866E-06*(VD**2)           DN12 1
     1-7.923484E-10*(VD**3)+2.126357E-13*(VD**4)-2.807806E-17           DN12 2
     2*(VD**5)+1.433924E-21*(VD**6))*(XD/100.)                          DN12 3
C     FOURTEEN INCH DIA DN
      DPFD=(-4.649544E-02+1.857951E-04*VD-1.666552E-07*(VD**2)          DN14 1
     1+1.869205E-10*(VD**3)-7.536571E-14*(VD**4)+1.439629E-17           DN14 2
     2*(VD**5)-1.034001E-21*(VD**6))*(XD/100.)                          DN14 3
C     SIXTEEN INCH DIA DN
      DPFD=(-8.561152E-02+3.777864E-04*VD-4.603074E-07*(VD**2)          DN16 1
     1+3.555021E-10*(VD**3)-1.250044E-13*(VD**4)+2.175208E-17           DN16 2
     2*(VD**5)-1.488497E-21*(VD**6))*(XD/100.)                          DN16 3
```

COMPUTER SYMBOLS FOR TABLE C-1

Symbol	Description	Dimensions
DPFB	Friction loss from branch station to fitting center	in. of H_2O
DPFD	Friction loss from downstream station to fitting center	in. of H_2O
DPFU	Friction loss from upstream station to fitting center	in. of H_2O
VB	Mean velocity in branch	ft./min.
VD	Mean velocity in downstream	ft./min.
VU	Mean velocity in upstream	ft./min.
XB	Distance from branch station to fitting center	ft.
XD	Distance from downstream station to fitting center	ft.
XU	Distance from upstream station to fitting center	ft.

APPENDIX D

GENERALIZED LOSS COEFFICIENT GRAPHS

The branch and main loss coefficient curves in Figures D-1 through D-48 were generated by equations 4.17 and 4.18. These equations were

$$CB = CB_t + \Delta CB \qquad 4.17$$

$$CM = CM_t + \Delta CM \qquad 4.18$$

where CB_t and CM_t were evaluated by equations 4.13 and 4.14 respectively for all A_b/A_d, A_u/A_d, and all branch angles. Table 4-1 lists the equation numbers pertaining to ΔCB and ΔCM for different branch angles and specifies the reliaility restrictions based on comparison between the analytical equations and the experimental data. These plots are to be used directly for design work where the total pressure drops from branch to downstream and from upstream to downstream are

$$\Delta P_{tbd} = CB\left(\frac{V_d}{4005}\right)^2$$

$$\Delta P_{tud} = CM\left(\frac{V_d}{4005}\right)^2$$

where, CB $\triangleq$ branch loss coefficient from graph, dimensionless

CM $\triangleq$ main loss coefficient from graph, dimensionless

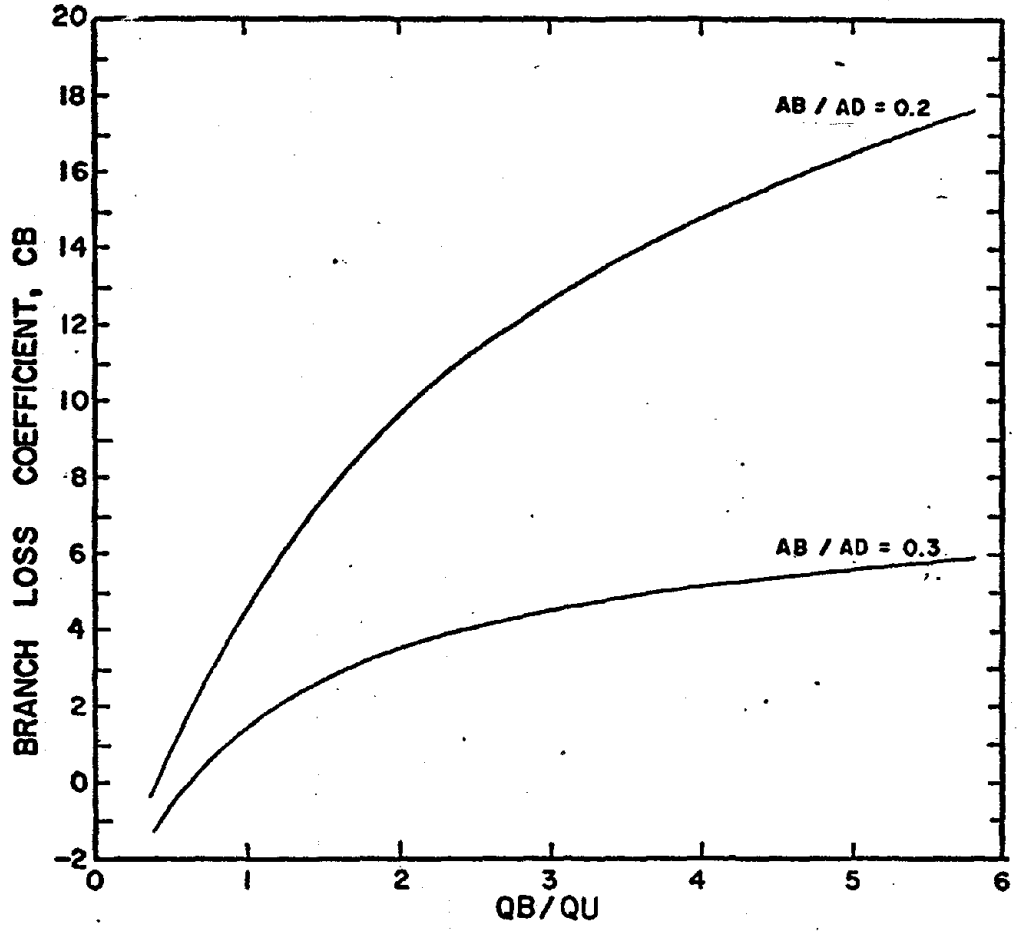

FIGURE D-1 BRANCH ANGLE=30°, AU/AD=0.3

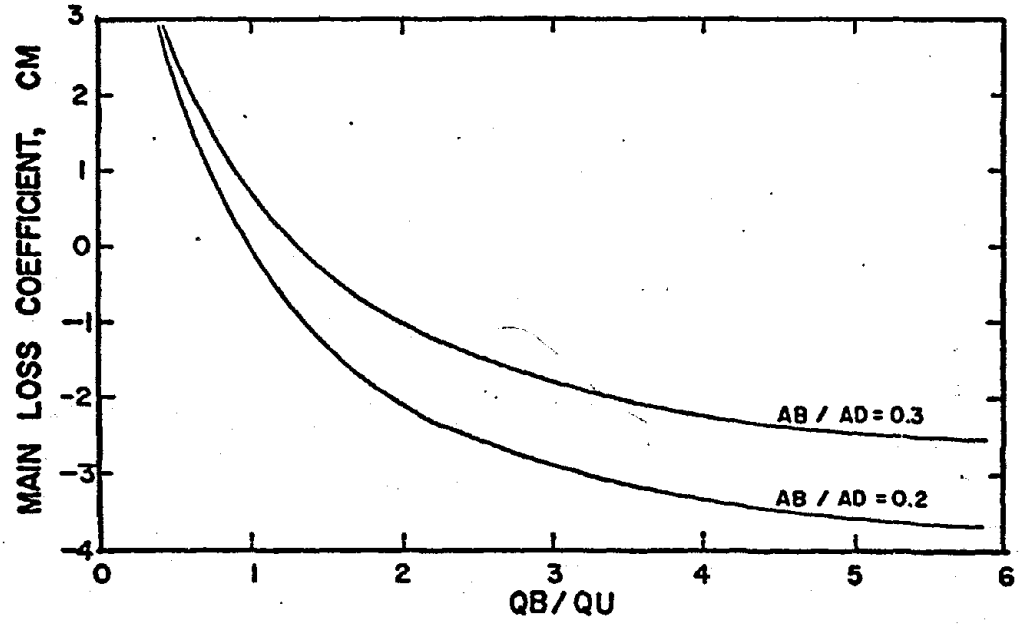

FIGURE D-2 BRANCH ANGLE=30°, AU / AD=0.3

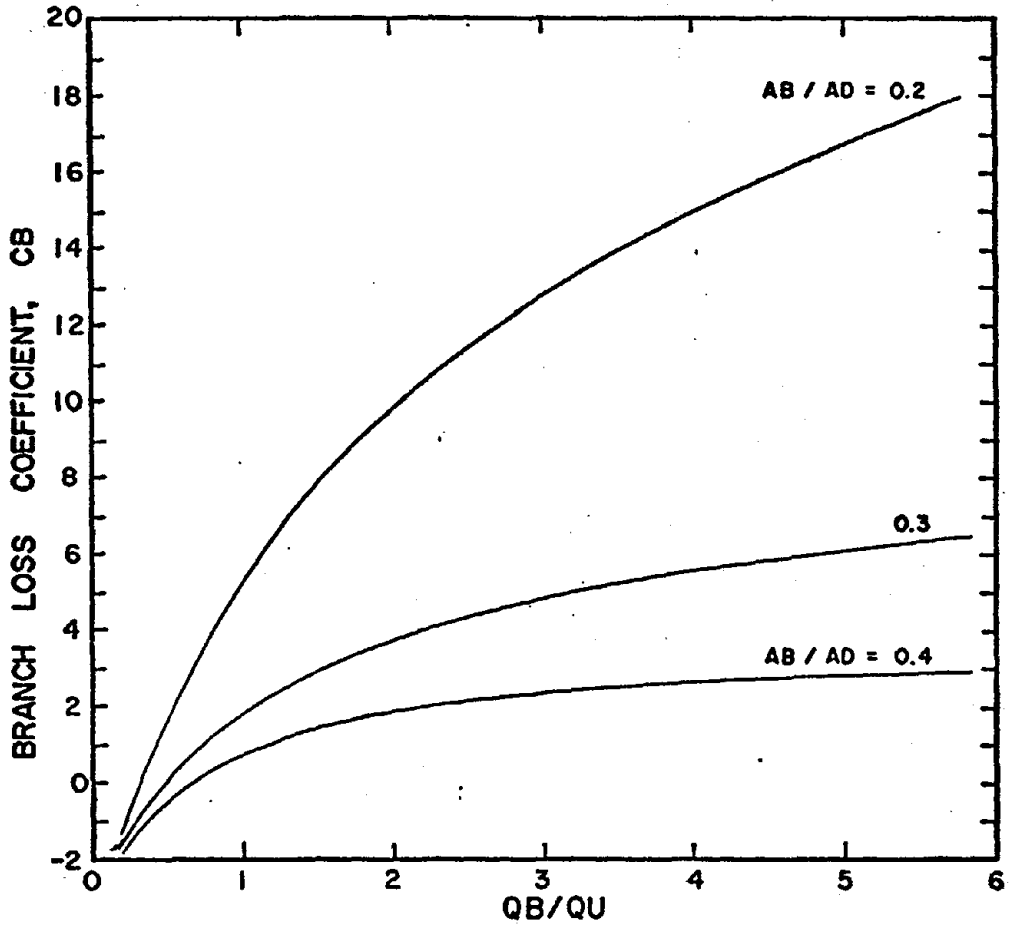

FIGURE D-3 BRANCH ANGLE=30°, AU/AD=0.4

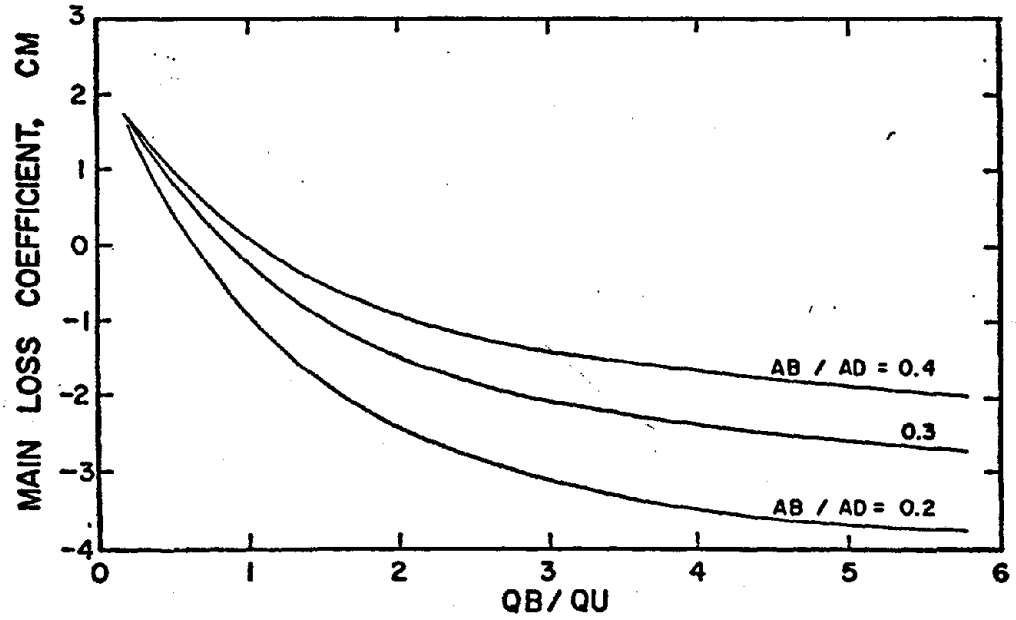

FIGURE D-4 BRANCH ANGLE=30°, AU/AD=0.4

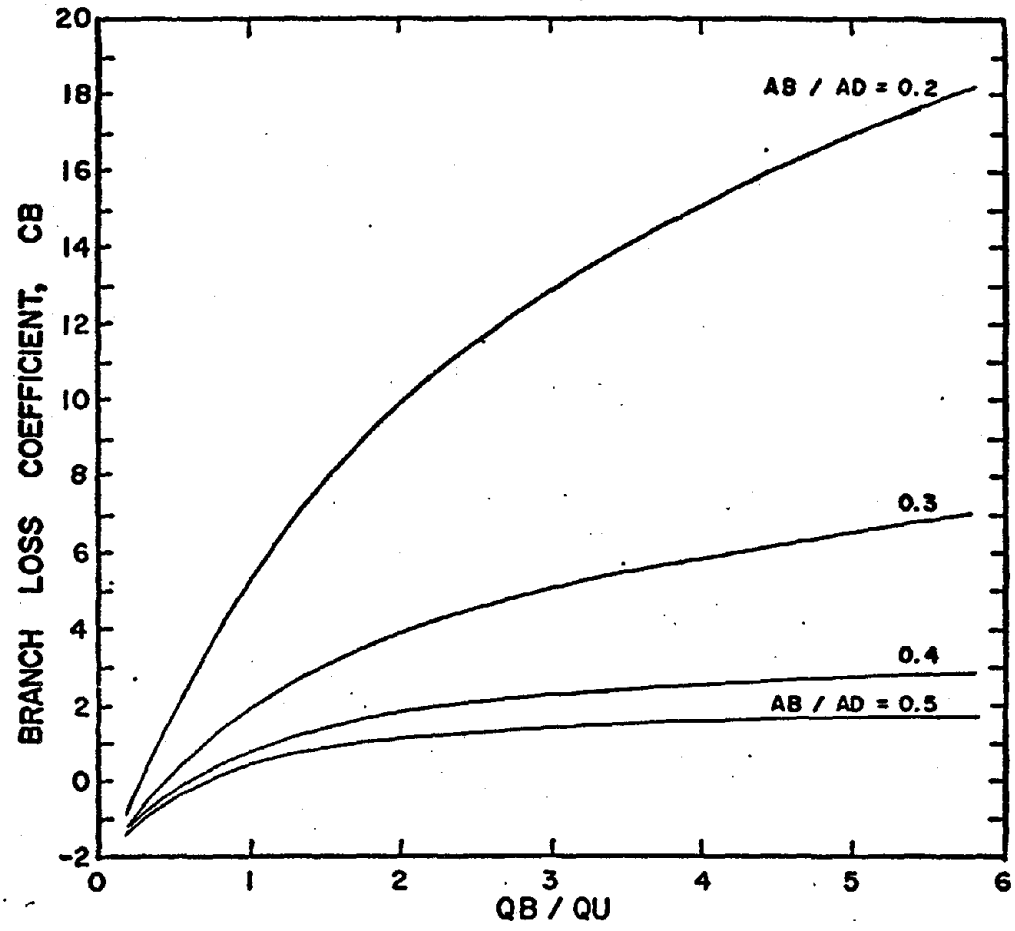

FIGURE D-5 BRANCH ANGLE=30°, AU/AD = 0.5

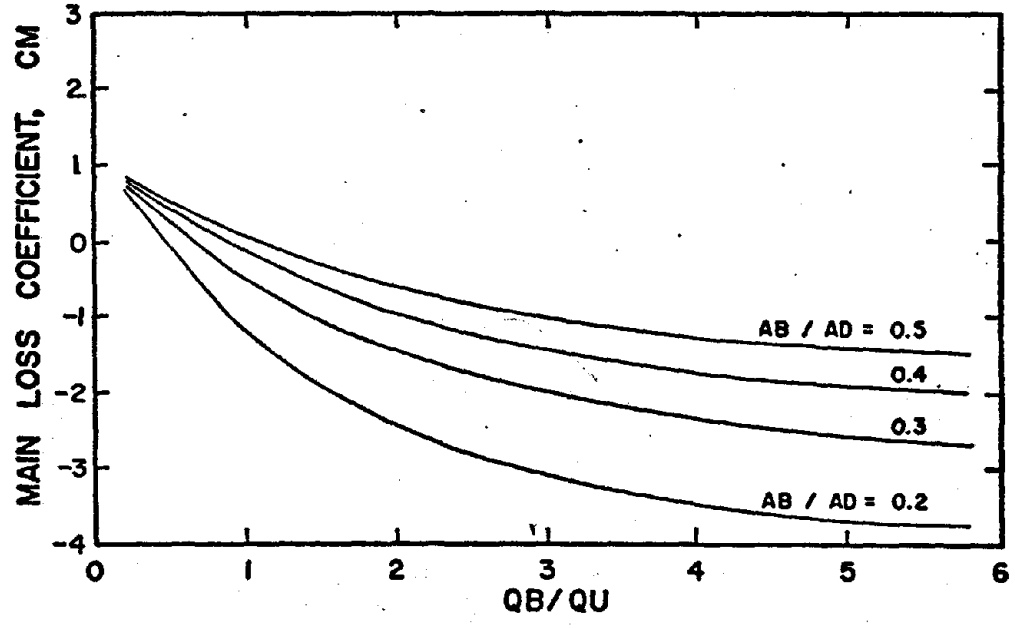

FIGURE D-6 BRANCH ANGLE=30°, AU/AD=0.5

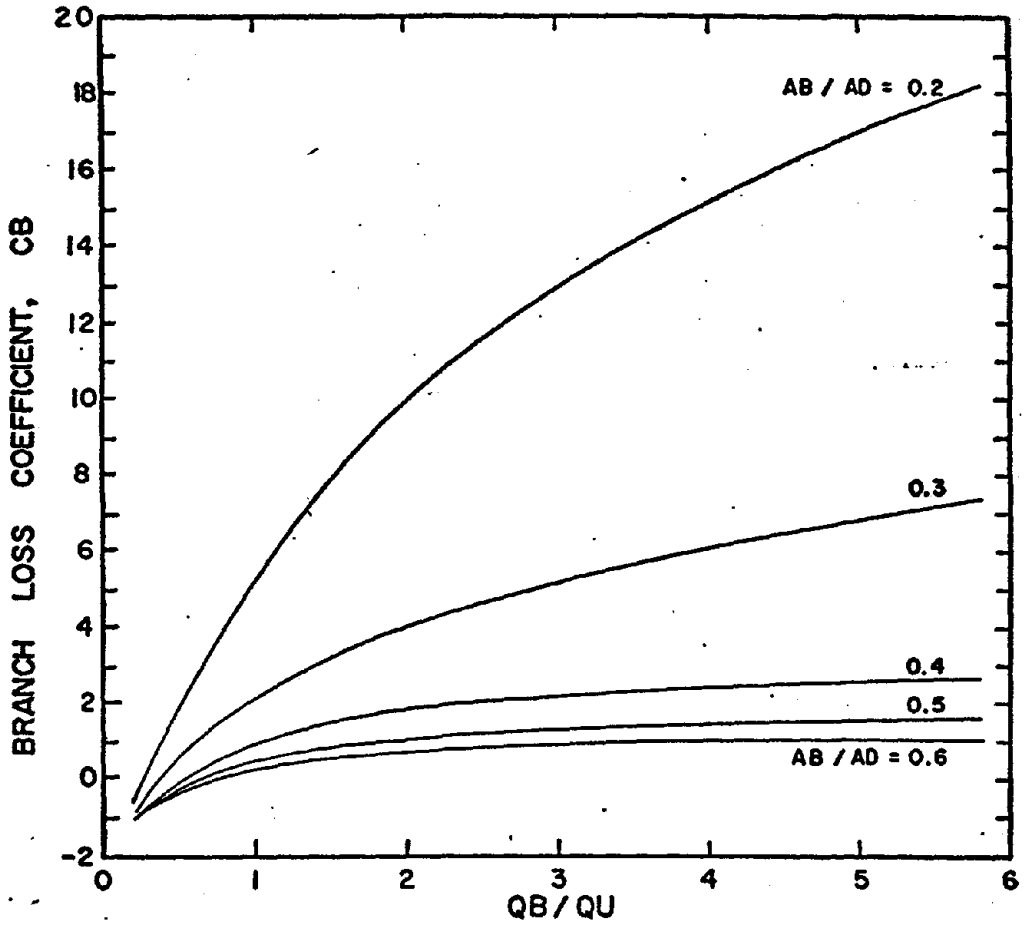

FIGURE D-7 BRANCH ANGLE=30°, AU/AD=0.6

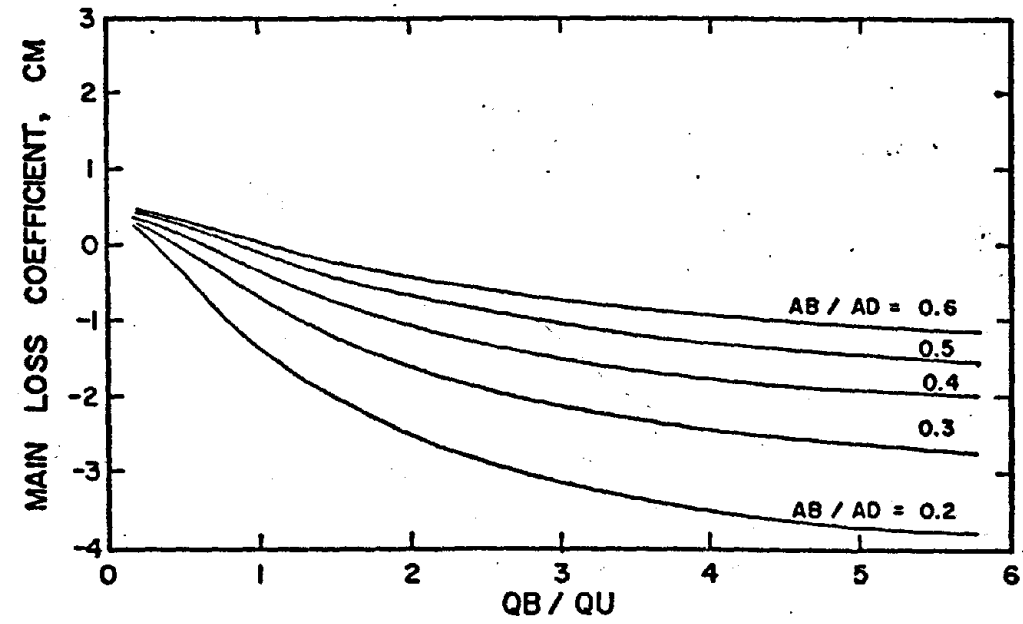

FIGURE D-8 BRANCH ANGLE=30°, AU/AD=0.6

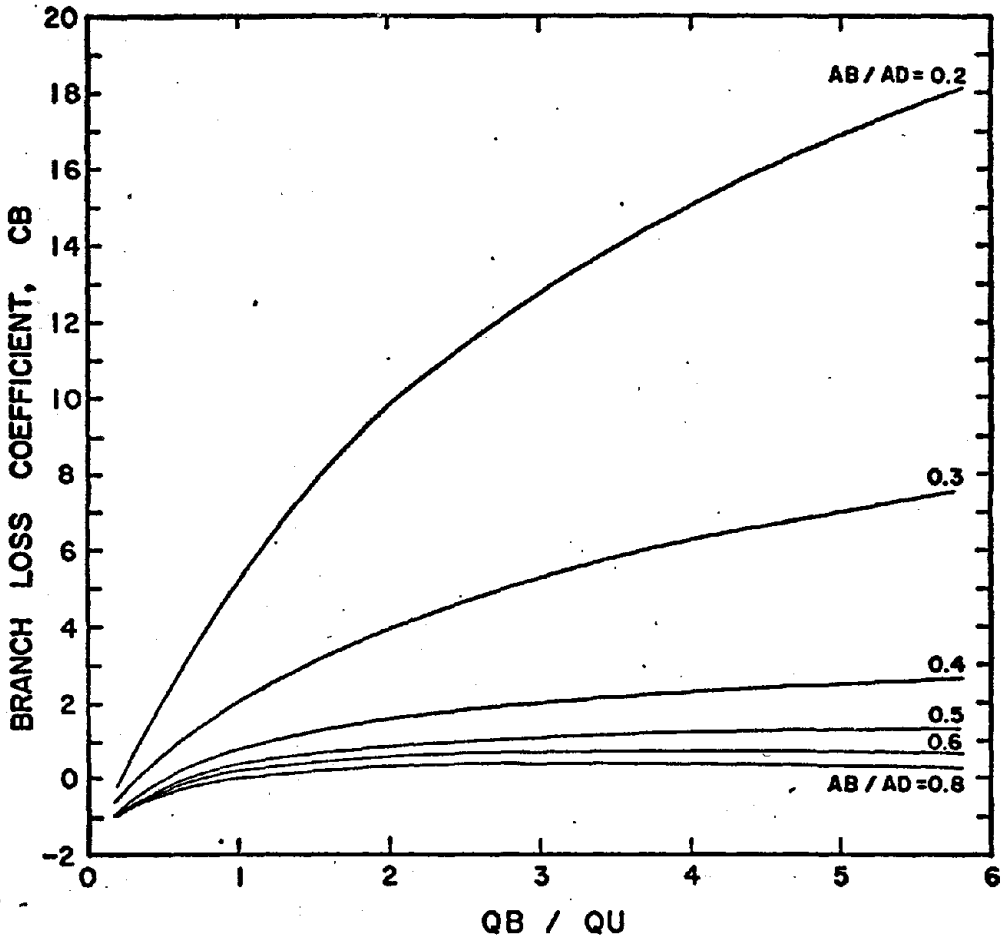

FIGURE D-9 BRANCH ANGLE = 30°, AU / AD = 0.8

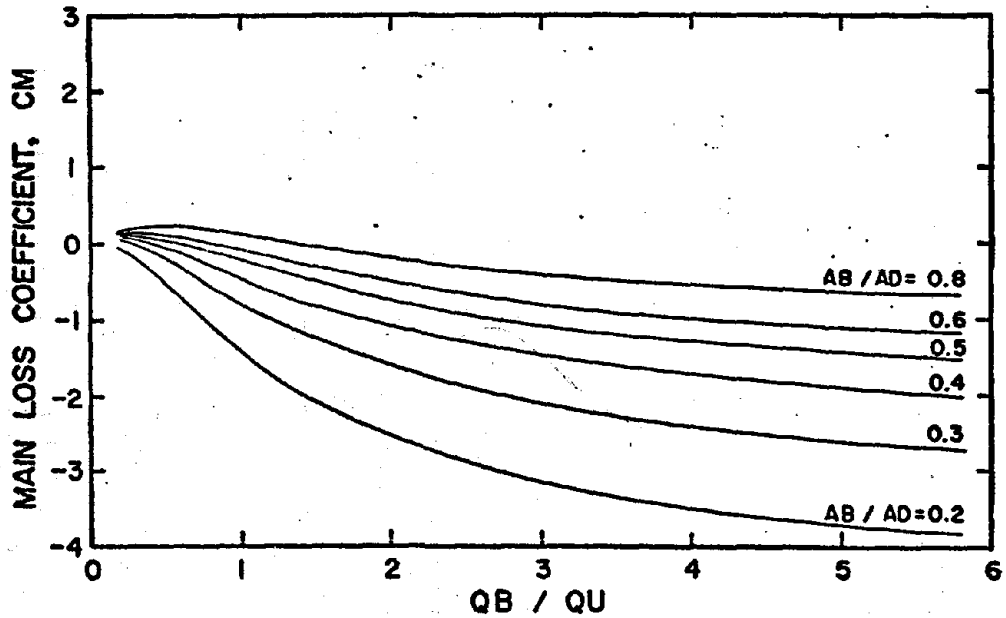

FIGURE D-10 BRANCH ANGLE = 30°, AU / AD = 0.8

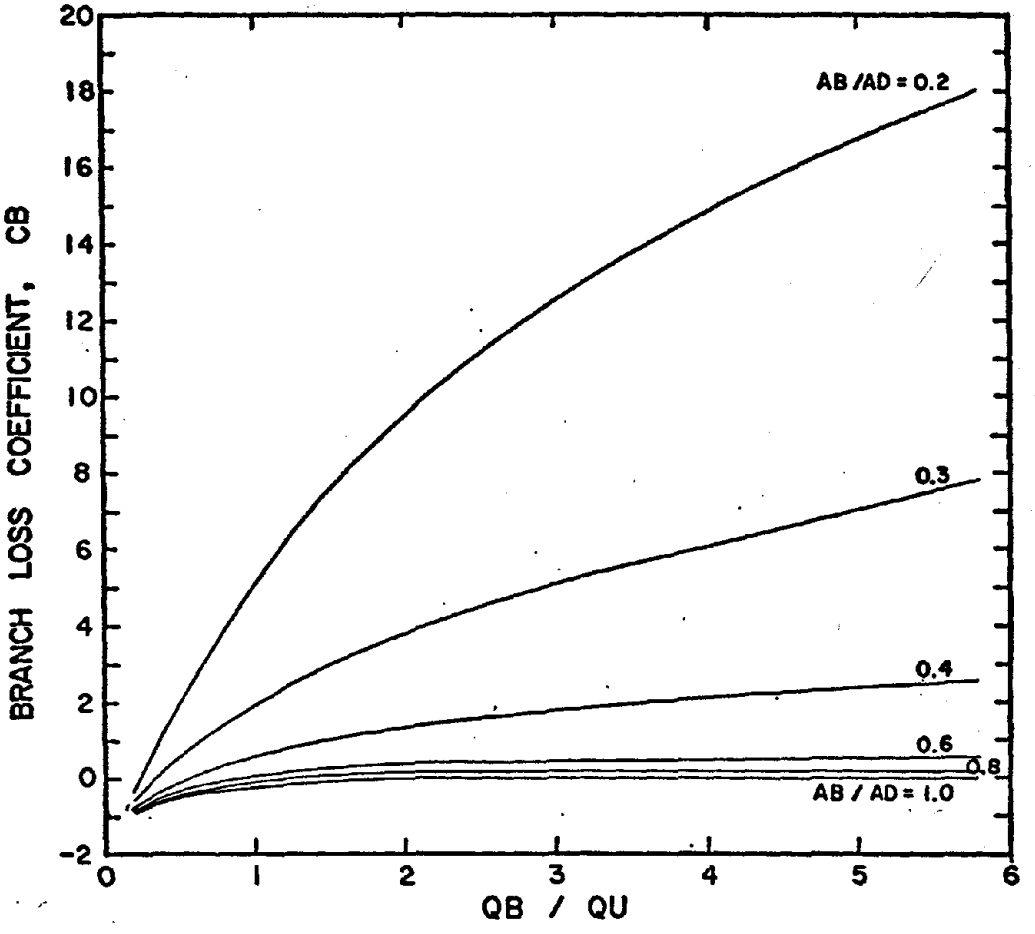

FIGURE D-11 BRANCH ANGLE = 30°, AU / AD = 1.0

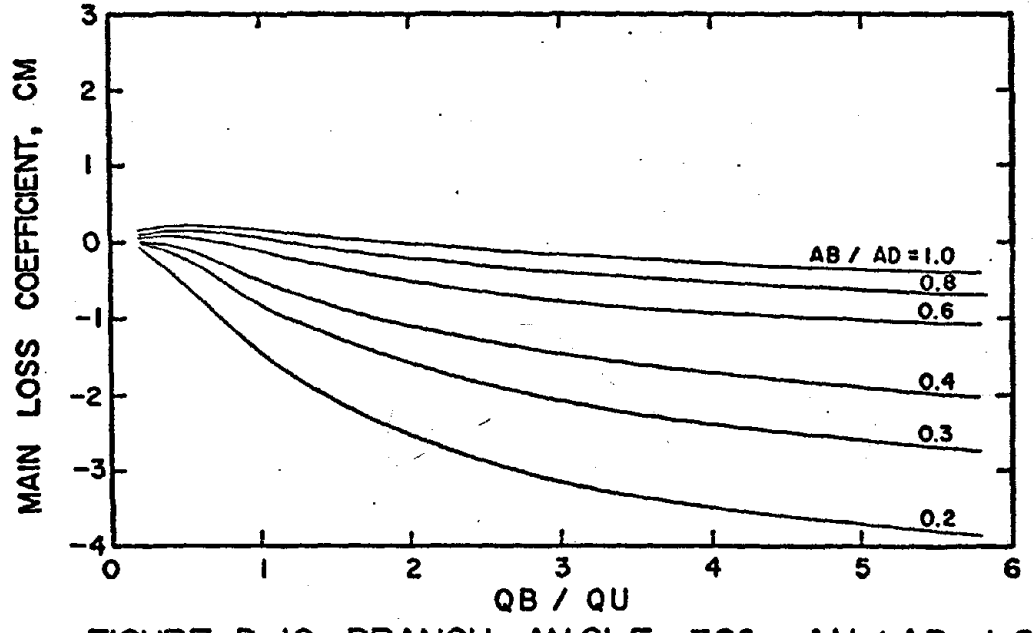

FIGURE D-12 BRANCH ANGLE = 30°, AU / AD = 1.0

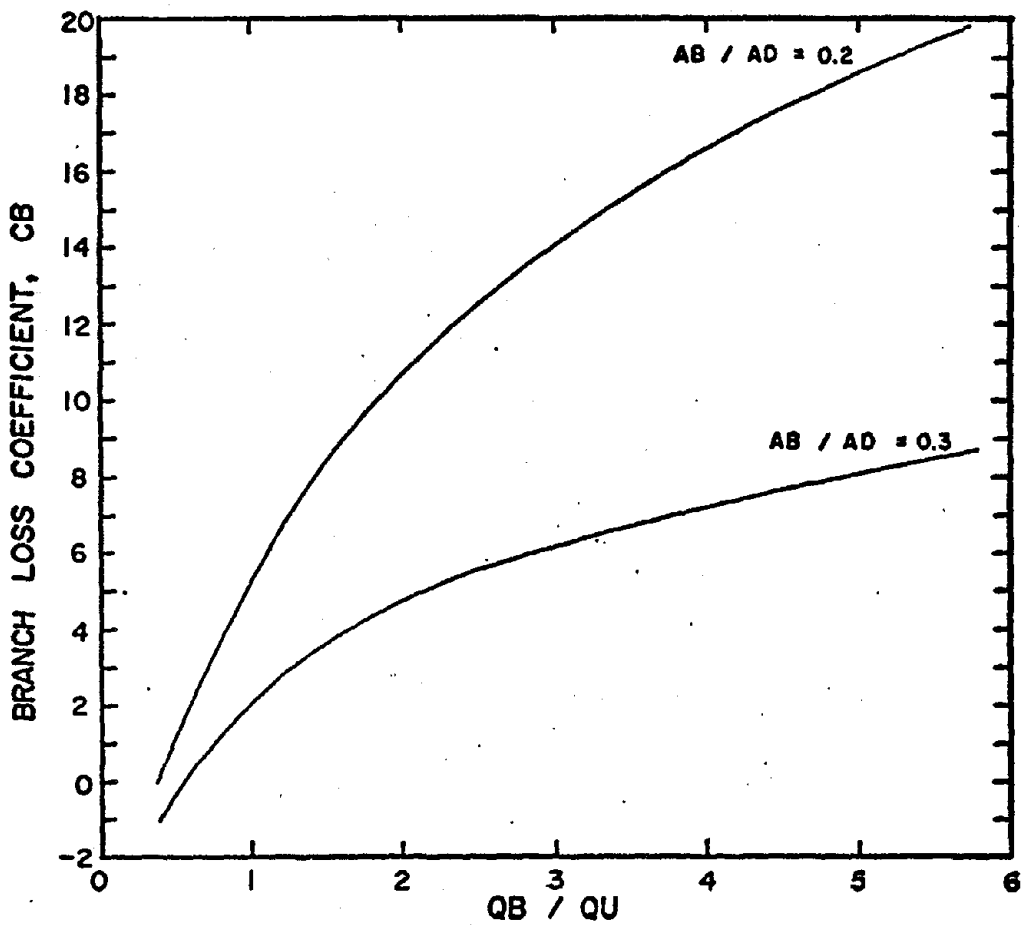

FIGURE D-13 BRANCH ANGLE = 45°, AU / AD = 0.3

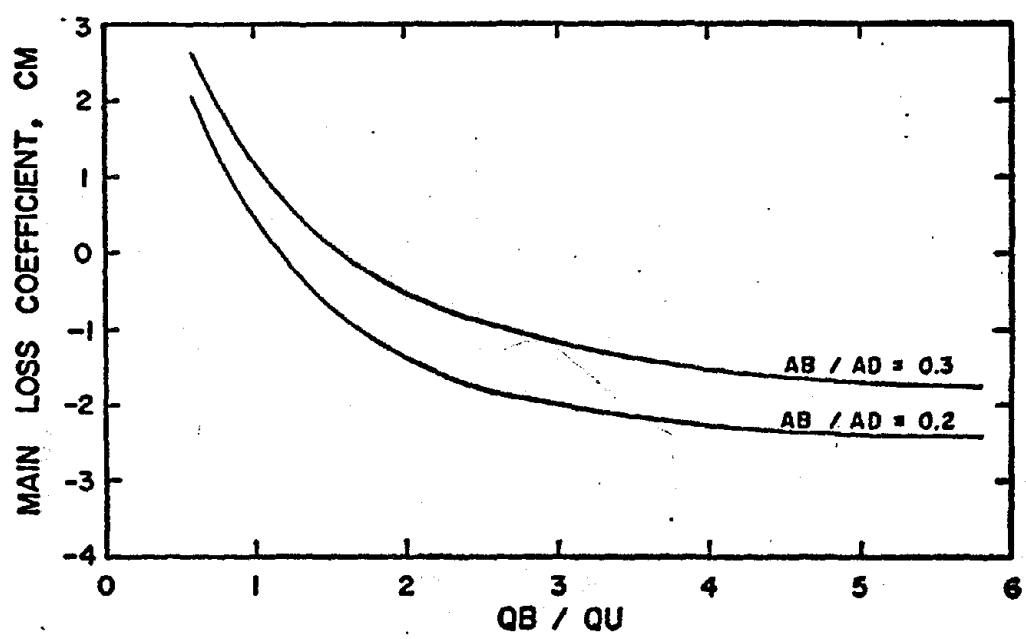

FIGURE D-14 BRANCH ANGLE = 45°, AU / AD = 0.3

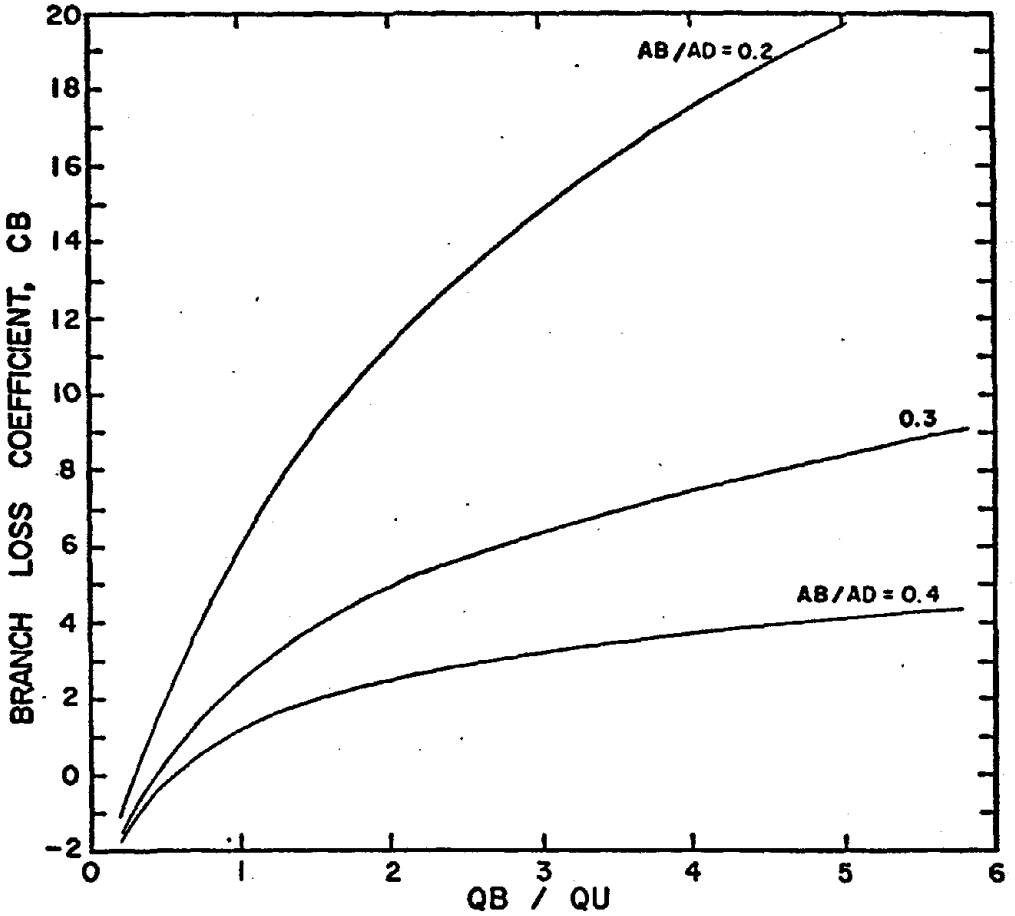

FIGURE D-15 BRANCH ANGLE=45°, AU / AD=0.4

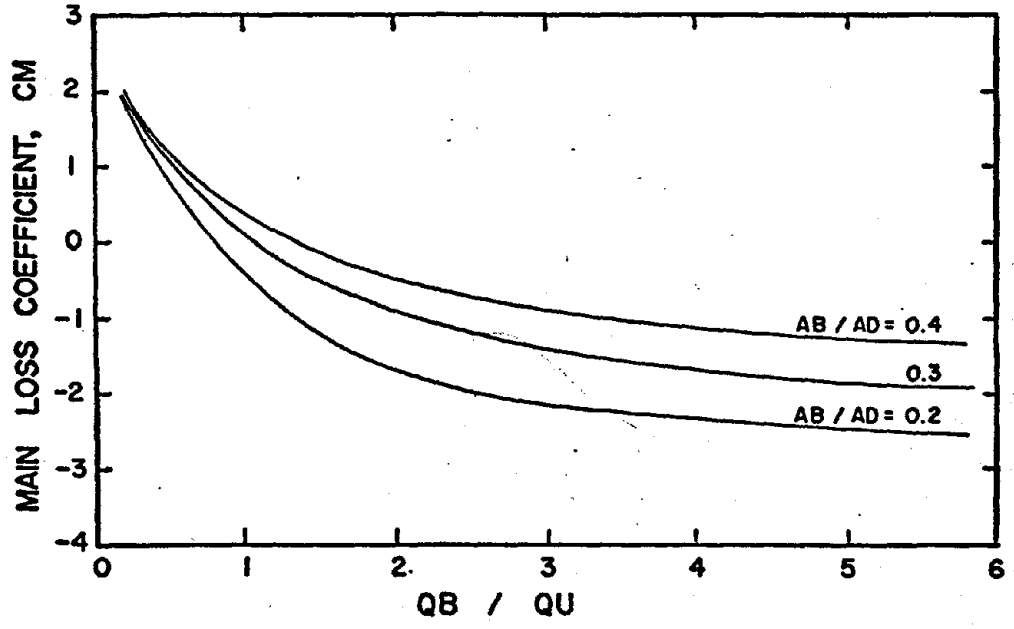

FIGURE D-16 BRANCH ANGLE=45°, AU / AD = 0.4

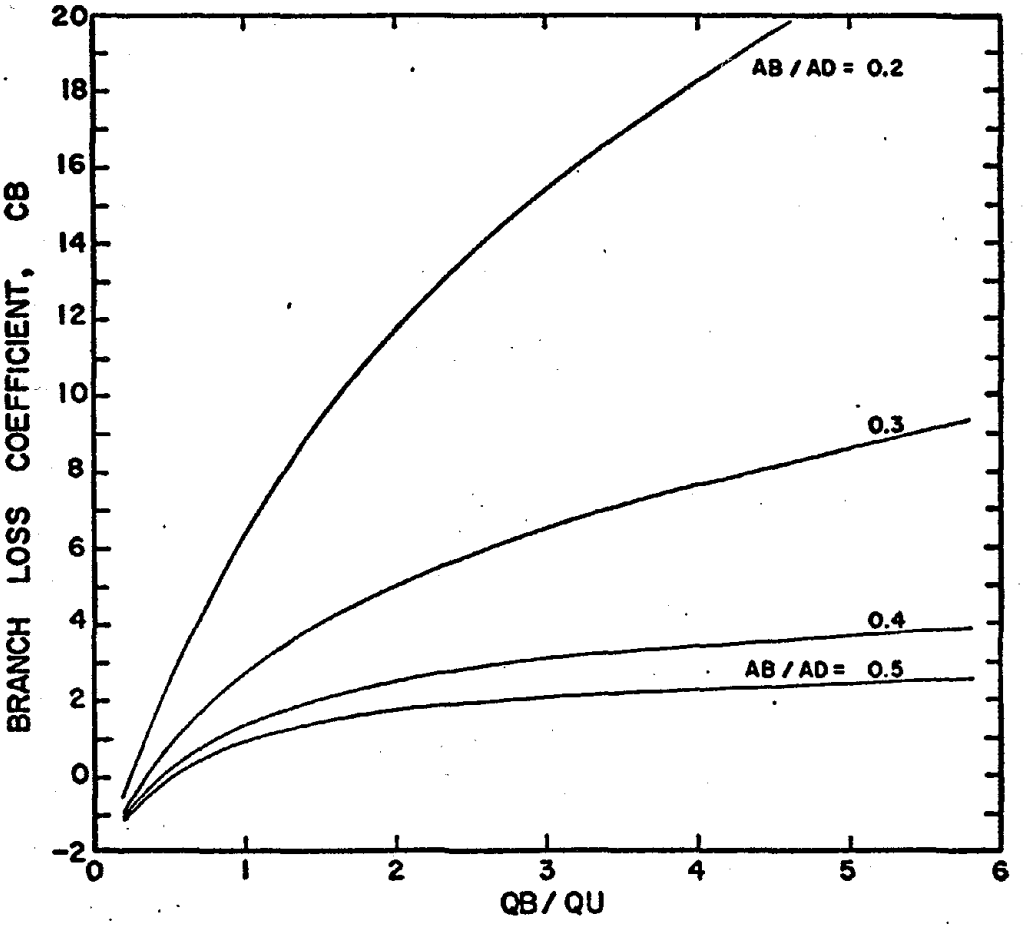

FIGURE D-17 BRANCH ANGLE = 45°, AU / AD = 0.5

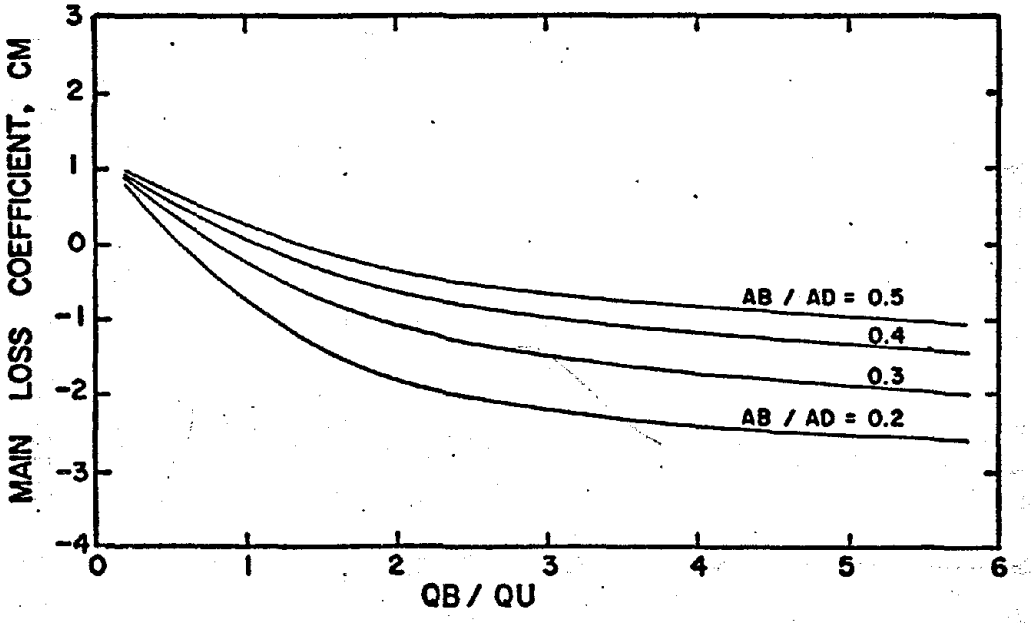

FIGURE D-18 BRANCH ANGLE = 45°, AU / AD = 0.5

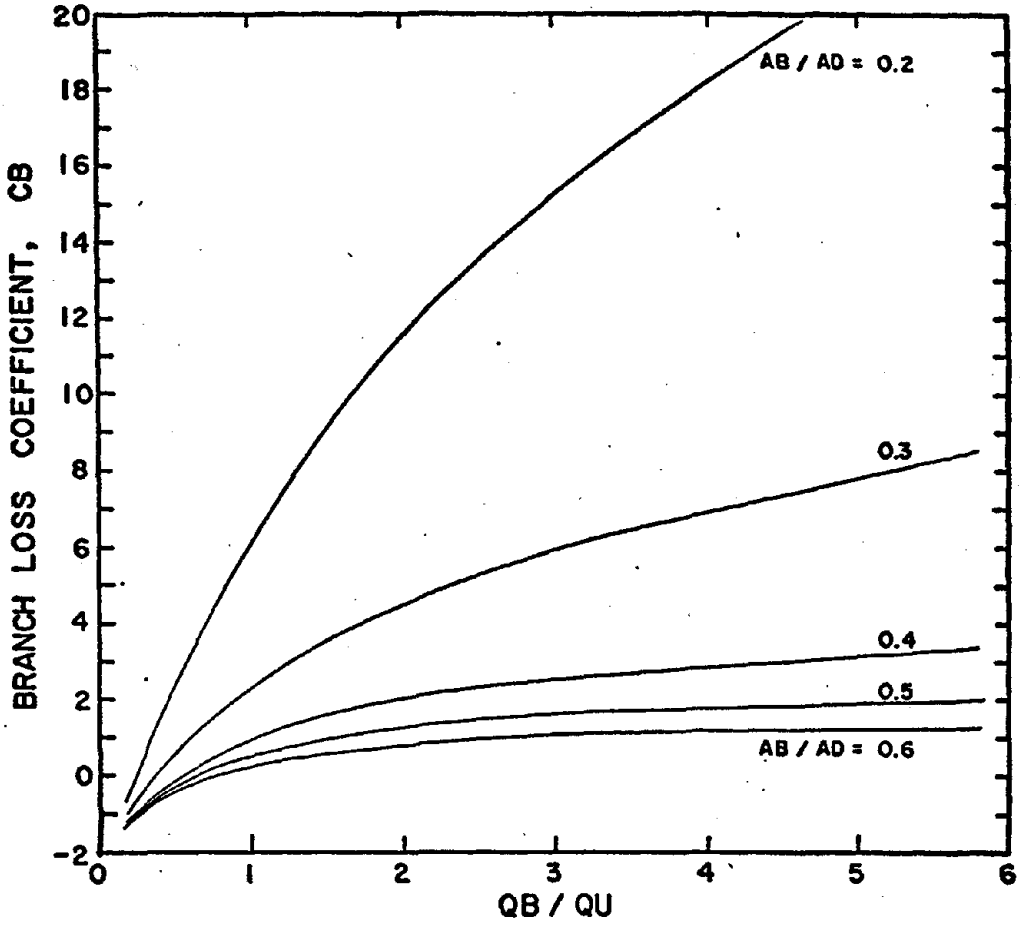

FIGURE D-19 BRANCH ANGLE = 45°, AU / AD = 0.6

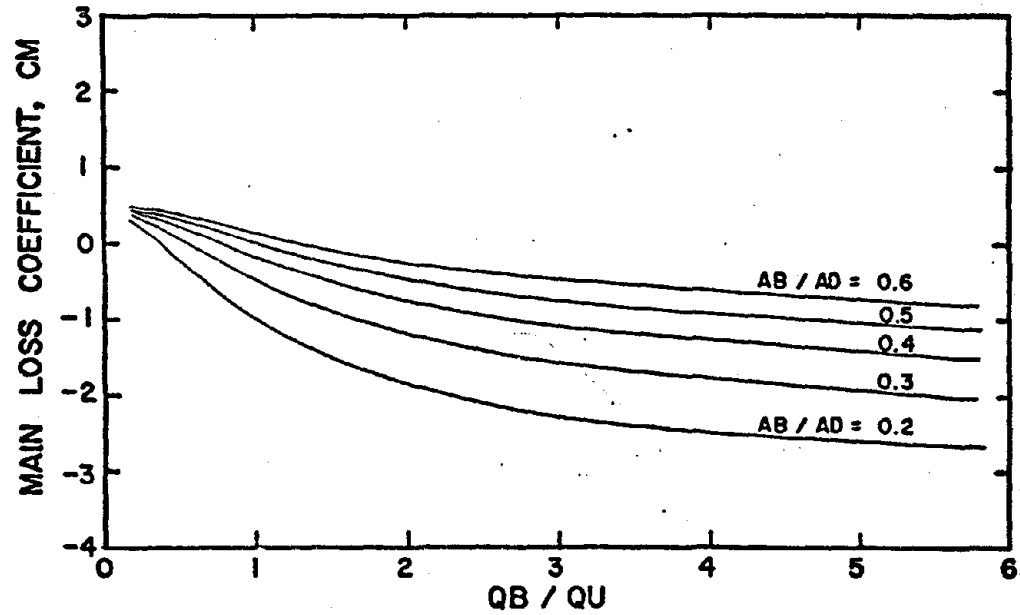

FIGURE D-20 BRANCH ANGLE = 45°, AU / AD = 0.6

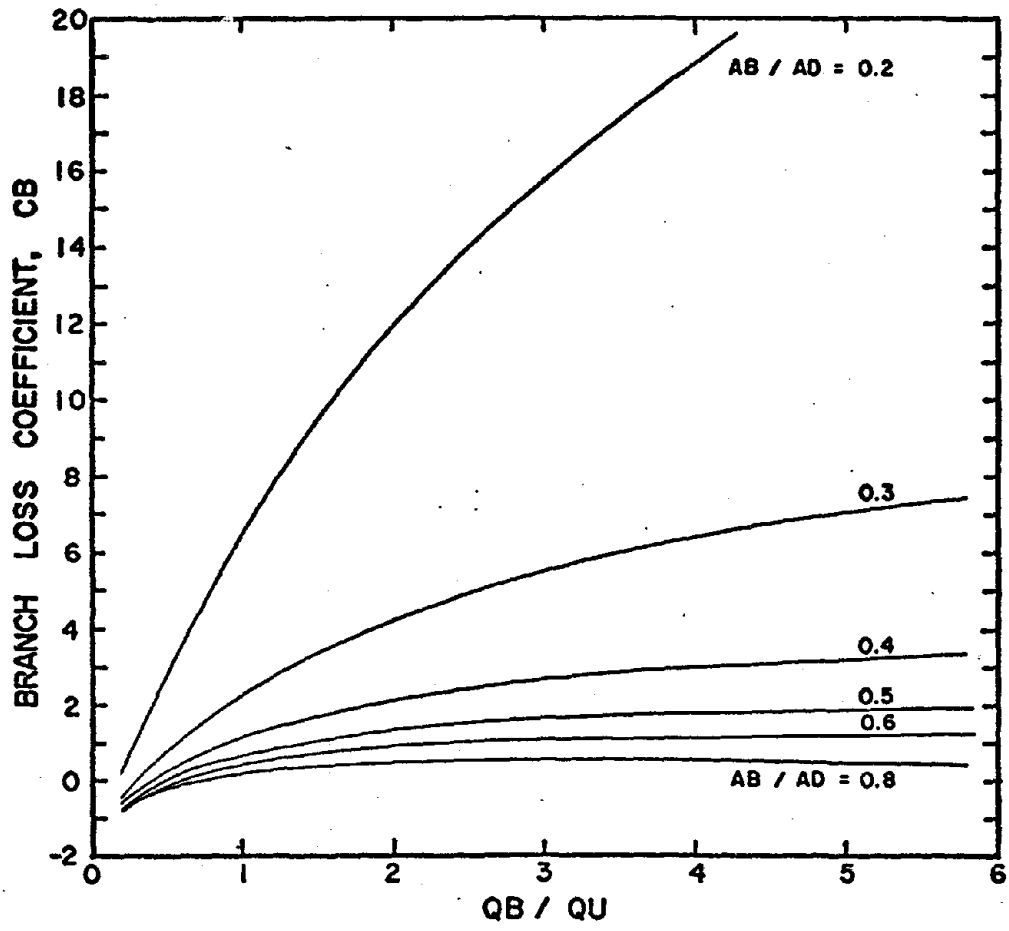

FIGURE D-21 BRANCH ANGLE = 45°, AU / AD = 0.8

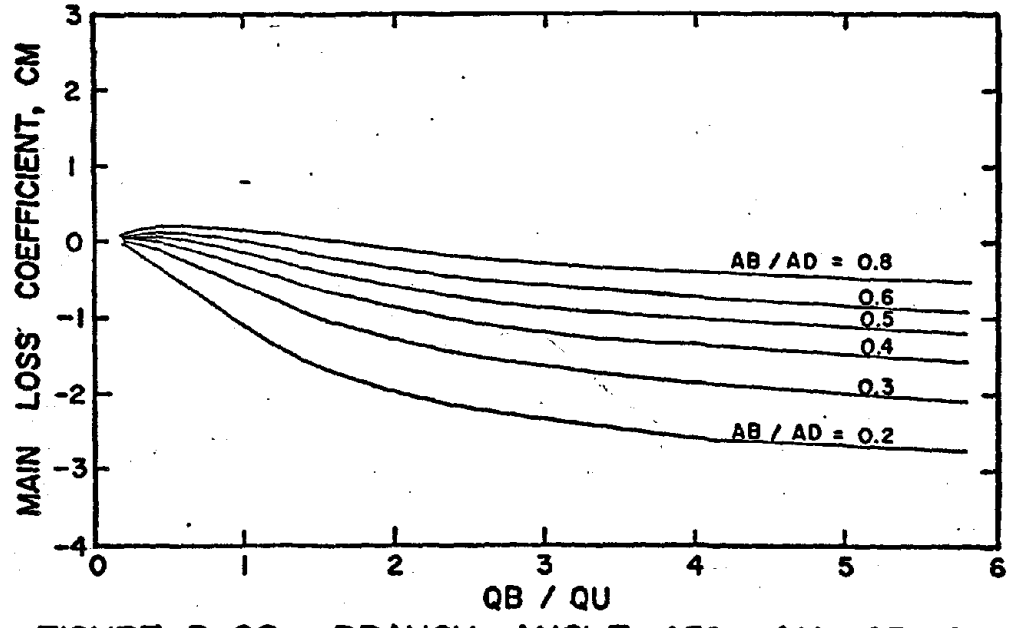

FIGURE D-22 BRANCH ANGLE = 45°, AU / AD = 0.8

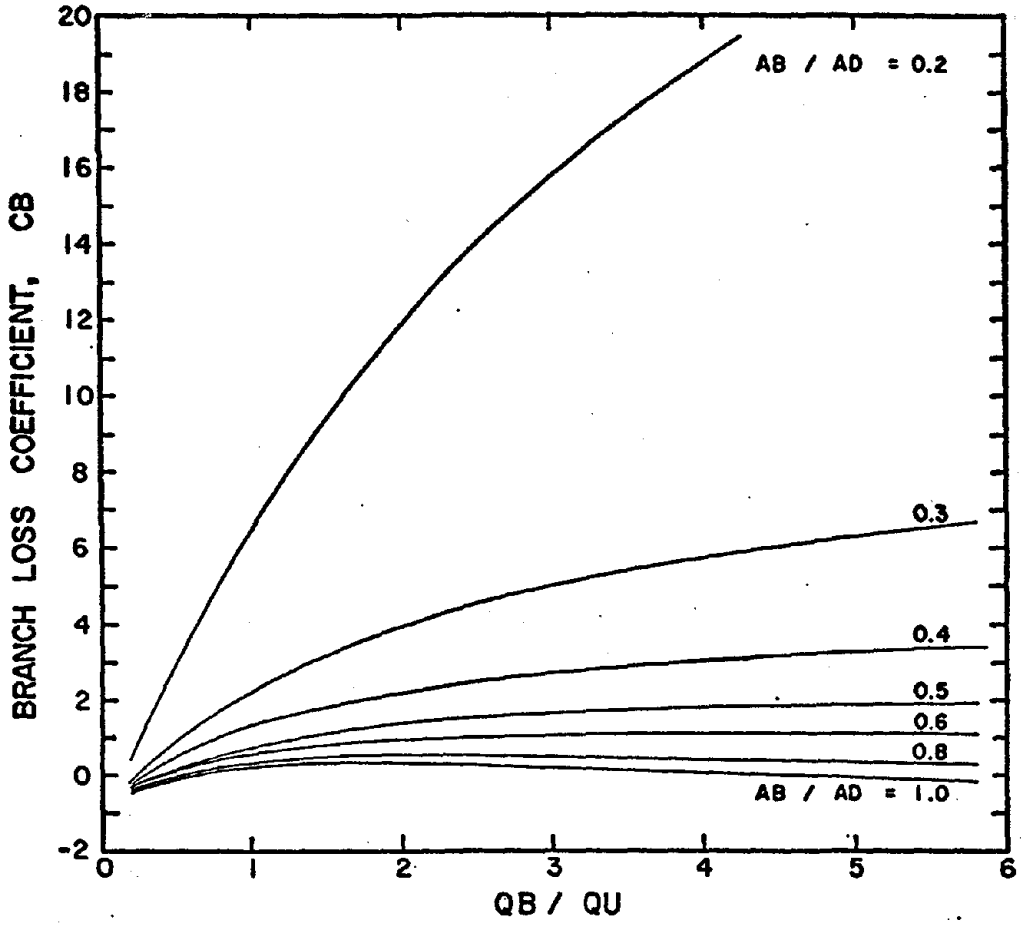

FIGURE D-23 BRANCH ANGLE = 45°, AU / AD = 1.0

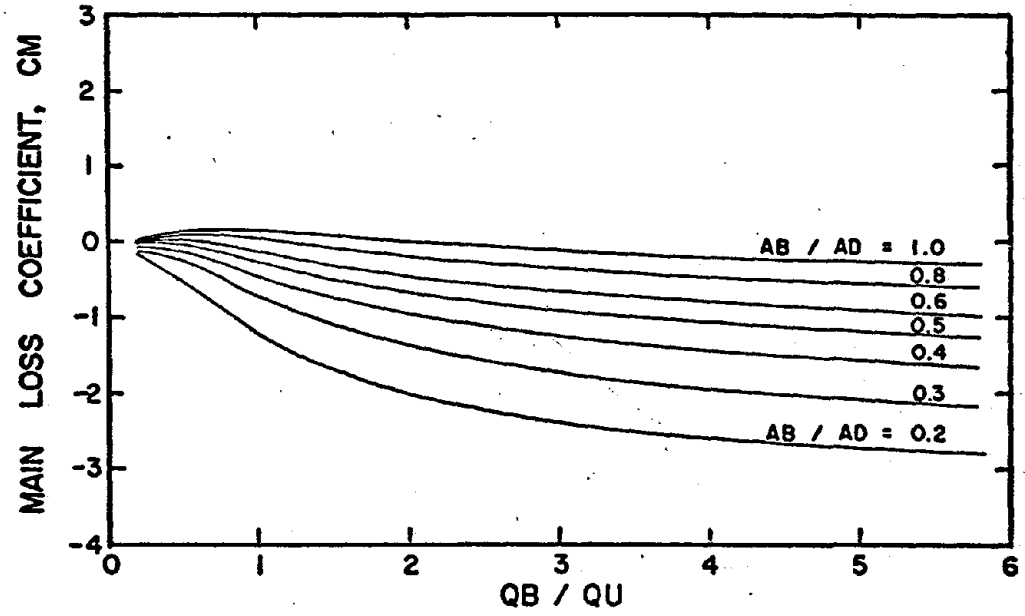

FIGURE D-24 BRANCH ANGLE = 45°, AU / AD = 1.0

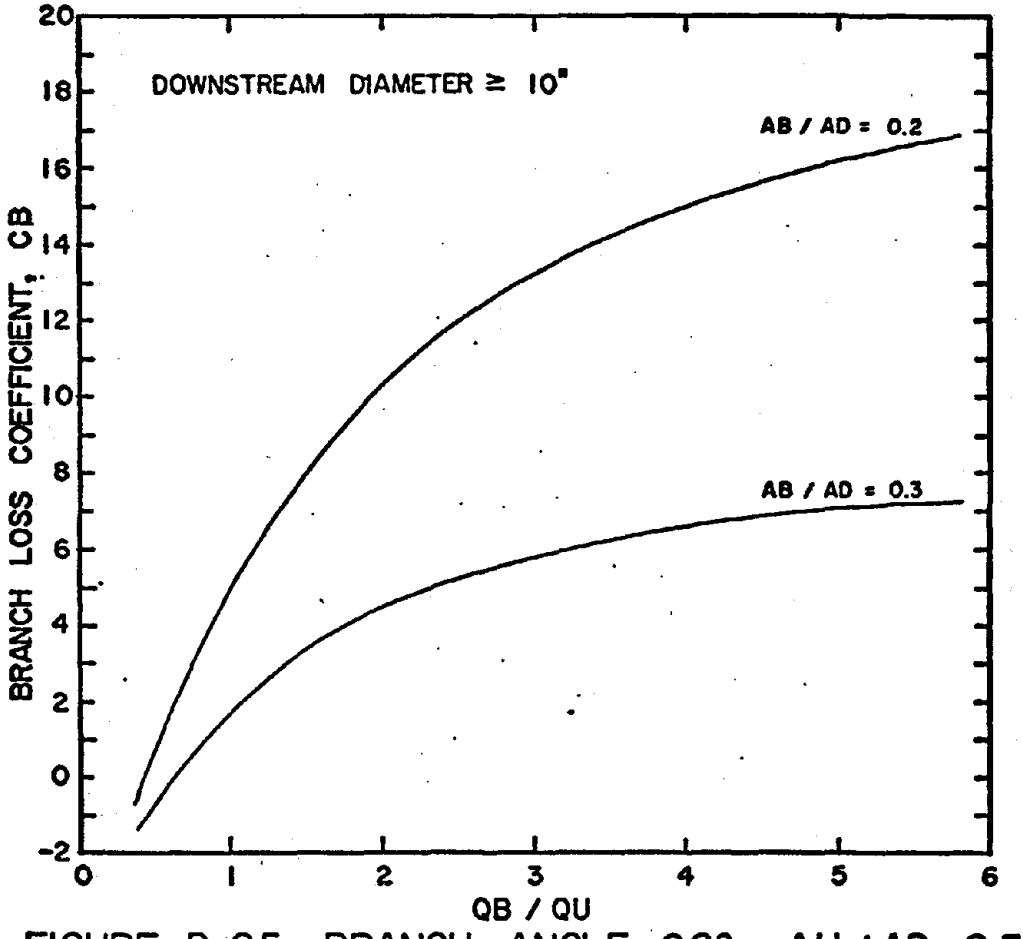

FIGURE D-25 BRANCH ANGLE = 90°, AU / AD = 0.3

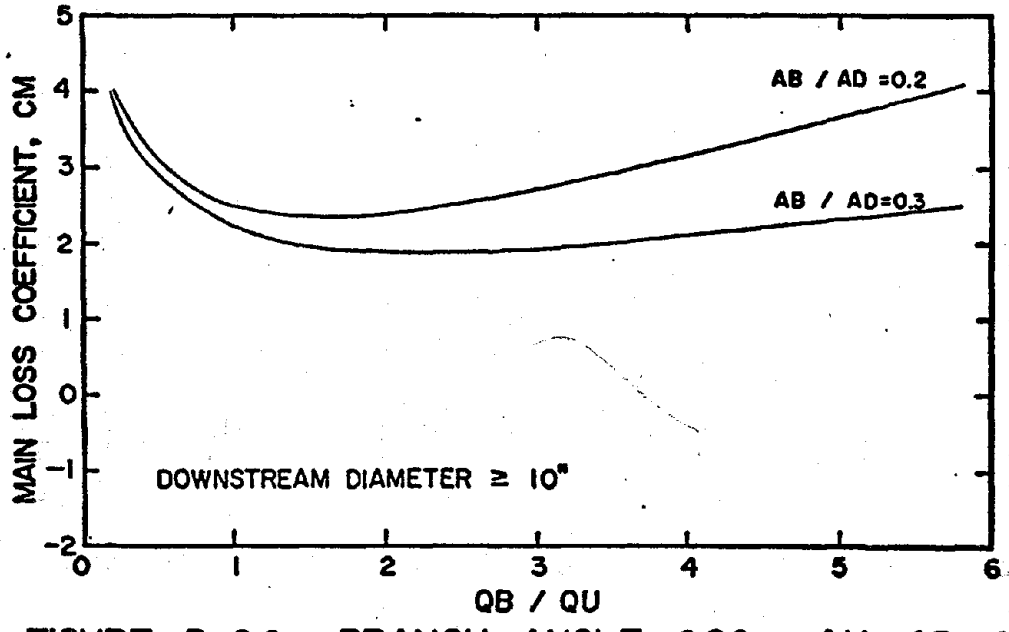

FIGURE D-26 BRANCH ANGLE = 90°, AU / AD = 0.3

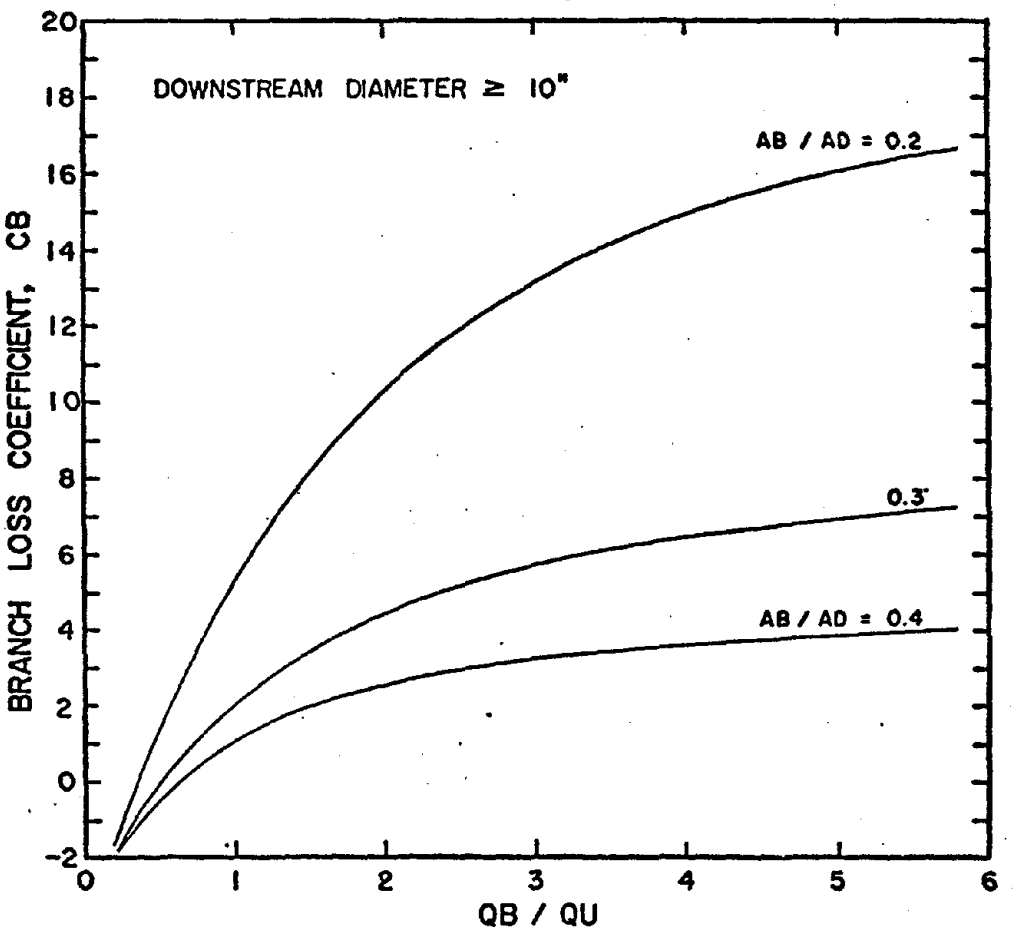

FIGURE D-27 BRANCH ANGLE = 90°, AU/AD = 0.4

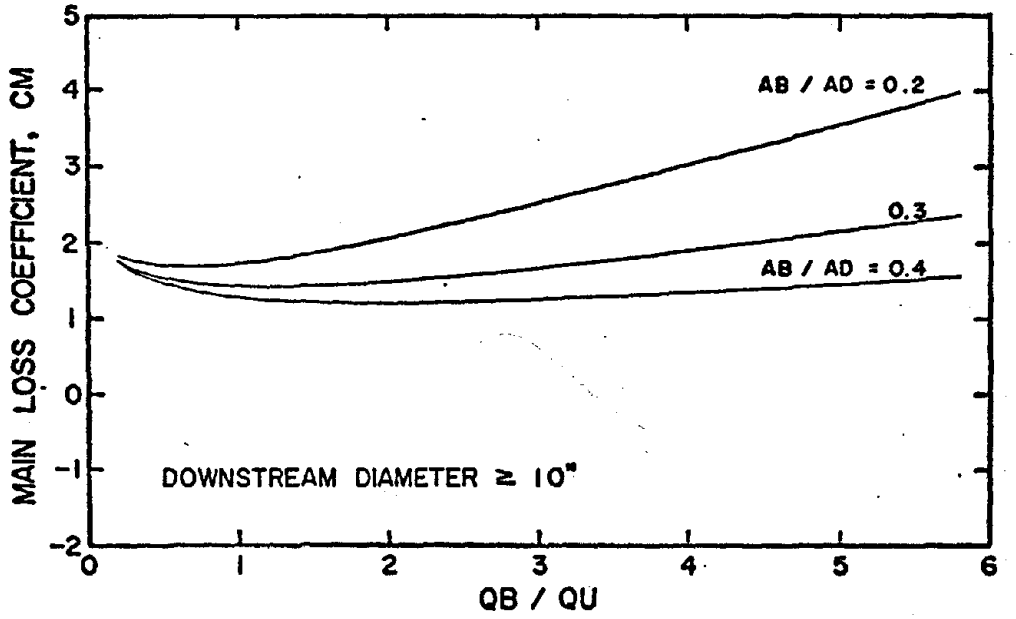

FIGURE D-28 BRANCH ANGLE = 90°, AU/AD = 0.4

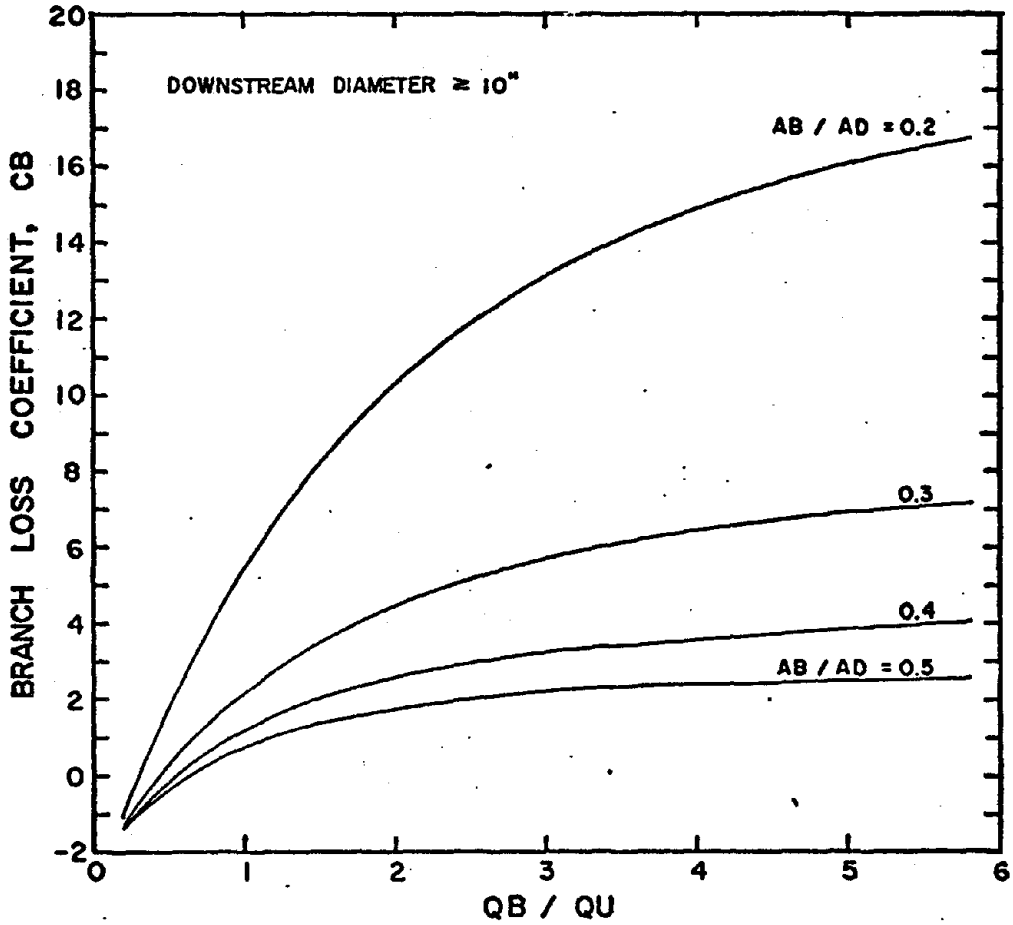

FIGURE D-29 BRANCH ANGLE=90°, AU / AD=0.5

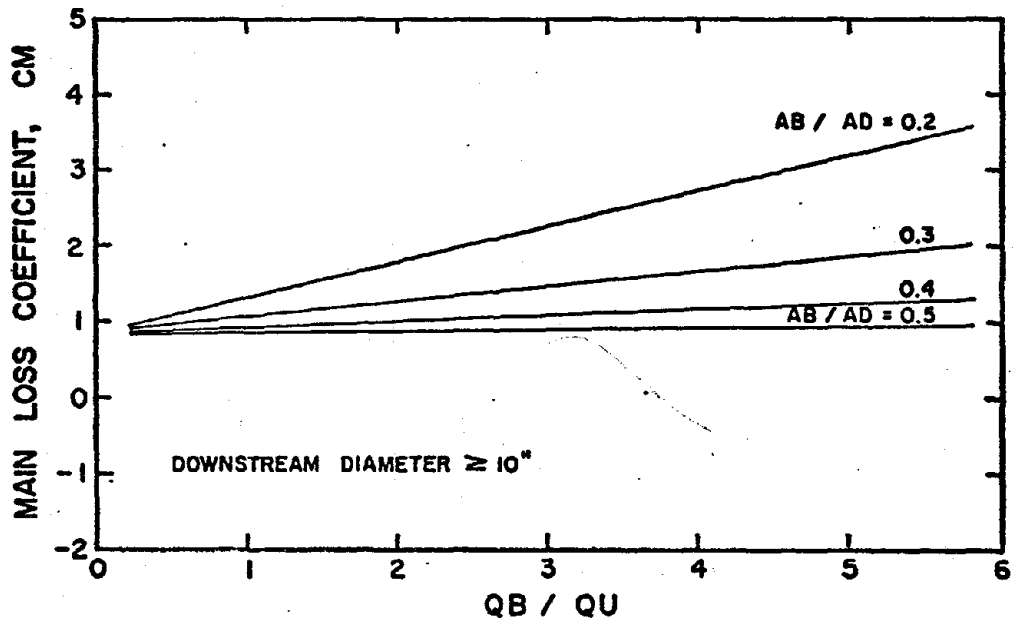

FIGURE D-30 BRANCH ANGLE=90°, AU / AD=0.5

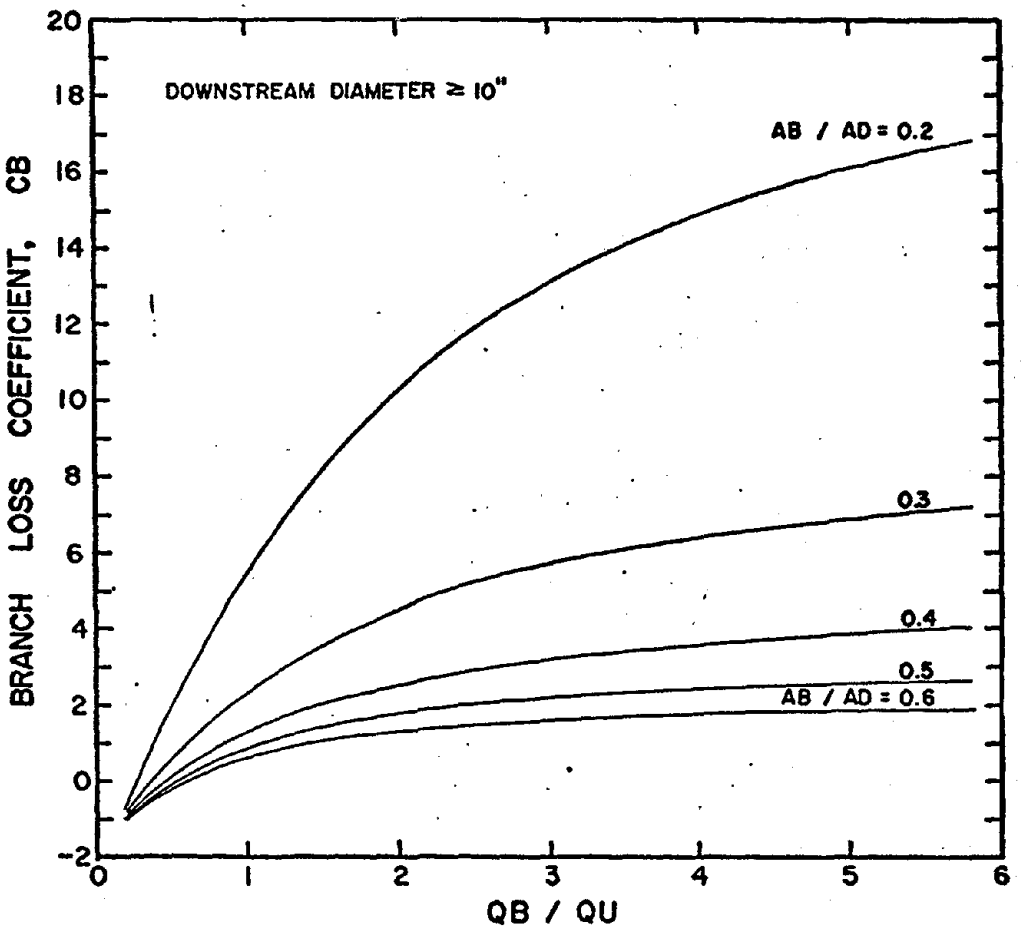

FIGURE D-31 BRANCH ANGLE = 90°, AU / AD = 0.6

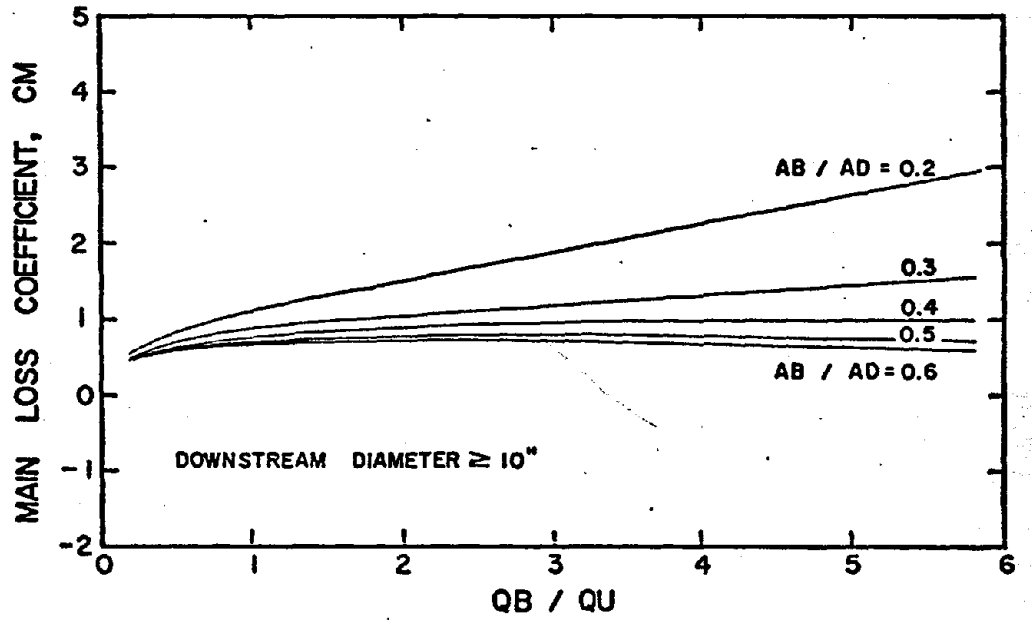

FIGURE D-32 BRANCH ANGLE = 90°, AU / AD = 0.6

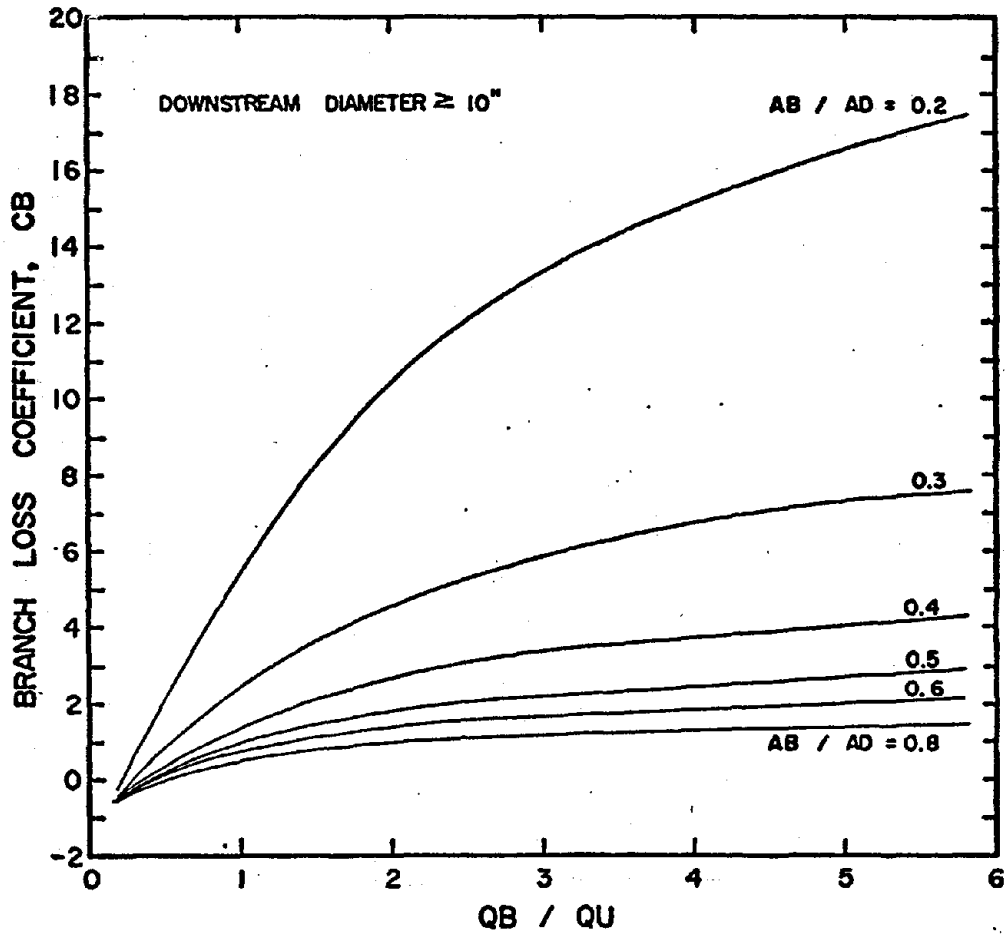

FIGURE D-33 BRANCH ANGLE = 90°, AU / AD = 0.8

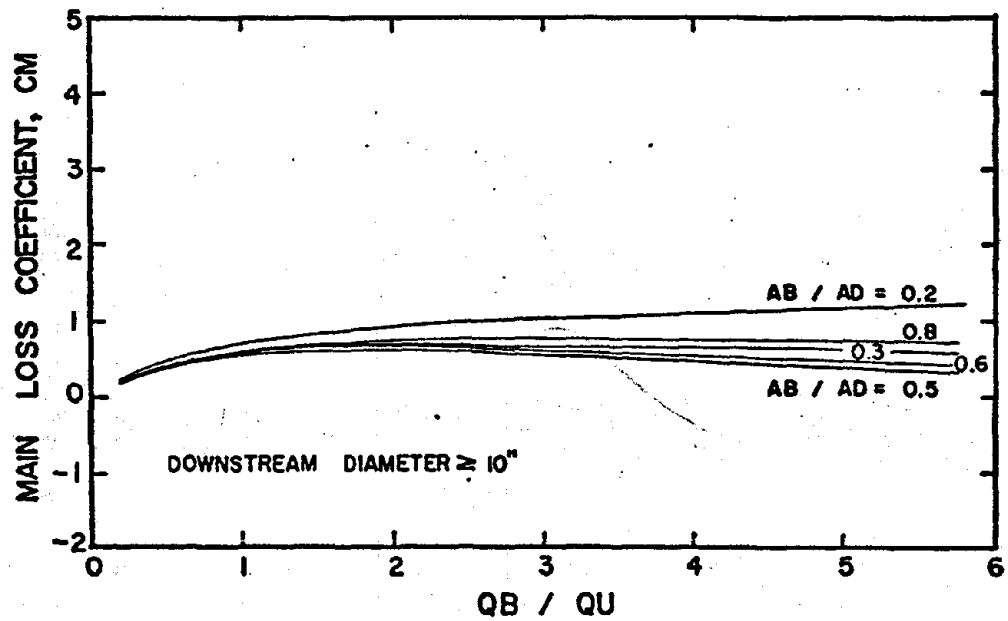

FIGURE D-34 BRANCH ANGLE = 90°, AU / AD = 0.8

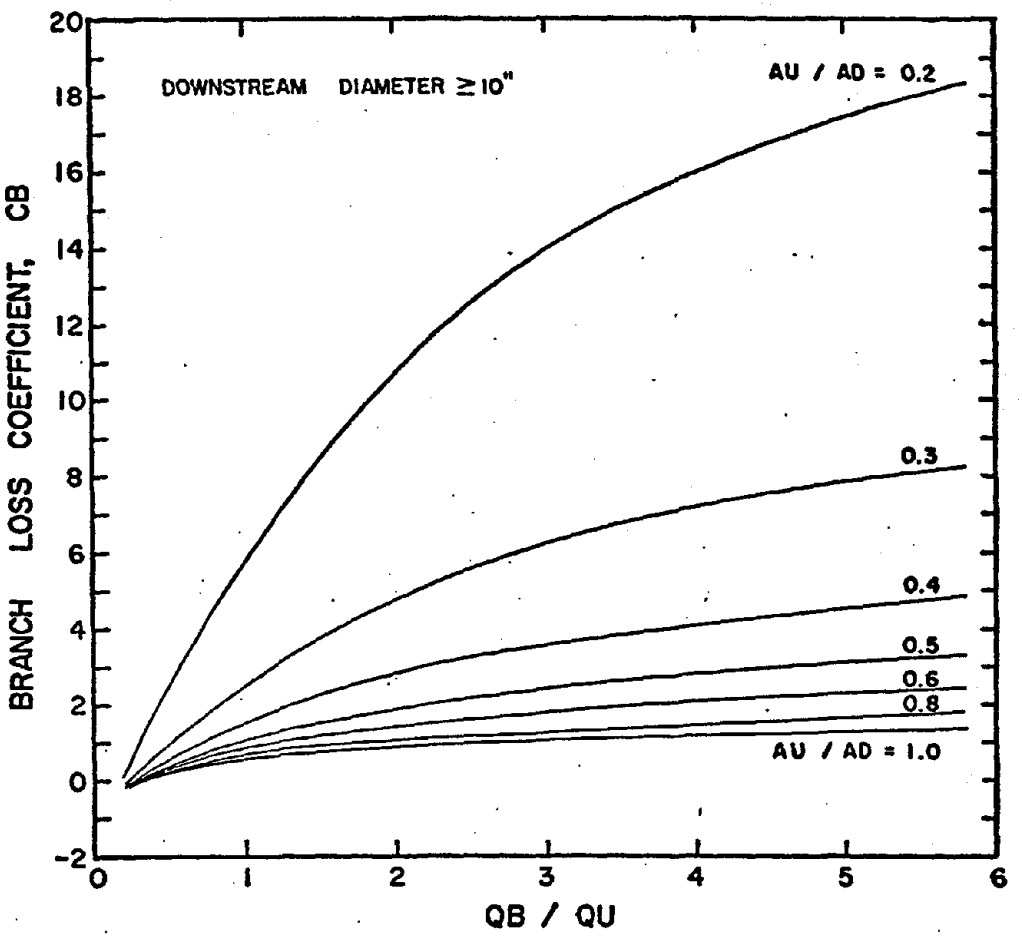

FIGURE D-35 BRANCH ANGLE = 90°, AU / AD = 1.0

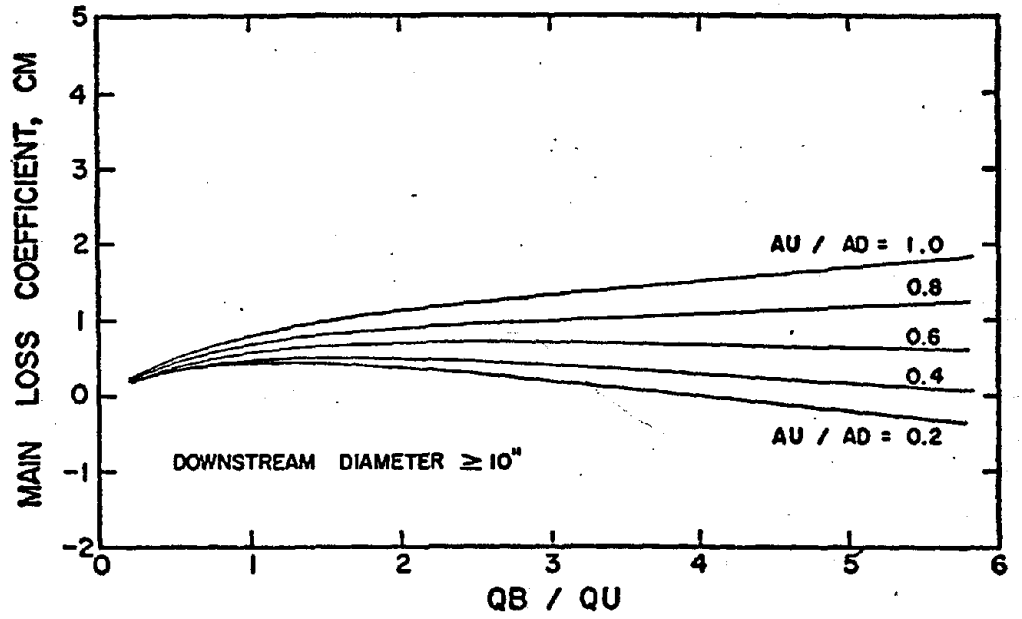

FIGURE D-36 BRANCH ANGLE = 90°, AU / AD = 1.0

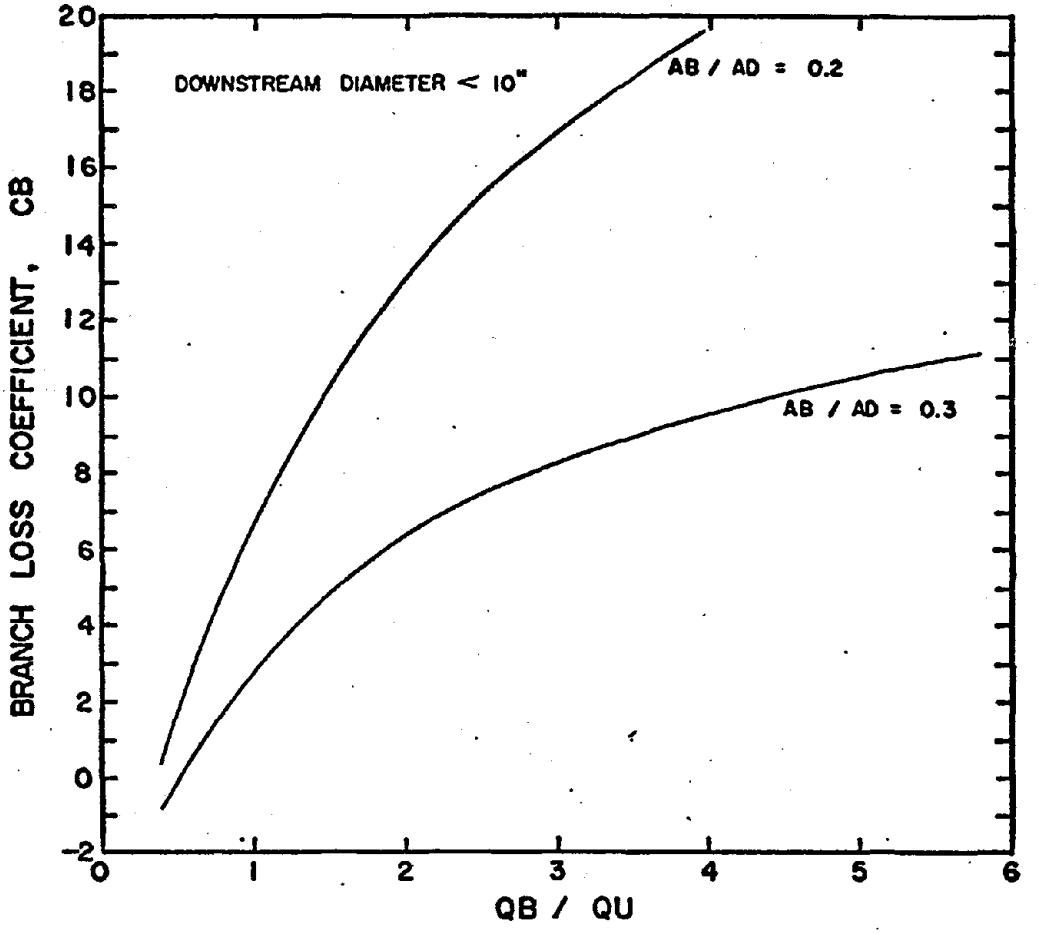

FIGURE D-37 BRANCH ANGLE = 90°, AU / AD = 0.3

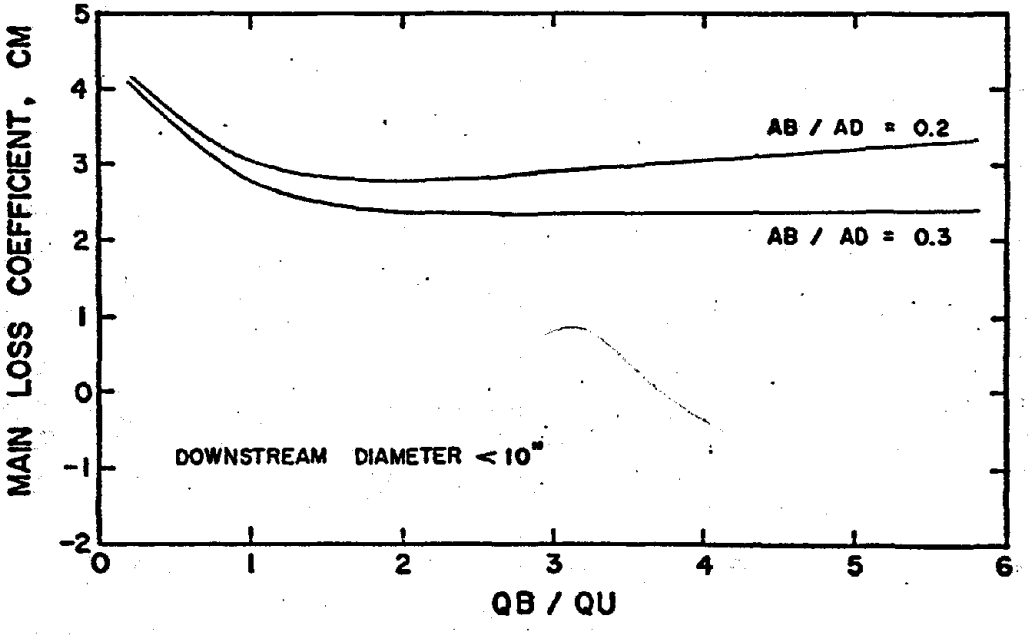

FIGURE D-38 BRANCH ANGLE = 90°, AU / AD = 0.3

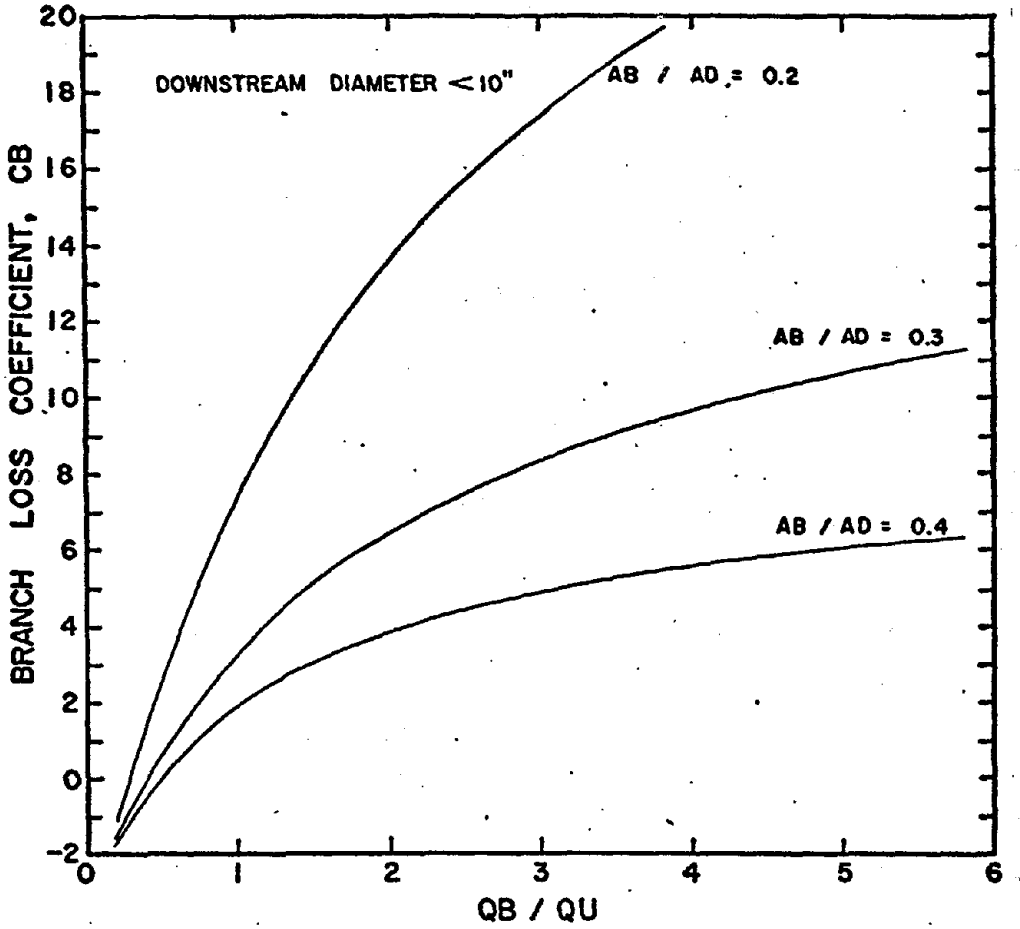

FIGURE D-39 BRANCH ANGLE = 90°, AU / AD = 0.4

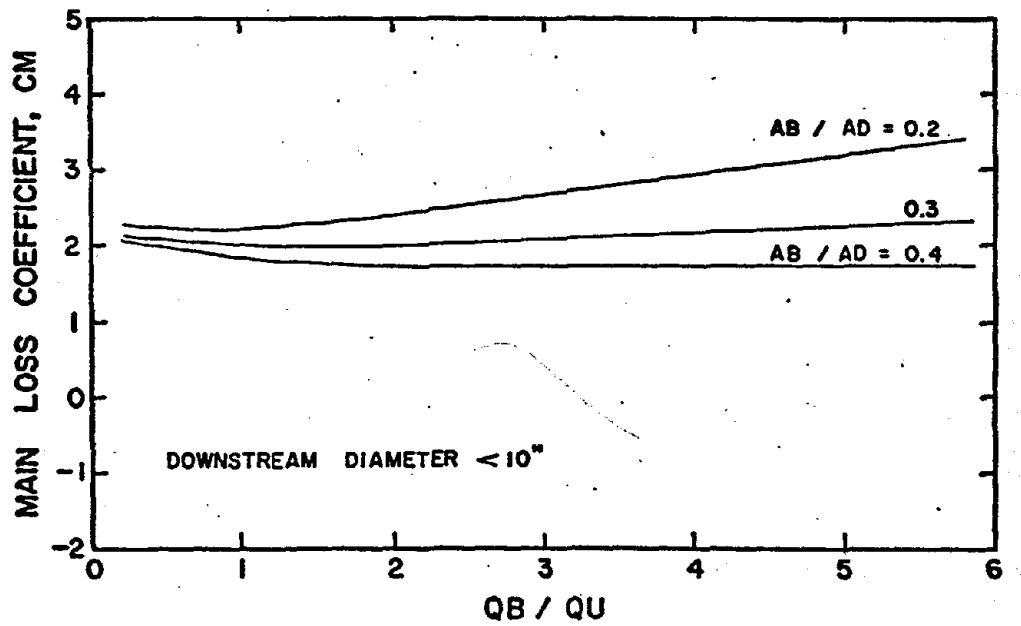

FIGURE D-40 BRANCH ANGLE = 90°, AU / AD = 0.4

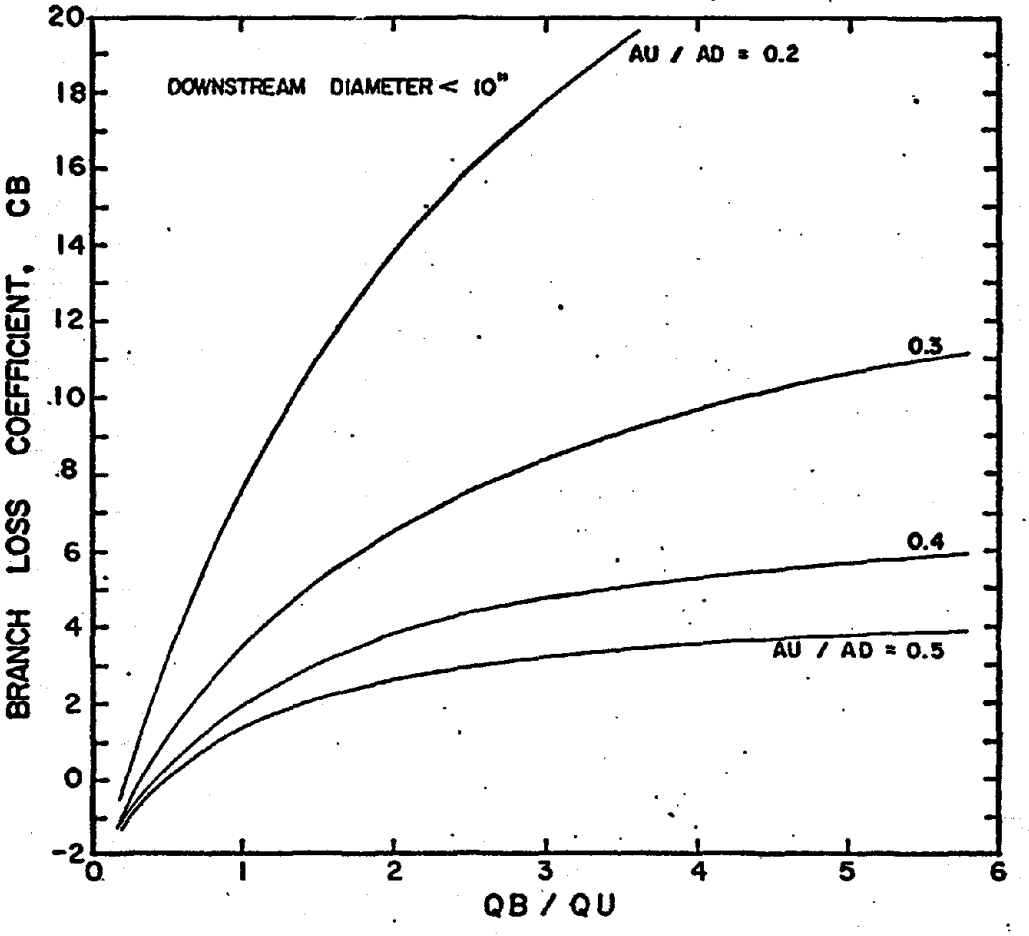

FIGURE D-41 BRANCH ANGLE = 90°, AU / AD = 0.5

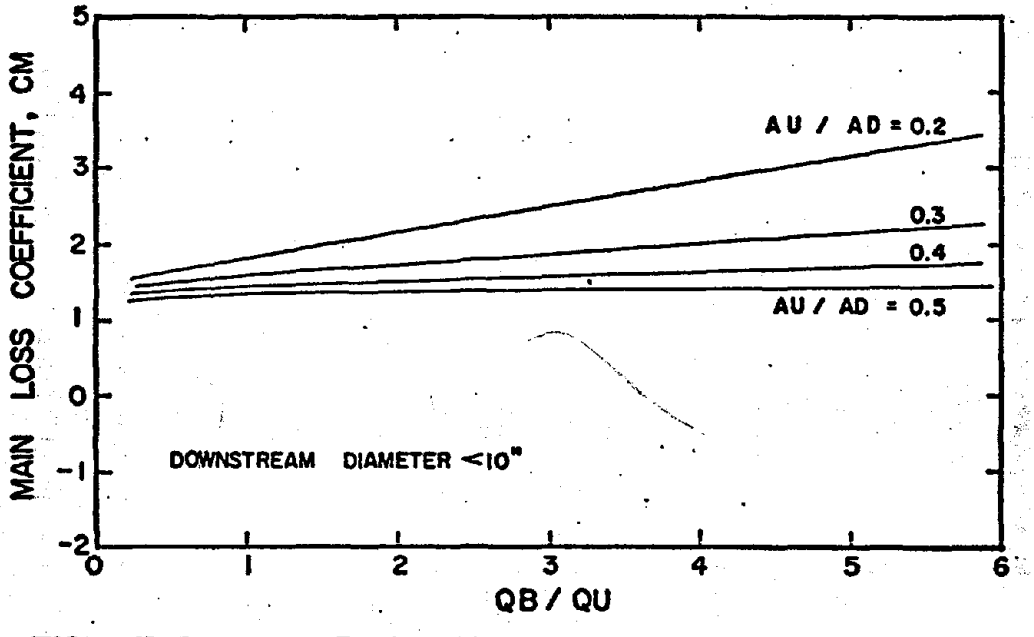

FIGURE D-42 BRANCH ANGLE = 90°, AU / AD = 0.5

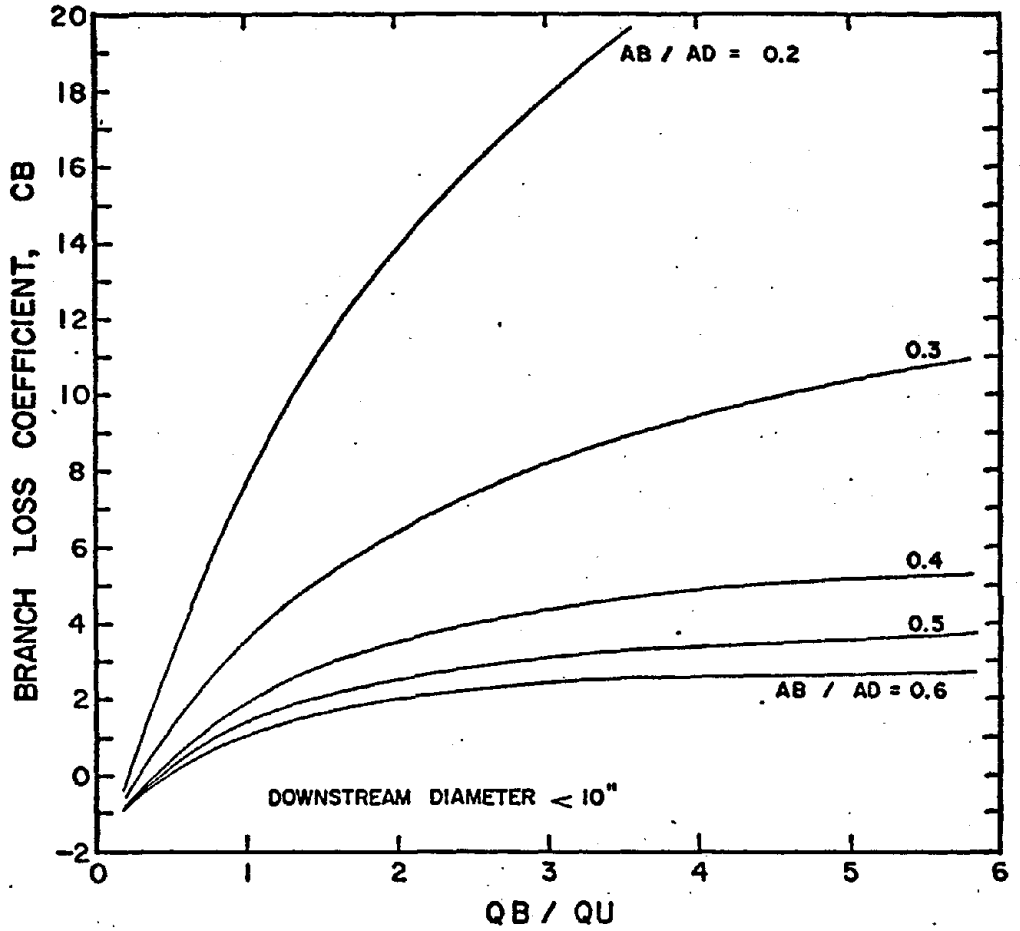

FIGURE D-43 BRANCH ANGLE = 90°, AU / AD = 0.6

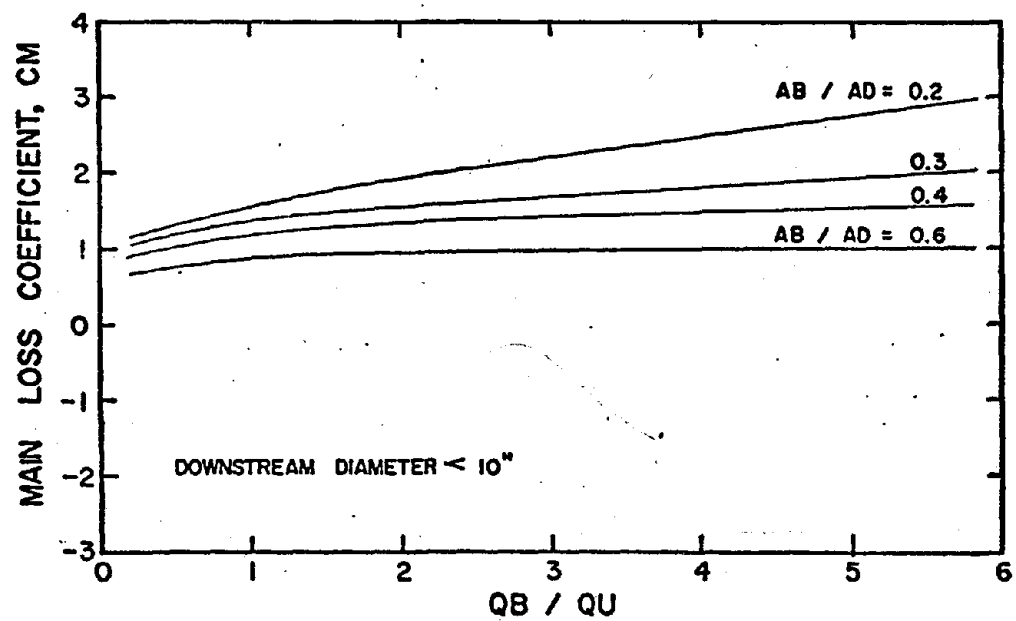

FIGURE D-44 BRANCH ANGLE = 90°, AU / AD = 0.6

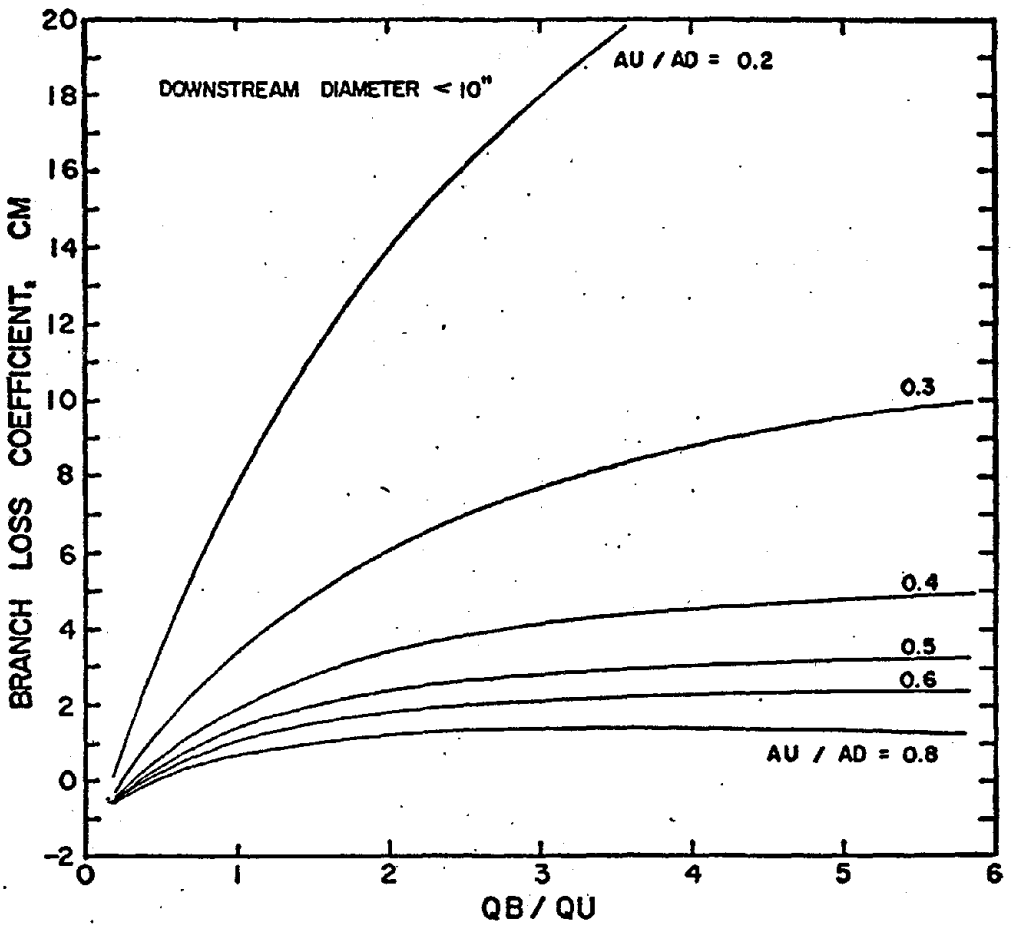

FIGURE D-45 BRANCH ANGLE = 90°, AU/AD = 0.8

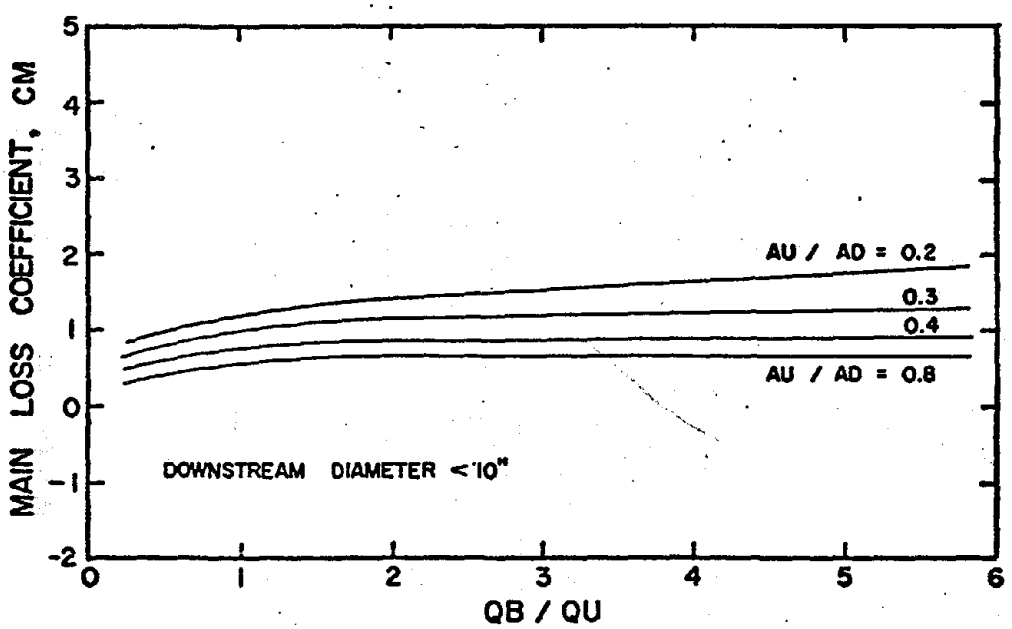

FIGURE D-46 BRANCH ANGLE = 90°, AU/AD = 0.8

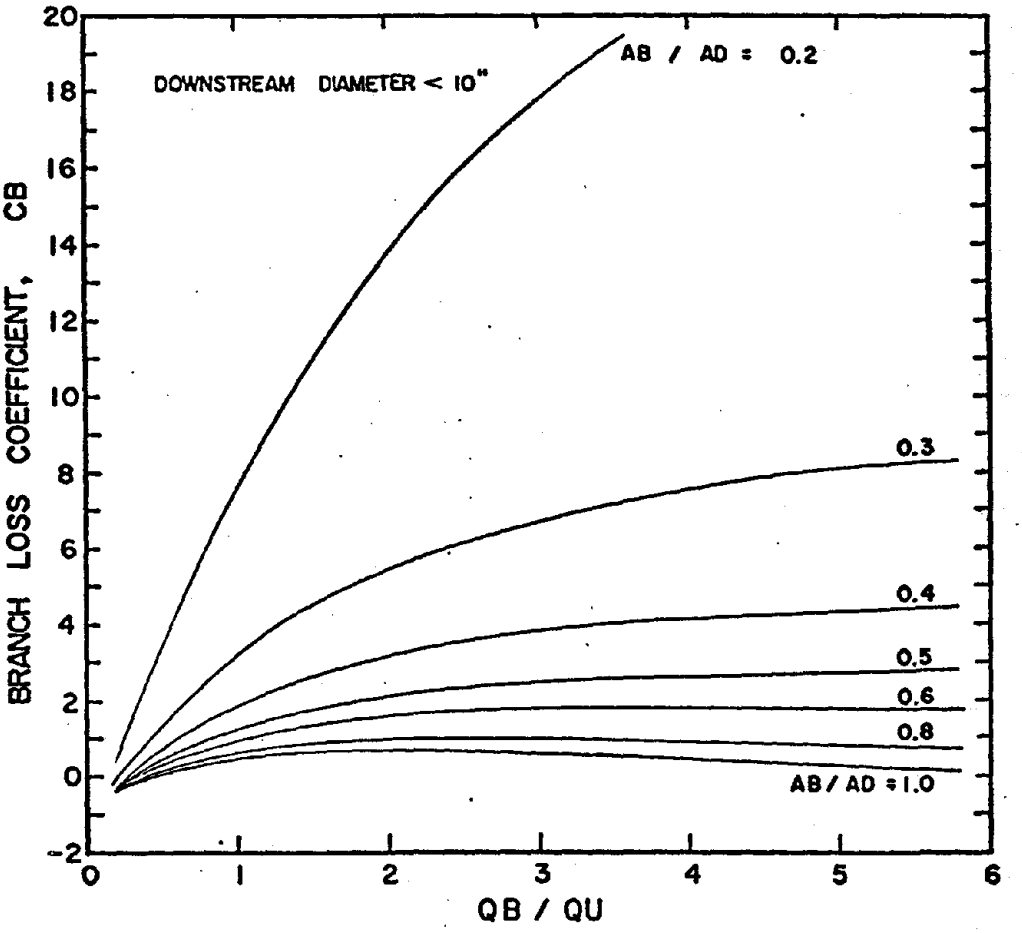

FIGURE D-47 BRANCH ANGLE = 90°, AU / AD = 1.0

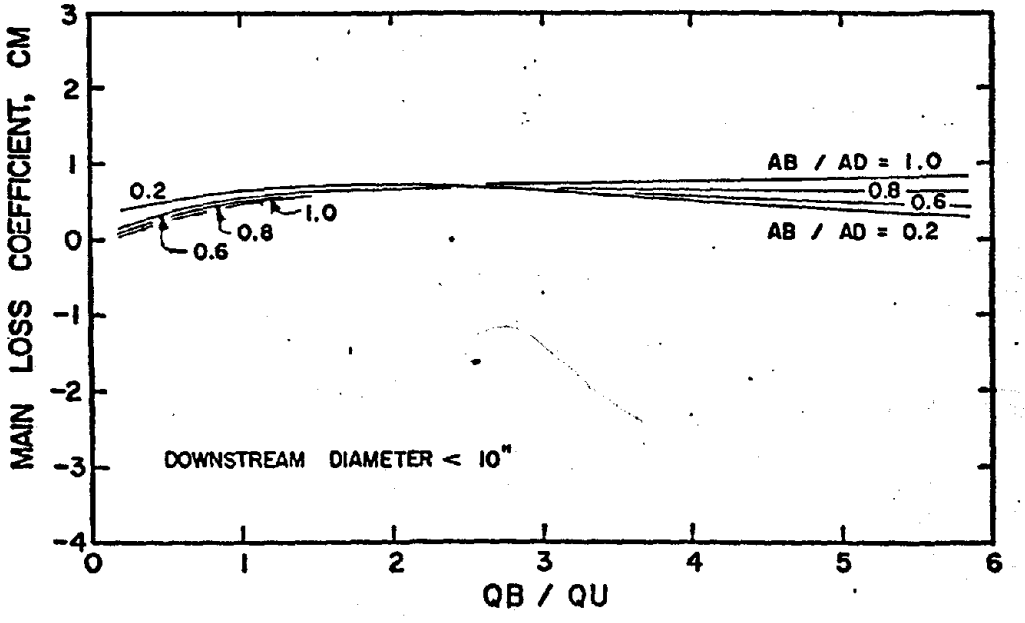

FIGURE D-48 BRANCH ANGLE = 90°, AU / AD = 1.0

APPENDIX E

UNCERTAINTY ANALYSIS OF EXPERIMENTAL RESULTS

Random error in the final results is that error due to fluctuations in the measurements. The uncertainty analysis described by Doebelin (see ref. 6) allows prediction of the maximum random error in the results. This maximum error would occur when all measurements were assumed to be taken at the greatest limits of fluctuation. Applying the uncertainty analysis to this pressure loss study, uncertainty intervals could be established for the branch and main loss coefficients for any specified flow rate. The procedure also broke the uncertainty interval into a number of terms where each term represented the uncertainty a particular parameter contributed to the loss coefficient.

General representations of uncertainty in the branch and main loss coefficients are given by

$$UNCB = \sum_{i=1}^{m} \Delta n_i \frac{\partial CB}{\partial n_i} \qquad E.1$$

$$UNCM = \sum_{i=1}^{m} \Delta n_i \frac{\partial CM}{\partial n_i} \qquad E.2$$

where, UNCB $\triangleq$ uncertainty interval in branch coefficient, dimensionless

UNCM $\triangleq$ uncertainty interval in main coefficient, dimensionless

$m \triangleq$ number of parameters which determine loss coefficient

$\Delta n_i \triangleq$ uncertainty in the i th parameter

$\frac{\partial}{\partial n_i} \triangleq$ partial derivative of loss coefficient with respect to i th parameter.

An analysis performed previously (see ref. 18) showed that the only parameters which had significant influence in the uncertainty of the loss coefficients were CLCB (centerline coefficient of the branch), CLCU (centerline coefficient of the upstream), FBD (friction between the branch and downstream), FUD (friction between the upstream and downstream), SPBD (static pressure drop from branch to downstream), SPUD (static pressure drop from upstream to downstream), VPB (centerline velocity head in the branch), and VPU (centerline velocity head in the upstream).

Equations E.1 and E.2 may then be rewritten as the sum of the uncertainties due to the parameters just mentioned. The new forms are

$$UNCB = UNCLCB + UNCLCU + UNFBD + UNSPBD + UNVPB + UNVPU \quad E.3$$

$$UNCM = UNCLCB + UNCLCU + UNFUD + UNSPUD + UNVPB + UNVPU \quad E.4$$

for UNCB: $UNCLCB = \left| \Delta CLCB \frac{\partial CB}{\partial CLCB} \right|$

$UNCLCU = \left| \Delta CLCU \frac{\partial CB}{\partial CLCU} \right|$

$UNFBD = \left| \Delta FBD \frac{\partial CB}{\partial FBD} \right|$

$UNSPBD = \left| \Delta SPBD \frac{\partial CB}{\partial SPBD} \right|$

$UNVPB = \left| \Delta VPB \frac{\partial CB}{\partial VPB} \right|$

$UNVPU = \left| \Delta VPU \frac{\partial CB}{\partial VPU} \right|$

and for UNCM:

$UNCLCB = \left| \Delta CLCB \frac{\partial CM}{\partial CLCB} \right|$

$UNCLCU = \left| \Delta CLCU \frac{\partial CM}{\partial CLCU} \right|$

$UNFUD = \left| \Delta FUD \frac{\partial CM}{\partial FUD} \right|$

$UNSPUD = \left| \Delta SPUD \frac{\partial CM}{\partial SPUD} \right|$

$$UNVPB = \left| \Delta VPB \frac{\partial CM}{\partial VPB} \right|$$

$$UNVPU = \left| \Delta VPU \frac{\partial CM}{\partial VPU} \right|$$

The measured downstream velocity head is noted not to influence the uncertainty of either loss coefficients because this velocity head was calculated using a mass balance as described in Chapter 3. Rewritting the loss coefficients in terms of mass balance, the branch and main loss coefficients may be rewritten as equations E.5 and E.6 respectively.

$$CB = \frac{A - B + SPBD - FBD}{C + B} \qquad E.5$$

$$CM = \frac{D - B + SPUD - FUD}{C + B} \qquad E.6$$

where, $A = CLCB^2\ VPB\left[1 - \left(\frac{DB}{DD}\right)^4\right] - CLCU^2\ VPU\left(\frac{DU}{DD}\right)^4$

$$B = 2\ \frac{DB^2 \times DU^2}{DD^4}\ (CLCB)(CLCU)[(VPB)(VPU)]^{1/2}$$

$$C = CLCB^2 \left(\frac{DB}{DD}\right)^4 VPB + CLCU^2 \left(\frac{DU}{DD}\right)^4 VPU$$

$$D = CLCU^2\ VPU\left[1 - \left(\frac{DU}{DD}\right)^4\right] - CLCB^2 VPB \left(\frac{DB}{DD}\right)^4$$

Partial derivatives of equations E.5 and E.6 were then made and used in the equations for UNCB and UNCM. These derivatives gave very complicated forms and are not included in this discussion.

Uncertainties in the various parameters were made by careful judgement after observing the trends of accuracy with which pressure measurements could be taken. The uncertainties were selected as:

$\Delta CLCB = 0.01$

$\Delta CLCU = 0.01$

$\Delta FBD = 0.005$ in. of H_2O

$\Delta FUD = 0.005$ in. of H_2O

$\Delta SPBD = 0.01$ in. of H_2O

$\Delta SPUD = 0.01$ in. of H_2O

$\Delta VPB = 0.01 \times VPB$ in. of H_2O

$\Delta VPU = 0.01 \times VPU$ in. of H_2O

Hand calculations of UNCB and UNCU (Eq.'s E.3 and E.4) were felt unfeasible due to the complicated forms after taking the partial derivatives, but use of the computer made computations possible. Since the computer program became somewhat involved and lengthy, it was decided that only the results of the analysis would be presented. Although the uncertainty analysis was performed on all fittings, only the results for five random fittings are presented. These

uncertainties are listed on two pages per fitting where the first page lists the terms of equation E.3 and the latter page lists the terms of equation E.4.

T-1-EF FITTING, DB= 3.0 INCHES, DU= 6.0 INCHES, DD= 6.0 INCHES, BRANCH ANGLE=90.0

RUN	UNCB	UNCLCB	UNCLCU	UNFBD	UNSPBD	UNVPB	UNVPU
1	0.2898	0.0043	0.0262	0.0620	0.1239	0.0221	0.0512
2	0.2906	0.0169	0.0412	0.0428	0.0857	0.0685	0.0356
3	0.3249	0.0242	0.0522	0.0330	0.0661	0.1182	0.0312
4	0.3968	0.0267	0.0637	0.0261	0.0521	0.2004	0.0279
5	0.4084	0.0270	0.0659	0.0234	0.0469	0.2191	0.0261
6	0.4230	0.0253	0.0687	0.0215	0.0429	0.2396	0.0251
7	0.4483	0.0238	0.0709	0.0194	0.0387	0.2722	0.0233
8	0.3766	0.0232	0.0714	0.0154	0.0308	0.2145	0.0214
9	0.0962	0.0017	0.0157	0.0195	0.0389	0.0011	0.0192
10	0.0970	0.0048	0.0206	0.0175	0.0349	0.0019	0.0173
11	0.1002	0.0077	0.0241	0.0162	0.0325	0.0027	0.0170
12	0.1099	0.0140	0.0318	0.0139	0.0277	0.0053	0.0172
13	0.1401	0.0235	0.0487	0.0104	0.0209	0.0178	0.0187
14	0.1418	0.0257	0.0534	0.0085	0.0170	0.0190	0.0182
15	0.1585	0.0254	0.0589	0.0086	0.0171	0.0296	0.0190
16	0.0556	0.0024	0.0148	0.0090	0.0179	0.0005	0.0110
17	0.0606	0.0043	0.0185	0.0085	0.0169	0.0009	0.0115
18	0.0663	0.0072	0.0221	0.0078	0.0157	0.0016	0.0119
19	0.0793	0.0127	0.0300	0.0069	0.0139	0.0023	0.0135
20	0.0881	0.0165	0.0361	0.0062	0.0124	0.0025	0.0145
21	0.0975	0.0201	0.0435	0.0053	0.0106	0.0023	0.0155
22	0.0420	0.0025	0.0143	0.0052	0.0104	0.0010	0.0085
23	0.0491	0.0050	0.0186	0.0047	0.0094	0.0021	0.0094
24	0.0611	0.0089	0.0246	0.0044	0.0088	0.0036	0.0109
25	0.0674	0.0115	0.0281	0.0039	0.0077	0.0048	0.0115
26	0.0745	0.0142	0.0318	0.0035	0.0069	0.0060	0.0121
27	0.0356	0.0025	0.0140	0.0035	0.0069	0.0013	0.0074
28	0.0380	0.0035	0.0159	0.0030	0.0061	0.0018	0.0077
29	0.0471	0.0061	0.0202	0.0029	0.0059	0.0031	0.0089
30	0.0539	0.0080	0.0233	0.0026	0.0053	0.0041	0.0097
31	0.0598	0.0100	0.0265	0.0026	0.0052	0.0051	0.0105

T-1-FE FITTING, D8= 3.0 INCHES, DU= 6.0 INCHES, DD= 6.0 INCHES, BRANCH ANGLE=90.0

RUN	UNCM	UNCLCB	UNCLCU	UNFUD	UNSPUD	UNVPR	UNVPU
1	0.2770	0.0054	0.0116	0.0620	0.1239	0.0274	0.0465
2	0.2132	0.0108	0.0122	0.0428	0.0857	0.0467	0.0150
3	0.1946	0.0149	0.0131	0.0330	0.0661	0.0584	0.0091
4	0.1872	0.0192	0.0131	0.0261	0.0521	0.0710	0.0057
5	0.1796	0.0203	0.0128	0.0234	0.0469	0.0715	0.0048
6	0.1780	0.0219	0.0131	0.0215	0.0429	0.0743	0.0044
7	0.1735	0.0231	0.0125	0.0194	0.0387	0.0761	0.0036
8	0.1441	0.0225	0.0120	0.0154	0.0308	0.0603	0.0030
9	0.0962	0.0028	0.0074	0.0195	0.0389	0.0043	0.0233
10	0.0963	0.0046	0.0087	0.0175	0.0349	0.0068	0.0138
11	0.0841	0.0060	0.0099	0.0162	0.0325	0.0087	0.0108
12	0.0795	0.0085	0.0107	0.0139	0.0277	0.0117	0.0070
13	0.0772	0.0131	0.0117	0.0104	0.0209	0.0172	0.0040
14	0.0724	0.0146	0.0118	0.0085	0.0170	0.0171	0.0032
15	0.0786	0.0165	0.0127	0.0086	0.0171	0.0204	0.0033
16	0.0499	0.0031	0.0071	0.0090	0.0179	0.0022	0.0105
17	0.0491	0.0043	0.0083	0.0085	0.0169	0.0031	0.0081
18	0.0497	0.0056	0.0092	0.0078	0.0157	0.0040	0.0064
19	0.0490	0.0078	0.0101	0.0069	0.0139	0.0057	0.0046
20	0.0497	0.0095	0.0109	0.0062	0.0124	0.0068	0.0039
21	0.0506	0.0116	0.0117	0.0053	0.0106	0.0080	0.0033
22	0.0333	0.0031	0.0067	0.0052	0.0104	0.0013	0.0067
23	0.0329	0.0044	0.0077	0.0047	0.0094	0.0019	0.0049
24	0.0348	0.0061	0.0088	0.0044	0.0088	0.0028	0.0039
25	0.0355	0.0073	0.0098	0.0039	0.0077	0.0032	0.0035
26	0.0354	0.0083	0.0101	0.0035	0.0069	0.0036	0.0031
27	0.0253	0.0030	0.0062	0.0035	0.0069	0.0009	0.0048
28	0.0240	0.0035	0.0065	0.0030	0.0061	0.0010	0.0039
29	0.0259	0.0048	0.0075	0.0029	0.0059	0.0015	0.0033
30	0.0273	0.0058	0.0087	0.0026	0.0053	0.0017	0.0032
31	0.0291	0.0067	0.0095	0.0026	0.0052	0.0021	0.0031

COMPILE TIME= 0.49 SEC,EXECUTION TIME= 0.34 SEC,OBJECT CODE= 12216 BYTES,ARRAY AREA= 2800 BYTES,UNUSED= 4984 BYTES

0.C L-IRT-## FITTING, DB= 3.0 INCHES, DU= 3.0 INCHES, DD= 4.0 INCHES, BRANCH ANGLE=45.0

RUN	UNCB	UNCLCB	UNCLCU	UNFBD	UNSPBD	UNVPB	UNVPU
1	0.4353	0.0054	0.0233	0.0808	0.1616	0.0845	0.0797
2	0.2551	0.0056	0.0190	0.0388	0.0775	0.0885	0.0256
3	0.1947	0.0086	0.0168	0.0227	0.0455	0.0886	0.0125
4	0.1553	0.0108	0.0143	0.0138	0.0276	0.0824	0.0063
5	0.1447	0.0121	0.0135	0.0114	0.0228	0.0900	0.0049
6	0.1384	0.0139	0.0129	0.0096	0.0192	0.0788	0.0040
7	0.1408	0.0180	0.0128	0.0084	0.0167	0.0814	0.0035
8	0.1204	0.0152	0.0125	0.0074	0.0149	0.0672	0.0031
9	0.1190	0.0154	0.0124	0.0072	0.0143	0.0668	0.0030
10	0.2027	0.0007	0.0183	0.0415	0.0830	0.0121	0.0471
11	0.1715	0.0012	0.0195	0.0334	0.0667	0.0153	0.0355
12	0.1336	0.0022	0.0200	0.0230	0.0459	0.0211	0.0214
13	0.1070	0.0039	0.0194	0.0155	0.0309	0.0242	0.0131
14	0.0861	0.0098	0.0174	0.0078	0.0156	0.0297	0.0057
15	0.0889	0.0126	0.0177	0.0071	0.0143	0.0318	0.0054
16	0.0815	0.0134	0.0178	0.0059	0.0119	0.0277	0.0048
17	0.0841	0.0010	0.0149	0.0161	0.0323	0.0014	0.0183
18	0.0785	0.0002	0.0181	0.0135	0.0270	0.0030	0.0167
19	0.0700	0.0009	0.0192	0.0108	0.0217	0.0043	0.0131
20	0.0602	0.0031	0.0200	0.0073	0.0146	0.0064	0.0088
21	0.0617	0.0074	0.0209	0.0056	0.0112	0.0096	0.0070
22	0.0557	0.0074	0.0209	0.0046	0.0092	0.0073	0.0063
23	0.0554	0.0012	0.0143	0.0092	0.0183	0.0005	0.0119
24	0.0507	0.0002	0.0176	0.0074	0.0147	0.0001	0.0107
25	0.0481	0.0016	0.0198	0.0056	0.0112	0.0012	0.0087
26	0.0504	0.0047	0.0215	0.0046	0.0092	0.0029	0.0076
27	0.0460	0.0046	0.0215	0.0037	0.0075	0.0018	0.0069
28	0.0429	0.0014	0.0137	0.0059	0.0118	0.0013	0.0088
29	0.0432	0.0038	0.0158	0.0055	0.0109	0.0012	0.0090
30	0.0414	0.0004	0.0186	0.0045	0.0089	0.0009	0.0082
31	0.0434	0.0029	0.0211	0.0039	0.0077	0.0001	0.0078
32	0.0412	0.0029	0.0211	0.0032	0.0063	0.0005	0.0072

OC.

T-PIPE-MW FITTING, DB= 3.0 INCHES, DU= 3.0 INCHES, DD= 4.0 INCHES, BRANCH ANGLE=45.0

RUN	UNCM	UNCLCB	UNCLCU	UNFUD	UNSPUD	UNVPB	UNVPU
1	0.3559	0.0150	0.0029	0.0808	0.1616	0.0554	0.0402
2	0.1741	0.0138	0.0012	0.0388	0.0775	0.0371	0.0058
3	0.1050	0.0111	0.0009	0.0227	0.0455	0.0240	0.0008
4	0.0642	0.0077	0.0009	0.0138	0.0276	0.0138	0.0004
5	0.0541	0.0070	0.0009	0.0114	0.0228	0.0117	0.0005
6	0.0456	0.0061	0.0008	0.0096	0.0192	0.0095	0.0005
7	0.0414	0.0061	0.0006	0.0084	0.0167	0.0091	0.0004
8	0.0375	0.0060	0.0007	0.0074	0.0149	0.0091	0.0005
9	0.0360	0.0057	0.0007	0.0072	0.0143	0.0076	0.0005
10	0.2034	0.0121	0.0083	0.0415	0.0930	0.0184	0.0401
11	0.1598	0.0132	0.0061	0.0334	0.0667	0.0186	0.0210
12	0.1110	0.0143	0.0031	0.0230	0.0459	0.0183	0.0063
13	0.0776	0.0132	0.0023	0.0155	0.0309	0.0149	0.0009
14	0.0461	0.0106	0.0011	0.0078	0.0156	0.0101	0.0009
15	0.0443	0.0139	0.0009	0.0071	0.0143	0.0101	0.0008
16	0.0396	0.0110	0.0008	0.0059	0.0119	0.0091	0.0009
17	0.0989	0.0110	0.0103	0.0161	0.0323	0.0073	0.0119
18	0.0739	0.0125	0.0072	0.0135	0.0270	0.0083	0.0054
19	0.0611	0.0136	0.0048	0.0108	0.0217	0.0088	0.0015
20	0.0479	0.0133	0.0031	0.0073	0.0146	0.0082	0.0013
21	0.0417	0.0135	0.0018	0.0056	0.0112	0.0081	0.0015
22	0.0379	0.0133	0.0019	0.0046	0.0092	0.0072	0.0018
23	0.0575	0.0109	0.0106	0.0092	0.0183	0.0049	0.0038
24	0.0474	0.0126	0.0070	0.0074	0.0147	0.0056	0.0000
25	0.0427	0.0134	0.0045	0.0056	0.0112	0.0062	0.0019
26	0.0392	0.0139	0.0030	0.0046	0.0092	0.0065	0.0021
27	0.0363	0.0134	0.0033	0.0037	0.0075	0.0057	0.0026
28	0.0437	0.0104	0.0115	0.0059	0.0118	0.0035	0.0037
29	0.0425	0.0114	0.0094	0.0055	0.0109	0.0039	0.0014
30	0.0399	0.0125	0.0067	0.0045	0.0089	0.0045	0.0028
31	0.0375	0.0135	0.0045	0.0039	0.0077	0.0052	0.0028
32	0.0354	0.0137	0.0044	0.0032	0.0063	0.0048	0.0031

COMPILE TIME= 0.51 SEC,EXECUTION TIME= 0.38 SEC,OBJECT CODE= 12216 BYTES,ARRAY AREA= 2800 BYTES,UNUSED= 4984 BYTES

O.C.

-IRT-3A FITTING, DR= 6.0 INCHES, DU= 8.0 INCHES, DD=10.0 INCHES, BRANCH ANGLE=30.0

RUN	UNCR	UNCLCR	UNCLCU	UNERD	UNSERD	UNVRD	UNVRU
1	0.2695	0.0236	0.0206	0.0494	0.0953	0.0536	0.0228
2	0.2354	0.0287	0.0224	0.0327	0.0655	0.0710	0.0151
3	0.2118	0.0308	0.0227	0.0223	0.0445	0.0812	0.0103
4	0.1978	0.0320	0.0222	0.0188	0.0375	0.0796	0.0086
5	0.1889	0.0328	0.0218	0.0165	0.0330	0.0773	0.0075
6	0.1723	0.0330	0.0215	0.0137	0.0274	0.0703	0.0064
7	0.1502	0.0358	0.0199	0.0109	0.0218	0.0659	0.0049
8	0.1324	0.0359	0.0183	0.0097	0.0194	0.0609	0.0043
9	0.1248	0.0093	0.0111	0.0299	0.0599	0.0091	0.0146
10	0.1192	0.0131	0.0160	0.0244	0.0489	0.0121	0.0148
11	0.1105	0.0176	0.0214	0.0176	0.0352	0.0057	0.0130
12	0.0946	0.0247	0.0238	0.0102	0.0203	0.0072	0.0084
13	0.0923	0.0278	0.0237	0.0082	0.0164	0.0094	0.0068
14	0.0950	0.0291	0.0234	0.0080	0.0159	0.0123	0.0063
15	0.0749	0.0058	0.0092	0.0162	0.0324	0.0019	0.0065
16	0.0770	0.0092	0.0135	0.0141	0.0283	0.0021	0.0107
17	0.0745	0.0106	0.0164	0.0114	0.0229	0.0028	0.0103
18	0.0754	0.0156	0.0206	0.0087	0.0174	0.0038	0.0093
19	0.0752	0.0185	0.0227	0.0071	0.0141	0.0043	0.0085
20	0.0764	0.0239	0.0235	0.0062	0.0123	0.0035	0.0071
21	0.0514	0.0054	0.0086	0.0094	0.0189	0.0124	0.0066
22	0.0570	0.0084	0.0137	0.0078	0.0155	0.0036	0.0060
23	0.0608	0.0109	0.0171	0.0066	0.0132	0.0047	0.0052
24	0.0656	0.0148	0.0207	0.0053	0.0105	0.0063	0.0050
25	0.0695	0.0181	0.0223	0.0048	0.0096	0.0072	0.0075
26	0.0405	0.0052	0.0090	0.0061	0.0121	0.0026	0.0056
27	0.0441	0.0066	0.0116	0.0054	0.0107	0.0034	0.0064
28	0.0490	0.0090	0.0150	0.0045	0.0089	0.0047	0.0069
29	0.0524	0.0110	0.0180	0.0034	0.0069	0.0061	0.0070
30	0.0590	0.0138	0.0199	0.0037	0.0073	0.0072	0.0072

-IRT-3A FITTING, DB= 6.0 INCHES, DU= 9.0 INCHES, DD=10.0 INCHES, BRANCH ANGLE=30.0

RUN	UNCM	UNCLCB	UNCLCD	UNCUD	UNSPUD	UNVPB	UNVPU
1	0.1762	0.0037	0.0093	0.0496	0.0993	0.0123	0.0329
2	0.1113	0.0004	0.0080	0.0327	0.0655	0.0011	0.0036
3	0.0914	0.0041	0.0075	0.0223	0.0445	0.0096	0.0324
4	0.0956	0.0059	0.0073	0.0189	0.0375	0.0129	0.0332
5	0.0840	0.0079	0.0074	0.0165	0.0330	0.0162	0.0330
6	0.0825	0.0108	0.0078	0.0137	0.0274	0.0199	0.0329
7	0.0756	0.0125	0.0069	0.0109	0.0218	0.0212	0.0323
8	0.1589	0.0057	0.0127	0.0357	0.0714	0.0032	0.0253
9	0.1767	0.0070	0.0103	0.0299	0.0598	0.0097	0.0100
10	0.1023	0.0078	0.0085	0.0244	0.0489	0.0102	0.0325
11	0.0783	0.0072	0.0076	0.0176	0.0352	0.0094	0.0322
12	0.0471	0.0027	0.0077	0.0102	0.0203	0.0026	0.0077
13	0.0357	0.0002	0.0073	0.0082	0.0164	0.0002	0.0023
14	0.0377	0.0017	0.0072	0.0080	0.0159	0.0017	0.0071
15	0.0776	0.0063	0.0111	0.0162	0.0324	0.0045	0.0071
16	0.0663	0.0073	0.0095	0.0141	0.0283	0.0057	0.0019
17	0.0573	0.0079	0.0086	0.0114	0.0229	0.0057	0.0013
18	0.0439	0.0077	0.0077	0.0087	0.0174	0.0049	0.0036
19	0.0436	0.0070	0.0072	0.0071	0.0141	0.0043	0.0038
20	0.0363	0.0039	0.0074	0.0062	0.0123	0.0026	0.0038
21	0.0502	0.0060	0.0117	0.0064	0.0129	0.0027	0.0014
22	0.0456	0.0074	0.0095	0.0078	0.0155	0.0033	0.0021
23	0.0431	0.0080	0.0083	0.0066	0.0132	0.0036	0.0034
24	0.0390	0.0081	0.0073	0.0053	0.0105	0.0037	0.0041
25	0.0365	0.0072	0.0072	0.0048	0.0096	0.0035	0.0042
26	0.0393	0.0060	0.0117	0.0061	0.0121	0.0019	0.0016
27	0.0384	0.0068	0.0104	0.0054	0.0107	0.0022	0.0029
28	0.0365	0.0077	0.0089	0.0045	0.0089	0.0025	0.0040
29	0.0333	0.0084	0.0076	0.0034	0.0069	0.0026	0.0045
30	0.0341	0.0082	0.0075	0.0037	0.0073	0.0029	0.0046

COMPILE TIME= 0.52 SEC,EXECUTION TIME= 0.32 SEC,OBJECT CODE= 11880 BYTES,ARRAY AREA= 2800 BYTES,UNUSED= 5320 BYTES

O.C.

L-1RT-3H FITTING, DB= 8.0 INCHES, DU=10.0 INCHES, DD=12.0 INCHES, BRANCH ANGLE=45.0

RUN	UNCR	UNCLCR	UNCLCU	UNFBD	UNSPBD	UNVPR	UNVPU
1	0.2052	0.0126	0.0161	0.0359	0.0718	0.0483	0.0205
2	0.1676	0.0152	0.0164	0.0270	0.0439	0.0585	0.0117
3	0.1419	0.0180	0.0150	0.0146	0.0293	0.0580	0.0070
4	0.1339	0.0182	0.0147	0.0126	0.0251	0.0573	0.0059
5	0.1379	0.0184	0.0139	0.0109	0.0218	0.0683	0.0047
6	0.1101	0.0178	0.0145	0.0090	0.0179	0.0465	0.0045
7	0.1020	0.0182	0.0139	0.0074	0.0148	0.0442	0.0036
8	0.1068	0.0041	0.0063	0.0274	0.0549	0.0002	0.0138
9	0.1027	0.0059	0.0095	0.0236	0.0472	0.0016	0.0147
10	0.0942	0.0093	0.0140	0.0178	0.0356	0.0050	0.0135
11	0.0801	0.0105	0.0160	0.0124	0.0248	0.0061	0.0103
12	0.0678	0.0136	0.0171	0.0077	0.0143	0.0093	0.0063
13	0.0633	0.0145	0.0168	0.0058	0.0116	0.0095	0.0051
14	0.0648	0.0151	0.0165	0.0056	0.0113	0.0117	0.0047
15	0.0615	0.0037	0.0091	0.0125	0.0251	0.0008	0.0104
16	0.0596	0.0050	0.0120	0.0105	0.0210	0.0007	0.0103
17	0.0557	0.0062	0.0144	0.0082	0.0164	0.0010	0.0094
18	0.0532	0.0086	0.0168	0.0064	0.0127	0.0008	0.0079
19	0.0508	0.0101	0.0173	0.0051	0.0102	0.0012	0.0068
20	0.0479	0.0119	0.0177	0.0038	0.0076	0.0015	0.0054
21	0.0417	0.0032	0.0089	0.0070	0.0139	0.0014	0.0074
22	0.0454	0.0050	0.0132	0.0057	0.0114	0.0022	0.0079
23	0.0461	0.0061	0.0160	0.0046	0.0091	0.0027	0.0076
24	0.0464	0.0079	0.0168	0.0038	0.0077	0.0034	0.0067
25	0.0461	0.0092	0.0175	0.0031	0.0062	0.0041	0.0060
26	0.0476	0.0105	0.0178	0.0035	0.0069	0.0032	0.0057
27	0.0330	0.0027	0.0100	0.0040	0.0081	0.0017	0.0064
28	0.0354	0.0036	0.0117	0.0038	0.0075	0.0022	0.0066
29	0.0396	0.0046	0.0147	0.0035	0.0069	0.0029	0.0070
30	0.0404	0.0052	0.0169	0.0026	0.0053	0.0036	0.0068

L-1RT-3H FITTING, DB= 8.0 INCHES, DU=10.0 INCHES, DD=12.0 INCHES, BRANCH ANGLE=45.0

RUN	UNCM	UNCLCR	UNCICU	UNFUD	UNSPUD	UNVPR	UNVPU
1	0.1460	0.0074	0.0033	0.0359	0.0718	0.0242	0.0034
2	0.0911	0.0061	0.0024	0.0220	0.0439	0.0164	0.0003
3	0.0549	0.0020	0.0031	0.0146	0.0293	0.0045	0.0014
4	0.0456	0.0011	0.0030	0.0126	0.0251	0.0024	0.0014
5	0.0388	0.0007	0.0027	0.0109	0.0218	0.0015	0.0013
6	0.0312	0.0001	0.0029	0.0090	0.0179	0.0001	0.0014
7	0.0293	0.0012	0.0028	0.0074	0.0148	0.0019	0.0012
8	0.1319	0.0058	0.0075	0.0274	0.0549	0.0088	0.0276
9	0.1086	0.0072	0.0052	0.0236	0.0472	0.0106	0.0147
10	0.0808	0.0083	0.0037	0.0178	0.0356	0.0113	0.0041
11	0.0584	0.0083	0.0031	0.0124	0.0248	0.0097	0.0001
12	0.0383	0.0061	0.0028	0.0072	0.0143	0.0062	0.0017
13	0.0313	0.0048	0.0028	0.0059	0.0116	0.0046	0.0017
14	0.0290	0.0038	0.0029	0.0056	0.0113	0.0037	0.0017
15	0.0649	0.0064	0.0059	0.0125	0.0251	0.0049	0.0099
16	0.0533	0.0074	0.0048	0.0105	0.0210	0.0055	0.0040
17	0.0431	0.0083	0.0036	0.0082	0.0164	0.0057	0.0008
18	0.0379	0.0089	0.0027	0.0064	0.0127	0.0059	0.0013
19	0.0339	0.0086	0.0026	0.0051	0.0102	0.0055	0.0019
20	0.0291	0.0075	0.0025	0.0038	0.0076	0.0047	0.0021
21	0.0403	0.0062	0.0058	0.0070	0.0139	0.0029	0.0046
22	0.0331	0.0081	0.0037	0.0057	0.0114	0.0039	0.0003
23	0.0310	0.0087	0.0031	0.0046	0.0091	0.0041	0.0014
24	0.0294	0.0091	0.0025	0.0038	0.0077	0.0043	0.0020
25	0.0271	0.0092	0.0021	0.0031	0.0062	0.0043	0.0022
26	0.0280	0.0086	0.0023	0.0035	0.0069	0.0046	0.0022
27	0.0268	0.0064	0.0053	0.0040	0.0081	0.0020	0.0010
28	0.0256	0.0072	0.0044	0.0038	0.0075	0.0023	0.0003
29	0.0262	0.0084	0.0031	0.0035	0.0069	0.0030	0.0013
30	0.0242	0.0096	0.0016	0.0026	0.0053	0.0033	0.0018

COMPILE TIME= 0.50 SEC,EXECUTION TIME= 0.36 SEC,OBJECT CODE= 11880 BYTES,ARRAY AREA= 2800 BYTES,UNUSED= 5320 BYTES

L-1RT-3N FITTING, DR=12.0 INCHES, DU=14.0 INCHES, DD=16.0 INCHES, BRANCH ANGLE=30.0

RUN	UNCR	UNCLCR	UNCLCU	UNFRD	UNSPRD	UNVPR	UNVPU
1	0.1853	0.0066	0.0114	0.0268	0.0535	0.0714	0.0156
2	0.1349	0.0080	0.0102	0.0150	0.0301	0.0641	0.0074
3	0.1125	0.0090	0.0090	0.0101	0.0202	0.0599	0.0043
4	0.1008	0.0097	0.0084	0.0083	0.0166	0.0544	0.0034
5	0.0902	0.0096	0.0082	0.0069	0.0137	0.0491	0.0028
6	0.0839	0.0095	0.0079	0.0059	0.0118	0.0463	0.0024
7	0.0759	0.0101	0.0073	0.0048	0.0096	0.0423	0.0018
8	0.1133	0.0045	0.0124	0.0188	0.0376	0.0248	0.0152
9	0.0959	0.0057	0.0120	0.0128	0.0257	0.0307	0.0090
10	0.0784	0.0066	0.0110	0.0085	0.0170	0.0330	0.0054
11	0.0717	0.0073	0.0103	0.0069	0.0139	0.0292	0.0041
12	0.0655	0.0076	0.0100	0.0060	0.0119	0.0265	0.0035
13	0.0622	0.0079	0.0095	0.0052	0.0103	0.0264	0.0029
14	0.0568	0.0084	0.0089	0.0043	0.0085	0.0244	0.0023
15	0.0619	0.0011	0.0119	0.0106	0.0212	0.0021	0.0152
16	0.0563	0.0010	0.0129	0.0089	0.0178	0.0028	0.0123
17	0.0524	0.0021	0.0136	0.0076	0.0151	0.0028	0.0103
18	0.0480	0.0013	0.0152	0.0047	0.0095	0.0052	0.0071
19	0.0389	0.0033	0.0136	0.0042	0.0084	0.0038	0.0057
20	0.0368	0.0029	0.0132	0.0037	0.0074	0.0039	0.0048
21	0.0443	0.0038	0.0105	0.0070	0.0141	0.0002	0.0117
22	0.0436	0.0010	0.0121	0.0064	0.0128	0.0004	0.0109
23	0.0383	0.0013	0.0130	0.0051	0.0102	0.0002	0.0091
24	0.0362	0.0014	0.0148	0.0039	0.0078	0.0010	0.0073
25	0.0335	0.0014	0.0149	0.0033	0.0066	0.0006	0.0065
26	0.0281	0.0008	0.0057	0.0043	0.0086	0.0005	0.0063
27	0.0302	0.0010	0.0093	0.0039	0.0078	0.0007	0.0075
28	0.0320	0.0011	0.0120	0.0035	0.0069	0.0009	0.0076

B220
5

L-I-T-3N FITTING, DB=12.0 INCHES, DU=14.0 INCHES, DD=16.0 INCHES, BRANCH ANGLE=30.0

RUN	UNC*	UNCLCB	UNCLCU	UNEUD	UNSPUL	UNVPB	UNVPU
1	0.1201	0.0069	0.0007	0.0268	0.0535	0.0291	0.0032
2	0.0632	0.0040	0.0012	0.0150	0.0301	0.0127	0.0032
3	0.0364	0.0010	0.0016	0.0101	0.0202	0.0027	0.0008
4	0.0274	0.0009	0.0016	0.0083	0.0166	0.0001	0.0008
5	0.0261	0.0010	0.0017	0.0069	0.0137	0.0021	0.0008
6	0.0264	0.0020	0.0019	0.0059	0.0118	0.0040	0.0008
7	0.0256	0.0030	0.0017	0.0048	0.0096	0.0056	0.0007
8	0.0914	0.0027	0.0001	0.0188	0.0376	0.0206	0.0056
9	0.0614	0.0069	0.0008	0.0128	0.0257	0.0146	0.0007
10	0.0308	0.0044	0.0013	0.0085	0.0170	0.0090	0.0006
11	0.0316	0.0032	0.0014	0.0069	0.0139	0.0054	0.0008
12	0.0263	0.0023	0.0016	0.0060	0.0119	0.0036	0.0009
13	0.0213	0.0013	0.0016	0.0052	0.0103	0.0019	0.0009
14	0.0162	0.0004	0.0016	0.0043	0.0085	0.0006	0.0008
15	0.0603	0.0077	0.0003	0.0106	0.0212	0.0074	0.0138
16	0.0505	0.0086	0.0004	0.0089	0.0178	0.0081	0.0068
17	0.0440	0.0091	0.0005	0.0076	0.0151	0.0084	0.0034
18	0.0318	0.0094	0.0005	0.0047	0.0095	0.0076	0.0001
19	0.0285	0.0087	0.0000	0.0042	0.0084	0.0068	0.0004
20	0.0263	0.0080	0.0003	0.0037	0.0074	0.0062	0.0008
21	0.0437	0.0105	0.0009	0.0070	0.0141	0.0041	0.0111
22	0.0386	0.0076	0.0001	0.0064	0.0128	0.0049	0.0069
23	0.0321	0.0083	0.0002	0.0051	0.0102	0.0050	0.0033
24	0.0291	0.0097	0.0011	0.0039	0.0078	0.0059	0.0007
25	0.0271	0.0110	0.0017	0.0033	0.0066	0.0058	0.0001
26	0.0335	0.0045	0.0028	0.0043	0.0086	0.0016	0.0118
27	0.0272	0.0062	0.0010	0.0039	0.0078	0.0024	0.0058
28	0.0246	0.0079	0.0001	0.0035	0.0069	0.0034	0.0026

COMPILE TIME= 0.48 SEC,EXECUTION TIME= 0.29 SEC,OBJECT CODE= 11880 BYTES,ARRAY AREA= 2800 BYTES,UNUSED= 5320 BYTES